Functional and biochemical analysis of the *Capsicum annuum* resistance protein Bs3

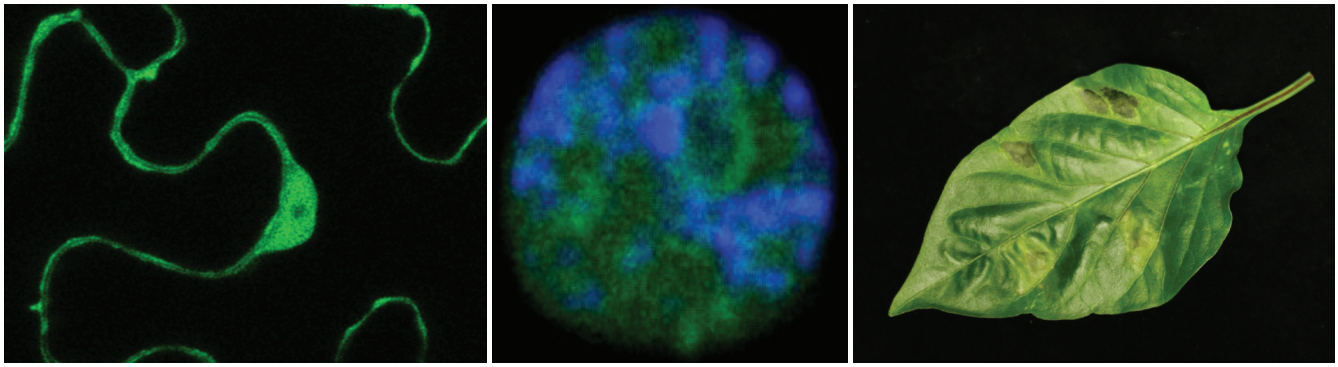

Dissertation
der Mathematisch-Naturwissenschaftlichen Fakultät
der Eberhard Karls Universität Tübingen
zur Erlangung des Grades eines
Doktors der Naturwissenschaften
(Dr. rer. nat.)

Christina Krönauer

Functional and biochemical analysis of the *Capsicum annuum* resistance protein Bs3

Dissertation

der Mathematisch-Naturwissenschaftlichen Fakultät

der Eberhard Karls Universität Tübingen

zur Erlangung des Grades eines

Doktors der Naturwissenschaften

(Dr. rer. nat.)

vorgelegt von

Christina Krönauer

aus Peißenberg

Tübingen

2019

Gedruckt mit Genehmigung der Mathematisch-Naturwissenschaftlichen Fakultät der Eberhard Karls Universität Tübingen.

Tag der mündlichen Qualifikation:	06.02.2020
Dekan:	Prof. Dr. Wolfgang Rosenstiel
1. Berichterstatter:	Prof. Dr. Thomas Lahaye
2. Berichterstatter:	Prof. Dr. Ulrike Zentgraf

List of publications

Parts of this work have been published:

Christina Krönauer, Joachim Kilian, Tina Strauß, Mark Stahl, Thomas Lahaye

Cell death triggered by the YUCCA-like Bs3 protein coincides with accumulation of SA and Pip but not of IAA

Plant Physiology, Published July 2019. DOI: https://doi.org/10.1104/pp.18.01576

From the work presented in this thesis the following manuscript is in preparation:

Christina Krönauer, David Ballou, Yunde Zhao, Thomas Lahaye

Bs3 is an FMO that triggers cell death in plants and impairs growth in yeast

From work not presented in this thesis the following manuscript has been published:

Deepak Shantharaj, Patrick Römer, Josef Figueiredo, Gerald V. Minsavage, Christina Krönauer, Robert E. Stall, Gloria A. Moore, Latanya C. Fisher, Yang Hu, Diana M. Horvath, Thomas Lahaye and Jeffrey B. Jones.

An engineered promoter driving expression of a microbial avirulence gene confers recognition of TAL effectors and reduces growth of diverse *Xanthomonas* strains in citrus.

Molecular Plant Pathology (2017) 18(7), 976–989

Dass ich erkenne, was die Welt, im Innersten zusammenhält

(J.W. v. Goethe, Faust I)

Contents

Abbreviations

35S	Cauliflower mosaic virus *35S* promoter
aa	Amino acid
Avr	Avirulence
bp	Base pair
C4a	C4a-(hydro)peroxyflavin
CC	Coiled-coil
CDS	Coding sequence
DAB	3,3'-Diaminobenzidine
ETI	Effector triggered immunity
FAD	Flavin adenine dinucleotide
FMO	Flavin-containing monooxygenase
GC/MS	Gas chromatography mass spectrometry
GSH	Glutathione
GSSG	Glutathione disulfide
hpi	Hours post infiltration
HR	Hypersensitive response
IAA	Indole-3-acetic acid
IPA	Indole-3-pyruvic acid
LC/MS	Liquid chromatography mass spectrometry
MS	Mass spectrometry
NADH	Nicotinamide adenine dinucleotide
NADPH	Nicotinamide adenine dinucleotide phosphate
N-OH-Pip	N-hydroxypipecolic acid
NLR	Nucleotide-binding leucine-rich repeat
PAMP	Pathogen associated molecular pattern
Pip	Pipecolic acid
PTI	PAMP-triggered immunity
R gene	Resistance gene
ROS	Reactive oxygen species
RLP	Receptor-like protein
RLK	Receptor-like kinase
SA	Salicylic acid
SAR	Systemic acquired resistance
TALE	Transcription activator like effector
TIR	Toll/IL-1 receptor
TMA	Trimethylamine
TMAO	Trimethylamine-N-oxide
TRV	Tobacco rattle virus
VIGS	Virus induced gene silencing

Abstract

The pepper (*Capsicum annuum*) bacterial spot 3 (Bs3) protein confers resistance against bacteria of the genus *Xanthomonas* which are the causal agent of bacterial spot disease. During infection, *Xanthomonas* injects effector proteins into the plant cell to reprogram the host´s protein biosynthesis and to enhance virulence. In return, plants evolved mechanisms that sense bacterial components and activate an immune response. The Bs3 resistance reaction is induced by the *Xanthomonas* transcription activator like effector (TALE) AvrBs3, which binds to a specific sequence element within the *Bs3* promoter. Activation of *Bs3* subsequently triggers a fast and local cell death reaction known as the hypersensitive response (HR), which limits spread of the pathogen.

Sequence-based comparisons revealed that Bs3 belongs to the family of flavin containing monooxygenases (FMOs) and has highest similarity to YUCCA (YUC) proteins, a family of enzymes which produce the major plant hormone auxin, thereby playing a critical role in growth and development. This raised the question of why Bs3 fulfils such a different function compared to YUCs, despite its striking similarity.

In the first part of this work, the Bs3 and YUC amino acid (aa) sequences were compared with the aim to identify sections that could be responsible for the different function of the two proteins. We conducted mutant analyses and gene shuffling experiments and identified sequence elements that are exchangeable. Furthermore, we found that Bs3 expression does not increase auxin levels but correlates with accumulation of the immune associated metabolites salicylic acid (SA) and pipecolic acid (Pip).

In the second part of this thesis, a protocol for Bs3 protein purification was established which enabled the biochemical characterization of Bs3 and *in vitro* enzyme assays. We validated that Bs3 indeed functions as FMO and found oxidation of NADPH as well as production of H_2O_2 *in vitro* and *in vivo*. The creation and analysis of the $Bs3_{S211A}$ mutant derivative, which functions as NADPH oxidase but does not trigger HR, clarified that oxidase function is not sufficient to trigger cell death. In order to identify the putative Bs3 substrate, metabolite experiments were started that will have to be pursued in the future.

Zusammenfassung

Das Bs3 Protein aus Paprika (*Capsicum annuum*) vermittelt Resistenz gegenüber pflanzenpathogenen Bakterien der Gattung *Xanthomonas*. Während einer Infektion nutzt *Xanthomonas* sogenannte Effektorproteine, um die biochemischen Prozesse innerhalb der Pflanze zum eigenen Vorteil zu verändern. Dagegen haben Pflanzen verschiedene Mechanismen entwickelt, die Effektorproteine direkt oder indirekt erkennen und eine Immunantwort auslösen. Die Bs3 Resistenzreaktion wird von dem *Xanthomonas* Effektor AvrBs3 ausgelöst, der spezifisch and ein Sequenzelement im *Bs3* Promotor bindet und dadurch Transkription des *Bs3* Gens induziert. Die daraufhin ausgelöste hypersensitive Reaktion (HR), ein schnelles und lokal begrenztes Zelltodereignis, verhindert die weitere Ausbreitung der Bakterien.

Basierend auf Sequenzvergleichen wird Bs3 der Familie der Flavin-monooxygenasen (FMOs) zugeordnet. Innerhalb der FMOs besteht die größte Ähnlichkeit gegenüber YUCCA (YUC) Proteinen, die das Phytohormon Auxin produzieren und daher eine wichtige Rolle für Pflanzenwachstum und -entwicklung spielen. Daher stellt sich die Frage, warum Bs3, trotz seiner auffallenden Ähnlichkeit zu YUCs, eine so andersartige Funktion in der Pflanze ausübt.

Im ersten Teil dieser Arbeit wurden vergleichende Analysen zwischen YUC und Bs3 Aminosäuresequenzen durchgeführt, um mögliche Sequenzabschnitte zu identifizieren, die für die unterschiedliche Funktionen der homologen Proteine innerhalb der Zelle verantwortlich sein könnten. Durch funktionale Analyse von Einzelmutationsderivaten und chimären Proteinen konnten austauschbare Regionen in Bs3 und YUC identifiziert werden. Darüber hinaus wurde festgestellt, dass *Bs3* Expression zur Anreicherung der zwei Metaboliten Salicylsäure und Pipecolinsäure führt, welche eine wichtige Rolle in der Regulation pflanzlicher Resistenzreaktionen spielen.

Im zweiten Teil dieser Arbeit wurde ein Protokoll zur nativen Reinigung von Bs3 Protein aus *E. coli* Kulturen etabliert. Mit der daraus entstehenden Möglichkeit, biochemische Studien zur enzymatischen Funktion von Bs3 *in vitro* durchzuführen, konnte gezeigt werden, dass Bs3 nicht nur strukturell, sondern auch funktional eine FMO darstellt. Bs3 bindet den Kofaktor FAD und produziert H_2O_2 durch die Oxidation von NADPH. Zur Durchführung funktionaler

Vergleiche wurde das Bs3 Derivat $Bs3_{S211A}$ erstellt, das zwar NADPH-Oxidaseaktivität besitzt, jedoch keinen Zelltod in Pflanzen auslöst. Anhand des Vergleichs von Bs3 mit $Bs3_{S211A}$ konnte gezeigt werden, dass diese NADPH-Oxidaseaktivität allein jedoch nicht ausreicht, um eine HR auszulösen. Zur weiteren Erforschung des Signalwegs der Bs3 Resistenzreaktion wurde daher mit Experimenten zur Identifizierung des Bs3 Substrats begonnen.

1 Introduction

The aim to fight plant pests and diseases is probably as old as breeding of crops itself. With the increasing awareness of the ecological impact of pesticides and the emergence of resistant pathogen strains, new ways of plant protection become necessary. The understanding of the molecular basis of plant immune responses might help to exploit the natural abilities of plants to fight pathogens and to create biocompatible and durable resistances in plants. This work focusses on the genetic and biochemical dissection of how the pepper Bs3 resistance protein triggers an immune reaction in response to *Xanthomonas* infection in pepper.

1.1 The origin of *Capsicum* and its pathogens

Peppers (*Capsicum* spp.) have their origin in the region of what is considered present day´s Northeast Mexico (Kraft et al., 2014), and are by now grown in all temperate parts of the world (Bosland and Votava, 2012). Ever since their domestication 6000 years ago, chili peppers have been an important part of South American culture (Figure 1.1) and used as a vegetable, spice, and medical compound. Christopher Columbus brought peppers to Europe, and is not only responsible for their designation as "pepper" similar to black pepper (*Piper nigrum*) but also for a revolution of Spanish cuisine. By now, peppers of sweet and pungent varieties are grown all around the world. The genus *Capsicum* comprises 38 species known to date (USDA, 2019) whereof five are domesticated: *C. annuum*, *C. chinense*, *C. frutescens*, *C. baccatum* and *C. pubescens* (Pickersgill, 1997). Of these, *C. annuum* is by far the most abundant species. The other domesticated species are mostly grown in South America and only play a minor role in Europe with only some known uses, for example in Tabasco sauce, which is made from *C. frutescens* and Habanero (*C. chinense*). In 2017, around 36 million metric tons of green pepper and 4.6 million metric tons of dry pepper were produced worldwide, with China and India being the leading producers (FAO, 2017).

In parallel with increasing cultivation of pepper, pests and diseases emerged and spread to producing areas. Besides insects, viruses and fungi, bacteria of the genus *Xanthomonas* are a major threat to pepper plants. *Xanthomonas* causes bacterial spot disease, which was first described in tomato and pepper in the 1920s

(Higgins, 1922; Gardner and Kendrick, 1923). The causal bacterium was designated as *Bacterium vesicatorium* (Doidge, 1920) according to the characteristic pustules it causes on all plant parts (Figure 1.1 B). Currently, bacteria causing bacterial spot disease are reclassified into four species: *X. euvesicatoria*, *X. vesicatoria*, *X. gardneri*, and *X. perforans*, which all cause similar symptoms but possess different metabolic and phenotypic characteristics (Jones et al., 2004; Stoyanova et al., 2014).

Figure 1.1: Early signs of the importance of chili peppers in South American cultures and signs of *Xanthomonas* causing bacterial spot on pepper A) Bowl with aji (chili peppers), Nasca culture, Peru, 100 BCE - 600 CE, ceramic, slip paints with slip paints. With kind permission of the Department of Art and Art History, College of Fine Arts, The University of Texas at Austin B) Symptoms of bacterial spot disease on *Capsicum* leaves. Photograph by Chelsea Hardin (2014).

In humid and warm conditions, which are favourable for the pathogen, bacterial spot disease is devastating and can lead to defoliation and massive crop loss. Since these pathogens can be transmitted via wind and rain and are introduced into new areas via contaminated seeds or potentially symptomless non-host plants, control of the disease is challenging (Gitaitis and Walcott, 2007). Currently, chemical treatment, field rotation, seed sterilization, and introduction of resistance genes from wild cultivars are used to contain bacterial disease outbreaks (Ritchie, 2000). However, *Xanthomonas* strains rapidly develop resistances to chemical treatment (Marco and Stall, 1983; Jones and Jones, 1985) and evolve mechanisms to avoid host recognition (Gassmann et al., 2000). In this context, understanding the molecular mechanisms of resistance could help to create more durable resistance in plants.

1.2 Plant immunity in response to pathogen attack

1.2.1 Pathogen and effector triggered immune responses

Plants are able to fight pathogenic invaders at several levels of infection (Figure 1.2). The first layer of immunity is the presence of receptors in the plasma membrane, facing the apoplastic space. These receptor-like proteins (RLPs) or receptor like kinases (RLKs) carry an extracellular domain which can sense pathogen derived molecules, known as pathogen associated molecular patterns (PAMPs), and subsequently trigger a signalling cascade to activate basal plant defence mechanisms. Plants contain multiple receptors that differ in their ectodomain, creating specificity for different types of PAMPs. The immune reactions triggered by these RLPs/RLKs are designated as PAMP-triggered immunity (PTI).

Many bacteria inject proteins, called effectors, via a type-III-secretion system into the host cytoplasm to restrict these basal plant immune responses. This is known as effector-triggered susceptibility. Plants in turn contain proteins of the nucleotide-binding leucine-rich repeat (NLR) type, that sense these bacterial effectors (Figure 1.2). NLR type *R* genes account for 60% of the more than 300 resistance genes that have been cloned thus far (Kourelis and van der Hoorn, 2018). NLRs are multidomain proteins that can either bind directly, or indirectly via other binding proteins, to bacterial effectors. Upon effector recognition, NLRs induce an immune response that often results in cell death. In general, immune responses triggered upon effector recognition are designated as effector triggered immunity (ETI). ETI is described to trigger a faster and more pronounced response than PTI (Jones and Dangl, 2006). However, the clear distinction between ETI and PTI is challenged by some immune responses showing overlapping characteristics (Tsuda and Katagiri, 2010).

1.2.2 ROS and SA are important signalling compounds

Plant immune reactions are dependent on signalling molecules like hydrogen peroxide (H_2O_2) and hormonal compounds like salicylic acid (SA) that are produced at the infection site, and operate as signals that are transmitted to cells distant from the infection site (Figure 1.2).

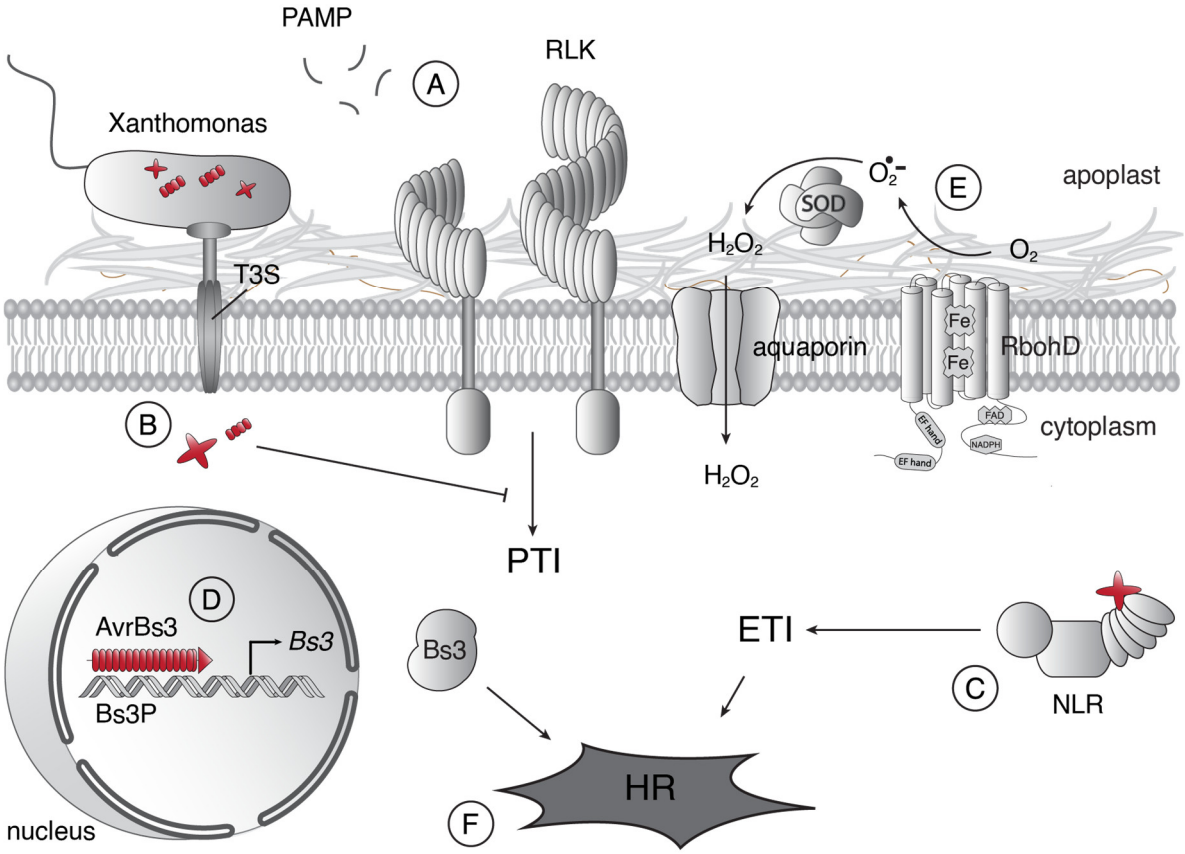

Figure 1.2 The plant immune system and activation of Bs3 HR. A) During infection, pathogen associated molecular patterns (PAMP) are perceived by membrane bound receptor-like kinases (RLKs) B) Many pathogens inject bacterial proteins, called effectors, via a Type-3-secretion system (T3S) into the plant cell to promote infection. C) Within the cell, nucleotide binding–leucine-rich repeat (NLR) proteins can perceive bacterial effectors and induce effector triggered immunity (ETI) D) The TALE AvrBs3 binds a sequence element within the *Bs3* promoter (*Bs3P*) and activates transcription of *Bs3*. F) Activation of Bs3, similar ETI mediated by NLRs, causes a hypersensitive response (HR).

SA is an important immunity associated compound, which increases upon microbial infection. In plants, SA is synthesized via two different pathways, either from cinnamic acid by phenylalanine ammonia lyase (PAL) or from isochorismate via the isochorismate pathway (Dempsey and Klessig, 1994; Wildermuth et al., 2001; Chen et al., 2009; Zhang and Li, 2019). Recently, the acyl adenylase avrPphB SUSCEPTIBLE3 (PBS3) and the acyltransferase ENHANCED PSEUDOMONAS SUSCEPTIBILTY 1 (EPS1) were found to catalyse the previously unknown final reactions in SA biosynthesis in *Arabidopsis*. Together, they form a two-step metabolic pathway to produce SA from isochorismate (Rekhter et al., 2019; Torrens-Spence et al., 2019). Plants that are deficient in SA production show reduced systemic acquired resistance (SAR) and increased pathogen growth (Gaffney et al., 1993; Nawrath and Metraux, 1999). Examples are *Arabidopsis sid2* lines that carry a mutation within the *ISOCHORISMATE*

SYNTHASE 1 (*ICS1*) gene, or plants that express the *Pseudomonas putida* salicylate hydroxylase gene (*NahG*) which diminishes SA quantity by reducing it into catechol (Gaffney et al., 1993; Nawrath and Metraux, 1999; Wildermuth et al., 2001; van Wees and Glazebrook, 2003).

Reactive oxygen species (ROS) are oxygen-containing, reactive molecules like H_2O_2, superoxide anion ($O_2^{\bullet-}$) and hydroxyl radical ($^{\bullet}OH$). At low levels, ROS are unavoidable by-products of aerobic metabolism and for a long time were viewed as being detrimental to cells. As of recently, however, their role as a signalling compound has been highlighted. ROS are produced at various locations within the cell, especially at the plasma membrane, in the mitochondria, chloroplasts, and peroxisomes (Figure 1.3, Corpas et al., 2015). ROS levels are tightly regulated by scavengers like catalase, superoxide dismutase and peroxidase. In response to microbial infection, plants exhibit a rapid increase in ROS levels known as the oxidative burst. Membrane bound NADPH oxidases and cell wall associated peroxidases are the source of ROS generated during pathogen attack (Wojtaszek, 1997; Torres et al., 2006). Notably, NADPH oxidases produce $O_2^{\bullet-}$ in the apoplastic space, which is converted to H_2O_2 by superoxide dismutase and re-enters the cell via aquaporins (Figure 1.3).

1.3 *Bs3* activation triggers a hypersensitive response

1.3.1 *Bs3* is transcriptionally activated by AvrBs3 and AvrHah1

Bs3 belongs to a class of resistance (*R*) genes, the executor *R* genes, that are activated by transcription activator like effector (TALE) proteins. TALEs are bacterial derived effectors that act as eukaryotic transcription factors and reprogram host gene expression (Boch and Bonas, 2010). TALEs are injected by bacteria into the host cytoplasm to increase virulence and promote bacterial growth. However, during plant-pathogen co-evolution, some plants have established TALE activation-based resistance mechanisms. Five members of the executor *R* genes, *Bs3*, *Xa10, Xa23, Bs4-C* and *Xa27* have been cloned so far (Zhang et al., 2015) and are known to constitute a "promoter-trap" for the respective TALEs. In case of *Bs3*, the *Xanthomonas* derived TALE AvrBs3 binds to a 19 bp long sequence in the *Bs3* promoter and activates transcription. (Figure 1.2, Bonas et al., 1989; Römer et al., 2007). Notably, binding occurs in a sequence

specific manner. The specificity of TALEs is based on their distinct repeat structure and determined by the base specifying residue, an amino acid side chain located within each repeat of TALEs, mediating the contact to the bases within the target sequence in the promoter. Interestingly, a second TAL-effector, AvrHah1 of *Xanthomonas gardneri* which is only distantly related to AvrBs3, is able to activate *Bs3* transcription (Schornack et al., 2008). Upon activation, *Bs3* triggers a HR (Boch et al., 2009; Deng et al., 2012; Mak et al., 2012).

1.3.2 The hypersensitive response

The HR is a type of programmed cell death in plants that occurs in conjunction with resistance reactions during pathogen attack. By contrast, cell death during manifested disease is usually designated as necrosis. Notably, these designations are not based on mechanistic differences (Morel and Dangl, 1997).

Hallmarks of the HR are an oxidative burst, accumulation of SA, increased ion leakage and an induction of defence gene expression. Macroscopically, HR causes dry lesions at the infection site that are clearly delimited from surrounding tissue (Lam, 2004). On a subcellular level, mitochondrial swelling, membrane dysfunction and lytic vacuoles can be observed (van Doorn et al., 2011). All of these features overlap with senescence or disease phenotypes and no unique factor defining HR is known thus far. What is known however, is that HR reactions are dependent on active protein biosynthesis in plants as substances that block metabolic processes have been described to impair HR development (He et al., 1994). The isolation of lesions from the surrounding tissue is an interesting feature of HR, and there are multiple theories on how this localized cell death is achieved. One possibility is that high SA contents leads to cell death while low SA contents serve as survival signal (Fu et al., 2012). Other studies show that NADPH oxidases supress SA mediated cell death (Torres et al., 2005).

There are a myriad of distinct immune pathways that all converge to the final result of HR. For example, the HR in *Arabidopsis*, triggered by the *P. syringae* effector AvrRps4 via recognition by the Toll/IL-1 receptor-(TIR) NLR Rps4 is dependent on autophagy related proteins. By contrast, the HR triggered by the *P. syringae* effector AvrRpt2 which is sensed by the coiled-coil (CC) NLR type R protein resistant to *P. syringae* 2 (RPS2) is not dependant on

autophagy but on the NON RACE-SPECIFIC DISEASE RESISTANCE (NDR1, Hofius et al., 2009).

Finally, it is still under discussion, if cell death is the cause or consequence of the immune reaction and if it is needed for impairment of bacterial growth (Kiraly et al., 1972; Greenberg and Yao, 2004). It seems to be likely, that cell death during HR is predominantly a signal to the surrounding plant tissue to establish systemic immunity (Heath, 2000).

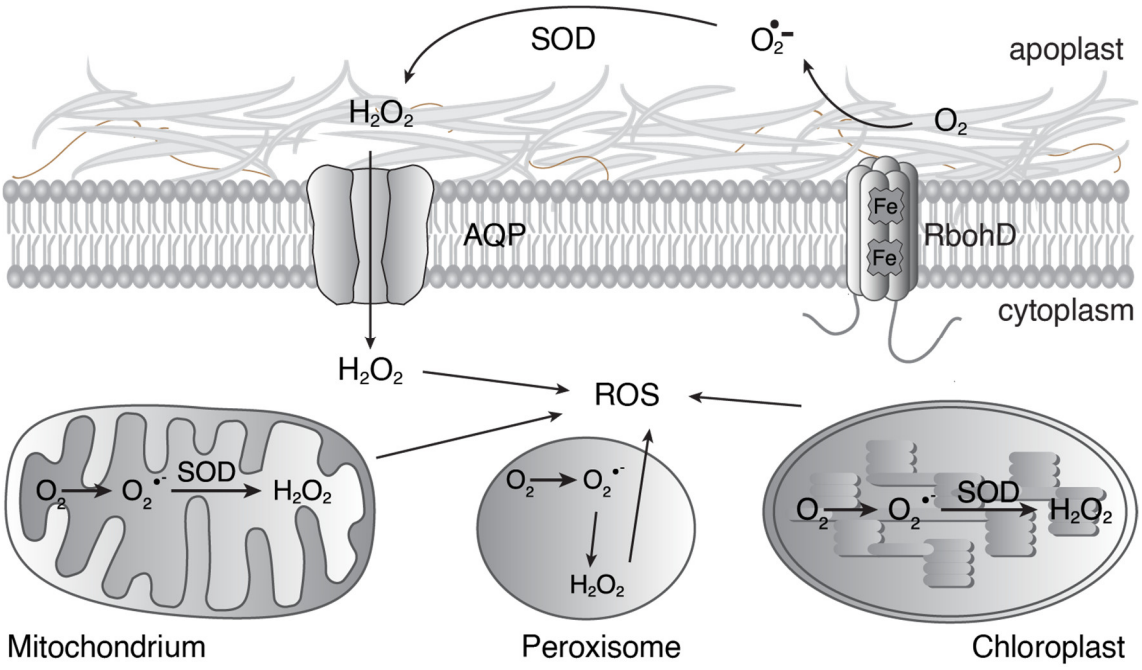

Figure 1.3 Sources of ROS in the plant cell. Reactive oxygen species (ROS) are produced in mitochondria, peroxisomes, chloroplasts and by membrane localized NADPH oxidases. Superoxide ($O_2^{\bullet-}$) is converted to H_2O_2 by superoxide dismutase (SOD). Notably, the membrane bound plant NADPH oxidases (respiratory burst oxidase homologs, RbohD) produce superoxide in the apoplast. The H_2O_2 generated by SOD re-enters the cell via aquaporins (AQP).

1.4 The *Bs3* resistance gene

1.4.1 Identification and cloning of *Bs3*

Different *Capsicum* varieties have always shown variable susceptibility or resistance to bacterial spot disease in the field (Horsfall and McDonnell, 1940). The *Bs3 R gene* was first mentioned in 1985 when Kim and Hartmann analysed a *C. annuum* line of Indian origin (PI 271322) that appeared to be resistant against bacterial spot disease. They found development of HR after inoculation with specific *Xanthomonas* strains and an inheritance pattern that suggested a dominant gene to be responsible for this resistance (Kim and Hartmann, 1985). Following the nomenclature of two previously discovered *R* genes, *Bs1* and *Bs2*, the gene causing HR in PI 271322 was designated as *Bs3* (Kim and Hartmann, 1985). These three *R* genes were crossed into the pepper variety Early California Wonder (ECW) to create the near isogenic lines ECW-10R, ECW-20R and ECW-30R (Stall et al., 2009).

The *Bs3* locus was isolated via a map based cloning strategy. Amplified Fragment Length Polymorphism (AFLP) analysis (Pierre M et al., 2000) and screening of yeast- and bacterial artificial chromosome (YAC and BAC) libraries delimited the Bs3 locus to a segment of approximately 60 kb (Jordan, 2005; Jordan et al., 2006). Fragments of a BAC were cloned into a plant expression vector and tested via *Agrobacterium* mediated co-transformation with *avrBs3* in *N. benthamiana.* The *Bs3* gene was finally identified and its gene product was determined to be 342 amino acids (aa) long. Surprisingly, the protein was not found to be similar to any known R proteins but showed a striking similarity to the enzyme family of flavin-containing monooxygenases (FMOs) (Römer et al., 2007).

1.4.2 Bs3 is similar to flavin-containing monooxygenases

FMOs are found in mammals, plants, yeast and bacteria where they fulfil a plethora of different functions like detoxifications of xeno-substrates, hormone production, and redox homeostasis (Suh et al., 1999; Zhao et al., 2001; Eswaramoorthy et al., 2006). The number of FMOs varies across different phyla. While there are five FMOs in humans, there is only a single FMO in yeast. Far more FMOs are found in plants, for example there are 29 in *Arabidopsis* (Suh et

al., 1996; Krueger and Williams, 2005; Schlaich, 2007). FMOs share several conserved sequence motifs that are also present in Bs3 (Figure 1.4 A, Krönauer et al., 2019). Two conserved GxGxxG motifs build a beta-strand-alpha helix-beta strand (called βαβ fold or Rossmann fold) supersecondary structure (Rao and Rossmann, 1973) and serve as FAD and NADPH binding sites. The WL(I/V)VATGENAE motif is conserved in plant FMOs (Exposito-Rodriguez et al., 2007). The further downstream located FxGxxxHxxx(Y/F) sequence, designated as FMO identifying motif, discriminates FMOs from another class of monooxygenases, the Baeyer-Villiger monooxygenases (BVMOs) that contain the slightly different FxGxxxHxxxW(P/D) motif (Fraaije et al., 2002). The F/LATGY motif near the C-terminus is described to be common in N-hydroxylating enzymes (Stehr et al., 1998) and possibly serves as linker in between the NADPH domain and the active site (2010). Within the family of FMOs, Bs3 surprisingly shows highest homology to YUCCA FMOs, an enzyme family which produces auxin in plants (Zhao, 2010).

1.5 Structure and Function of FMOs

1.5.1 YUCCAs produce the plant hormone auxin

Auxins are a class of essential growth hormones in plants. YUCCAs (YUCs) are FMOs, which catalyse the rate limiting step in tryptophan dependent auxin biosynthesis, the oxidative decarboxylation of indole-pyruvate (IPA) to indole-3-acetic acid (IAA, Figure 1.2, Dai et al., 2013) . IAA is the major form of auxin in plants and is essential for many developmental processes (Normanly et al., 2004). In adult plants, high auxin levels cause downward curled and epinastic leaves, a phenotype which in *Arabidopsis*, resembles the appearance of yucca plants (*Agave* sp.) and led to the designation of this enzyme family (Zhao et al., 2001). The first identified member of the YUC family was discovered in an activation tagging screen in *Arabidopsis*, in which the isolated YUC overexpressing mutant seedlings showed long hypocotyls and internodes (Weigel et al., 2000). Most plants contain several members of the YUC family, and all of the eleven YUCs in *Arabidopsis* produce auxin (Cheng et al., 2006, 2007; Lee et al., 2012; Ishida et al., 2016; Muller-Moule et al., 2016). Due to this high level of redundancy, single gene knockouts usually do not cause severe phenotypes in

Arabidopsis. However, in other plants like rice, which has at least seven YUCs, the knock down of a single gene can be sufficient to cause abnormal phenotypes (Yamamoto et al., 2007). In general, the large number of YUC genes allows for a high degree of temporal and spatial control of gene expression and subsequent production of auxin.

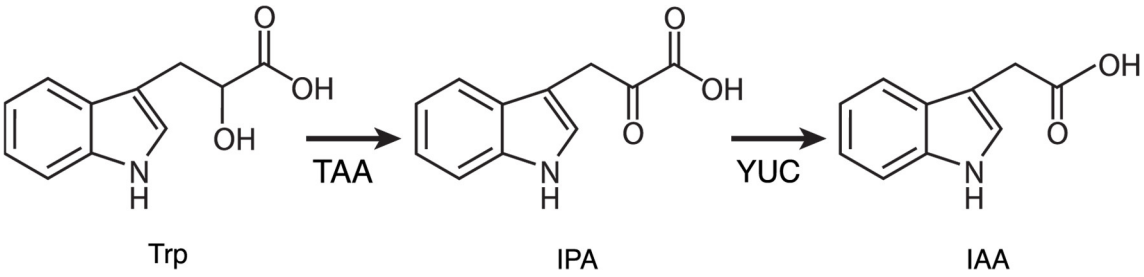

Figure 1.3: Tryptophan dependent auxin biosynthesis. In the first step, tryptophan (Trp) is converted into indole-pyruvic acid (IPA) by tryptophan aminotransferase (TAA). YUCCA enzymes (YUC) subsequently convert IPA into indole-3-acetic acid (IAA).

1.5.2 The FMO enzymatic cycle

As the name implies, FMOs carry out monooxygenation reactions, which means that they transfer one atom of oxygen to a substrate. During the enzymatic cycle (Figure 1.4 B), the tightly bound FAD cofactor is reduced by NADPH and subsequently reacts with molecular oxygen. A stable C4a-(hydro)peroxyflavin (C4a) intermediate is built, which is assumed to be the predominant state of FMOs inside the cell in which they are able to react with a substrate. This state is often referred to a "cocked gun" (Krueger and Williams, 2005). In the event that a suitable substrate enters the active site, one atom of oxygen is transferred to the substrate and one atom of oxygen forms H_2O. Finally, $NADP^+$ is released. In a side reaction, breakdown of the C4a-intermediate can be observed without substrate oxygenation and $NADP^+$ and H_2O_2 are released. This consumption of NADPH without simultaneous substrate oxygenation is referred to as an "uncoupled" reaction or NADPH oxidase activity (Figure 1.4 B).

Typically, C4a-intermediates have a half-life ranging from a few seconds up to several minutes. The crystal structure of *Methylophaga* FMO reveals that binding of $NADP^+$ is crucial for stabilization of the C4a-intermediate and substrate oxygenation (Alfieri et al., 2008; Orru et al., 2010). Since the stability of the C4a-intermediate correlates with the percentage of uncoupling that leads

to production of H_2O_2, information about the characteristics of this reaction give valuable insights into enzymatic function. Due to the spectroscopic properties of FAD (Figure 1.4 C), the build-up and decay of the C4a-intermediate can be followed via stopped flow spectrometry (Beaty and Ballou, 1980). Similarly, the oxidation of NADPH can be observed via the decrease of absorption at 340 nm.

While the production of H_2O_2 via the uncoupling reaction was considered to be detrimental or at least wasteful in the past, it is now conceivable that H_2O_2 is probably produced as physiological signal. This assumption is supported by the observation that some FMOs produce high amounts of H_2O_2 also in the presence of substrate (Fiorentini et al., 2016).

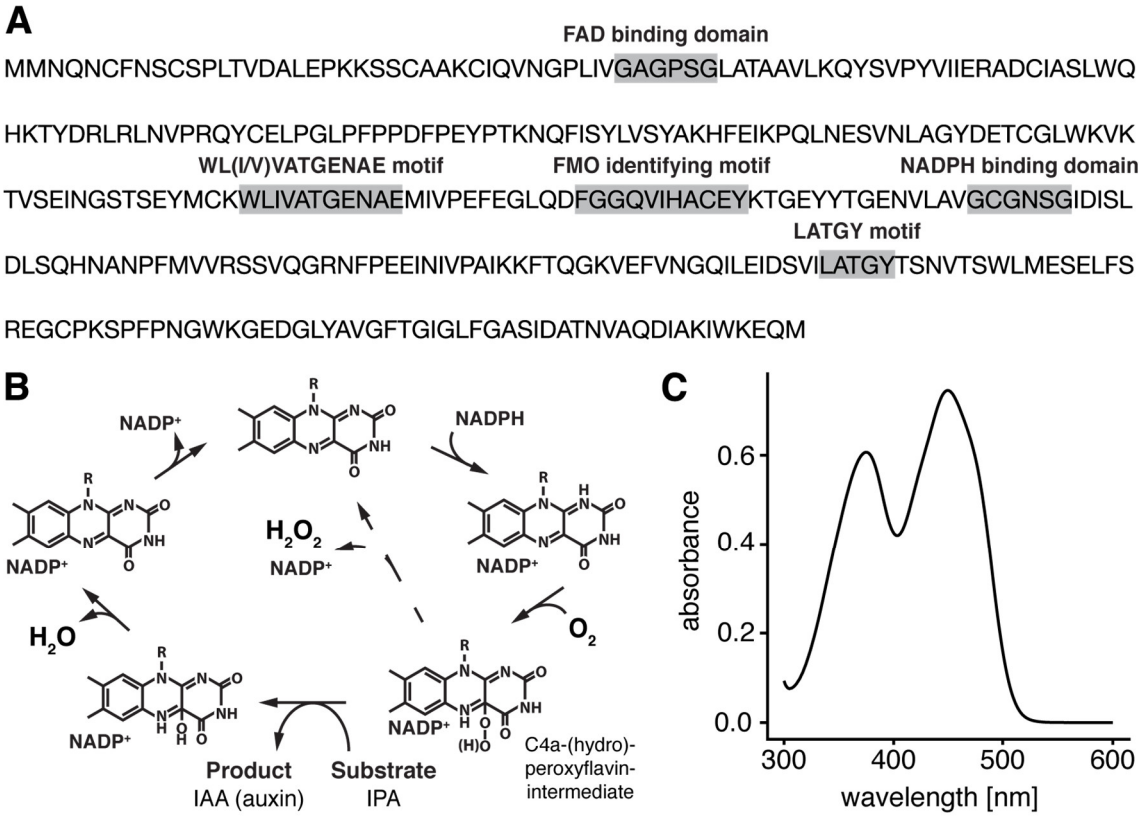

Figure 1.4: Bs3 contains features of FMOs. A) Amino acid sequence of Bs3. Domains that are conserved within the family of FMOs are highlighted in grey. B) The FMO catalytic cycle. The FAD cofactor is reduced by NADPH. Binding of oxygen results in a stable C4a-(hydro)peroxyflavin intermediate, that can react with any suitable substrate. In case of YUCs, IPA is converted to IAA. Finally, water and $NADP^+$ are released and the enzyme returns to its original state (Image modified from Alfieri et al., 2008. C) Absorption spectrum of FAD with characteristic peaks at 350 nm and 450 nm.

1.5.3 Structure and substrate specificity of FMOs

Human FMOs generally oxygenize a wide range of preferably amine- and sulfur-containing nucleophilic substances, thereby converting them into more polar, easily excretable substances (reviewed in Cashman and Zhang, 2006). Human FMOs show tissue and developmental specific expression patterns and distinct, but partially overlapping substrate specificities (Hines et al., 1994; Dolphin et al., 1996). The most prominent example of an FMO substrate is trimethylamine (TMA), a small tertiary amine (Figure 1.5) with a characteristic fishy odour. It is converted into trimethylamine-N-oxide (TMAO) by human FMO3 (hFMO3), the predominant FMO in human liver. The fact that other human FMOs, despite their broad substrate specificity, show only minor activity for this small tertiary amine (Lang et al., 1998) illustrates the complexity to predict a putative FMO substrate.

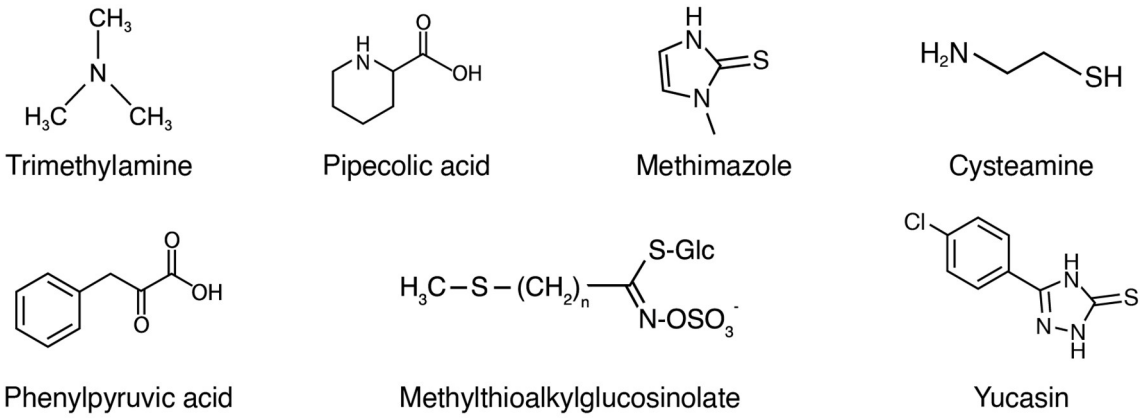

Figure 1.5 Common substrates of FMOs. Trimethylamine is a prominent substrate of hFMO3. Phenylpyruvic acid is a substrate of YUCs. Yucasin and methimazole can act as competitive inhibitors of FMOs. Pipecolic acid is the substrate of AtFMO1. Cysteamine is a substrate of yeast FMO. Methylthioalkylglucosinolates are substrates of GS-OX-like FMOs.

Most research on substrate specificity of FMOs is done by analysis of bacterial FMOs. The most similar candidate compared to Bs3 of which a crystal structure is available is TMA-oxidase of *Roseovarius nubinhibens* (*Rn*). This RnTMA-oxidase exists as a homodimer with bound FAD and NADPH cofactors (Bienert et al., 2017; Li et al., 2017; Fig. 1.6). Due to the low similarity, a model of Bs3 created with the RnTMA-oxidase as template using SWISS-MODEL (Figure 1.6 B, Waterhouse et al., 2018) can yield only limited information.

However, it illustrates the orientation of the FAD and NADPH cofactors and the active site within FMO proteins. The broad substrate specificity of FMOs is based on the fact that activation of oxygen occurs without binding of a substrate. The energy required for oxygenation reaction is inherent to the C4a-intermediate and any metabolite, that is able to access the active site can be oxygenized (Poulsen and Ziegler, 1995). However, the FAD cofactor is usually located in the interior of the protein and the bound $NADP^+$ is co-localized in a way that the nicotinamide ring is in parallel orientation with the isoalloxazine moiety of the FAD (Alfieri et al., 2008; Li et al., 2017). Metabolites can be excluded from entering the active site because of their size or biochemical properties.

Substances that enter the active site usually build a series of transient interactions with numerous amino acid side chains, acting as gatekeepers on their way through the protein. Notably, it is possible that different molecules enter the protein via distinct channels (Gygli et al., 2017; Fürst et al., 2018). Therefore, it is contentious to what degree characteristics of these FMOs are transferrable to the plant FMOs and it remains an open question why plant FMOs show a much higher substrate specificity than human FMOs.

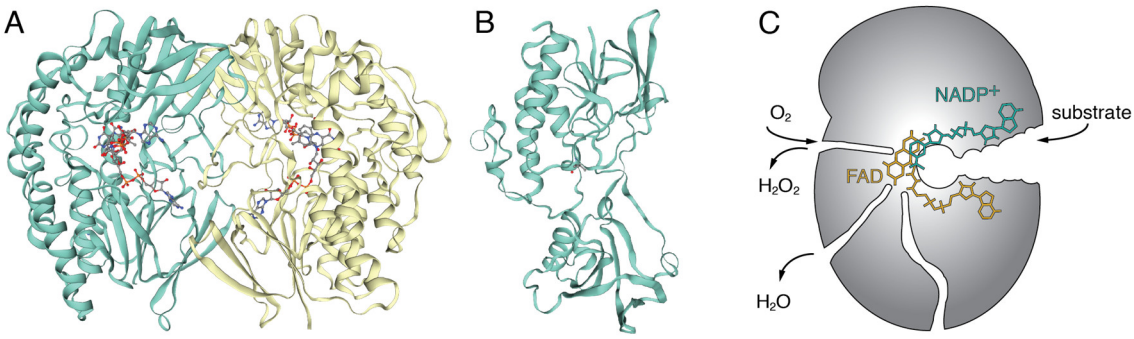

Figure 1.6 Substrate specificity of FMOs is dependent on accessibility of the active site. A) Structure of the TMA oxidase of *Roseovarius nubinhibens* (*Rn*TMA-oxidase). The Structure shows the homodimer with bound FAD and NADPH cofactors as ball-and-stick model. The monomers are coloured in yellow and turquoise, respectively. B) *Rn*TMA-oxidase based homology model of Bs3 aa 33 – 337. Models were created with the SWISS Model workspace. (Waterhouse et al., 2018) C) Scheme of an FMO with bound cofactors. The FAD cofactor (yellow) is located inside the protein. NADPH (blue) and metabolites access the enzyme via different routes, depending on their biochemical properties. (Modified from Romero et al., 2018).

1.6 Aims of this work

The major aim of this work was to get further insights into the molecular mechanism of how Bs3 triggers HR.

In experiments prior to this work, the *Bs3 R* gene had been cloned and its sequence similarity to the YUC family of FMOs was obvious (Römer et al., 2007). Moreover, an effect of Bs3 on yeast growth had been discovered (Römer, Piprek and von Roepenack-Lahaye, unpublished) and extensive analysis of Bs3 mutants revealed functional and non-functional Bs3-derivatives (Piprek unpublished, Strauß, 2008). Experiments with the aim of finding putative signal components of the Bs3 triggered HR, like the screening of a pepper cDNA library (Jaenecke, 2011) and a mutant yeast library (Piprek, unpublished) had not been successful. Despite these preceding efforts, the putative enzymatic function of Bs3 was not yet confirmed and the events that follow *Bs3* activation and finally lead to cell death remained elusive.

The first aim of this study was to analyse the structure-function relationship of Bs3 compared to YUCs and to investigate why the two proteins, despite their close homology, induce such a distinct phenotype *in planta*.

The second aim was to establish a protocol for the expression and purification of the Bs3 protein with the intention to study its biochemical properties. In this regard, the putative FMO function and the potential effects of H_2O_2 production were of particular interest.

The results of our first experiments finally renewed the desire to identify metabolites and signalling pathway components that are required for the induction of Bs3 HR.

2 Results

2.1 Comparison of Bs3 with its nearest homolog AtYUC8

Chapter 2.1 comprises the manuscript "**Cell Death Triggered by the YUCCA-like Bs3 Protein Coincides with Accumulation of Salicylic Acid and Pipecolic Acid But Not of Indole-3-Acetic Acid**"

Christina Krönauer, Joachim Kilian, Tina Strauß, Mark Stahl, Thomas Lahaye
Plant Physiology Jul 2019, 180 (3) 1647-1659; DOI: 10.1104/pp.18.01576

Christina Krönauer (1st author) performed the experiments, analysed the data, created all the figures and wrote the manuscript. **Joachim Kilian** and **Mark Stahl** (2nd and 4th author) conducted the mass spectrometry measurements of auxin and salicylic acid. **Tina Strauß** (3th author) created the Bs3 mutants derivatives via error prone PCR. **Thomas Lahaye** (corresponding author) conceived the original idea, supervised the project and wrote the manuscript.

2.1.1 YUC manuscript

Cell Death Triggered by the YUCCA-like Bs3 Protein Coincides with Accumulation of Salicylic Acid and Pipecolic Acid But Not of Indole-3-Acetic Acid[1]

Christina Krönauer,[a,2] Joachim Kilian,[a] Tina Strauß,[b,c] Mark Stahl,[a] and Thomas Lahaye[a,c,3,4]

[a]Center for Plant Molecular Biology, Eberhard-Karls-University Tuebingen, Tuebingen 72076, Germany
[b]Integrated Plant Genetics, Inc., Gainesville, Florida 32653
[c]Genetics, Faculty of Biology, Ludwig-Maximilians-University, D-82152 Munich Martinsried, Germany

ORCID IDs: 0000-0002-3172-5149 (C.K.); 0000-0001-5711-3688 (J.K.); 0000-0002-5834-2527 (T.S.); 0000-0002-1139-4178 (M.S.); 0000-0001-5257-336X (T.L.).

The pepper (*Capsicum annuum*) resistance gene *bacterial spot3* (*Bs3*) is transcriptionally activated by the matching *Xanthomonas euvesicatoria* transcription-activator–like effector (TALE) AvrBs3. AvrBs3-induced *Bs3* expression triggers a rapid and local cell death reaction, the hypersensitive response (HR). Bs3 is most closely related to plant flavin monooxygenases of the YUCCA (YUC) family, which catalyze the final step in auxin biosynthesis. Targeted mutagenesis of predicted NADPH- and FAD-cofactor sites resulted in Bs3 derivatives that no longer trigger HR, thereby suggesting that the enzymatic activity of Bs3 is crucial to Bs3-triggered HR. Domain swap experiments between pepper *Bs3* and Arabidopsis (*Arabidopsis thaliana*) *YUC8* uncovered functionally exchangeable and functionally distinct regions in both proteins, which is in agreement with a model whereby *Bs3* evolved from an ancestral *YUC* gene. Mass spectrometric measurements revealed that expression of *YUC*s, but not expression of *Bs3*, coincides with an increase in auxin levels, suggesting that Bs3 and YUCs, despite their sequence similarity, catalyze distinct enzymatic reactions. Finally, we found that expression of *Bs3* coincides with increased levels of the salicylic acid and pipecolic acid, two compounds that are involved in systemic acquired resistance.

Analysis of plant immune reactions triggered by transcription-activator–like effectors (TALEs) from the bacterial genus *Xanthomonas* uncovered a mechanistically novel plant resistance (*R*) gene class, whereby TALEs bind to corresponding effector binding elements within *R* gene promoters. Upon binding, they activate transcription and translation of the downstream encoded R protein (Boch et al., 2014). In such TALE-activated *R* genes, the encoded R protein is not involved in effector recognition but only in the execution of the plant immune reaction. Accordingly, these R proteins have been designated executors (Boch et al., 2014; Zhang et al., 2015). Conceptually, TALE-specific *R* genes are two-component systems, consisting of a pathogen-inducible promoter and a downstream encoded immune executor protein. Such modular systems are more amenable to engineering approaches, when compared to other systems, where effector recognition and defense execution are functionally combined in one protein, as is the case for the most prevalent class of native plant R proteins, the nucleotide-binding Leu-rich repeat (NLR)-type plant R proteins.

Engineering of plant *R* genes through rational design relies on well-characterized functional modules. TALE-inducible plant *R* promoters are well understood, which allows for the design of *R* promoters that are capable of recognizing multiple TALEs instead of the single-TALE recognition of native *R* promoters (Hummel et al., 2012; Strauß et al., 2012; Shantharaj et al., 2017). In contrast to our detailed understanding of TALE-specific *R* promoters, the molecular basis of executor R protein triggered defense reactions remains mostly obscure. For example, the functionality of an executor R protein may be restricted to the *R*-gene donor or closely related plant species, as is the case for plant NLR proteins (Tai et al., 1999). The lack of knowledge on the mechanistic principles of executor proteins substantially limits their application in rationalized design approaches. Thus, elucidation of the molecular mechanisms of executor R proteins is needed to eliminate current constraints in the deployment of executor R proteins in rationalized design approaches of synthetic plant *R* genes.

[1]This work was supported by the Deutsche Forschungsgemeinschaft (SFB 1101 project D08 to T.L. and DFG grant no. LA1338/10-1). [2]Present address: Department of Molecular Biology and Genetics, Aarhus University, 8000 Aarhus C, Denmark.

[3]Author for contact: thomas.lahaye@zmbp.uni-tuebingen.de.

[4]Senior author.

The author responsible for distribution of materials integral to the findings presented in this article in accordance with the policy described in the Instructions for Authors (www.plantphysiol.org) is: Thomas Lahaye (thomas.lahaye@zmbp.uni-tuebingen.de).

C.K. performed and analyzed the experiments and wrote the article with contributions from all authors; J.K. and M.S. performed mass spectrometry; T.S. planned and performed the epPCR mutagenesis;

The pepper (*Capsicum annuum*) *R* gene *Bs3* mediates the recognition of the *Xanthomonas euvesicatoria* effector protein AvrBs3. A major aim of our work is to clarify how the executor R protein Bs3 triggers plant defense and whether Bs3 makes use of immune signaling components employed by other plant R proteins.

Pepper Bs3 has no sequence homology to any other known plant R protein but shows striking similarity to the family of flavin monooxygenases (FMOs). FMOs are found in bacteria, yeast, mammals, and plants, where they carry out an FAD- and NADPH-dependent oxidation reaction (van Berkel et al., 2006). Besides an FAD- and NADPH-binding site with the conserved sequence motif GxGxxG, plant FMOs comprise several other conserved motifs, including the FMO identifying motif (FxGxxxHxxxY), the L/FATGY motif, and the WL(I/V)VATGENAE motif, which is highly conserved in plant FMOs (Exposito-Rodriguez et al., 2007; Schlaich, 2007). FMOs fulfill a plethora of different functions like detoxification of xenobiotics in mammals and redox homeostasis in yeast (*Saccharomyces cerevisiae*; Suh et al., 1999; Krueger and Williams, 2005). In plants, there are three clades of FMOs described so far that fulfill different functions (Schlaich, 2007). Arabidopsis (*Arabidopsis thaliana*) FMO1 is the only member of clade I and catalyzes N-hydroxylation of pipecolic acid (Pip) to N-hydroxypipecolic acid, which is required for induction of systemic acquired resistance (SAR; Bernsdorff et al., 2016; Chen et al., 2018; Hartmann et al., 2018). Arabidopsis clade III FMOs comprise seven members of the glucosinolate *S*-oxygenase like FMOs ($FMO_{GS\text{-}OX\ 1\text{-}7}$) that catalyze the conversion of methylthioalkyl glucosinolates into methylsulfinylalkyl glucosinolates, a group of compounds that play a role in defense to pathogens and pests (Hansen et al., 2007; Kong et al., 2016).

Pepper Bs3 is most related to clade II FMOs, also known as YUCCA (YUC) proteins. YUCs catalyze the conversion of indole-pyruvic acid (IPA) into indole-3-acetic acid (IAA) via oxidative decarboxylation (Dai et al., 2013). IAA is the most abundant auxin in plants and a major regulator of plant growth and development. Accordingly, constitutive in planta expression of YUCs causes high auxin phenotypes like long hypocotyls and epinastic leaves (Zhao et al., 2001).

The Arabidopsis genome encodes 11 YUC proteins (AtYUCs), which are assumed to catalyze the same enzymatic reaction. Yet, differences in the promoters of *AtYUC*s facilitate restricted expression of YUCs in certain cell types or defined developmental stages (Cheng et al., 2007). Phylogenetically, AtYUCs can be divided into four distinct groups. AtYUCs originating from the same group typically share similar features like tissue-specific expression in either the root or the shoot. Furthermore, AtYUCs within distinct phylogenetic groups often have distinct subcellular localizations, which are generally mediated by the presence or absence of a transmembrane domain (TMD) that anchors YUCs to the endoplasmic reticulum (ER; Cheng et al., 2006; Poulet and Kriechbaumer, 2017).

In this study we compared pepper Bs3 to structurally related YUCs from pepper and Arabidopsis. A sequence-based comparison of Bs3 and YUCs shows that some sequence stretches are highly conserved while others show marked differences. Gene shuffling experiments with pepper *Bs3* and *AtYUC8* from Arabidopsis uncovered sequence stretches that are functionally exchangeable between both proteins, possibly suggesting that *Bs3* evolved from an ancestral *YUC* gene. Constitutive in planta expression of pepper *Bs3* and related *YUC* genes revealed that only *Bs3* activates hypersensitive response (HR) while all other pepper YUCs cause high auxin phenotypes. Given the high structural relatedness of Bs3 and YUC proteins, we hypothesized that both enzymes catalyze the same enzymatic reaction and that the Bs3-triggered HR would be simply the consequence of high auxin levels produced by Bs3. However, mass spectrometry (MS) analysis revealed that in planta expression of *YUC* genes, but not of *Bs3*, coincides with high auxin levels. Reciprocally, expression of Bs3, but not of YUCs, coincides with increased levels of the immunity-related phytohormone salicylic acid (SA) as well as with increased levels of Pip, a metabolite that is involved in SAR (Shan and He, 2018). The observation that Bs3 HR coincides with accumulation of defense-related metabolites is not in agreement with a model where Bs3 triggers cell death simply by accumulation of a toxic compound but suggests that Bs3 triggers cell death via a signaling cascade.

RESULTS

Comparison of Bs3 and YUCs Reveals Pronounced Differences within their N-Termini and a Bs3-Specific 70 Amino Acid Deletion with Unknown Functional Impact

Pepper Bs3 is a structurally unique R protein that shows no similarity to any known plant R protein (Römer et al., 2007). To identify Arabidopsis orthologs, the 342-amino acid–long Bs3 sequence was used for a nonredundant similarity search against the Arabidopsis database using BLASTp (Altschul et al., 1990). All sequences with significant similarity ($S \geq 100$, $E \leq 10^{220}$) to Bs3 are members of the YUC family (AtYUC1-AtYUC11). AtYUC8 is 64% identical to Bs3 and thus is most closely related to Bs3 within the AtYUC proteins (Fig. 1). The sequence alignment between Bs3 and AtYUCs uncovers three major differences between Bs3 and YUCs, which could cause their functional disparity (Supplemental Fig. S1). First, there is an ;70-amino acid–long sequence element that is conserved in YUCs (matching to residues 217–295 in AtYUC1) but absent from Bs3. Notably, this 70-amino acid region does not contain any motifs of known function and thus its biological function remains unclear. Second, the N-terminus of Bs3 shows little conservation to the

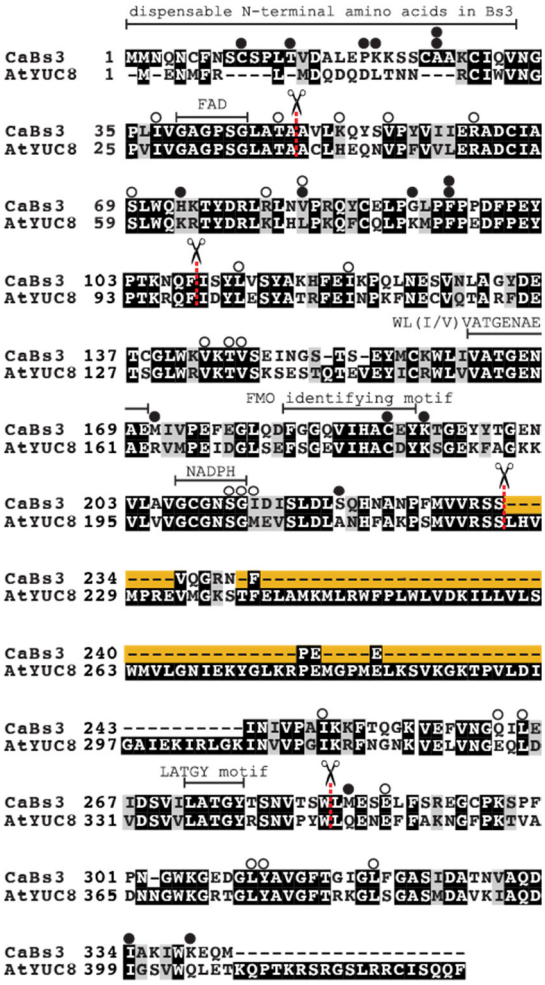

Figure 1. Pepper Bs3 (CaBs3) and AtYUC proteins are highly related but also display characteristic differences. Sequence alignment of CaBs3 and AtYUC8 proteins. The ~70-amino acid sequence that is present in all YUC proteins including AtYUC8 but absent from Bs3 is highlighted by yellow background. The conserved FAD and NADPH binding sites (GxGxxG) as well as the conserved WL(I/V)VATGENAE, FMO-identifying, and LATGY motifs are designated accordingly. Scissors mark the borders used for Golden-Gate–based assembly of the Bs3-AtYUC8 chimeras (see Fig. 6). Open and solid circles mark Bs3 residues that were mutated by error-prone PCR (epPCR) and did or did not cause a loss of function, respectively (see Fig. 3). Alignment was done with CLC Main Workbench (QIAGEN). Gaps in the alignment are indicated with dashes. Identical amino acids (black background) and similar amino acids (gray background) were defined using BoxShade (https://embnet.vital-it.ch/software/BOX_form.html).

N-termini of AtYUC proteins. Third, there are a number of amino acid residues across the aligned proteins that are conserved in YUCs but differ with respect to Bs3 (Supplemental Fig. S1). Apart from YUCs, other plant FMOs show only minor similarity to Bs3. For example, Bs3 and Arabidopsis FMO1 share only 26% identity and Bs3 and Arabidopsis GS-OX like FMOs ~23% (Supplemental Fig. S2). In summary, Bs3 and AtYUCs have high overall sequence homology but show clear differences at the amino acid level, which could possibly be the reason for the functional differences between Bs3 and YUCs.

Constitutive In Planta Expression of Bs3-Related Pepper YUCs Induces Leaf Curling Indicative of Auxin Production

Previous studies have shown that the vast majority of pepper species and at least one *Capsicum chinense* genotype encode a functional *Bs3* coding sequence (CDS; Römer et al., 2009). We inspected the recently published *Capsicum baccatum* genome (Kim et al., 2017) and uncovered a CDS that translates into a protein that is highly related to the pepper and *C. chinense* Bs3 proteins (Supplemental Fig. S3). Translated BLAST searches in other sequenced plant genomes did not uncover any putative proteins that resemble the characteristic domain structure of Bs3, which makes it clearly distinct from YUC proteins. Thus, Bs3-like proteins seem to occur exclusively in *Capsicum* species.

The biological and enzymatic function of pepper YUCs (CaYUCs) has not been studied thus far. Given the high similarity of Bs3 and YUCs, we wanted to clarify if the CaYUCs that are most similar to Bs3 would either trigger HR or produce auxin. To find YUCs in pepper, a BLASTp search against the pepper var Zunla genome (v2.0) was performed (http://peppersequence.genomics.cn/pa-ge/species/index.jsp). Nine sequences in total with alignment scores ~ 100 were found, whereof one was Bs3. We constructed a phylogenetic tree (Supplemental Fig. S4) based on the alignment of all amino acid sequences of Arabidopsis YUCs, pepper Bs3, and pepper YUCs. CaYUCs were numbered in ascending order based on the group and position of AtYUCs in the phylogenetic tree (Supplemental Fig. S4). Similar to the 11 AtYUCs (Poulet and Kriechbaumer, 2017), the eight CaYUCs cluster into four clades. CaYUC1 groups with AtYUC1 and AtYUC4, CaYUC2 groups with AtYUC2, and AtYUC6 and CaYUC7-8 cluster with AtYUC10-11. Bs3 forms one monophyletic group together with CaYUC3-6 and AtYUC3,5,7-9 (Supplemental Fig. S4). To study the in planta function of the four Bs3-related CaYUC3-6 proteins, the corresponding CDSs were PCR-amplified from genomic DNA (Supplemental Table S1). PCR products were cloned into a transfer (T-DNA) vector downstream of the constitutively active Cauliflower mosaic virus 35S (*35S*) promoter. Expression of the four distinct *CaYUC3-6* in *Nicotiana benthamiana* leaves via *Agrobacterium tumefaciens*-mediated transient transformation (agroinfiltration) caused, in all cases, a leaf curling phenotype, which is indicative of the production of auxin (Supplemental Fig. S5). Thus, Bs3 is the only YUC-like protein encoded in the pepper genome that triggers HR and not leaf curling.

Mutations in FAD or NADPH Binding Sites Abolish Bs3-Mediated HR

Bs3 as well as YUCs belong to the family of FMOs that generally contain two conserved GxGxxG motifs, which are predicted to serve as binding sites for FAD and NADPH (Supplemental Fig. S1). To clarify if Bs3-triggered HR is dependent on the integrity of both nucleotide-binding sequences, we created six Bs3 mutant derivatives. In each of these mutants, a single Gly of the predicted FAD and NADPH motifs was changed to Ala. The six distinct *Bs3* mutant derivatives were each agroinfiltrated along with a *35S*-promoter-driven *avrBs3* gene into *N. benthamiana* leaves. The Bs3 wild type triggered HR, but none of the Bs3 derivatives with mutations in the predicted FAD and NADPH binding site did (Fig. 2A). This suggests that activation of HR is dependent on cofactor binding and therefore enzymatic function of Bs3.

Pathogen-induced HR typically coincides with an increase in reactive oxygen species (ROS). To see if the generated Bs3 derivatives are null- or partial loss-of-function mutants, we conducted 3,39-diaminobenzidine (DAB) staining to visualize accumulation of ROS. To do so, *35S*-promoter–driven *Bs3* and *Bs3*-derivatives were agroinfiltrated into *N. benthamiana* leaves and DAB staining was carried out at 24, 48, and 72 h post infiltration (hpi). Leaf discs containing the Bs3 wild-type protein showed increased brown staining, indicative of ROS accumulation, at 48 and 72 hpi (Fig. 2B). Notably, DAB staining in leaves containing the Bs3 mutants $Bs3_{G44A}$, $Bs3_{G207A}$, and $Bs3_{G209A}$ was delayed, and was visible only at 72 hpi. The staining in these Bs3 mutants was also less intense than for the Bs3 wild-type protein, but clearly stronger than the staining observed for $Bs3_{G39A}$ and $Bs3_{G41A}$ (Fig. 2B). In summary, these data indicate that the $Bs3_{G44A}$, $Bs3_{G207A}$, and $Bs3_{G209A}$ mutants are not null-mutants but partial loss-of-function mutants that induce minor ROS accumulation and do not trigger HR.

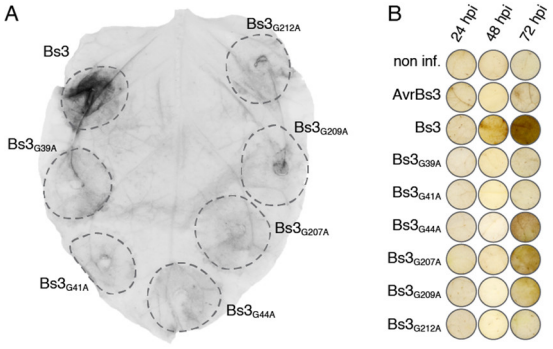

Figure 2. Mutations with conserved glycines of the Bs3 FAD- and NADPH-binding sites abolish the Bs3-triggered HR. The depicted *Bs3* derivatives were expressed in *N. benthamiana* leaves. *Agrobacterium* strains carrying the indicated gene constructs under transcriptional control of the pepper *Bs3* promoter were coinfiltrated with *Agrobacterium* strains carrying the *Xanthomonas* TAL effector gene *avrBs3* under control of the constitutive cauliflower mosaic virus *35S* promoter. A, Four d post infiltration, leaves were harvested and cleared with ethanol to visualize HR (dark). Dashed lines mark the infiltrated leaf areas. B, At 24, 48, and 72 hpi, leaf discs were excised and incubated in DAB solution. Brown color indicates accumulation of hydrogen peroxide.

Error-Prone PCR Mutagenesis Uncovers Residues that Are Crucial to Bs3 Function

To find residues that, apart from the FAD and NADPH binding sites, are indispensable for Bs3 function, we conducted PCR-based random mutagenesis. To do so, the *Bs3* CDS was amplified by epPCR, and products were cloned into a T-DNA vector downstream of the *Bs3* promoter. DNA sequencing identified 154 *Bs3* mutants. *Bs3* derivatives with (1) silent mutations, (2) more than one mutation resulting in an amino acid exchange, or (3) deletions were excluded from further analysis. Thirty-nine *Bs3* derivatives encoding proteins with a single amino acid exchange were studied at the functional level. not affect function, seems nonrandom, suggesting that different protein regions seem to differ in their tolerance to amino acid changes. For example, none of the six distinct amino acid changes within the far N-terminal region of Bs3 impacted the Bs3-triggered HR, possibly suggesting the N-terminal region is dispensable for Bs3 function (Fig. 3). Apart from this N-terminal region, mutations that abolish Bs3 HR are found across all regions of the Bs3 protein. Interestingly, we found one position in which a mutation encoding the change of Val to Glu (V83E) but not to Ala (V83A) causes loss of function (Supplemental Fig. S6). This random mutagenesis thus demonstrates that mutations aside from the two nucleotide-binding–sequence encoding regions can impair functionality of Bs3, most likely by causing an overall change of its protein structure.

The 32 N-Terminal Amino Acids of Bs3 Can Be Deleted without Loss of Function

The sequence alignment of Bs3 and YUCs shows that the N-terminal 30 amino acids of Bs3 have no homology to the N-terminal region of any of the YUC proteins (Supplemental Fig. S1). These residues within the Bs3 N-terminus might cause functional differences between the Bs3 and YUC proteins. However, our functional analysis of the six epPCR-generated Bs3-derivatives with amino acid changes in the Bs3 N-terminus did not affect Bs3 HR (Fig. 3; Supplemental Fig. S6), possi- bly suggesting that the Bs3 N-terminus is functionally dispensable. To clarify the functional relevance of Bs3 N-terminal amino acids, we generated a set of dele- tion derivatives and tested their functionality by agroinfiltration of *N. benthamiana* leaves (Fig. 4). These studies

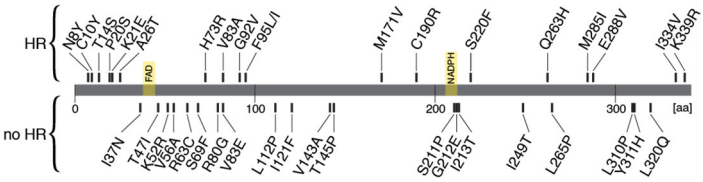

Figure 3. EpPCR uncovers residues that are crucial to Bs3 function. The 342-amino acid–long Bs3 protein is depicted as a horizontal gray bar. FAD and NADPH binding sites are designated and highlighted by yellow background. Point mutations that do not or do impair HR are displayed above and below the bar, respectively.

showed that 32 N-terminal amino acids (including V32) of the Bs3 protein can be deleted without affecting the Bs3-triggered HR. The shortest functional Bs3 derivative ($Bs3_{DN32}$) contains only seven amino acids in between the first Met and the FAD binding site located at position 39–44 in the Bs3 wild-type protein (Fig. 1).

Deletion of a ~70-Amino Acid Stretch Present in YUCs But Absent from Bs3 Does Not Yield HR-Inducing YUC-Derivatives

A characteristic feature of Bs3 upon comparison to YUCs is the absence of a ~70-amino acid stretch that is present in all YUCs (Supplemental Fig. S1). Careful inspection of this region uncovers nine amino acids in Bs3 (VQGRNFPEE) that do not align unequivocally to any region within the ~70-amino acid sequence present in YUCs. One plausible scenario could be that this sequence polymorphism causes functional differences between Bs3 and YUC proteins. To test this hypothesis, we initiated reciprocal domain swaps between Bs3 and AtYUC8 (Fig. 5A) and tested if functional specificity of these chimeras, HR versus leaf curling, would be dictated by the transferred gene segments. We created one Bs3-derived chimera (Bs31aa), where the *Bs3*-derived gene segment encoding nine amino acids was replaced by the corresponding *AtYUC8*-derived gene segment encoding 81 amino acids. Similarly, we replaced the *AtYUC8* gene segment encoding an 81-amino acid sequence with the *Bs3*-derived gene segment encoding nine amino acids (AtYUC8Daa). Agroinfiltration of *N. benthamiana* leaves revealed that the two chimeras induced neither HR nor leaf curling (Fig. 5, B and C). Together, these results suggest that the functional differences between AtYUC8 and Bs3 are not exclusively due to the amino acids that are absent from Bs3.

Gene Shuffling of *Bs3* and *AtYUC8* Reveals Functionally Exchangeable Sequence Segments

Mutational studies typically aim to confirm the functional relevance of protein residues that, due to their positioning in a protein structure, are assumed to be of particular importance. The epPCR of Bs3 uncovered numerous residues that, when being replaced by another amino acid, resulted in Bs3 derivatives that no longer trigger HR (Fig. 3). It is conceivable that these random amino acid replacements often cause structural changes, and thus typically do not uncover functional key residues of a protein. To overcome this limitation of the epPCR approach, we decided to create chimeric proteins based on Bs3 and AtYUC8 sequences to further study the structure–function relationship of these two proteins. In contrast to the epPCR approach, where codons are exchanged regardless of the properties of the encoded amino acids, in chimeras, gene segments are substituted by gene segments derived from genes encoding highly related, functional proteins. Given the relatedness of Bs3 and AtYUC8, we would expect that the functional properties of the chimeras are typically dictated by the functionally distinct sections of Bs3 and AtYUC proteins. Moreover, this approach should enable us to identify amino acid polymorphisms between Bs3 and YUCs that do not translate into functional differences.

To carry out Golden-Gate shuffling, the *AtYUC8* and the *Bs3* CDSs were split into five parts, labeled with Roman numerals as parts I–V (Fig. 6, A and B). Split points were chosen according to intron–exon boundaries of *Bs3* and sequence similarity in between Bs3 and YUC8. The five gene segments were amplified, cloned, and sequence-validated. Subsequently all possible 32 segment combinations (Bs3, chimeras #2–#31, and AtYUC8) were assembled via Golden-Gate cloning. The chimeric CDSs were cloned in a T-DNA vector downstream of the *35S* promoter and translationally fused to *GFP* at their 39 end. Functionality of these

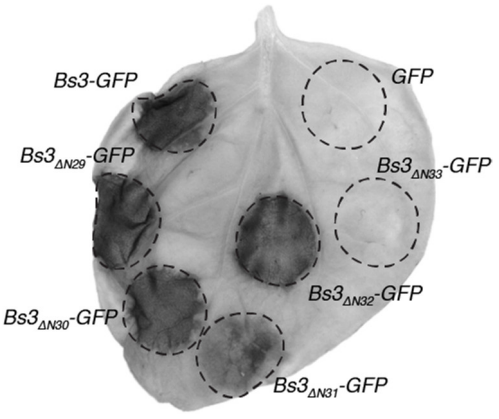

Figure 4. The first 32 amino acids of the Bs3 N terminus are functionally dispensable. Depicted N-terminal deletion derivatives of Bs3 were expressed in *N. benthamiana* via *Agrobacterium*-mediated transient transformation. Four d post infiltration, leaves were harvested and cleared with ethanol to visualize HR (dark area). Dashed lines mark the infiltrated area.

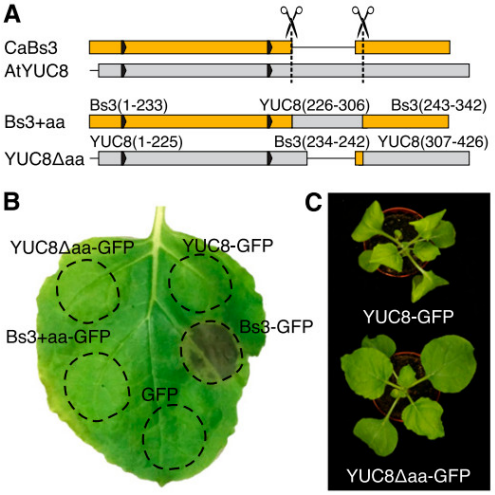

Figure 5. Reciprocal domain swaps suggest that a 70-amino acid sequence present in YUCs and absent from Bs3 does not on its own define functional specificity of Bs3 and YUC proteins. A, Horizontal yellow and gray bars indicate the pepper Bs3 (CaBs3) and AtYUC8 protein sequences, respectively. Black arrowheads indicate the predicted FAD- and NADPH binding sites, respectively. Designations above the chimeric proteins (Bs31aa and AtYUC8Daa) indicate the Bs3- and AtYUC8-derived residues encoding the given chimeras. B and C, Constructs depicted in (A) were expressed in *N. benthamiana* leaves under control of the *35S* promoter via *Agrobacterium*-mediated transient transformation. Pictures of leaves showing HR were taken 4 d post infiltration and pictures of plants with curly leaves were taken 2 d post infiltration. Dashed lines mark the infiltrated leaf area.

chimeras was tested via agroinfiltration in *N. benthamiana* leaves. The assembly of chimeric genes also resulted in reconstitution of the *Bs3* and *AtYUC8* genes. The reconstituted *Bs3* and *AtYUC8* genes triggered HR and leaf curling phenotypes, respectively, thus confirming that our Golden-Gate–based assembly approach can yield functional gene constructs (Fig. 6C). Six out of 30 chimeras were functional and showed either a leaf curling or an HR phenotype. Three chimeras (#2, #4, and #6), which contained *AtYUC8*-derived gene segment I, III, or V and were otherwise composed of *Bs3*-derived gene segments only, triggered HR (Fig. 6, C and D; Supplemental Fig. S7). Reciprocally, three chimeras (#20, #27, and #28) that contained the *Bs3*-derived parts I, V and I + V but were otherwise composed of *AtYUC8*-derived segments only, caused a leaf curling phenotype (Fig. 6C). Thus, Bs3 as well as AtYUC8 maintained their functionality when either the N-terminal part I or the C-terminal part V were exchanged. If part I and part V of *AtYUC8* together are replaced by the corresponding segments of *Bs3*, the resulting chimera #20 still causes leaf curling. Interestingly, however, the reciprocal chimera #10, in which part I and part V of *Bs3* are replaced by the corresponding segments of *AtYUC8*, does not trigger HR. Moreover, Bs3, but not AtYUC8, remains functional when only part III is replaced (chimeras #4 and #30, respectively; Fig. 6). Together, these observations suggest that gene segments I, III, and V encode functionally interchangeable domains of Bs3 and AtYUC8. Yet it is notable that most, but not all, of the changes function reciprocally. Because no mixed phenotypes were observed, we wondered if leaf curling and HR phenotypes are mutually exclusive. However, coexpression of 35S-driven *Bs3* and *AtYUC8* in *N. benthamiana* leaves shows that HR is induced to a similar extent in curly and control leaf areas and that leaf curling is not affected by expression of Bs3 (Supplemental Fig. S8).

Bs3 and AtYUC8 Show Different Subcellular Localization

Agroinfiltration of *35S*-promoter–driven T-DNA constructs encoding GFP-tagged fusion proteins shows that Bs3 and AtYUC8 differ in their subcellular localization. Bs3 is located in the cytoplasm and the nucleus whereas AtYUC8 is excluded from the nucleus (Fig. 7). To dissect their subcellular localization, the GFP-tagged chimeras were expressed in *N. benthamiana* and analyzed by confocal laser scanning microscopy (CLSM). We noted that all chimeras that contain part IV of AtYUC8 show no GFP fluorescence in the nucleus (Fig. 7, Supplemental Fig. S9). This includes chimera Bs31aa, in which the Bs3-specific nine amino acids are replaced by the corresponding 81-amino acid sequence of AtYUC8 (Fig. 5; Supplemental Fig. S10). To test our hypothesis that part IV of AtYUC8 determines nuclear exclusion, the corresponding gene segment was fused to GFP under transcriptional control of the *35S* promoter. Agroinfiltration in *N. benthamiana* leaves and subsequent CLSM indeed showed that this GFP fusion protein was excluded from the nucleus (Fig. 7). To clarify the localization of Bs3 and AtYUC8, we conducted colocalization analyses with an mCherry derivate containing the ER peptide targeting signal HDEL (mCherry-HDEL). The *35S* promoter-driven, GFP-tagged variants of Bs3, AtYUC8, AtYUC8-part IV, and a GFP control were agroinfiltrated in *N. benthamiana* together with a *35S*-promoter–driven mCherry-HDEL. Bs3-GFP showed a similar nuclear-cytoplasmatic localization as the GFP control (Supplemental Fig. S11). AtYUC8-partIV-GFP, AtYUC8-GFP, and mCherry-HDEL all showed a similar subcellular distribution and localized to the ER, but not the nucleus (Supplemental Fig. S11). These data suggest that the amino acid stretch composing part IV of AtYUC8 is sufficient for localization to the ER.

None of the chimeras that contain part IV of AtYUC8 triggered HR (Supplemental Fig. S7). This raises the question of whether either localization of Bs3 to the nucleus is important for HR activation or if AtYUC8 part IV is disturbing Bs3 protein conformation in a way that abolishes HR activation. To test whether the subcellular localization of Bs3 and AtYUC8 is crucial to their functionality, gene segments encoding either nuclear localization signal (NLS) or a nuclear export signal (NES) were fused to the 59 end of Bs3 and AtYUC8

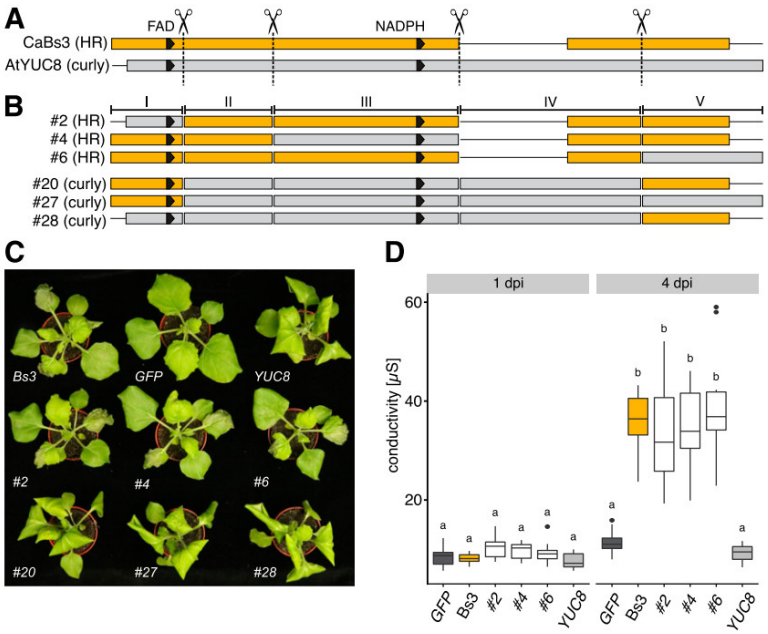

Figure 6. Golden-Gate–based gene shuffling uncovers protein regions that are functionally interchangeable between pepper Bs3 (CaBs3) and AtYUC8. A, Schematic depiction of CaBs3 (yellow horizontal bar) and AtYUC8 (gray horizontal bar) proteins. FAD and NADPH binding sites are depicted as black arrowheads. Gaps in the alignment are indicated as dashes. Scissors above dashed vertical lines indicate split points that were used for gene-shuffling. B, Schematic depiction of six functional CaBs3-AtYUC8 chimeras. Note, that all possible 30 chimeras were generated and functionally tested. The figure shows the composition of the six chimeras that either triggered HR (#2,#4, and #6) or induced a leaf curling phenotype (#20, #27, and #28). C, *Bs3*, *AtYUC8*, the six functional chimeras and *GFP* control were expressed in *N. benthamiana* leaves via *Agrobacterium*-mediated transient transformation. AtYUC8 and chimeras #20, #27, and #28 cause epinastic leaves. Bs3 and chimeras #2, #4, and #6 trigger HR. The picture was taken 4 d post infiltration. D, Ion leakage measurements. Indicated constructs were expressed in *N. benthamiana* via *Agrobacterium*-mediated transient transformation. One and 4 d post infiltration, leaf discs were harvested and incubated in ultrapure water. Conductivity was measured 20 hpi. Boxplots represent the values of 10 replicates. Different letters denote significant differences ($P = 0.05$, ANOVA with posthoc Tukey Honest Significant Difference test).

CDSs. Next, the *35S*-promoter–driven gene constructs were agroinfiltrated into *N. benthamiana* leaves, and GFP fluorescence was studied by CLSM. NLS-AtYUC8 and NES-AtYUC8 both show cytoplasmic fluorescence (Fig. 8A), which indicates that the NLS is not sufficient to reroute AtYUC8 quantitatively to the nucleus. Transient expression of *NES-YUC8* and *NLS-YUC8* in *N. benthamiana* caused a leaf curling phenotype, which shows that neither fusion of a NES nor of a NLS disturbs AtYUC8 function (Fig. 8C). NLS-Bs3 and NES-Bs3 produced predominantly the expected nuclear and cytoplasmic fluorescence, respectively, and both produced an HR. These data suggest that Bs3 triggers HR irrespective of whether it is localized in the nucleus or the cytoplasm (Fig. 8B).

IAA Levels Increase upon In Planta Expression of YUC8 But Not Bs3

YUC proteins catalyze the final step in auxin biosynthesis (Zhao, 2018). Given that the sequence of Bs3 is related to that of YUC proteins, we wondered if expression of Bs3 coincides with accumulation of auxin. To clarify if Bs3 catalyzes IAA synthesis, we agroinfiltrated the *35S*-promoter–driven T-DNA constructs *Bs3-GFP*, *AtYUC8-GFP*, or *GFP* in *N. benthamiana* and quantified IAA levels in leaf tissue by gas chromatography-mass spectrometry (GC-MS). We noted that leaves infiltrated with *A. tumefaciens* carrying *35S-AtYUC8-GFP* had elevated IAA concentrations immediately after infiltration (Supplemental Fig. S12), suggesting that *A. tumefaciens* strains containing *AtYUC8-GFP* produce auxin. To avoid expression of YUC protein in *A. tumefaciens*, we replaced the intron-less *AtYUC8* gene with the intron-containing *CaYUC3* gene. Overexpression of *CaYUC3* caused an increase of IAA levels that became apparent only at 24 hpi, correlating with the amount of protein detected (Fig. 9). By contrast, overexpression of Bs3 caused similar IAA levels as observed in plants expressing the GFP control (Fig. 9), suggesting that Bs3-triggered HR does not involve depletion or accumulation of IAA.

Bs3 Triggered Cell Death Coincides with Accumulation of SA

A hallmark of plant immune signaling is the accumulation of the phytohormone SA (Seyfferth and Tsuda,

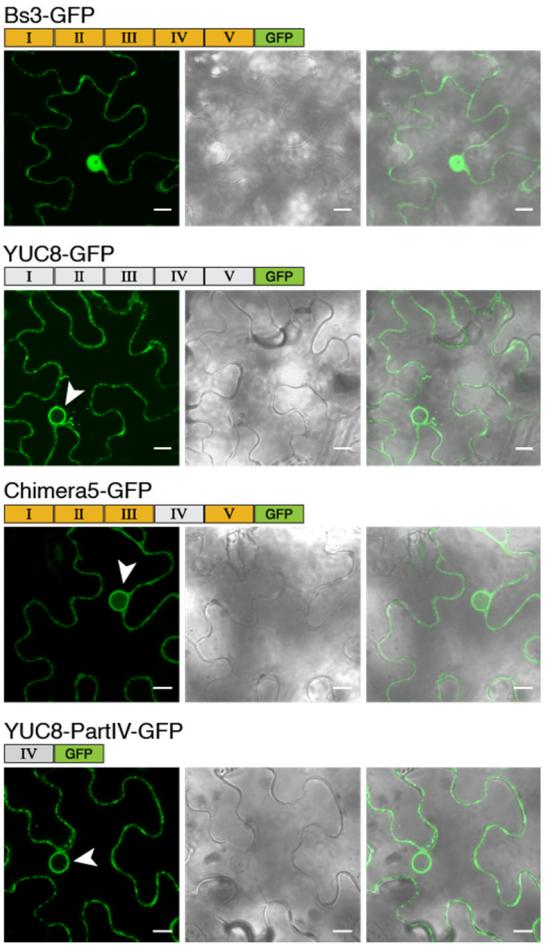

Figure 7. An amino acid stretch within AtYUC8 (L226–W347) determines nuclear exclusion. Bs3, AtYUC8, Chimera #5 and AtYUC8-PartIV were expressed as GFP fusions in *N. benthamiana* leaves via *Agrobacterium*-mediated transient transformation. The composition of each fusion protein is shown schematically above the microscopic pictures. The five parts are numbered with Roman numerals (see also Fig. 6B). Yellow and gray boxes represent Bs3- and AtYUC8-derived protein segments, respectively. Leaf discs for microscopy were collected 30 hpi. Pictures show GFP fluorescence (left), brightfield (center), and image overlay (right). White arrowheads point to nuclei that show no GFP fluorescence. Scale bar = 10 μm.

2014). To clarify if *Bs3* expression coincides with an increase in SA, we agroinfiltrated *N. benthamiana* leaves with *35S*-promoter–driven *Bs3-GFP*, *CaYUC3-GFP*, and *GFP*. Subsequently inoculated leaf tissue was harvested at different time points, and SA levels were quantified by GC-MS (Fig. 9). Although basal SA levels in leaves of *N. benthamiana* expressing the *GFP* control were low (<10 ng/g fresh weight [FW]), levels rose up to 1,500 ng/g FW in plants that expressed *Bs3*. No elevated SA levels were measured in plants that expressed *CaYUC3* (Fig. 9). During transient expression of *Bs3*, SA levels declined after 30–36 h, coinciding with the decline of Bs3 protein levels (Fig. 9). Given that *Bs3* expression coincides with increased SA levels, this suggests that Bs3 employs established immune signaling pathways to trigger HR.

Bs3-Triggered Cell Death Coincides with Accumulation of Pip

Pip is an immune regulatory metabolite in plants, and elevated Pip levels induce AtFMO1-dependent SAR in plants (Návarová et al., 2012; Bernsdorff et al., 2016). To test whether Bs3 expression coincides with increased Pip levels, we agroinfiltrated *N. benthamiana* leaves with *35S*-promoter–driven *Bs3-GFP*, *CaYUC3-GFP*, and *GFP*. Inoculated leaf tissue was harvested at different time points, and Pip levels were quantified by GC-MS (Fig. 9). We found that Pip levels were significantly increased in leaves expressing *Bs3* at 48 hpi (Fig. 9). Notably, the *Bs3* dependent increase of Pip is independent of contact with a plant pathogen or pathogen-associated molecular pattern.

DISCUSSION

Golden-Gate–based Domain Swaps Facilitate Identification of Functionally Exchangeable and Functionally Distinct Domains in Bs3 and YUC Proteins

Knowledge of the mechanistic basis of plant defense is a prerequisite for molecular breeding of pest-resistant crops. Accordingly, much effort has been devoted to clarify defense pathways engaged by the prevalent NLR-type plant R proteins. This resulted in the identification of various proteins required for NLR function, like enhanced disease susceptibility 1 (EDS1), required for Mla12 resistance 1 (RAR1), and suppressor of the G2 allele of skp1 (SGT1; Kadota et al., 2010), as well as the identification of defense-associated metabolites like SA and ROS (Herrera-Vásquez et al., 2015). By contrast, the molecular basis of executor-type R protein-induced plant defense remains enigmatic, and it remains to be clarified whether executor-mediated HR relies on signaling components as is the case for NLRs. Thus far five plant *R* genes have been cloned that are transcriptionally activated by and mediate recognition of matching *Xanthomonas* TALE proteins (*Bs3*, *Bs4C*, *Xa10*, *Xa23*, and *Xa27*; Zhang et al., 2015). Within these five known executor R proteins, Bs3 is exceptional because it is the only one that has homology to a protein of known function, which provides unique opportunities to clarify how Bs3 initiates a defense reaction. Pepper Bs3 is most related to YUC proteins but can be easily distinguished by the characteristic 70-amino acid deletion (Fig. 1; Supplemental Fig. S1). Notably, Bs3 with its characteristic 70-amino acid indel was found in three *Capsicum* species, but not in any other plant species,

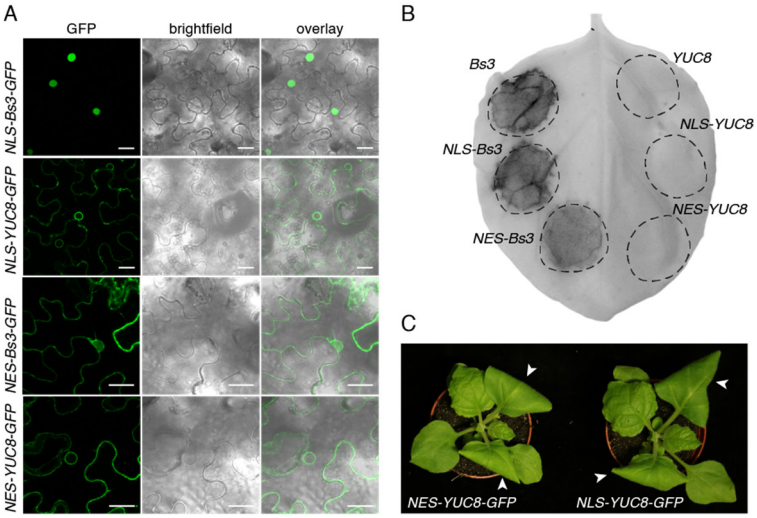

Figure 8. NLS or NES interfere neither with Bs3 nor with AtYUC8 function. A, Depicted gene constructs were expressed in *N. benthamiana* via *Agrobacterium*-mediated transient transformation. Leaf discs for CLSM were harvested 30 hpi. Pictures show GFP fluorescence (left), brightfield (center), and image overlay (right). Scale bars = 20 μm. B, Depicted constructs were expressed in *N. benthamiana* via *Agrobacterium*-mediated transient transformation. Four d post infiltration, the leaf was harvested and cleared with ethanol to visualize HR (dark). Dashed lines mark the infiltrated area. C, Depicted constructs were expressed in *N. benthamiana* leaves under control of the *35S* promoter via *Agrobacterium*-mediated transient transformation. White arrows point to infiltrated leaves.

suggesting that it evolved in an ancestral *Capsicum* species (Supplemental Fig. S3). Given the high relatedness of Bs3 and YUC proteins, it seems likely that Bs3 evolved in *Capsicum* from a YUC progenitor that acquired polymorphisms that made it functionally distinct from YUC proteins. In our studies, we aimed to clarify which residues or domains within Bs3 and YUC proteins dictate the functional specificity as inducers of either HR or leaf curling phenotypes, respectively. Our domain swap experiments demonstrated that three out of five defined segments (I, III and V) within the Bs3 protein can be functionally replaced by sequence-related segments from AtYUC8 (Fig. 6). Although these Bs3 and AtYUC8 regions are functionally equivalent, they differ in numerous residues that seemingly have no functional relevance. Thus, the domain-swaps experiments provide a convenient tool to discriminate between functionally relevant and functionally irrelevant amino acid polymorphisms.

The most significant difference between Bs3 and YUCs is the 70-amino acid sequence that is present in YUCs but absent from Bs3 (Fig. 1). It seemed plausible that this region defines functional specificity of Bs3 and AtYUC8. In our gene-shuffling experiments, the

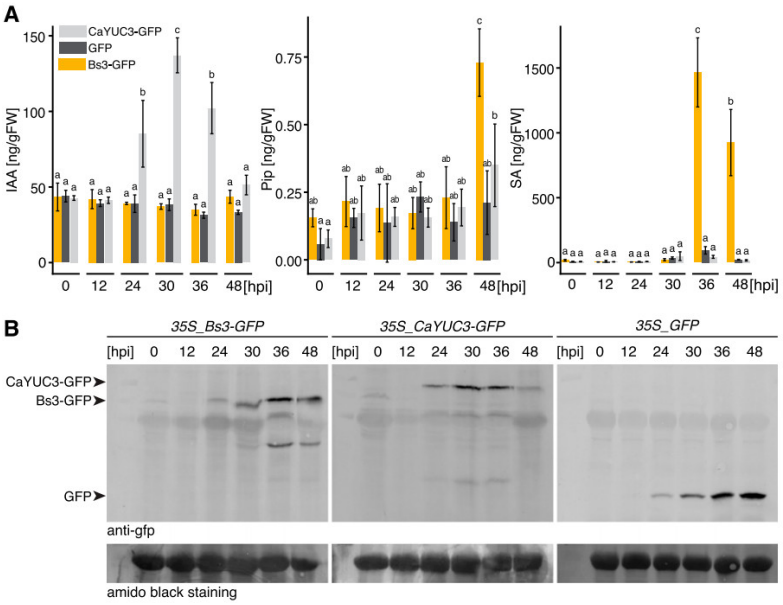

Figure 9. In planta expression of *Bs3* correlates with increased levels of SA and Pip but not with increased levels of IAA. The *35S*-promoter-driven *Bs3-GFP* (yellow), *CaYUC3-GFP* (light gray), and *GFP* (dark gray) CDSs were expressed in *N. benthamiana* leaves via *Agrobacterium*-mediated transient transformation. One-hundred mg of leaf material was harvested at indicated time points. A, SA, Pip, and IAA contents were quantified by MS. Bars = mean of three replicates ±SD. Different letters denote statistically significant differences (P<0.05, ANOVA with posthoc Tukey Honest Significant Difference test). B, Protein expression was monitored via an anti-GFP western blot. Black arrows indicate the expected position of the recombinant proteins. Amido black staining was used to visualize total protein load.

70-amino acid indel was contained in segment IV of Bs3 (234–284) and AtYUC8 (226–347; Fig. 1). A chimera in which the Bs3 segment IV was integrated into an AtYUC8 context (chimera #5; Supplemental Fig. S7) was nonfunctional. Reciprocally, integration of AtYUC8 segment IV into a Bs3 context (chimera #31; Supplemental Fig. S7) also resulted in a nonfunctional chimera. One plausible explanation for these nonfunctional chimeras is that our domain swaps separated functional domains that coevolved within Bs3 and/or YUC proteins. Another explanation is that deletion or integration of segment IV causes a slight disturbance in the protein structure that changes the relative position of the FAD to the NADPH cofactor. This causes loss of substrate oxygenation and therefore protein function. This is in line with the finding that single amino acid changes are sufficient to abolish Bs3 function.

Bs3-YUC8 Chimeras Containing a Putative AtYUC8 Membrane Anchor Do Not Trigger Bs3 HR

Notably, segments IV of Bs3 and AtYUC seem to dictate the different localization of Bs3 and AtYUC8. The observation that all chimeras that carry part IV of AtYUC8 are excluded from the nucleus (Supplemental Fig. S9) and that AtYUC8-part IV alone is sufficient to change localization of GFP (Fig. 7; Supplemental Fig. S11) is in line with previous studies on AtYUC proteins that show that some YUCs are anchored to the ER via a TMD (Kriechbaumer et al., 2016). Our colocalization studies of AtYUC8 and AtYUC8-part IV with ER-targeted mCherry confirm localization to the ER of AtYUC8 without much doubt due to the presence of a TMD within the C-terminal half of the protein (Supplemental Fig. S11). The exact position and length of the TMD remains to be clarified. There is no evidence that the enzymatic function of cytoplasmic and ER-anchored AtYUCs is distinct. On the other hand, it seems plausible that distinct subcellular localizations of enzymes with identical catalytic functions can have a profound impact on the cellular consequences. Thus, it remains to be clarified if the lack of biological activity in given chimeras is due to changed subcellular localization or due to structural changes that affect enzymatic activity.

Bs3-Triggered HR Is Not Caused by Auxin

Given that YUC proteins catalyze the conversion of IPA to IAA, it seemed reasonable to assume that the sequence-related Bs3 protein would catalyze the same reaction. Given that auxin is not only known as a growth hormone but also as modulator of defense responses to pathogens (for review, see Kazan and Manners, 2009), we originally hypothesized that Bs3 triggers HR by the deregulated production of auxin. In one possible scenario, Bs3 would have lost regula- tory protein domains and thus would produce toxic amounts of auxin. Another possibility would be that Bs3 decreases cellular auxin levels by competing with YUCs for the substrate IPA. Our measurements show that in planta auxin levels of Bs3-expressing plants are not changed compared to control plants, suggesting that Bs3 does not synthesize auxin (Fig. 9). Our studies also revealed that *Agrobacterium* containing intronless *AtYUC8* but not *Agrobacterium* containing *Bs3* had increased auxin levels (Supplemental Fig. S12). This observation also indicates that only AtYUC8, but not Bs3, catalyzes auxin biosynthesis. Notably, leaf curling phenotypes induced by AtYUC8-mediated auxin synthesis were not suppressed in leaves coexpressing *Bs3* and *AtYUC8* (Supplemental Fig. S8), thus demonstrating that Bs3-triggered HR is not epistatic to the auxin-induced leaf curling phenotype. Together, these observations suggest that Bs3-triggered HR does not rely on changed auxin levels and that Bs3 catalyzes an enzymatic reaction that is different from YUC-catalyzed reactions.

How Does Bs3 Trigger HR?

Due to the fact that in planta expression of *Bs3* does not coincide with elevated auxin levels (Fig. 9), we assume that sequence signatures that are unique to Bs3 and that are not found in YUCs change the conformation of the active site. We envision two possible consequences: One possible scenario could be that Bs3 might have a substrate specificity that is distinct from YUCs, resulting in synthesis of a possibly cytotoxic product. Alternatively, we envision that substrate-binding, but not cofactor-binding, is impaired in Bs3. This raises the question of how impaired substrate binding in Bs3 could possibly translate into an immune reaction? A possible explanation is provided by the reaction mechanism that has been studied in great detail for YUC proteins (Dai et al., 2013). YUCs first bind NADPH and molecular oxygen to produce an O_2-charged intermediate that is the most abundant form of YUC proteins. If no substrate is available, some FMOs, including YUCs, release the reduction equivalents coming from NADPH in the form of H_2O_2 (Siddens et al., 2014). The lack of a functional substrate binding site in the Bs3 protein could cause it to produce significant levels of H_2O_2. ROS, including H_2O_2, are key mediators of plant cell death reactions during biotic and abiotic stress (Mittler et al., 2011) Thus, the possible inability of Bs3 to bind and convert a substrate might cause Bs3 to convert NADPH into ROS that in turn trigger an HR. Interestingly, our studies uncovered some Bs3 mutants that induce elevated ROS levels in the plant tissue but do not trigger HR (Fig. 2). The question remains, however, if ROS are the initial trigger of cell death in Bs3-triggered HR. In this regard, a major challenge of future experiments will be to distinguish ROS that are directly produced by Bs3 from ROS that are indirectly produced during HR (e.g. by respiratory burst oxidases or peroxidases).

Does Bs3 Engage Known Immune Signaling Components to Execute HR?

As outlined in the preceding paragraph, expression of Bs3 might simply cause accumulation of a cytotoxic metabolite resulting in an HR phenotype. In this regard, it is interesting that we found that Bs3 HR correlates with an ~150× increase of SA and an ~3× increase of Pip (Fig. 9). SA is involved in pattern-triggered immunity and effector-triggered immunity, and, together with Pip, is a major regulator of SAR (Bernsdorff et al., 2016). Although the low sequence similarity of Bs3 compared to AtFMO1 and the different overexpression phenotype in planta (Koch et al., 2006) make it unlikely that Bs3 and AtFMO1 have a similar function, they seem to influence similar signaling pathways. Notably, Pip levels observed in Bs3-triggered HR are significant but far lower than what can be observed after pathogen inoculation in Arabidopsis (Hartmann et al., 2018). In general, the expression of SA and Pip supports the hypothesis that Bs3 is not simply cytotoxic but uses established immune signaling pathways to trigger HR. In this context, it will be interesting to clarify in the future to what extent Bs3 and other executor R proteins share immune signaling components with NLR-type R proteins.

MATERIALS AND METHODS

Plants and Growth Conditions

Nicotiana benthamiana plants were grown in a glasshouse at 22°C with 35% humidity and a light intensity of 12.3 klx on a 16-h light/8-h dark cycle. Four- to

Expression Plasmid Construction

Binary plasmids containing *Bs3* or *YUC* under control of the *35S* promoter were constructed via Golden-Gate–based cloning (Binder et al., 2014). Sequences were amplified with Type II restriction sites (*Bsa*I or *Esp3*I) and specific 4-bp overlaps flanking the gene of interest. PCR products were cloned into a pUC57 vector. Assembly of copy DNA sequences of *Bs3* derivatives and *YUCs*, *35S* promoter, and *NOS* terminator into the LII backbone (based on pICH50505; iCON Genetics) was done by simultaneous restriction digest and ligation. Single-bp mutants were obtained by mutagenesis PCR (see Supplemental Table S2 for Oligonucleotide sequences). Signal sequences, either the NLS (MLQPKKKRKVGGVDSSAAA) or the NES (MLQNELALKLAGLDINK), were

Creation of *Bs3* Mutants by epPCR Mutagenesis

Taq polymerase and M13 primers (see Supplemental Table S2 for Oligonucleotide sequences) were used to amplify the *Bs3* copy DNA flanked by *att*L sites from pENTR_Bs3 (Römer et al., 2007). To achieve a single-bp exchange, 0.5–1 ng of plasmid DNA was used as template, and the PCR was run for 35 cycles. *Dpn*I was used to digest the template DNA after amplification. An AvrBs3-inducible 360-bp promoter fragment of *Bs3* was amplified from pGWB1-Bs3 (Römer et al., 2007) with flanking *Hin*dIII and *Xba*I restriction sites and cloned into pCR-Blunt II Topo resulting in pCR-Blunt II-Topo 360-bp Bs3prom. *Hin*dIII and *Xba*I restriction-based replacement of the Ampicillin- resistant cassette (*Hin*dIII + *Xba*I flanked) in pK7T1WG1Amp with the Bs3 promoter fragment of pCR-Blunt II-Topo 360-bp Bs3prom resulted in pK7-360bp-WG1. PCR fragments were cloned into pK7-360bp-

Transient Expression in *N. benthamiana*

Agrobacterium tumefaciens (strain GV3101) was grown overnight in yeast extract broth medium (5 g/L of beef extract, 1 g/L of yeast extract, 5 g/L of peptone, 5 g/L of Suc, and 0.5 g/L of mM MgSO4 at pH 7.2) containing Rifampicin and either Spectinomycin or Kanamycin (concentration = 100 μg/mL), depending on the selection marker of given expression plasmids. Cultures were pelleted and resuspended in water. *35S*-driven *Bs3* or *YUC* constructs were adjusted to an OD_{600} = 0.4. For PCR mutant experiments, equal amounts of *A. tumefaciens* strains containing the *35S*-promoter–driven *avrBs3* gene and the strain containing the *Bs3* mutant CDS under control of the *Bs3* promoter were adjusted to an OD_{600} 5 0.8 and mixed in a 1:1 ratio. Infiltration into *N. benthamiana* leaves was performed using a blunt-end syringe. Leaf curling was monitored 1 d post infiltration. HR was monitored 3–4d post infiltration. For better visualization of the HR, leaves were bleached by incubation in 80% (v/v) ethanol at 60°C.

Microscopy

Leaf discs were cut with a cork-borer 30–36 h after infiltration with *A. tumefaciens*. Images were acquired using a TCS SP8 confocal microscope (Leica) equipped with an HCX PL APO CS 633 1.2 water objective (Leica). Excitation/emission was 488 nm/498–530 nm for GFP and 561 nm/571–610 nm for mCherry. For colocalization studies, mCherry containing a C-terminal HDEL motif was used as an ER marker. Image analysis and processing was performed using the software Fiji (Schindelin et al., 2012).

Ion Leakage Measurements

Ion leakage measurements were conducted using the CM100-2 conductivity meter (Reid & Associates). Each well was filled with 1-mL ultrapure water. Leaf discs with 4-mm diameter were harvested at the indicated time points. One disc was added per well and incubated at room temperature. Ion leakage was measured at indicated time points, usually after 10–20 h of incubation.

Gel Electrophoresis and Immunoblotting

Two leaf discs with 9-mm diameter were harvested at indicated time points after infiltration with *A. tumefaciens* and flash-frozen in liquid nitrogen. Leaf material was ground and mixed with 50-μL SDS buffer, then incubated at 98°C for 10 min. Ten-μL samples were loaded onto a 10% (w/v) polyacrylamide gel. The protein ladder #26616 (Thermo Fisher Scientific) was used as a size standard. Electrophoresis was done at 120 V for 90 min. Protein was transferred to a polyvinylidene fluoride membrane using a semidry transfer system (neoLab) for 70 min at 0.8 mA/cm^2. An α-GFP primary antibody (ab290/Abcam) and α-rabbit secondary antibody (IRdye680/LI-COR) were used for protein detection. The conjugated fluorophore signal was visualized with an Amersham Typhoon scanner (GE Healthcare Life Sciences) equipped with a BPFR 700 filter at 680 nm. To control protein transfer, the membrane was stained with Amido

Sequence Homology Analysis

Multiple sequence alignments were made using CLC Main Workbench (QIAGEN). Sequence alignments were shaded using the software BoxShade v3.21 (https://embnet.vital-it.ch/software/BOX_form.html). The tree representation of the Alignment was generated with the software "R" (www.r-project.org) and the "ggtree" package (Yu et al., 2017).

Quantification of SA and Auxin by GC-MS

Two-hundred mg of *N. benthamiana* leaf tissue was ground in liquid nitrogen and mixed thoroughly with 1.5-mL extraction solution (Ethyl-acetate, 0.1% [v/v] formic acid containing 16.7 ng/mL of 3-hydroxybenzoic acid, and 23.34 ng/mL of indole-5-carboxylic acid as internal standards). Samples were treated for 10 min in an ultrasonic water bath and incubated at 28°C with shaking (1,600 rpm). After centrifugation at 18,500*g* at 4°C, 1.2 mL of the supernatant was transferred to a fresh 1.5-mL tube, and the solvent was evaporated in a vacuum concentrator. The dried samples were derivatized in 60-μL N-Methyl-N-(trimethylsilyl)trifluoroacetamide (Sigma-Aldrich) for 30 min at 40°C and 1,200 rpm. Samples were transferred to 2-mL GC Vials with 100-μl

inserts and sealed with Polytetrafluoroethylene rubber septa lids. A 1-μL sample was subjected to GC-MS analysis.

GC-MS analysis was performed on a model no. TQ-8040 GC-MS system (Shimadzu). The injector, fitted with a custom glass liner (cat. no. 550733; Restek), was set to splitless mode at 280°C. Compounds were separated on a glass capillary column (30 m x 0.25 mm x 0.25 μm, cat. no. SH-Rxi-17SIL-MS; Restek). Helium at 1 mL/min column flow and a controlled linear velocity of 36.7 cm/s was used as carrier gas. Septum purge was set to 3 mL/min. The oven program was set as follows: initial temperature of 70°C for 5 min, followed by a gradient of 15°C/min to a final temperature of 280°C, which was held for 10 min (Total run time: 30 min). The interface of the mass spectrometer and the ion source were set to 250°C and 200°C, respectively. "Multiple Reaction Monitoring" was used as the acquisition mode.

Quantification of Pip via LC-MS

Two-hundred milligrams of fresh leaf material was directly frozen in liquid nitrogen and lyophilized. Afterward, samples were homogenized with a ball mill (twice for 30 s) and extracted with 80% (v/v) methanol containing 0.1% (v/v) formic acid. This was followed by a second extraction step with 20% (v/v) methanol also containing 0.1% (v/v) formic acid. Both supernatants were combined and dried. Samples were redissolved in 120-μL 20% (v/v) methanol containing 0.1% (v/v) formic acid. Five microliters were injected for analysis.

Analysis was done with a model no. UPLC-SynaptG2 LC/MS system (Waters) operated in "electrospray ionization positive" mode. The mass spectrometer was scanned in MS and MS^E mode from 50 to 2,000 mass to charge ratio at a scan rate of 0.2 s For separation, a flow rate of 200 µL/min and a 10-min gradient from 99% (v/v) water to 99% (v/v) methanol (both with 0.1% [v/v] formic acid) was used on an Acquity C18 HSST3, 100 mm 32.1 mm, 1.8-μm column (Waters). Compounds were quantified by integration of the extract ion chromatograms and external calibration.

Accession Numbers

C. annuum Cv ECW-30R Bs3: EU078684; Arabidopsis, YUC8: NM_119016.

Supplemental Data

The following supplemental materials are available.

Supplemental Figure S1. Bs3 is highly similar to pepper and Arabidopsis YUC proteins.

Supplemental Figure S2. Bs3 is only distantly related to AtFMO1 and AtFMO GS-OX-like1.

Supplemental Figure S3. Bs3 is present in the different *Capsicum* species *C. annuum* (Ca), *C. baccatum* (Cb), and *C. chinense* (Cc).

Supplemental Figure S4. Arabidopsis and *C. annuum* YUC families show a similar phylogenetic composition.

Supplemental Figure S5. Constitutive expression of *CaYUCs* causes leaf curling indicative of auxin accumulation.

Supplemental Figure S6. Random mutagenesis uncovers residues crucial to Bs3 function.

Supplemental Figure S7. Bs3-AtYUC8 chimeras trigger HR.

Supplemental Figure S8. HR and leaf curling phenotypes are not mutually exclusive.

Supplemental Figure S9. Composition and subcellular localization of Bs3-AtYUC8 chimeras.

Supplemental Figure S10. AtYUC8Daa and Bs31aa show altered subcellular localization compared to AtYUC8 and Bs3.

Supplemental Figure S11. Bs3 localizes to the nucleus and cytoplasm whereas AtYUC8 is anchored to the ER.

Supplemental Figure S12. IAA levels in leaves at timepoint 0 indicate auxin production in *A. tumefaciens*.

Supplemental Table S1. Genomic DNA sequences of *CaYUC3-6*.

Supplemental Table S2. Oligonucleotides used in this study.

ACKNOWLEDGMENTS

We thank D. Holmes for helpful comments on earlier versions of the article.

Received December 19, 2018; accepted April 29, 2019; published May 8, 2019.

LITERATURE CITED

Altschul SF, Gish W, Miller W, Myers EW, Lipman DJ (1990) Basic local alignment search tool. J Mol Biol 215: 403–410

Bernsdorff F, Döring AC, Gruner K, Schuck S, Bräutigam A, Zeier J (2016) Pipecolic acid orchestrates plant systemic acquired resistance and defense priming via salicylic acid-dependent and -independent path- ways. Plant Cell 28: 102–129

Binder A, Lambert J, Morbitzer R, Popp C, Ott T, Lahaye T, Parniske M (2014) A modular plasmid assembly kit for multigene expression, gene silencing and silencing rescue in plants. PLoS One 9: e88218

Boch J, Bonas U, Lahaye T (2014) TAL effectors—pathogen strategies and plant resistance engineering. New Phytol 204: 823–832

Chen YC, Holmes EC, Rajniak J, Kim JG, Tang S, Fischer CR, Mudgett MB, Sattely ES (2018) N-hydroxy-pipecolic acid is a mobile metabolite that induces systemic disease resistance in *Arabidopsis*. Proc Natl Acad Sci USA 115: E4920–E4929

Cheng Y, Dai X, Zhao Y (2006) Auxin biosynthesis by the YUCCA flavin monooxygenases controls the formation of floral organs and vascular tissues in Arabidopsis. Genes Dev 20: 1790–1799

Cheng Y, Dai X, Zhao Y (2007) Auxin synthesized by the YUCCA flavin monooxygenases is essential for embryogenesis and leaf formation in Arabidopsis. Plant Cell 19: 2430–2439

Dai X, Mashiguchi K, Chen Q, Kasahara H, Kamiya Y, Ojha S, DuBois J, Ballou D, Zhao Y (2013) The biochemical mechanism of auxin biosynthesis by an Arabidopsis YUCCA flavin-containing monooxygenase. J Biol Chem 288: 1448–1457

Exposito-Rodriguez M, Borges AA, Borges-Perez A, Hernandez M, Perez JA (2007) Cloning and biochemical characterization of *ToFZY*, a tomato gene encoding a flavin monooxygenase involved in a tryptophan- dependent auxin biosynthesis pathway. J Plant Growth Regul 26: 329–340

Hansen BG, Kliebenstein DJ, Halkier BA (2007) Identification of a flavin-monooxygenase as the S-oxygenating enzyme in aliphatic glucosinolate biosynthesis in Arabidopsis. Plant J 50: 902–910

Hartmann M, Zeier T, Bernsdorff F, Reichel-Deland V, Kim D, Hohmann M, Scholten N, Schuck S, Bräutigam A, Hölzel T, et al (2018) Flavin monooxygenase-generated N-hydroxypipecolic acid is a critical element of plant systemic immunity. Cell 173: 456–469.e16

Herrera-Vásquez A, Salinas P, Holuigue L (2015) Salicylic acid and reac- tive oxygen species interplay in the transcriptional control of defense genes expression. Front Plant Sci 6: 171

Hummel AW, Doyle EL, Bogdanove AJ (2012) Addition of transcription activator-like effector binding sites to a pathogen strain-specific rice bacterial blight resistance gene makes it effective against additional strains and against bacterial leaf streak. New Phytol 195: 883–893

Kadota Y, Shirasu K, Guerois R (2010) NLR sensors meet at the SGT1-HSP90 crossroad. Trends Biochem Sci 35: 199–207

Kazan K, Manners JM (2009) Linking development to defense: Auxin in plant-pathogen interactions. Trends Plant Sci 14: 373–382

Kim S, Park J, Yeom SI, Kim YM, Seo E, Kim KT, Kim MS, Lee JM, Cheong K, Shin HS, et al (2017) New reference genome sequences of hot pepper reveal the massive evolution of plant disease-resistance genes by retroduplication. Genome Biol 18: 210

Koch M, Vorwerk S, Masur C, Sharifi-Sirchi G, Olivieri N, Schlaich NL (2006) A role for a flavin-containing mono-oxygenase in resistance against microbial pathogens in Arabidopsis. Plant J 47: 629–639

Kong W, Li J, Yu Q, Cang W, Xu R, Wang Y, Ji W (2016) Two novel flavin-containing monooxygenases involved in biosynthesis of aliphatic glucosinolates. Front Plant Sci 7: 1292

Kriechbaumer V, Botchway SW, Hawes C (2016) Localization and interactions between Arabidopsis auxin biosynthetic enzymes in the TAA/YUC-dependent pathway. J Exp Bot 67: 4195–4207

Krueger SK, Williams DE (2005) Mammalian flavin-containing monooxygenases: Structure/function, genetic polymorphisms and role in drug metabolism. Pharmacol Ther 106: 357–387

Mittler R, Vanderauwera S, Suzuki N, Miller G, Tognetti VB, Vandepoele K, Gollery M, Shulaev V, Van Breusegem F (2011) ROS signaling: The new wave? Trends Plant Sci 16: 300–309

Návarová H, Bernsdorff F, Döring AC, Zeier J (2012) Pipecolic acid, an endogenous mediator of defense amplification and priming, is a critical regulator of inducible plant immunity. Plant Cell 24: 5123–5141

Poulet A, Kriechbaumer V (2017) Bioinformatics analysis of phylogeny and transcription of TAA/YUC auxin biosynthetic genes. Int J Mol Sci 18: E1791

Römer P, Hahn S, Jordan T, Strauss T, Bonas U, Lahaye T (2007) Plant pathogen recognition mediated by promoter activation of the pepper *Bs3* resistance gene. Science 318: 645–648

Römer P, Strauss T, Hahn S, Scholze H, Morbitzer R, Grau J, Bonas U, Lahaye T (2009) Recognition of AvrBs3-like proteins is mediated by specific binding to promoters of matching pepper *Bs3* alleles. Plant Physiol 150: 1697–1712

Schindelin J, Arganda-Carreras I, Frise E, Kaynig V, Longair M, Pietzsch T, Preibisch S, Rueden C, Saalfeld S, Schmid B, et al (2012) Fiji: An open-source platform for biological-image analysis. Nat Methods 9: 676–682

Schlaich NL (2007) Flavin-containing monooxygenases in plants: Looking beyond detox. Trends Plant Sci 12: 412–418

Seyfferth C, Tsuda K (2014) Salicylic acid signal transduction: The initiation of biosynthesis, perception and transcriptional reprogramming. Front Plant Sci 5: 697

Shan L, He P (2018) Pipped at the post: Pipecolic acid derivative identified as SAR regulator. Cell 173: 286–287

Shantharaj D, Römer P, Figueiredo JFL, Minsavage GV, Krönauer C, Stall RE, Moore GA, Fisher LC, Hu Y, Horvath DM, et al (2017) An engineered promoter driving expression of a microbial avirulence gene confers recognition of TAL effectors and reduces growth of diverse *Xanthomonas* strains in citrus. Mol Plant Pathol 18: 976–989

Siddens LK, Krueger SK, Henderson MC, Williams DE (2014) Mammalian flavin-containing monooxygenase (FMO) as a source of hydrogen peroxide. Biochem Pharmacol 89: 141–147

Strauß T, van Poecke RM, Strauß A, Römer P, Minsavage GV, Singh S, Wolf C, Strauß A, Kim S, Lee H-A, et al (2012) RNA-seq pinpoints a Xanthomonas TAL-effector activated resistance gene in a large-crop genome. Proc Natl Acad Sci USA 109: 19480–19485

Suh JK, Poulsen LL, Ziegler DM, Robertus JD (1999) Yeast flavin-containing monooxygenase generates oxidizing equivalents that con- trol protein folding in the endoplasmic reticulum. Proc Natl Acad Sci USA 96: 2687–2691

Tai TH, Dahlbeck D, Clark ET, Gajiwala P, Pasion R, Whalen MC, Stall RE, Staskawicz BJ (1999) Expression of the *Bs2* pepper gene confers resistance to bacterial spot disease in tomato. Proc Natl Acad Sci USA 96: 14153–14158

van Berkel WJ, Kamerbeek NM, Fraaije MW (2006) Flavoprotein monooxygenases, a diverse class of oxidative biocatalysts. J Biotechnol 124: 670–689

Yu GC, Smith DK, Zhu HC, Guan Y, Lam TTY (2017) GGTREE: An R package for visualization and annotation of phylogenetic trees with their covariates and other associated data. Methods Ecol Evol 8: 28–36

Zhang J, Yin Z, White F (2015) TAL effectors and the executor *R* genes. Front Plant Sci 6: 641

Zhao Y (2018) Essential roles of local auxin biosynthesis in plant development and in adaptation to environmental changes. Annu Rev Plant Biol 69: 417–435

Zhao Y, Christensen SK, Fankhauser C, Cashman JR, Cohen JD, Weigel D, Chory J (2001) A role for flavin monooxygenase-like enzymes in auxin biosynthesis. Science 291: 306–309

Supplemental Table S1. Genomic DNA sequences of *CaYUC3-6.* The genomic sequences were amplified from ATG and stop. Grey background indicates exons.

>Capsicum anuum ECW-30R YUC3

ATGAATCAATATTGTAATAGTCCTTGTTCACCTCTAATGGTTCATGCACTTGAACAAGAAGAGGACTTGTTCCTTGGTAGATGCATAC
TAGTAAATGGTCCTGTCATCGTTGGTGCTGGTCCATCAGGACTAGCAGTTGGCGCGGGCCTAAAACAACAAGGGGTTCCCTTTGTTAT
TTTGGACCGCGCCAACTGCATTGCGTCCTTATGGCAAAACAGGACTTATGATCGCCTTAAACTTCACCTCCCGCGACAATTCTGTGAA
TTGCCTTACTTCCCATTTCCAAAAAACTTCCCTGAATACCCTACAAAGTACCAATTCATCAACTACCTTGAATCATATGCCAAGAATT
TCGAGATCAAGCCAAGGTTCAATGAGTCAGTCCACTCTGCCAAGTATGATGAAACATGTGGTTTGTGGAGGGTGAAAACAGTTTGTAG
AGATGGTTCAATCACTGAATATATATGCAGGTGGCTTGTTGTAGCTACCGGAGAGAATGCAGAAAAAGTTGTACCCGAATTCGAAGGA
TTAGAAGATTTTGGTGGACATGTTATGCATGCTTGTGACTACAAAACAGGGGAAACTTATCAAGGGAAGAATGTGTTAGTTGTTGGTT
GTGGCAATTCAGGCATGGAAGTTTCTCTTGATCTTTGTCATCATAATGCAAGTCCATCCATGGTTGTTCGAAGCTCGGTAAGTCTCAT
TTTTTCTCATCTAATATCTTTATGTCTGCGTCCTTCATTTGCCAGAAAATCGACACTTAACATCTTCAATACCTCATGACAAGTACCT
AATCAAATATACTATCTTTCAATCCTCCAGCGCGATTGACATAACAAATCTTCTTTATGTCTGTGTCCTTCAATTGCCAGAAAATCCG
CGCATTACGTCTCTGATTCCTCATGAAAAGTATATAATCATATGATATCTAATGAAACGTTCAATATTTTCATGAACAGGTTCATGTT
TTACCAAGGGAAATTCTTGGAAAATCGACGTTTGATTTAGGAGTATCAATGATGAAATGGCTACCCATTGATGTAGTTGACAAGATAT
TGCTAGTTGCAGCAAGGTTACTTCTTGGAAACATAGAAAAGTATGGTTTAAAAAGGCCATCTATTGGACCTTTACAACTCAAAAACAC
AGAAGGGAAAACTCCTGTTTTAGACATAGGTGCATTACAAAAGATTAAATCTGGAGAAATAAAGATAGTTCCAGCAATCAAGAAATTT
TCTCAAGGGAAAGTGGAGTTTGTGAATGGTCAAATTCTTGATATTGATTGTGTCATTTTGGCTACTGGATATTGCAGCAATGTTCCTT
CCTGGTTAAAGGTGAGAAAAATAAACTCTCTCTTTCTTTTTCATAATCGTGGTGTTGGCATTAGTTTACACAAACCTCGACTAATTTG
ACGAGTTATCTGTCACCTCCTACCACGGTACATCAAGGTTAGGACAGACGAGAAAGAAGTCAAAAACAAACAATATTTTTCTTTCTTT
TTTTCATAATCGTGGTGTTCGGCCAGGTTACACGAATGATTCGACTAATTTGACGAGATACCTGTCACCTTCCACCACAGTCCACCAA
AGCTAGAACAGACGGGAAGAAGTCAAAAACAAGTTAATTTTTTTTTTTTTACAAAAAAAATAATAATAATTTTGTTGTGTATTCAAG
GTGGTGTATTTATTTTTAATTTATGGATTCTTGTGACAGTTATGGAAGTTGGTTTTCTTTTTTATATTCTCTGTTTCTATTTCTTGTA
TTTGTTAGTGAACAGGTGGATGATATTCTCATTTGCTTCAATATTTGTTTTTATTTTATTGGGAACATAGAAAAATATATTTTTCTTT
TTTCTTTTACTTGTGGTAATAATACTTTGAGAAATAAAAATTGAGCATTCCAAGATAATGGTTGAATGGATTAGATCATAGATATGAG
CTACAAATAAATTTTCTGTTTTTTTTTTTTTCTTTTTAAGGGTATTTCAAGAATATATTTCTTTGAATTTTGGTCTAATGATTTTTTA
TTTATTTTTTTGTATATAGGAAAGTGAATTTTTTTCAAGGGAGGGATTTCCAAAAAATCCATTTCCAAATGGATGGAAAGGAAAAGGT
GGTATATATGCAGTTGGATTTACAAGAAGAGGACTTTCTGGTGCTTCTTTAGATGCAATTAAAGTATCACAAGATATTGGCAAAATTT
GGAAAGAAGAAATTAAACAGAAAAATCAATCTGTTACTGTTGCATGTCATAGAAGAAGCAAGTCACATTTCTAA

>Capsicum anuum ECW-30R YUC4

ATGTTTAGTTTCTCAGAAAACGATTTCTTTGCCCGGAGATGTGTTTGGGTAAATGGCCCCGTTATTGTTGGTGCCGGTCCATCAGGAC
TAGCTGTGGGAGCTTGTTTGAAAGAACAAGGAGTACCTTGTGTTATCTTGGAAAGAGCTGATTGTATTGCCTCTTTGTGGCAAAAAAG
AACGTATGATCGGTTGAAACTTCACCTACCTAAGCAATTCTGTCAATTGCCCAAATTCCCATTTCCAGAATACTACCCTGAATACCCA
ACTAAGAGACAATTCATTGAATATCTTGAATCATATGCCAAGCACTTTGACATTAGCCCACAGTTCAATGAATGTGTGCAATCTGCTA
AGTACGACGAGGCTTGTCGATTGTGGAGGGTGAAAACTGTTTCAGCTGATGGCTCTGAAGTTGAGTACATTTGCCAGTGGCTTGTTGT
TGCCACTGGTGAGAATGCTGAGAAAGTTGTGCCTGAAATTGATGGGCTAAAAGAATTTGGTGGTGAAGTGATTCATGCTTGTGACTAT
AAGTCTGGTGAGAAATTCAGGGGAAAGAAAGTTCTTGTTGGTTGTGGAAATTCTGGCATGGAAGTGTCACTTGATCTTTTCAACCATG
ATGCTCAACCATCAATGGTTTGTCGTAGCTCGGTAAGTAATTAATACTGTACCAAGCTTTGGAATGAGATGGTCACAGTTTTGATAAG
AGTTTAGATTTCTAATGTACTTTCTTTTGTTTATTCAGGTTCATGTTTTGCCAAGAGAGATATTTGGGAAATCAACTTTCGAGTTGGC
TATGTTGTTGATGGCATGGCTGCCACTTTGGATAGTTGACAAGATTTTACTCACTTTGACAGGGTTCATTCTTGGAAACATTGAGAAA
TATGGACTAAAAAGACCATCAATTGGACCATTACAACTCAAGAACACTCAAGGAAAAACCCCTGTTCTTGACATTGGTGCTTTGGAAA
AAATCAGATCCGGAAAAGTTAAGGTTATCCCTGGACTCAAGAAGTTTTCATGTGGCACTGTTGAACTTGTCACTGGTGAAATACTTGA
AGTTGATTCAGTTGTTCTTGCTACTGGCTACTGCAGCAATGTTCCATATTGGCTACAGGTGAGTAAGTGTTCTATTTGAAAGTTCTGG
AAGTTTCTATTTATTTAAAGTAAAAGGAAAAATAAAATGCAAGATTCTTTAACAGTTGACAAATATATTTTTGTTATGTTATACAGGA
AAGTGAATTTTTCTCCAAGAATGGGTACCCAAAAGCACAATTTCCTAACAACTGGAAGGGAAAATCCGGGCTATATGCAGTTGGATTC
ACAAAGAGAGGGCTGGCTGGTGCTTCTGCTGATGCTATTAGAATTGCTAAAGATATTGGCAAAGTTCACAAAGAAGATCTCAAGCAAA
AGAAGCAAAAAGTTCCAACACACAGACGTTGCATCTCAACCTTCTAA

>Capsicum anuum ECW-30R YUC5

ATGGTTAACTTCAATGATCAAGATTTCTTTTCTAGTAGATGTGTATGGGTAAATGGACCTGTTATTGTCGGTGCAGGTCCATCGGGAC
TAGCTGTGGGAGCTTGTTTAAAAGAACAAGGCATCCCATTTGTAATCTTGGAAAAATCAGATTGCATTGCATCACTATGGCAAAAAAG
AACTTATGATAGACTAAAACTACACCTCCCTAAACAATTTTGTCAATTACCCAAATTCCCATTTCCACAACACTACCCTGAGTACCCT
ACAAAGAAACAATTCATTGATTATCTTGAATCATATGCAAGAAAATTTGACATTAACCCAATGTTCAATGAGTGTGTTCAATTTGCAA
AGTATGATAAATCTTGCAAATTGTGGAGGGTGAAAACTATTTCATCAAGTGGTTTAGAAGTTGAGTATATTTGTCAATGGCTTGTTGT
GGCTACTGGTGAAAATGCACAAAAAGTTGTGCCTAATATTGAAGGATTAAAAGAATTTGGAGGTGAAGTGATTCATGCTTGTGATTAT
AAGTCTGGTGAAAAGTTTAGTGGCAAGAAAGTTCTTGTTGTTGGTTGTGGGAATTCTGGTATGGAAGTTTCTCTTGATCTTTGCAATC
ATAATGCTCAACCATCATTGGTTTGTCGTAGCTCGGTAAGTTATATATACTGACAATATAAAGAACCTTTTAGAGTTTCAATGTACTT
TTAACCTTTTGTAGTAGGTTAGCCACCTCAATTTTCAGGCAGCTCGGTAAGTTATACATACTAATAATATAATGAACTTTTTACAGTC
CCAATGCACTTTAACCTTTTGTAGTAGGTTAGCCATCTTACTTTTCAGGCTAGTAATCCCCCTTACTGTTATCTTTTAGGTGATTTGA
TAGTATAAAATTTTTTTACGATGATGTCAGAGTAAAAGTTGAATTCTTATAGCTGACAATATTGTATATGAATTTGTACACTATCAAG
TCATATAAAAGATAATAAAGTGGGATTACTAAGTTGGAGAATAACACAGATAACCTGTTACAACATGTTAAAAATACTTTAAGTGTAC
ATAAGTTAAATCCTTTTTGAATTTGCTCATAGCAAACACAAAAGAAGTGAAAAGGGGAAGAAGAAAAAGAATTTTTAAACAAAATAGC
GGCTGACACAAGAAAAATAGTTGGCAAATGTATAATATATGTATATCAACTAGGGGCTAATTGTCAGAGGTGGAGCCAGCCTAGTAAC
AGGGGGTTCGTCCGAACTCCCTTCGACGAAAAATTATATTATTAATACATTATTAAAATAGATGTTGAATCTCCTTCGGCGAGCTTTT
CTTTAAATTTTGAACCTCGTCAACAGAAATCCTGGCTCCGCCTCTGTTAATTGTGTGACTTCCCAAAAAAAGAAACTATGAAGTTTGG
ACTAATGGATTTTTTTTCTATGTTTCTCTTCTTTAGGTTCATGTATTGCCAAGAGAAATCTTTGGGAAATCAATATTTGAGTTGGCTA
TGTTTATGATGAAATGGCTACCATTGTGGCTAGTTGACAAAATTTTACTCATTTTGACATGGTTCATTCTTGGTAACATTGAGAAATA
TGGTCTAAAAAGGCCAAAAATTGGACCATTGGAACTCAAGAATACACAAGGGAAAACTCCTGTTTTGGACATTGGTGCATTGGAAAGA
ATTAGATCAAGAAAAATTAATGTTGTACCTGGAATCAACAAGTTTTCATGTGGCACCGTTGAACTTGTCACTGGCGAAAAACTCAAAA
TTGATTCTGTTGTTCTTGCTACTGGCTATCGTAGCAATGTCCCTTTTTGGCTAAAGGTGAGAAAATGTTTACATTTTTCTTTTTTTGA
TAGTCTTTGTACCTTAAATTAACTCGATAGATTCTCAAACAGACACCTTAAATTGGTCAAAACACGTCTTTTCATAAAAAAAAGACCA

AGTTATATGATGTCTGTTTGAGAACTTGTGAAGTTAAGGGGTCACCACTAGAAAGTTGTGCAAGTACGATTGTCATATTGAAATTTTT
GAATGTTTCTTTTTATTTATATTTAGGTTTATTTAGGTTTAGTACCTAAATCAACATCATTACTTTGCTGACCCCTTCGTTTGACGGT
TCTCAAACAAACACCTCAGCTTGGTCAAAACACATCATCAATATATACGACTGAGTTATGGTGTTTGTCTGAAAACCAATCGAGTTAA
AGGAGTCAGGACTAAAAAGTTGTCCAAGTAGGATTGTCAAATTGAAAACTATTGAAATTTTTGAATGTCTCCTTTTATTTATATTTAG
GTTTAGTACCTAAATCAACATCATTACATGTACAAGTCTCTAATGCTGACCCCTTCATTTGACGGCTCTCAAACAAACACCTCAACTT
GGTCAAAACACATCTTCCGTAAGACCGAGTTATGGTGTTTGCTTGAACACCAATCGAGTTAATGAGGTCAGGACTAGAAAGTTGTCCA
AGTACGATTGTCAAATCGAAAAATATTGAAATTTTTGAATGTCTCCTTTTATTTATATTTAGGTTTAGTACCTAAATCAACATCATTA
CTTGCACGAGTTTCTAATGCTGACCCCCTTCAATTGACGGTTCTCAAACAGACACCTTAGCTTGGTCAAAACACATTGTCAGTAAGAT
CGAGTTATGCTGTTTGTTTGAAAACCAGTTGAGTTAAGGGTGTCAGGACTAGAAAGTTGTCCAAGTATATACGAGTGTCAAATCTACT
AATGTTGAATTTTATGAAAAGATTCTTGAATAGTGGAGTAATGTTATTTTTGTTATTTTTTTTATATAGGAAAGTGAATTCTTTGCCA
AGAATGGATTTCCAAAAGCACCATTTCCAAATTGTTGGAAAGGAAAATATGGATTATATGCAGTTGGTTTCACAAGGAGAGGGTTAGC
TGGTGCTTCTAGTGATGCTATTAGAATTGCACAAGATATTAGCAAAGTTTACAATGAAGATATTATGCAAAAAAAGCAAAATTTTTCT
ACACATACAAGATGCATGTCAACCTTATGTGTAAATTAA

>*Capsicum anuum ECW-30R YUC6*
ATGTTTACCTTTTCGTCAGAACAAGATTTAATTTCCCGTAGATGTGTTTGGGTAAATGGCCCCGTGATCGTTGGTGCCGGTCCATCAG
GGCTAGCAGTAGGAGCTTGTTTAAGAGAACAAGGAGTTCCGTTTGTCGTTATAGAAAGATCTGACTGCATTGCATCATTATGGCAAAA
GCGAACTTACGATCGTTTAAAGCTCCACCTACCCAAAAAGTTCTGCCAATTACCAAAACTCCCATTTCCAAATCACTACCCTGAGTAT
CCAACAAAGAGACAATTCATAGAATACCTGGAACTGTATGCCAAACACTTTGACATTAAACCGCAGTTCAACGAGTGTGTTCAGTCAG
CTAAATACGACGAAACTTGCAGTGTTTGGAGGGTGAAAACTGGTTCACCAAACGGCTCTGAAGTCGAGTACATTTGCCAGTGGCTTGT
CGTAGCCACGGGCGAAAATGCTGAGAGAGTTGTCCCTGATATTGAAGGATTGAAAGATTTTGGAGGTGAAGTGATTCATGCTTGTGAT
TATAAGTCAGGGGGAAAATATCATGGAAAGAAAGTTGTTGTTGTTGGATGTGGAAATTCTGGTATGGAAGTTTCTCTTGATCTTTCAA
ATCATGGTGCTCAACCATCAATGGTTTGTCGTAGCTCGGTAAGCAAGCTATACAGAGACGTATTCAGAATTTAAATTTGATGATTAAG
AGTTCCACTTTACTAATGTTTTTTTCTTCTCCAGGTACATGTTTTGCCAAGAGAAATTTTTGGGAAATCAACATTTGAGCTAGCTATG
TTTATGATGAAATGGTTGCCTATATGGCTAGTTGACAAGATTCTACTTGTTCTTGCATGGTTTATATTGGGAAACATTGAGAATTATG
GACTAAAAAGGCCATCACTAGGACCATTGGAACTCAAGAACAAACAAGGGAAAACACCAGTTCTTGATATTGGTGCCTTGGAAAAAAT
TAGATCTGGACAAGTTAAGGTTGTCCCAGGAATCAAGAAGTTTTCATGTGGCACCGTTGAACTTGTCACGGGTGAAAAACTAGAAATT
GATTCTGTTGTTCTTGCTACTGGTTACTGCAGCAATGTTCCTTACTGGCTACAGGTGAGACAATGTCTCAATCCTTCTAGAACTCTTT
TCAACAACATTGACAGTCTTGGAAGTTTCAAATGAGTTTAAGTTATGTACACCGACCGACAGAGTGAACTCTTTTCACTCGCTATGTT
GCTCAGACTTTCTTAAAATGTTGTGGCCTAATGTTATTTTTTGTTATGTGATACAGGAAAGTGAATTTTTCTCCAAGAATGGCTTTCC
AAAAACACCATTTCCAAATAATTGGAAAGGAAACTCAGGCCTATATGCAATTGGATTTACAAAAAGAGGGCTAGCTGGTGCTTCTGCT
GATGCTATAAAAATTGCACAAGATATTGGCAAAGTATACAAAGAAGATCTCAAACAAAAAAAGCAAAAGGTTCCAACACATAGAAGAT
GCATCTCAACTTTTTAA

Supplemental Table S2. Oligonucleotides used in this study

NAME	SEQUENCE	EXPERIMENT
CKP34 Bs3partIfw	aaacgtctctCACCATGATGAATCAGAATTG	Gene shuffling
CKP35 Bs3partIrev	aaacgtctctAGCAGTAGCCAGCCCTG	Gene shuffling
CKP36 Bs3partIIfw	aaacgtctctTGCTGCCGTCCTTAAGC	Gene shuffling
CkP37 Bs3partIIrev	tttcgtctctTGAATTGGTTTTTGGTTGG	Gene shuffling
CKP38 Bs3partIIIfw	aaacgtctctTTCATCAGCTACCTGGTATC	Gene shuffling
CKP39 Bs3partIIIrev	aaacgtctctGAGCTTCGTACTACCATGAATG	Gene shuffling
CkP40 Bs3partIVfw	aaacgtctctGCTCGGTACAGGGTCGTA	Gene shuffling
CKP41 Bs3partIVrev	aaacgtctctCCAAGAAGTTACATTGCTGG	Gene shuffling
CKP42 Bs3partVfw	aaacgtctctTTGGTTAATGGAGAGTG	Gene shuffling
CKP43 Bs3partVrev	aaacgtctctCCTTCATTTGTTCTTTCC	Gene shuffling
CKP24 Yuc8partIfw	tttcgtctctCACCATGGAGAATATGTTTCG	Gene shuffling
CKP25 Yuc8partIrev	aaacgtctctAGCAGTCGCTAAGCCCG	Gene shuffling
CKP26 Yuc8partIIfw	aaacgtctctTGCTGCTTGTCTCCATG	Gene shuffling
CkP27 Yuc8partIIrev	aaacgtctctTGAACTGACGCTTCGTC	Gene shuffling
CKP28 Yuc8partIIIfw	aaacgtctctTTCATCGACTACCTCGAGTC	Gene shuffling
CKP29 Yuc8partIIIrev	aaacgtctctGAGCTTCTCACGACCATC	Gene shuffling
CKP30 Yuc8partIVfw	tttcgtctctGCTCTCTTCACGTGATGC	Gene shuffling
CKP31 Yuc8partIVrev	tttcgtctctCCAATATGGGACGTTGC	Gene shuffling
CKP32 Yuc8partVfw	aaacgtctctTTGGCTACAAGAGAATGAG	Gene shuffling
CKP33 Yuc8partVrev	aaacgtctctCCTTGAACTGTTGAGAGATAC	Gene shuffling
CKP125 CaYUC3fw	tttggtctctcaccATGAATCAATATTGTAATAGTCCTTGTTC	Capsicum YUCs
CKP126 CaYUC3rev	aaaggtctcaccttGAAATGTGACTTGCTTCTTCTATG	Capsicum YUCs
CKP127 CaYUC4fw	tttcgtctctcaccATGTTTAGTTTCTCAGAAAACGATTTC	Capsicum YUCs
CKP128 CaYUC4rev	aaacgtctcaccttGAAGGTTGAGATGCAACGTC	Capsicum YUCs
CKP129 CaYUC6fw	tttggtctctcaccATGTTTACCTTTTCGTCAGAAC	Capsicum YUCs
CKP130 CaYUC6rev	aaaggtctcaccttAAAAGTTGAGATGCATCTTCTATG	Capsicum YUCs
CKP131 CaYUC5fw	tttcgtctctcaccATGGTTAACTTCAATGATCAAG	Capsicum YUCs
CKP132 CaYUC5rev	aaacgtctcaccttATTTACACATAAGGTTGACATG	Capsicum YUCs
CKP88 Y8partIVfw	tttcgtctctCACCCTTCACGTGATGC	localization
CKP97 Y8partIVrev	aaacgtctctCCTTTGGGACGTTGCTGCG	localization
360-IQV-Bs3fw	aaacgtctctCACCATGATACAAGTAAATGGTCCTCTTAT	N-term. deletions
361-QVN-Bs3fw	aaacgtctctCACCATGCAAGTAAATGGTCCTCTTATTG	N-term. deletions
362-VNG-Bs3fw	aaacgtctctCACCATGGTAAATGGTCCTCTTATTGTT	N-term. deletions
363-NGP-Bs3fw	aaacgtctctCACCATGAATGGTCCTCTTATTGTTG	N-term. deletions
364-GPL-Bs3fw	aaacgtctctCACCATGGGTCCTCTTATTGTTGGA	N-term. deletions
CKP52 partIVa Bs3rev	aaacgtctctGAACCACGTTTATTTCCTCGG	Domain swaps
CKP53 partIVa Yuc8rev	aaacgtctctGAACTATGTTGATCTTTCCTAAG	Domain swaps
CKP54 partIVb Bs3fw	aaacgtctctGTTCCAGCAATCAAGAAATTTAC	Domain swaps
CKP55 partIVb Yuc8fw	aaacgtctctGTTCCCGGGATCAAAAG	Domain swaps
M13 fw	GTAAAACGACGGCCAGT	Sequencing
M13 rev	GGAAACAGCTATGACCATG	Sequencing

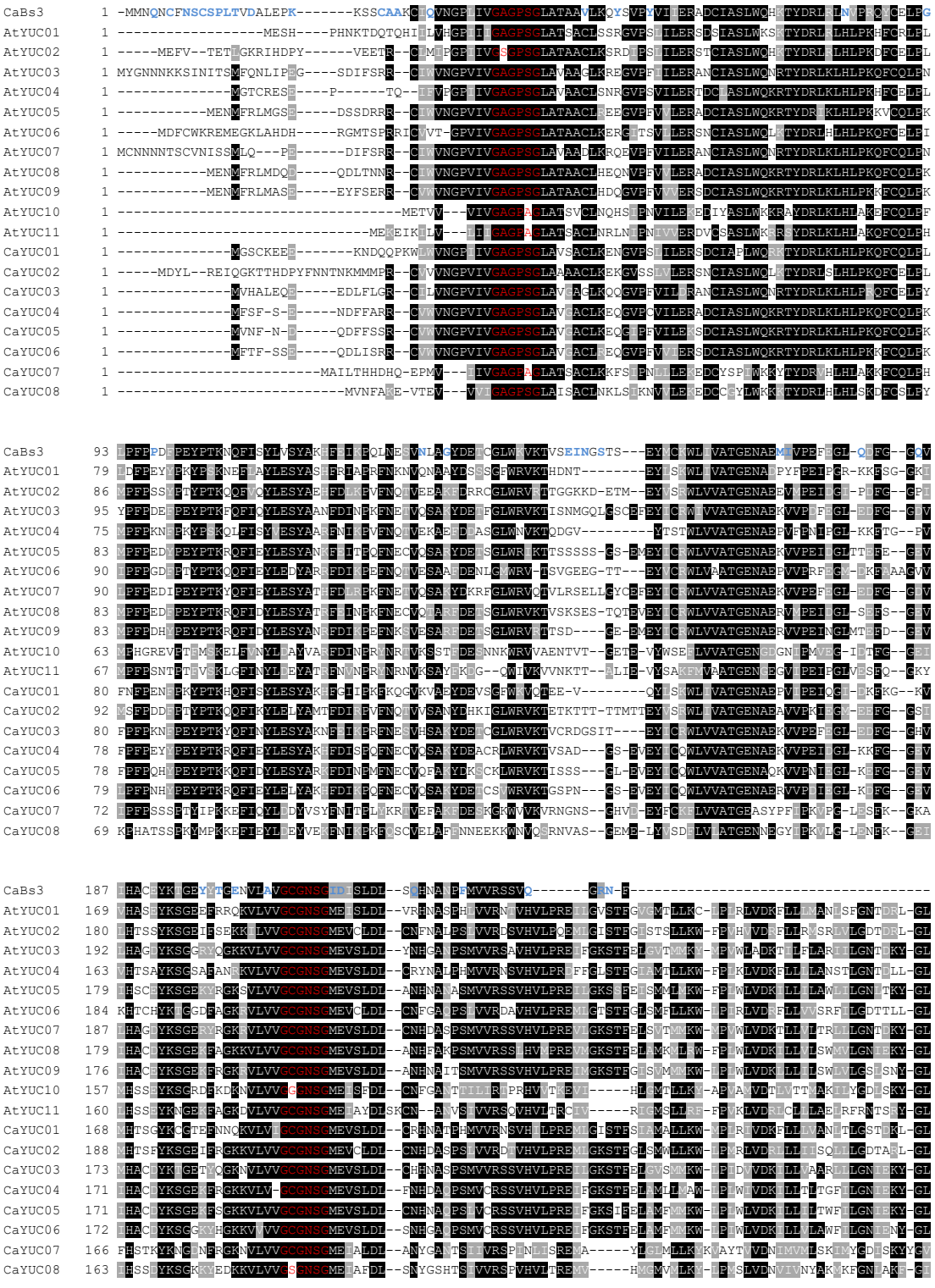

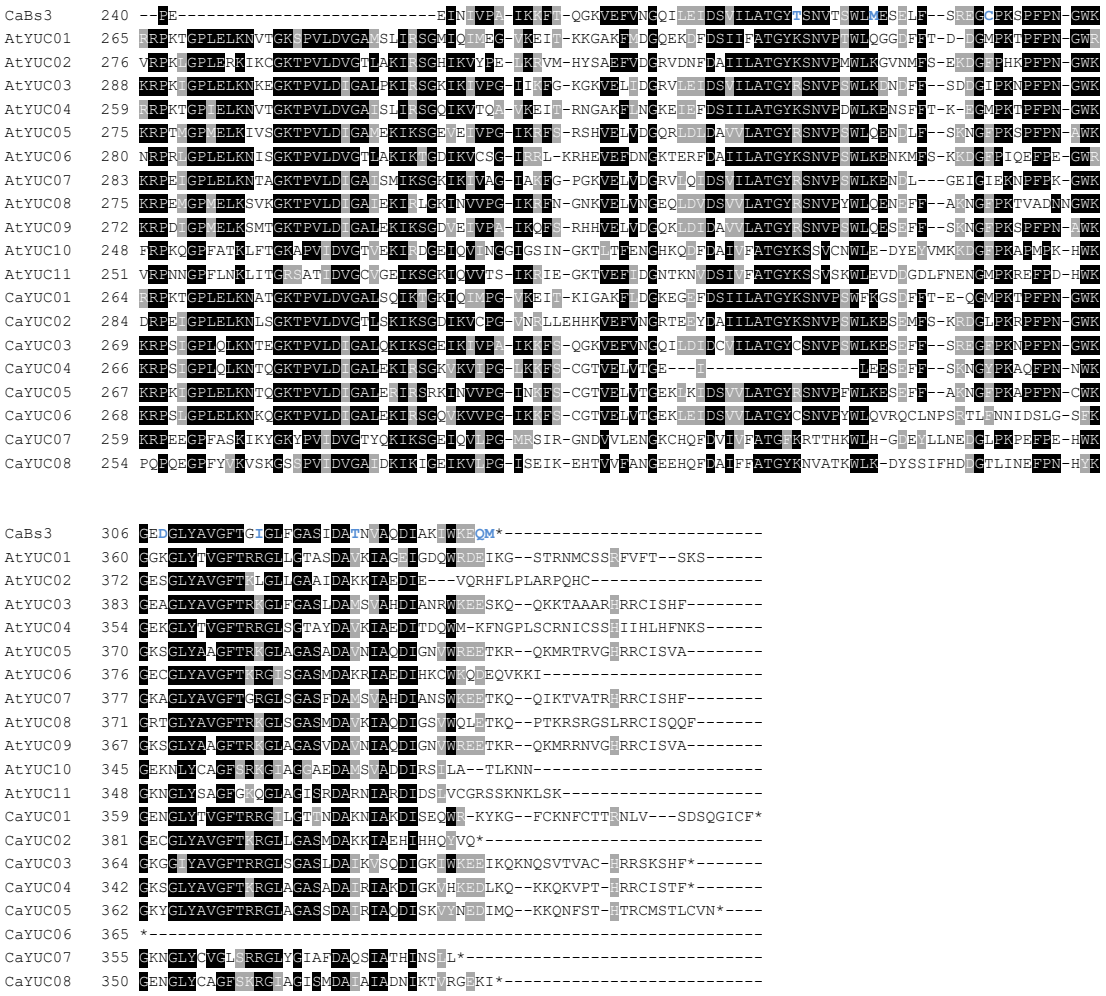

Supplemental Figure S1. Bs3 is highly similar to pepper and Arabidopsis YUC proteins. Amino acid sequence alignment of pepper Bs3 (CaBs3), all YUCs of pepper (CaYUCs) and all YUCs of Arabidopsis (AtYUCs). Alignment was done with CLC main Workbench. Identical amino acids (black background) and similar amino acids (grey background) were shaded using Boxshade. Gaps in the alignment are indicated as black horizontal lines. Red font indicates the predicted FAD (position 39 to 41 in Bs3) and NADPH (position 207 to 212 in Bs3) binding sites, respectively. Blue font highlights amino acids that are different in Bs3 compared to all other YUC proteins.

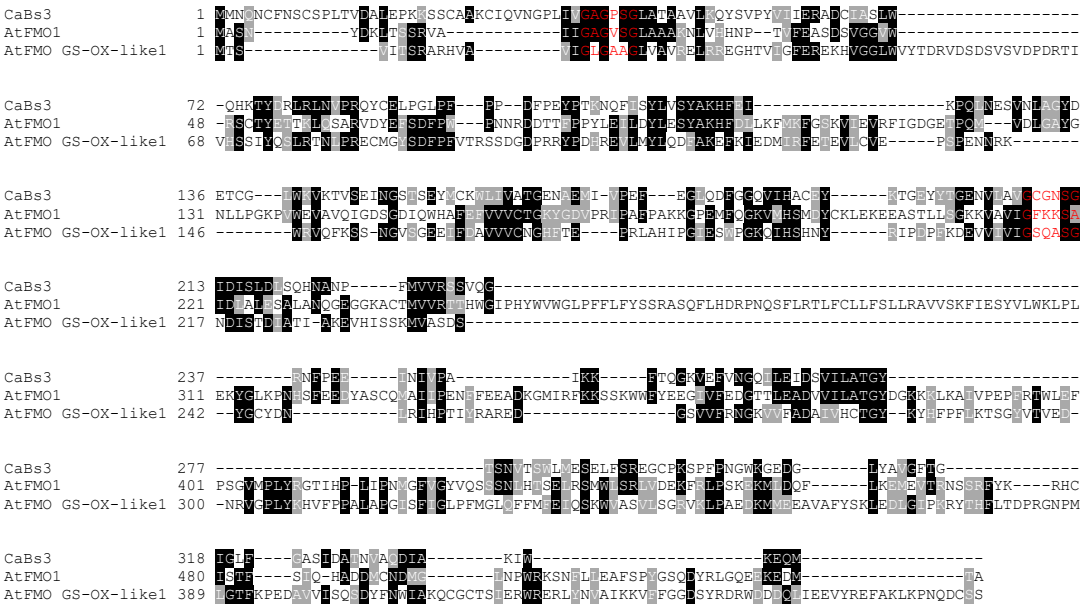

Supplemental Figure S2. Bs3 is only distantly related to AtFMO1 and AtFMO GS-OX-like1. Sequence alignment of Bs3 from pepper (CaBs3), Arabidopsis FMO1 (AtFMO1) and Arabidopsis FMO GS-OX-like1 (AtFMO GS-OX-like1). Alignment was done with CLC main Workbench. Identical amino acids (black background) and similar amino acids (grey background) were shaded using Boxshade. Gaps in the alignment are indicated as dashes. Red font indicates the predicted FAD and NADPH binding sites, respectively.

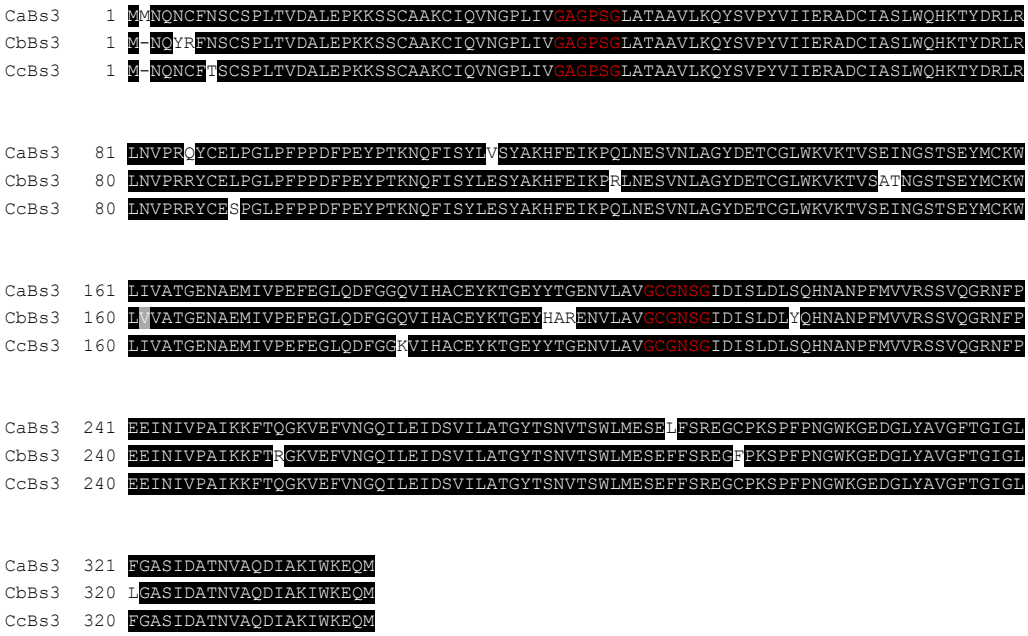

Supplemental Figure S3. Bs3 is present in the different *Capsicum* species *Capsicum annuum* (Ca), *Capsicum baccatum* (Cb) and *Capsicum chinense* (Cc). Alignment was done with CLC main Workbench. Identical amino acids (black background) and similar amino acids (grey background) were shaded using Boxshade. Gaps in the alignment are indicated as dashes. Red font indicates the predicted FAD and NADPH binding sites, respectively.

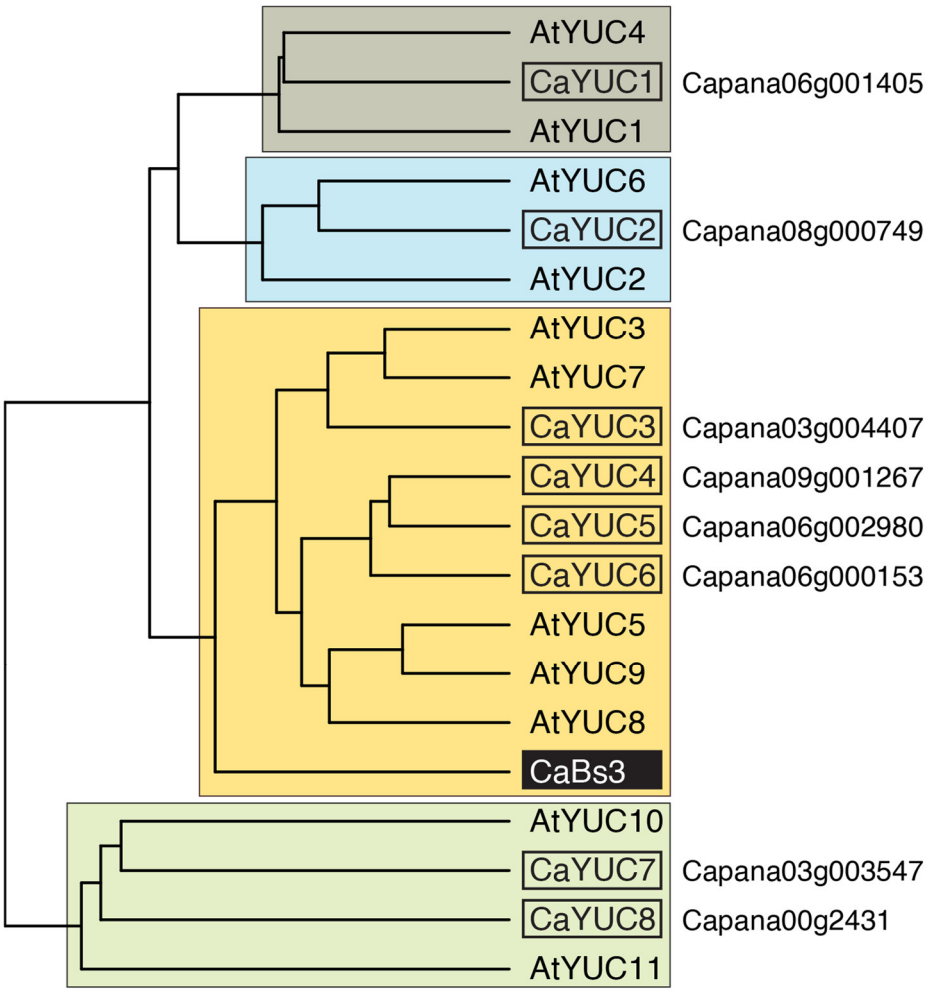

Supplemental Figure S4. Arabidopsis and pepper YUC families show a similar phylogenetic composition. Phylogenetic tree of pepper Bs3 and YUC proteins from pepper and Arabidopsis. The tree is based on the amino acid alignment in supplemental Figure S1. Construction was done by the UPGMA method. The pepper YUCs were numbered in ascending order based on their position in the tree. Colored boxes highlight the four phylogenetic groups.

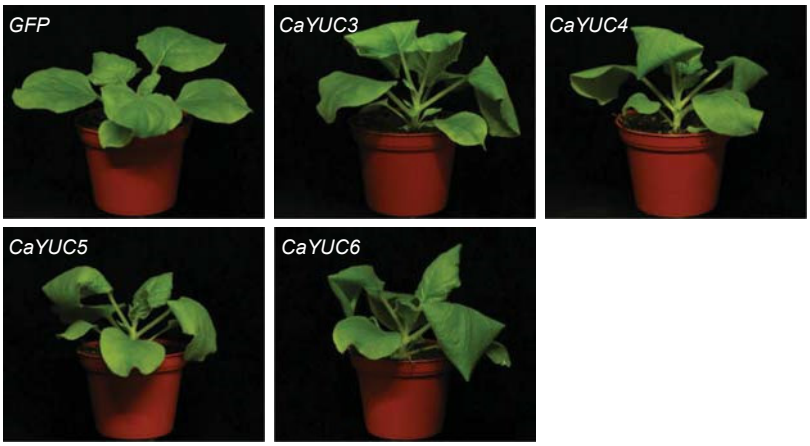

Figure S5. Constitutive expression of *CaYUCs* causes leaf curling indicative for accumulation of auxin. Depicted constructs were expressed under control of the *35S* promoter in *N. benthamiana* via *Agrobacterium*-mediated transient transformation. Pictures were taken 24 hours post infiltration.

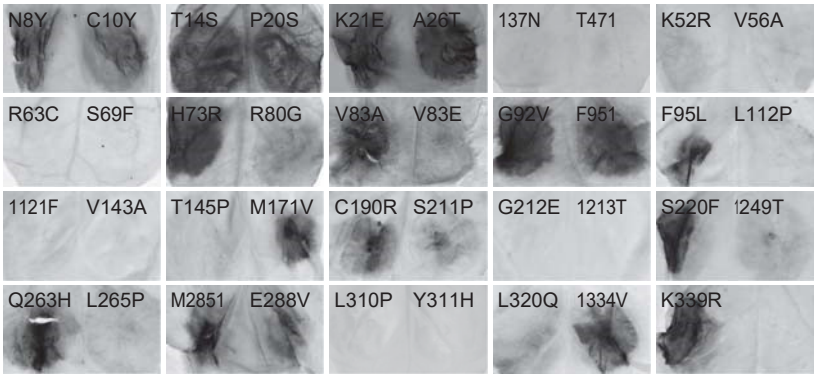

Supplemental Figure S6. Random mutagenesis uncovers residues crucial to Bs3 function. Indicated *Bs3* mutant derivatives (see Figure 3 for details) were expressed in *N. benthamiana* leaves. *Agrobacterium* strains carrying the indicated gene constructs under transcriptional control of the *Bs3* promoter were coinfiltrated with *Agrobacterium* strains containing *avrBs3* under control of the cauliflower mosaic virus *35S* promoter. Four days post infiltration, leaves were harvested and cleared with ethanol to visualize HR (dark). Dashed lines mark the infiltrated area.

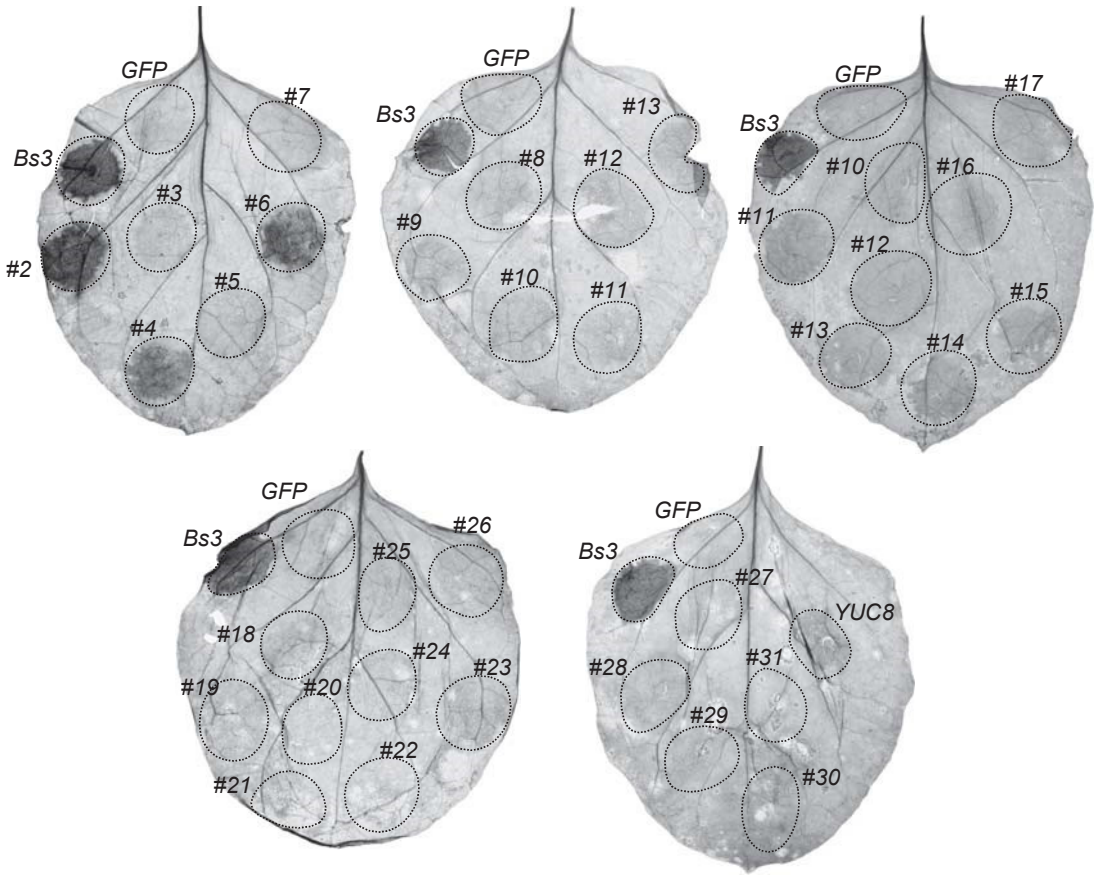

Supplemental Figure S7. Bs3-AtYUC8 chimeras trigger HR. *35S*-driven *Bs3*, *AtYUCB* and depicted chimeras (see Fig. S9 for details on composition of chimeras) were expressed in *N. benthamiana* leaves via *Agrobacterium*-mediated transient transformation. All depicted constructs are *GFP*-tagged. *Bs3* and *GFP* were infiltrated on every leaf as positive and negative controls, respectively. Four days post infiltration, leaves were harvested and cleared with ethanol to visualize HR (dark). Dashed lines mark the infiltrated area.

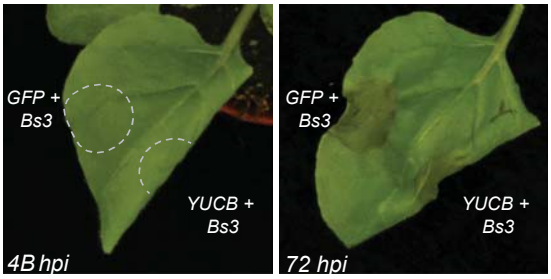

Supplemental Figure S8. HR and leaf curling phenotypes are not mutually exclusive. *35S-driven GFP* and *Bs3* or *AtYUC8* and *Bs3* were co-expressed in *N. benthamiana* via *Agrobacterium*-mediated transient transformation. Pictures were taken at 48 and 72 hours post infiltration (hpi). Dashed lines mark Bs3 infiltrated areas.

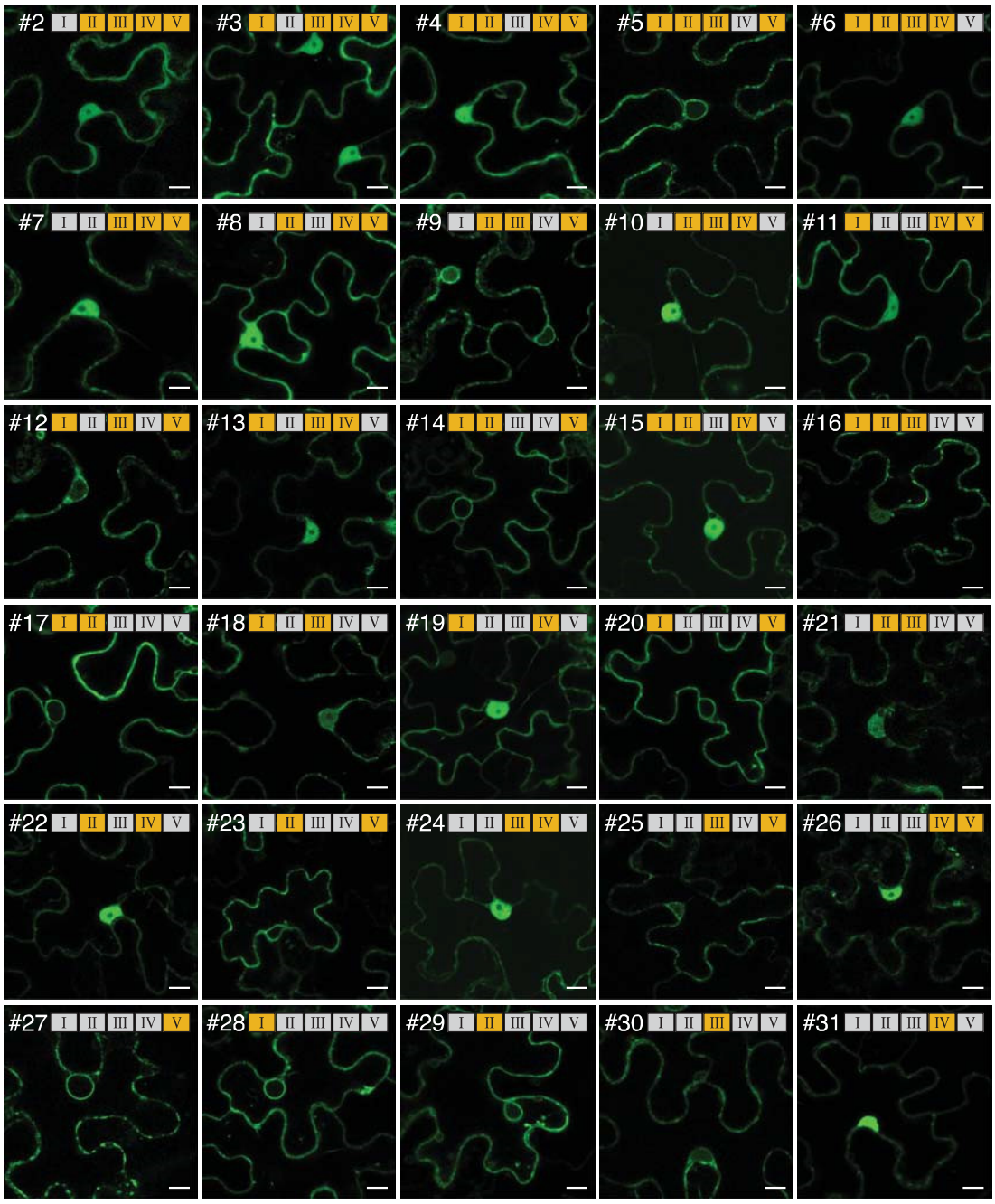

Supplemental Figure S9. Subcellular localization of Bs3-AtYUC8 chimeras. *GFP*-tagged chimeras #2 to #31 were expressed under control of the *35S* promoter in *N. benthamiana* leaves via *Agrobacterium*-mediated transient transformation. Leaf discs for microscopic investigation were harvested at 30 hours post infiltration. Scale bar = 10 μm. The composition of each chimera is shown schematically in the upper part of each microscopic image. The five Bs3/AtYUC8-derived protein segments are designated with roman numerals. Yellow and grey boxes represent protein segments derived from Bs3 or AtYUC8, respectively.

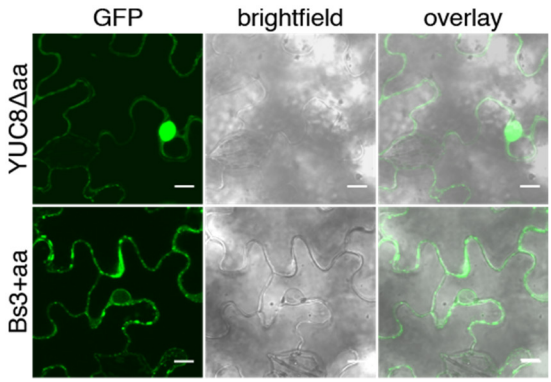

Supplemental Figure S10. AtYUC8Δaa and Bs3+aa show altered subcellular localization compared to AtYUC8 and Bs3 (Figure 7). *GFP*-tagged *AtYUC8Δaa* and *Bs3+aa* were expressed under transcriptional control of the cauliflower mosaic virus *35S* promoter in *N.benthamiana* via *Agrobacterium*-mediated transient transformation. Leaf discs for microscopy were harvested with a cork borer 30 hpi. Pictures show GFP fluorescence (left), brightfield (center) and image overlay. Scale bar = 10 μm

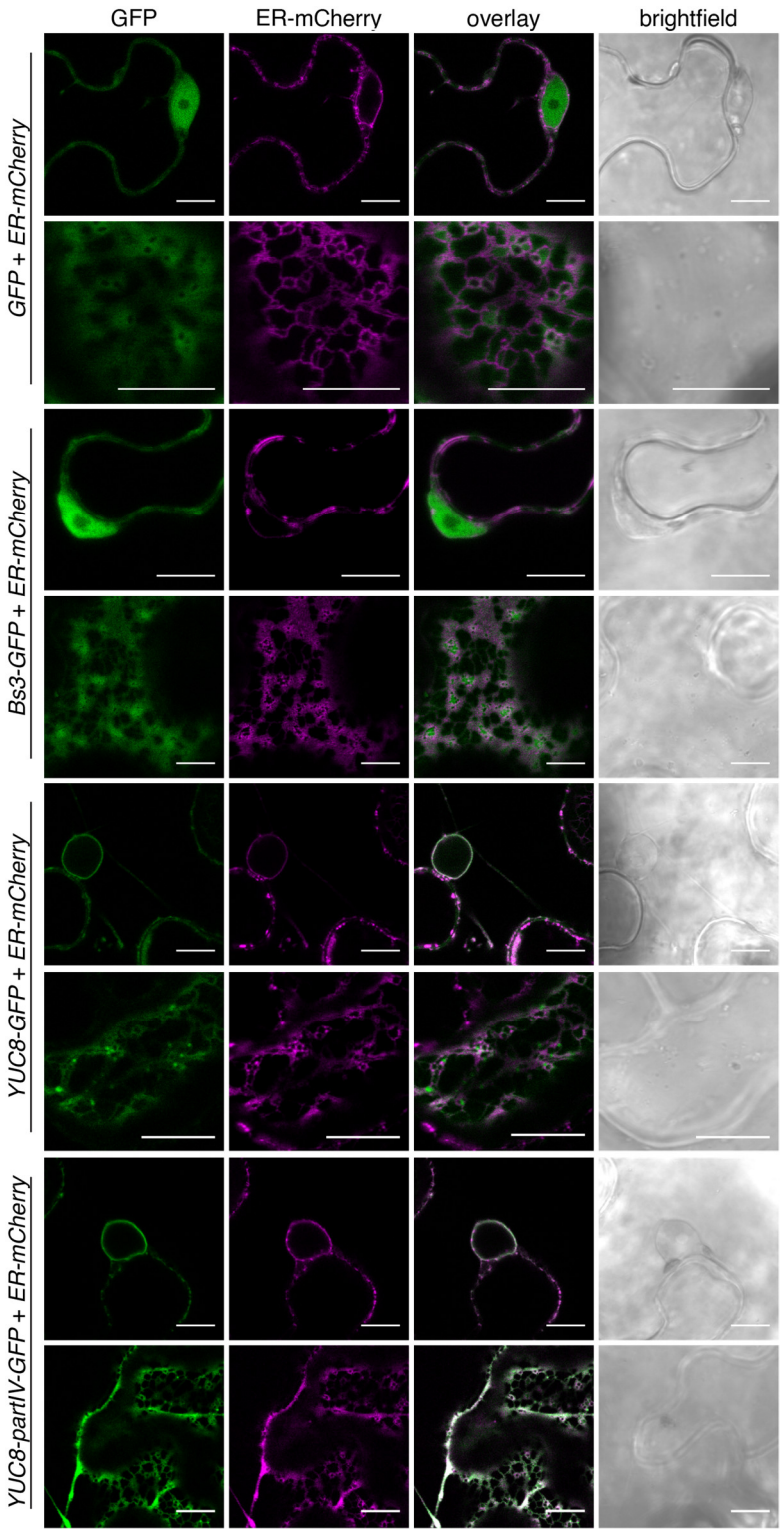

Supplemental Figure S11. Bs3 is located to nucleus and cytoplasm while AtYUC8 is anchored to the ER. GFP tagged Bs3, GFP, AtYUC8 and AtYUC8-partIV were co-expressed with mCherry-HDEL (ER targeted) under transcriptional control of the cauliflower mosaic virus *35S* promoter in *N. benthamiana* via *Agrobacterium*-mediated transient transformation. Leaf discs for microscopy were harvested with a cork borer 30 hpi. Pictures show GFP fluorescence, mCherry fluorescence, overlay of GFP and mCherry and brightfield. Scale bar = 10 μM.

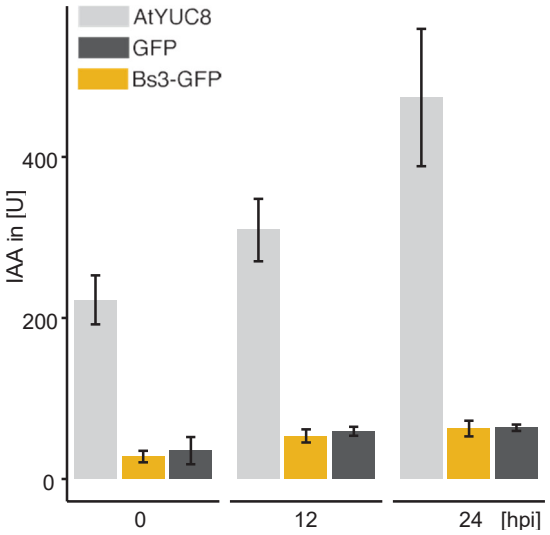

Supplemental Figure S12. Indole-3-acetic acid (IAA) levels in leaves at timepoint 0 indicate auxin production in *Agrobacterium*. *35S*-driven *Bs3-GFP*, *AtYUC8-GFP* and *GFP* were expressed in *N. benthamiana* via *Agrobacterium*-mediated transient transformation. 100 mg of leaf material were harvested at indicated time points. IAA was measured by GC-MS. Bars indicate mean of three replicates +/- sd. hpi = hours post infiltration, U = units

2.1.2 Exchange of part II.B causes loss of function

During the shuffling experiments with 32 chimeras (see Figure 6.3 for composition of all chimeras) we identified parts of Bs3 and AtYUC8 that are exchangeable between the two proteins without loss of function (Krönauer et al., 2019). One open question regarding the chimeric proteins was, why part II is not exchangeable despite its high similarity within Bs3 and AtYUC8. Part II was not exchangeable even though it comprises only 60 aa of which 40 (= 67%) are identical in Bs3 and AtYUC8. By contrast, part III, which is 125 amino acids long and contains 77 identical aa (= 62%), can be exchanged with Bs3 without loss of function. To narrow down the stretch of amino acids that are responsible for loss of function, part II was subdivided into two parts, designated as part II.A and part II.B. Four chimeras, designated as #34-37, were created (Figure 2.1 A) and tested via *35S* promoter driven, transient expression in *N. benthamiana*. Two of the four chimeras, #35 and #36, were functional and caused HR or curly leaves, respectively (Figure 2.1 B and C). Chimeras #34 and #37 were non-functional. In summary, part II.A is exchangeable while part II.B cannot be exchanged even though the alignment of these amino acid stretches shows that there are only 10 different amino acids (Figure 2.1 A).

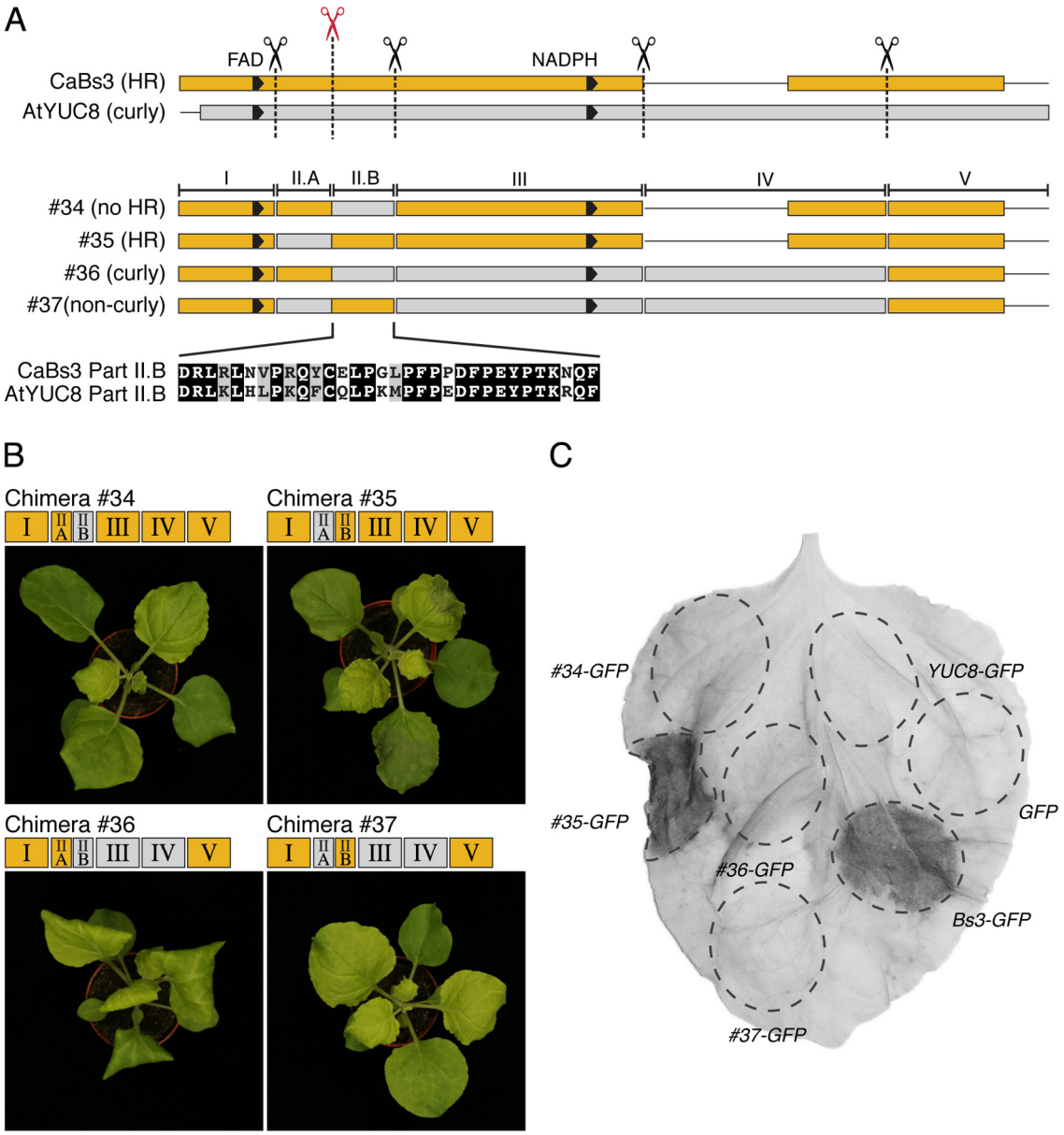

Figure 2.1 Part II.B in Bs3 and AtYUC8 is not exchangeable without loss of function. A) Schematic alignment of Bs3, AtYUC8 and the Bs3-AtYUC8 chimeras #34, #35, #36 and #37, in which Part II was subdivided to create Part II.A and Part II.B. Bs3 derived parts are depicted in yellow, AtYUC8 derived parts are depicted in grey. FAD and NADPH binding site are depicted as black arrows. Gaps are indicated by black lines. Scissor symbols indicate cutting points. The red Scissor indicates the split point within part II. The amino acids that comprise part II.B of Bs3 and AtYUC8 are shown below the scheme. Alignment was done with CLC main Workbench. Identical amino acids (black background) and similar amino acids (grey background) were defined using Boxshade. B) Full leaves of *N. benthamiana* plants were agroinfiltrated with chimeras #34-#37. Pictures were taken at 3 dpi. The composition of each chimera is shown schematically above each picture. The five parts are numbered with roman numerals. Yellow boxes represent sequence parts of Bs3. Grey boxes represent sequence parts of YUC8. C) *35S*-driven chimeras #34-#37 were expressed in *N. benthamiana* via *Agrobacterium*. Picture was taken at 3 dpi. The leaf was cleared with ethanol to visualize HR. Dashed lines mark the infiltrated areas. The HR is visible as dark spots.

2.2 Bs3 expression in yeast, bacteria and human cells

FMOs are present in all phyla studied so far. This raised the question if Bs3 is functional in other organisms than plants. Functionality of Bs3 in heterologous systems would be an interesting feature and open new options to study Bs3-triggered HR. In the course of this work, Bs3 expression and subsequent phenotypic changes were studied in bacteria, yeast and human cell culture.

2.2.1 *Bs3* expression in *E. coli*

In order to produce Bs3 protein for biochemical assays, the expression of *Bs3* in *E. coli* was required. The *Bs3* coding sequence (CDS) and two sequences encoding the Bs3 mutant derivatives $Bs3_{G41A}$ and $Bs3_{S211A}$ were cloned into the pET-53-DEST expression vector downstream of a T7 promoter. The constructs were transformed into *E. coli* Rosetta 2 containing an IPTG inducible T7 polymerase gene (see Table 4.1) and plated onto LB Agar medium without IPTG. After incubation at room temperature for two days, colonies of bacteria transformed with *Bs3* are lower in number and smaller compared to colonies formed by bacteria transformed with $Bs3_{G41A}$ or $Bs3_{S211A}$ (Figure 2.2). Remarkably, after incubation at 37°C over night, colonies of strains carrying *Bs3* are phenotypically similar to those carrying mutant *Bs3* derivatives and can be used for inoculation of preparatory cultures for protein expression. This obvious growth defect of *Bs3* containing cells, indicates the presence of background expression levels of *Bs3* that affect *E. coli* growth and survival in a temperature dependent manner.

2.2.2 *Bs3* expression in *S. cerevisiae* and *P. pastoris*

Interestingly, Bs3 not only triggers HR in plants but also causes a growth defect in yeast (see section 2.3.4, Piprek unpublished, von Roepenack Lahaye personal communication, Schiel, 2015, Figure 2.3). For expression in *Saccharomyces cerevisiae*, *Bs3* and *Bs3* mutant derivatives were cloned into the pYES-DEST-52 expression vector downstream of a galactose inducible promoter (*pGAL1*). Subsequently, strains containing either *Bs3* or a *Bs3* mutant derivative were grown either on repressing or inducing medium. No yeast colonies of strains carrying *Bs3* are visible after drop-out of cultures on solid inducing medium. (Figure 2.3 A).

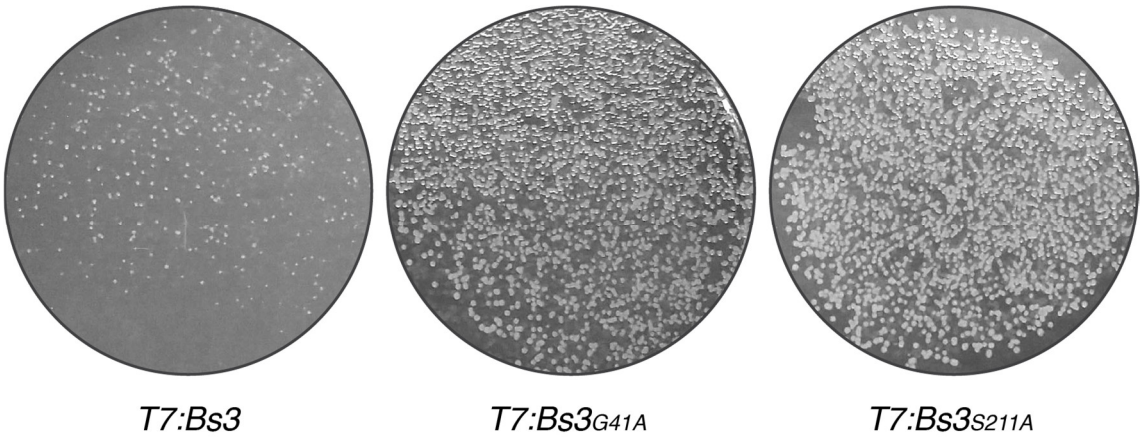

Figure 2.2 Presence of *T7:Bs3* impairs growth of *E. coli* at room temperature. *E. coli* Rosetta 2 were transformed with pET-53-DEST vectors containing either *Bs3*, $Bs3_{G41A}$ or $Bs3_{S211A}$ under control of the *T7* promoter and plated on LB Agar plates without inducing IPTG. Plates were incubated at room temperature for two days.

However, slow growth is observed when Bs3 expressing yeast is grown in liquid medium (Bs3 manuscript, Figure 2.4 B). Furthermore, bud formation of induced cultures can be observed (Figure 2.3 B) which indicates proceeding growth. Consequently, *Bs3* probably does not trigger cell death but rather causes a growth defect in yeast. Interestingly, the vacuole of yeast cells expressing *Bs3* is enlarged compared to yeast expressing $Bs3_{S211A}$ or control (Figure 2.3).

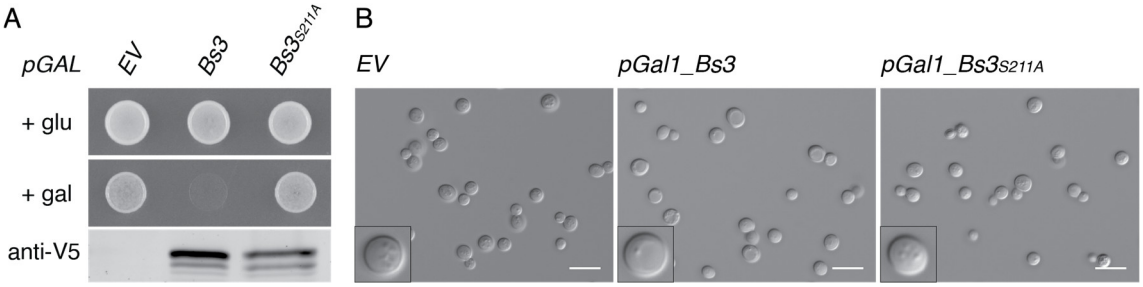

Figure 2.3 *Bs3* expression impairs yeast growth. A) *S. cerevisiae* (BY4742) carrying the indicated constructs under control of the inducible *Gal1* promoter was dropped onto SD plates containing either glucose (repressing) or galactose (activating). Pictures were taken after two days of incubation at 28°C. Protein expression was monitored in liquid culture via an anti-V5 Western Blot at 8 hpi. B) *S. cerevisiae* (BY4742) carrying the indicated constructs was grown in liquid culture containing galactose (inducing) for 6 hours. Scale bar = 10 μm. Inset pictures show a magnified representative cell.

The fission yeast *Pichia pastoris* is an established host for recombinant protein expression. To explore the possibility of large scale *Bs3* expression in yeast, sequences encoding Bs3 with either 6x-histidine (6xhis) or glutathione S-transferase (GST) tag, were cloned into the pPICZ expression vector with

methanol inducible promoter and transformed into *P. pastoris*. Single transformed yeast colonies were subsequently inoculated into non-inducing liquid medium and grown for 20 hours at 28°C. Absorption measurements at 600 nm reveal, that growth of yeast strains carrying *6xhis-Bs3* was strongly reduced, while strains carrying *GST-Bs3* showed similar growth compared to empty vector control (Figure 2.4 A). This is an indication for small levels of *Bs3* expression under non-inducing conditions, which seem to be sufficient to cause a growth defect. Furthermore, fusion of the GST-tag to Bs3 appears to impair either production or function of Bs3 and should be considered carefully in future experiments.

To test if temperature influences Bs3 function, yeast strains carrying either *Bs3*, $Bs3_{S211A}$ or the empty vector under control of a galactose inducible promoter were inoculated in inducing medium and incubated at 20, 28 or 37°C for 24 hours. Yeast growth of strains expressing *Bs3* is most severely impaired at 20°C while growth is less reduced at 28°C and similar to the empty vector control at 37°C (Figure 2.4 B). This indicates that either *Bs3* expression or Bs3 function is impaired at 37°C. This is in line with the observation that *E. coli* Rosetta strains only show a Bs3 induced growth defect after transformation when grown at room temperature but not at 37°C (see section 2.2.1).

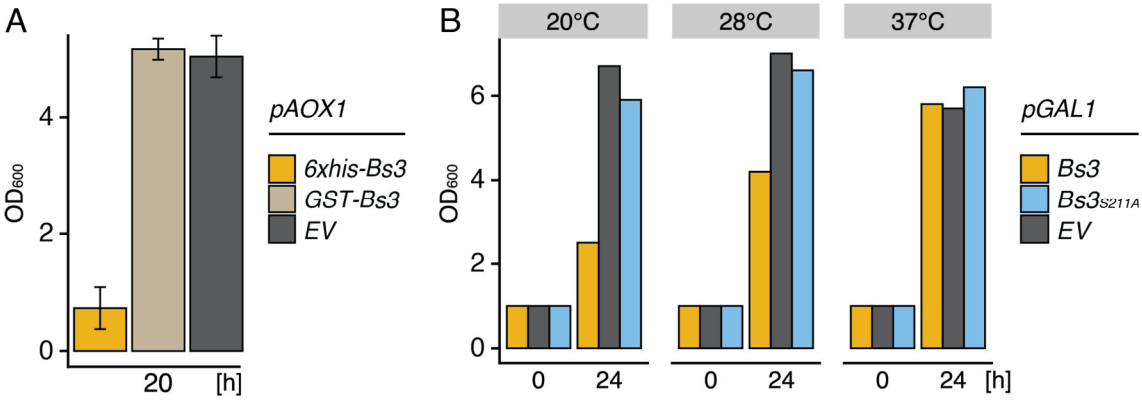

Figure 2.4 Fusion of a GST-tag and high temperature disturb Bs3 function A) *P. pastoris* (GS115) was transformed with pPICZ containing either *6xhis-Bs3* or *GST-Bs3* under control of the methanol inducible *AOX1* promoter (*pAOX1*) The empty vector (*EV*) was used as control. Four colonies were picked for each sample and grown in non-inducing medium. The OD_{600} was measured after 20 hours. B) *S. cerevisiae* (BY4742) strains were transformed with pYES-DEST-52 constructs containing either *Bs3* or $Bs3_{S211A}$ under control of the galactose inducible *GAL1* promoter (*pGAL1*). The strains were grown over night in glucose containing (repressing) medium, diluted to OD_{600} = 1 in galactose containing medium (inducing) and grown at either 20, 28 or 37°C. The OD_{600} was recorded after 24 hours.

2.2.3 *Bs3* expression in human cell culture

The executor *R* gene *Xa10* from rice (*Oryza sativa*) is transcriptionally activated by the TALE AvrXa10. Apart from its HR triggering function in plants, Xa10 is described to induce calcium depletion and subsequent cell death in the endoplasmic reticulum of HeLa cells (Tian et al., 2014). Since Bs3 does not only trigger HR in plants but also induces a growth defect in bacteria and yeast, we wondered if *Bs3* expression also affects human cells. Therefore, the *Bs3* CDS was cloned into a pVAX vector and expressed under control of the human elongation factor-1 alpha promoter (EF-1) promoter (Figure 2.5 A). *Xa10* and *GFP* served as positive and negative control, respectively. HEK-293T cells were transfected with *Bs3-GFP*, *Xa10-GFP* and *GFP* using the FuGENE reagent.

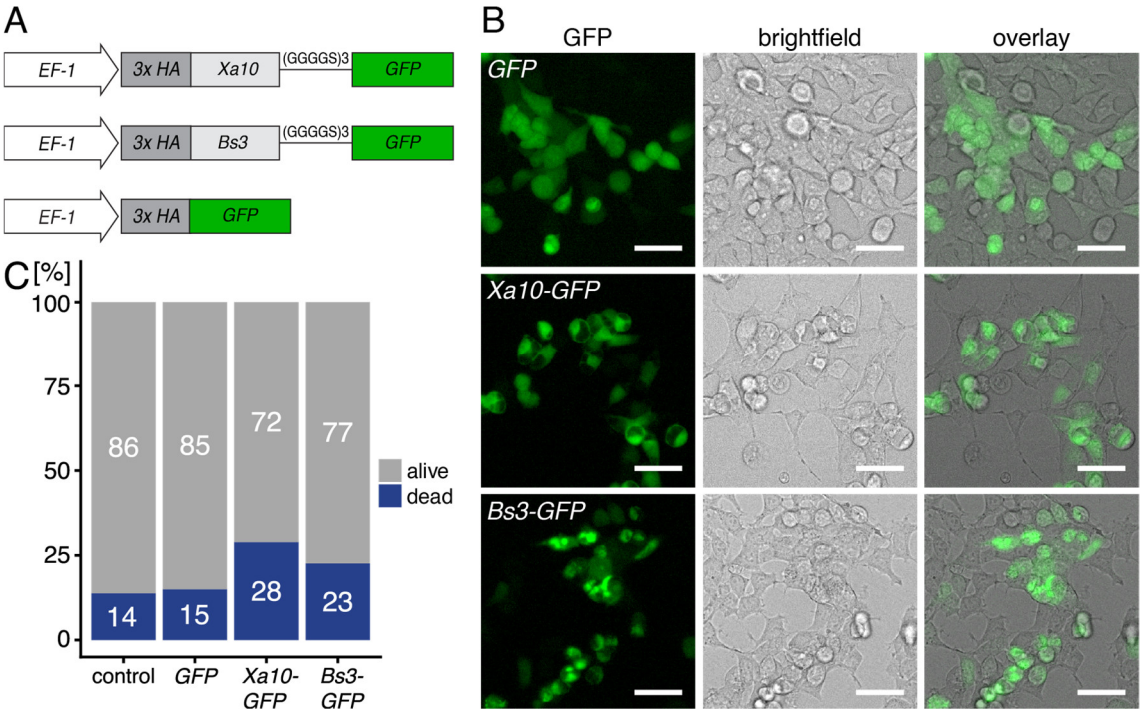

Figure 2.5 *Bs3* expression and localization in human cells. A) Scheme of the constructs that were cloned for the expression in human cells. *EF-1* = Human elongation factor-1 alpha promoter, HA = Human influenza hemagglutinin tag, GGGGS = sequence encoding a glycine/serine linker B) The constructs shown in A were transfected into HEK293T cells using FuGENE. Pictures were taken 48 hours post transfection with a Leica DMI300 epifluorescence microscope. Scale bar = 20 μM C) Trypan blue staining of HEK293T cells expressing either *Bs3-GFP*, *Xa10-GFP* or *GFP* compared to transfection control. Cells were detached, mixed 1:1 with trypan blue solution and transferred to a Neubauer chamber. Blue (dead) and white (viable) cells were counted.

Fluorescence signal in cells expressing only *GFP* was visible in the cytoplasm and nucleus. Xa10-GFP derived fluorescence is in accordance with its described localization to the ER (Figure 2.5 B, Tian et al., 2014). While Bs3 is

localized to the cytoplasm and nucleus in plants, localization is clearly different in HEK-293T cells. The spotty appearance of Bs3-GFP is reminiscent of mitochondrial localization (Figure 2.5 B). However, colocalization studies with mitochondrial markers are necessary to confirm this assumption.

A preliminary experiment was done to check if Bs3 would cause cell death in HEK-293T cells. Cells expressing *Bs3-GFP*, *Xa10-GFP*, or *GFP*, and a transfection control were stained with trypan blue to evaluate cell viability. With 28% and 23%, respectively, the number of dead cells in cultures expressing *Xa10-GFP* and *Bs3-GFP* was slightly increased compared to *GFP* and transfection control (Figure 2.5 C). This indicates, that Bs3 also affects human cells. In follow up experiments, transfection efficiency and temperature should be considered.

2.3 Biochemical characterization of Bs3

2.3.1 Protein purification of Bs3 and $Bs3_{S211A}$

The purification of native Bs3 protein and subsequent biochemical assays were a major goal of this PhD thesis. To optimize protein purification, several vectors and expression conditions were tested (see section 4.5). Despite the high similarity of Bs3 compared to the previously purified AtYUC6 (Dai et al., 2013), some protein characteristics which are relevant for purification are different. For example, the isoelectric point for YUC is 9.18 while it is only 5.82 for Bs3 (Table 2.1). Consequently, purification methods were based on the established protocol for AtYUC6 (Dai et al., 2013) and stepwise optimized for purification of Bs3. Major differences in buffer composition of Bs3 compared to AtYUC6 are the different glycerol content, which is 10% for Bs3 compared to 30% for YUC6, and low or no salt in Bs3 purification buffers, while AtYUC6 is purified with high amounts (0.5 M) of sodium chloride.

Table 2.1: NQN-Bs3 protein statistics. Calculations and predictions were done with the CLC Main Workbench 8.0.1; Pi = isoelectric point, ε 280 = extinction coefficient at 280 nm, Da = Dalton

PROTEIN	LENGTH (aa)	WEIGHT (Da)	PI	ε 280 (M-1 cm-1)
6xhis-Bs3	366	40224	5.82	53340
6xhis-NQN-Bs3	348	38368	5.61	52060
6xhis-NQN-Bs3S211A	348	38352	5.61	52060
6xhis-AtYUC6	441	49257	9.18	57040

E. coli cultures expressing *AtYUC8* are incubated for 48 hours after induction with IPTG. Notably, prolonged incubation of *Bs3* expression cultures after induction resulted in insoluble protein and best purification results were achieved with incubation times of less than three hours after induction. A major improvement of solubility of Bs3 was achieved by the deletion of amino acids derived from the recombination site of the Gateway compatible pET-53-DEST vector and of the first two methionines of the Bs3 sequence, finally resulting in the protein designated as NQN-Bs3, which is reduced by 18 amino acids and approximately two kilodalton (kDa) compared to the protein derived from the original vector (Table 2.1). Finally, supplementation of the lysis buffer with FAD is required to achieve higher amounts of active protein.

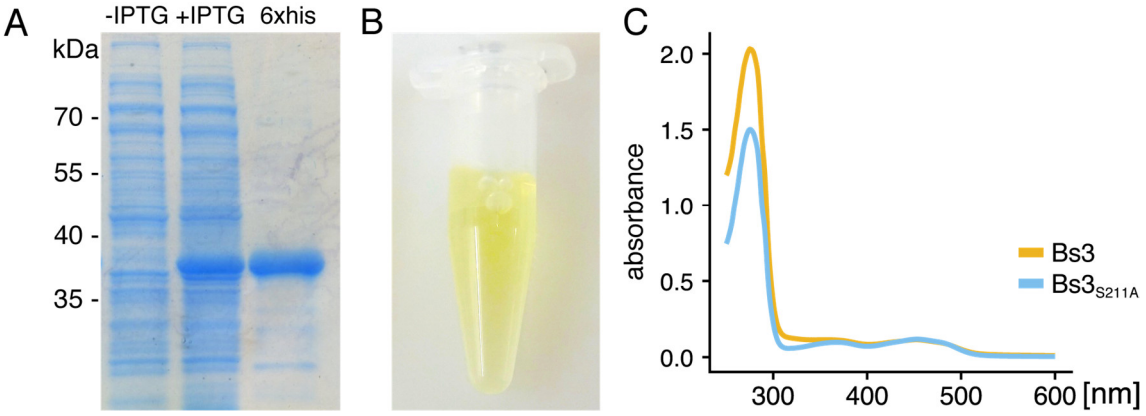

Figure 2.6 Native Bs3 protein is bright yellow due to the bound FAD cofactor. A) Coomassie stained denaturing polyacrylamide gel showing total protein extracts of *E. coli* Rosetta carrying pET-53-DEST_6xhis-Bs3 before (-) and after (+) induction with IPTG and after affinity purification (6xhis). B) Bs3 protein after affinity purification C) UV/vis spectra of Bs3 (yellow) and $Bs3_{S211A}$ (blue).

After purification, the Bs3 protein is bright yellow (Figure 2.6 B) and the UV/vis spectrum shows peaks at 370 and 450 nm (Figure 2.6 C), that indicate a bound FAD cofactor. Comparison of UV/vis spectra measured from two representative batches of Bs3 and $Bs3_{S211A}$ protein shows, that absorption at 280 nm is lower for $Bs3_{S211A}$ while peak height is similar at 450 nm (Figure 2.6 B). This indicates that an equal amount of Bs3 protein, measured from the tyrosine backbones at 280 nm, contains less FAD compared to $Bs3_{S211A}$. Given that a bound FAD cofactor is needed for enzymatic function, it can be assumed that a lower fraction of Bs3 compared to $Bs3_{S211A}$ is in the active state after purification. As a consequence, protein amounts used for activity measurements should be calculated on basis of the absorption at 450 nm.

2.3.2 Bs3 produces more H_2O_2 than AtYUC6 *in vitro*

It is known that many FMOs, besides substrate conversion, produce H_2O_2 to some extent. The amount of produced H_2O_2 is dependent on protein stability, cofactor and substrate availability. In order to evaluate the possibility that H_2O_2 accumulation triggers cell death, we investigated the amount of H_2O_2 produced by Bs3 compared to AtYUC6 and to what extent the availability of the different cofactors NADH and NADPH influences Bs3 or AtYUC6 activity. Therefore, 6xhis-Bs3 and 6xhis-AtYUC6 were purified and mixed with buffer containing either NADH or NADPH and incubated at room temperature. The amount of evolved H_2O_2 during the reactions was measured via Amplex Red (Figure 2.7). Only background levels of H_2O_2 are observed in the absence of NADH or NADPH. In the presence of NADH or NADPH Bs3 produces considerably more H_2O_2 compared to AtYUC6 or buffer control. Interestingly, H_2O_2 contents in AtYUC6 containing samples are decreased compared to buffer control, indicating either a putative H_2O_2 scavenging or a cofactor stabilizing effect of AtYUC6.

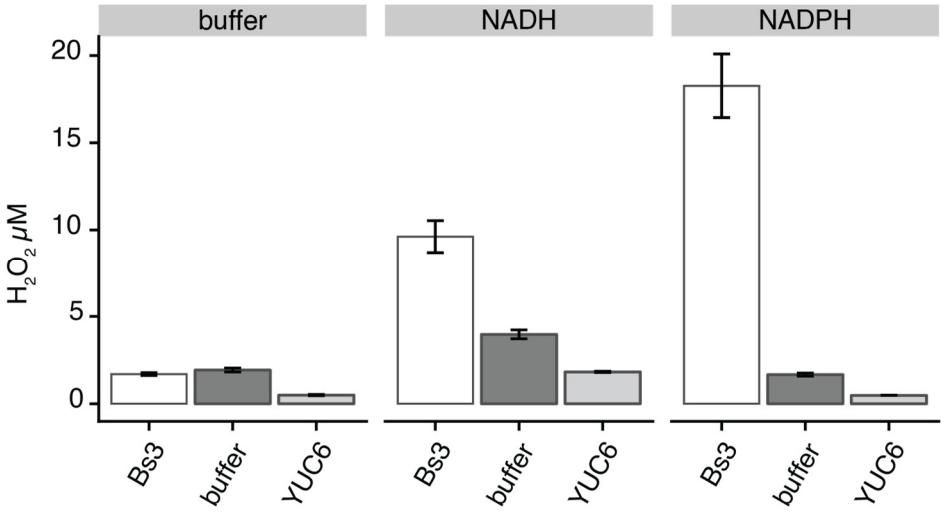

Figure 2.7 Bs3 produces more H_2O_2 than AtYUC6 *in vitro*. Buffer containing 100 μM NADH or NADPH was mixed with 1 μM of Bs3, AtYUC6 or an equal volume of buffer and incubated for 20 min at room temperature. The H_2O_2 content was determined via Amplex Red.

2.3.3 Bs3 is functional with C-terminal redox sensor fusion

One possible way to analyse the intracellular redox state in plants are redox sensitive fluorophores like roGFP2 and HyPer. Redox sensitivity of roGFP2 is based on two cysteines that are introduced into the GFP sequence and have the ability to form a disulfide bridge under oxidizing conditions (Hanson et al.,

2004). Redox sensitivity of HyPer is based on the combination of YFP with the regulatory domain of the H_2O_2 transcription factor OxyR from *E. coli* (Belousov et al., 2006). In both fluorophores, a different oxidation state leads to a change of protein conformation and consequently to a change in emission spectra of the fluorophore, which can be observed via fluorometric measurements. The additionally available fusion constructs of roGFP2 with human glutaredoxin 1 (GRX1) and yeast oxidase receptor peroxidase 1 (Orp1) ensure rapid equilibration with the glutathione pool and higher sensitivity towards H_2O_2, respectively.

To gain specificity for ROS produced by Bs3, translational fusions of the redox sensitive fluorophores to Bs3 were created. Since the described redox sensors have slightly different characteristics, they were all tested to find a suitable candidate to measure Bs3 induced intracellular redox changes. The first experiment was to confirm the functionality of Bs3-roGFP, Bs3-HyPer, Bs3-GRX1-roGFP2 and Bs3-roGFP2-Orp constructs (Figure 2.8 A). The fusion constructs were expressed in *N. benthamiana* via *Agrobacterium* mediated transient transformation. All tested constructs triggered HR, which shows, that the redox sensitive fluorophores do not impair Bs3 function (Figure 2.8 B).

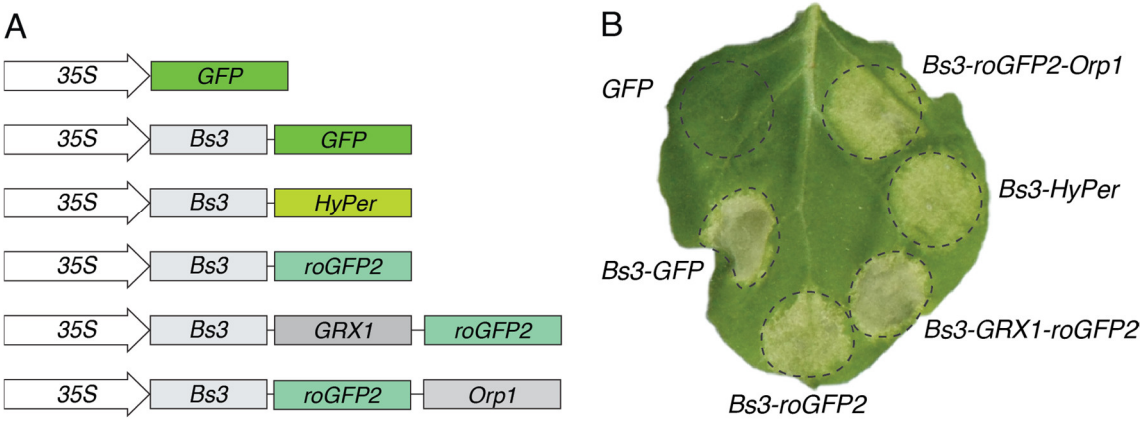

Figure 2.8 Fusion with redox sensitive fluorophores does not disturb Bs3 function. A) Scheme of the constructs that were cloned for transient expression *in planta*. GRX1 = human glutaredoxin 1, Orp1 = yeast oxidase receptor peroxidase 1, GFP = green fluorescent protein, roGFP2 = reduction-oxidation sensitive green fluorescent protein 2, HyPer = hydrogen peroxide sensing circularly permuted yellow fluorescent protein B) Indicated constructs were expressed under control of the 35S promoter (*35S*) in *N. benthamiana* via *Agrobacterium*-mediated transient transformation. Pictures were taken 4 days post infiltration. Dashed lines mark the infiltrated area.

2.3.4 Bs3 manuscript

The manuscript "**Bs3 is an FMO that triggers cell death in plants and impairs growth in yeast**" comprising chapter 2.3.4 is currently in preparation

Authors: Christina Krönauer, David Ballou, Yunde Zhao, Thomas Lahaye

Christina Krönauer (1st author) planned and performed most of the experiments, analysed the data, created the figures and wrote the manuscript. **David Ballou** and **Yunde Zhao** (2nd and 3rd author) conducted and analysed the stopped flow experiments. **Thomas Lahaye** (corresponding author) supervised the project and wrote the manuscript.

Bs3 is an FMO that triggers cell death in plants and impairs growth in yeast

Authors: Christina Krönauer, David Ballou, Yunde Zhao, Thomas Lahaye

Abstract

Bs3 is activated in pepper (*Capsicum annum)* via the transcription activator like effector AvrBs3, coming from a bacterial pathogen of the genus *Xanthomonas.* Bs3 triggers a hypersensitive response (HR) in plants which confers resistance against these bacterial pathogens. Bs3 shows no similarity to any other executor R protein and its molecular mechanism has remained elusive. However, it has high sequence similarity to flavin-containing monooxygenases (FMOs). In this study, we illustrate that *Bs3* expression does not only induce HR in plants, but also impairs growth in yeast. Since FMOs produce H_2O_2 as a side product of their enzymatic reactions, we wanted to investigate if Bs3 causes cell death by the production of H_2O_2. To study the enzymatic mechanism, we purified native Bs3 protein and measured Bs3-dependent NADPH oxidation and production of H_2O_2 *in vitro.* Previously created Bs3 derivatives harbouring mutations within their NADPH binding site do not trigger HR in plants or growth arrest in yeast. Herein, we describe a Bs3 derivative exchanging a serine to an alanine at the 211th residue, within the NADPH binding site, that does not cause HR but still has NADPH oxidase activity *in vitro*. Analysis of the intracellular oxidation state with the redox sensor roGFP2 shows that expression of $Bs3_{S211A}$ causes a similar increase of oxidation state compared to *Bs3* expression, even though it does not induce cell death. This indicates that H_2O_2 production of Bs3 is not sufficient to trigger HR. The results of our *in planta* experiments are corresponding to the observation of a stable C4a-intermediate, which thus indicates that Bs3 HR is probably triggered by catalysis of a so far unknown substrate.

Introduction

The bacterial pathogen *Xanthomonas euvesicatoria* elicits bacterial spot disease in pepper (*Capsicum annuum*) and tomato (*Solanum lycopersicum*), and therefore causes significant economic losses in production areas (Potnis et al., 2015). During infection, *X. euvesicatoria* injects effector proteins into the plant cell, that act as virulence factors and promote disease. Transcription activator like effectors (TALEs) are one class of bacterial effectors present in many xanthomonads that, upon injection into host cells, translocate to the plant nucleus where they transcriptionally activate host gene expression to promote disease. Plants evolved a class of resistance (*R*) genes, so called executor *R* genes, that are transcriptionally activated by specific TALEs and execute an immune reaction. The pepper *R* gene *Bs3* is transcriptionally activated by the corresponding TALE AvrBs3. Expression of Bs3 triggers a fast and local cell death reaction, known as the hypersensitive response (HR). This limits spread of the pathogen, and thus confers resistance against AvrBs3 carrying *X. euvesicatoria* strains. In contrast to other cell death activating R proteins, Bs3 belongs to the enzyme family of flavin-containing monooxygenases (FMOs), and shows around 60% sequence similarity to the YUCCA (YUC) family of FMOs (Krönauer et al., 2019). YUCs produce indole-3-acetic acid (IAA) from indole-3-pyruvate (IPA) via oxidative decarboxylation and are the rate-limiting enzymes of auxin biosynthesis in plants (Mashiguchi et al., 2011; Dai et al., 2013). During the FMO enzymatic cycle, reduction of the bound FAD cofactor by NADPH and binding of molecular oxygen results in a C4a-intermediate, which is ready to oxygenize suitable substrates. If no substrate is available, the C4a-intermediate breaks down without substrate oxygenation, a process referred to as the "uncoupled reaction", where reduction equivalents are released as H_2O_2 (Alfieri et al., 2008). The C4a stability in the absence of a substrate varies substantially among different FMOs and many FMOs produce considerable amounts of H_2O_2 (Thotsaporn et al., 2011; Siddens et al., 2014). While it is unclear if the production of H_2O_2 by FMOs is an undesired waste of NADPH, or if it potentially serves a biological function, the role of H_2O_2 as a signalling molecule of plant immune reactions is well established. Due to its comparably high stability within the cell, and its ability to modify the cysteine-thiol side chains of proteins to sulfenic acid, thereby creating a redox relay, H_2O_2 can act as signalling molecule (Marinho et al., 2014; Waszczak et al., 2014).

However, high concentrations of H_2O_2 are known to trigger autophagy and cell death (Montillet et al., 2005; Shibata et al., 2013).

Here, we show that Bs3 does not only trigger HR in plants, but also inhibits growth in yeast. In order to clarify the role of H_2O_2 in Bs3 triggered reactions, we analysed recombinant Bs3 protein, and conducted *in vivo* redox reporter studies. Our results are the first biochemical characterization of the enzymatic function of an executor R protein.

Results

Bs3 HR correlates with accumulation of H_2O_2 *in planta*

Despite its high similarity to YUCCA (YUC) FMOs, Bs3 does not produce auxin, and no substrate is known thus far (Krönauer et al., 2019). Since H_2O_2 causes oxidative damage at high concentrations, and H_2O_2 signalling is a hallmark of plant immune reactions, we hypothesized that Bs3 does not bind any substrate, but rather triggers HR by the excessive production of H_2O_2. In line with this hypothesis, accumulation of reactive oxygen species (ROS) can be observed in pepper plants containing the *Bs3* gene (ECW 123) upon infection with AvrBs3 carrying *Xanthomonas* strains (Fig. 1). Similarly, expression of Bs3 under control of the constitutive Cauliflower Mosaic Virus *35S* (*35S*) promoter caused ROS accumulation in *N. benthamiana* leaves (Krönauer et al., Fig. S1). Accumulation of ROS is known to be a general hallmark of plant stress and cell death reactions, which is illustrated in the accumulation of ROS via the HR activated by the NLR-type R protein pepper Bs2 (Tai et al., 1999, Fig 1). Therefore, it remains to be delineated if this ROS is being directly produced by Bs3, or if the Bs3 HR is activating other proteins that cause an increase in ROS.

Bs3$_{S211A}$ does not trigger HR in plants

FMO function is dependent on cofactor binding, and the mutation of the conserved glycines within the NADPH binding site has been shown to cause loss of function (Hou et al., 2011). Other studies uncovered mutations within FMOs that lead to derivatives with high uncoupling activity that produced increased amounts of H_2O_2. With the aim to modify putative H_2O_2 production of Bs3, we were inspired by a study on the *Aspergillus fumigatus* FMO SidA, where a specific

serine to alanine mutation within the NADPH binding site (GxGxSG) is described to preserve FMO activity, but alters the stability of the protein-NADPH interaction (Shirey et al., 2013). In a similar manner, we mutated the corresponding serine at position 211 in Bs3 to alanine, in order to create a Bs3 derivative which could conceivably create more H_2O_2. To test functionality of this mutant derivative, we expressed *35S*-driven *Bs3$_{S211A}$-GFP* alongside *Bs3-GFP* in *N. benthamiana* leaves via *Agrobacterium* mediated transient transformation (Fig. 1). We found that *Bs3* but not *Bs3$_{S211A}$* triggered HR in *N. benthamiana* leaves (Fig. 1). Western blot analysis showed that Bs3 and Bs3$_{S211A}$ fusion proteins were present in similar amounts suggesting that the S211A mutation does not cause reduced protein stability (Fig. 1). Therefore, the mutation of the serine within the NADPH binding site to an alanine resulted in a Bs3 derivative that does not trigger HR *in planta*.

Bs3 but not *Bs3$_{S211A}$* causes growth arrest in yeast

To gain further insights into the function of Bs3, we were interested in the effect of Bs3 expression in yeast. Therefore, we cloned *Bs3, Bs3$_{S211A}$* and the mutant derivatives *Bs3$_{G41A}$* and *Bs3$_{G209A}$*, that carry a mutation within the FAD and NADPH binding site, respectively, which lack an HR *in planta*, (Krönauer et al., 2019), into a yeast expression vector under control of a galactose inducible promoter (*pGAL1*). Transformed yeast was grown in liquid medium and dropped onto either glucose (repressing) or galactose (inducing) containing solid medium (Fig. 2). No colonies are visible after one day for yeast strains expressing wild type *Bs3*, while growth of strains expressing the *Bs3$_{S211A}$* and *Bs3$_{G41A}$* mutant derivatives is similar to the control strain transformed with empty vector (EV). The growth defect caused by *Bs3$_{G209A}$* expression is nearly as strong as that of *Bs3* expressing strains (Fig. 2). To monitor the effect of *Bs3* and its derivatives on yeast in liquid medium, yeast cultures were diluted to a starting OD_{600} of 1 in inducing medium containing galactose. Protein expression was monitored after six hours of incubation in inducing medium (Fig. 2) and yeast growth monitored over three days (Fig. 2). Similar to the growth phenotypes on solid plates, *Bs3* and *Bs3$_{G209A}$* showed reduced growth compared to the control. Interestingly, yeast strains expressing *Bs3* showed no growth arrest or cell death, but had a slower increase in culture density over the period of two days (Fig. 2). The effect of

Bs3$_{G209A}$ on growth was less pronounced than that of *Bs3*, and cultures of yeast strains containing *Bs3*$_{G209A}$ reached similar cell densities to that of control cultures (Fig. 2). The finding that *Bs3* affects yeast growth demonstrates that its function is not limited to the plant kingdom.

Expression and purification of Bs3 and Bs3$_{S211A}$

Since plant immune reactions generally correlate with the production of H_2O_2, it is not possible to clarify if the ROS release during *Bs3*-dependent cell death is produced by Bs3 directly, or if it is simply a consequence of *Bs3*-triggered immune reactions. Thus, we decided to test the potential of Bs3 to produce H_2O_2 by *in vitro* studies. To do so, Bs3 and Bs3$_{S211A}$ were expressed in *E. coli* and soluble Bs3 and Bs3$_{S211A}$ protein was affinity purified with yields of 2 mg per litre of culture (Fig. 3). Due to its homology to YUC proteins, we expected that Bs3 needed a bound FAD for activity. Indeed, supplementation with FAD was necessary to obtain active protein and increased yields. Notably, in contrast to the purification protocol established for YUC6 which uses extraction buffers containing 0.5 M NaCl (Dai et al., 2013), Bs3 purification works best under low sodium chloride conditions ($<$ 100 mM). The purified Bs3 and Bs3$_{S211A}$ proteins were bright yellow and the UV-vis spectra show characteristic peaks similar to FAD. Interestingly, we observed a slight shift of the local maxima of Bs3$_{S211A}$ (at 368 nm and 453 nm) compared to wild type Bs3 (373 and at 448 nm) respectively (Fig. 3). This is consistent with the expected slight structural change of the mutant Bs3$_{S211A}$ compared to wild type Bs3.

Bs3 and Bs3$_{S211A}$ oxidize NADPH and produce H_2O_2 *in vitro*

To measure the NADPH oxidase activity of Bs3 and Bs3$_{S211A}$, we mixed the two proteins with excessive amounts of NADPH and monitored the decrease of NADPH concentration via spectrometric measurements of absorbance at 340 nm. The active protein concentration was calculated from absorption at 450 nm and the extinction coefficient of FAD (ε = 11300 M^{-1} cm^{-1}). At 25°C, we measured an NADPH oxidation activity of 63 nmol/mg*min for Bs3 and 137 nmol/mg*min for Bs3$_{S211A}$ (Table 1, Fig. 4). These findings show that without a substrate, the Bs3$_{S211A}$ mutant has approximately two times higher NADPH oxidase activity

compared to that of the wild type Bs3 protein. This is in line with our expectation that the S to A mutation within the NADPH binding site is destabilizing the C4a-intermediate.

In addition, we tested if the two chemicals Yucasin or Methimazole (MMI), which are known to be competitive inhibitors of YUC function (Nishimura et al., 2014), had an influence on NADPH oxidation by Bs3. Both Yucasin and MMI decrease NADPH oxidation activity of Bs3 and $Bs3_{S211A}$ (Fig. 4), suggesting that the active site of Bs3 and $Bs3_{S211A}$ is accessible by these chemicals. As expected from experiments with YUCs and chemical inhibitors (Nishimura et al., 2014), Yucasin is a stronger inhibitor compared to MMI. In our experiments, Yucasin reduced NADPH oxidation of Bs3 to 5% of its original activity, while 20% oxidase activity remained upon MMI treatment (Fig. 4B). Interestingly, the two chemicals show a much weaker effect on $Bs3_{S211A,}$ which retains 84% and 61% of its activity when treated with MMI or Yucasin, respectively (Fig. 4).

Rapid kinetics reveal the formation of a C4a-intermediate for Bs3

In FMOs, a stable C4a-intermediate is a prerequisite to bind substrate. For AtYUC6, the half-life of the C4a-intermediate was determined to be relatively stable with a half-life of approximately 20 seconds (Dai et al., 2013). Instability of the C4a-intermediate is often observed with increased levels of H_2O_2 that are released during uncoupled reactions. Therefore, an instable C4a intermediate of Bs3 would support our hypothesis of strong NADPH oxidase activity. The Km for NADPH in the absence of any substrate was determined to be ~7 µM (Figure S2). Reduction of Bs3 by NADPH was visible as a decrease in absorbance at 380 and 450 nm (Figure 5). To test stability of the C4a-intermediate, reduced Bs3 was mixed with buffer containing 10% oxygen and the reaction was followed for 14 s. Immediately after mixing of protein and buffer, an intermediate formed with a maximum absorption at 388 nm. Re-oxidation was visible from the increasing peak at 450 nm, and appeared after approximately 6 s (Figure 5). Difference spectra, in which the first spectrum is subtracted from all subsequent spectra were generated for better visibility of the processes. The kinetics of formation and decay of the C4a-intermediate, as well as NADPH oxidation, can be followed in single wavelength traces (Figure 5D). In conclusion, the formation of a relatively stable

Bs3 C4a-intermediate indicates that the protein probably does not only have NADPH oxidase activity, but is also able to bind a substrate.

NADPH oxidase function is not sufficient to cause HR

The plant intracellular environment has been known to differ from an environment created *in vitro*, and we suspect that Bs3 is probably more stable *in* vivo, and might not produce H_2O_2 at high levels. So, to address whether Bs3 functions as an NADPH oxidase *in vivo,* and if this changes the intracellular oxidation state, we utilized the reduction-oxidation-sensitive green fluorescent protein roGFP2 in which two cysteines were introduced into GFP to create redox sensitive fluorophores, which lead to changed fluorescent properties depending on their oxidation state and allow for ratiometric measurements in plant cells (Hanson et al., 2004, Schwarzländer et al., 2008). In order to locate roGFP2 in close proximity to Bs3, we created translational fusions of *Bs3* and the mutant derivatives *Bs3*$_{G41A}$, *Bs3*$_{G209A}$ and *Bs3*$_{S211A}$ to *roGFP2* (Fig. 6). Functionality was tested via *Agrobacterium* mediated expression in *N. benthamiana* leaves. Expression of *Bs3*$_{S211A}$*-roGFP2* or *Bs3*$_{G41A}$*-roGFP2* does not cause HR. Notably, expression of *Bs3*$_{G209A}$*-roGFP2* triggers an HR with less pronounced phenotype compared to the HR caused by Bs3-roGFP2 (Fig. 6). To analyse changes of the intracellular oxidation state caused by Bs3 and its mutant derivatives, the *Bs3-roGFP2* fusions were expressed in *N. benthamiana* leaves and ratiometric analysis of roGFP2 fluorescence was performed by confocal laser scanning microscopy (CLSM) with excitation at 405 and 488 nm (Fig. 7). The ratiometric measurements revealed that roGFP2 showed similar relative fluorescent intensity (RFI) values to Bs3$_{G41A}$-roGFP2, indicating that the fusion of Bs3 derivatives has no impact on roGFP2 fluorescence itself, and that the non-functional Bs3$_{G41A}$ does not change the redox status of roGFP2 (Fig. 7). Interestingly, not only does expression of Bs3 and Bs3$_{G209A}$, both of which activate HR, increase the roGFP2 redox state, but the expression of the non-HR inducing Bs3$_{S211A}$ mutant also increases the roGFP2 redox state (Fig. 7). This conclusively illustrates that, in a similar fashion to the results obtained *in vitro*, Bs3 and Bs3$_{S211A}$ have NADPH oxidase function and most likely produce H_2O_2 *in planta*. Though Bs3$_{S211A}$ displays oxidase activity *in vivo*, it does not cause HR. This indicates that the sole production of H_2O_2 is not sufficient to trigger Bs3 HR.

Discussion

Bs3 is an FMO that triggers HR in plants and growth arrest in yeast

Bs3 is the superior example of an executor *R* gene that triggers HR upon activation by the corresponding TALE. Apart from Bs3, there are four other executor *R* genes that have been cloned thus far: *Bs4C* from pepper and *Xa10*, *Xa23* and *Xa27* from rice *(Zhang et al., 2015).* In contrast to all other executors, Bs3 does not contain potential transmembrane helices, which indicates a distinctly different molecular function. Indeed, Bs3 shows similarity to FMOs and is therefore the only executor that shows homology to a protein class of known function. However, the suggested enzymatic function of Bs3 has so far remained elusive. Our study on Bs3 found that it exhibits the biochemical properties of an FMO with a tightly bound FAD cofactor, and the ability to oxidize NADPH (Fig. 4). As expected, Bs3 activity is dependent on the integrity of the nucleotide binding sites (Fig 1 and Fig 2). Notably, the $Bs3_{G209A}$ mutant does not trigger HR under control of its native promoter and AvrBs3 activation (Krönauer et al., 2019), but it is able to trigger HR when expressed under the control of the *35S* Promoter (Fig. 6 B, C). Similar to the less pronounced phenotype in plants, the effect of $Bs3_{G209A}$ on growth in yeast is less severe than that of *Bs3*. These results confirm the assumption that Bs3 triggers HR via a FAD and NADPH dependent enzymatic reaction and that high protein levels can overcome putative reduction of enzyme activity.

Despite the fact that *Bs3* is only found in *Capsicum* species, and that *Bs3* is specifically activated by *Xanthomonas* strains carrying the TALE AvrBs3, the mechanism that Bs3 uses to trigger cell death seems to be not only exclusive to the plant kingdom. *Bs3* expression not only causes HR in a variety of plants, but also growth arrest in yeast (Fig 1, Fig 2). In case the putative signalling pathway triggered by Bs3, is conserved between plant and yeast, the yeast system could be a valuable tool to study the molecular mechanism in future. Besides Xa10, for which a cell death phenotype was shown in HeLa cells (Tian et al., 2014), Bs3 is the second candidate within the executor R protein family whose function seems not to be limited to the plant kingdom.

H_2O_2 production of Bs3 is not sufficient to trigger HR

Uncoupling ratios in FMOs range from around 4% in YUC6 (Dai et al., 2013) to 60% for hFMO5 (Fiorentini et al., 2016). The resulting production of H_2O_2 for a long time was considered to be detrimental to cellular processes, or at least cost-intensive, and therefore to be avoided during FMO function. By now, the function of H_2O_2 as highly abundant signalling molecule is accepted (Forman et al., 2010; Petrov and Van Breusegem, 2012), however, it is still unknown if the uncoupling reactions of FMOs fulfil any physiological function. Since Bs3 is the only known FMO thus far that triggers HR, a process known to be driven by ROS, we speculated that uncoupling and H_2O_2 production could be the predominant function of Bs3. Seeing as the half-life of FMOs can be reduced by their own H_2O_2 production *in vitro* (Goncalves et al., 2017), an impact on other cellular components is plausible. We envisioned two possible ways in which Bs3 could trigger HR by the production of H_2O_2. Firstly, Bs3 might produce excessive amounts of H_2O_2 that cause oxidative damage to the plant cell. Alternatively, Bs3 produces H_2O_2 as signalling molecule that activates a cascade leading to plant defence and HR. Our *in vitro* results show that NADPH oxidation by Bs3 is rather slow, thus indicating that excessive production of H_2O_2 is unlikely. Furthermore, the $Bs3_{S211A}$ mutant, despite not causing HR *in planta* or growth arrest in yeast, produces even higher amounts of H_2O_2 (Fig 4). In summary, the results of our *in vitro* experiments challenged our hypothesis that H_2O_2 production on its own can be the cause for HR induction. As a matter of course, we were interested in the function of these Bs3 derivatives *in vivo*. Due to the fact that there are multiple sources of H_2O_2 in plant cells, it is challenging to accurately measure small concentrations of H_2O_2, and almost impossible to identify its origin and distinguish Bs3-created H_2O_2 from other ROS within the cell. To circumvent these challenges, we translationally fused *roGFP2* to *Bs3* and its mutant derivatives. The ratiometric CLSM measurements show that not only Bs3 and $Bs3_{G209A}$ which trigger HR, but also the non-functional $Bs3_{S211A}$ increases the RFI of roGFP2 (Fig. 7). Since there is evidence that direct roGFP2 oxidation by H_2O_2 is slow (Winterbourn and Hampton, 2008), and that roGFP2 equilibrates with the glutathione pool (GSH/GSSG) via glutaredoxin (Meyer et al., 2007), we assume that the activity of Bs3 and its derivatives $Bs3_{G209A}$ and $Bs3_{S211A}$ induce the higher oxidation state of roGFP2 by an increase of GSSG concentration within the roGFP2 environment.

Bs3 builds a stable C4a-intermediate

There is evidence to suggest that the degree of uncoupling in FMOs is dependent on the stability of the C4a- intermediate. The finding that $Bs3_{S211A}$ produces more H_2O_2 is in harmony with the previously described finding that the serine within the NADPH binding site is important for stabilization of the C4a-intermediate by the $NADP^+$, which remains bound after reduction of FAD (Shirey et al., 2013). We were interested in the stability of the C4a-intermediate of Bs3 in order to further evaluate the importance of H_2O_2 production in the course of HR induction by Bs3. Our stopped flow analysis revealed that Bs3 builds a stable C4a-intermediate, which indicates that it should be able to bind and convert a substrate. However, it is evident from our Redox reporter experiments, that a certain amount of H_2O_2 is released, which may or may not fulfil a function during cell death progression. While human FMOs convert a broad spectrum of metabolites (Krueger and Williams, 2005), YUCs, which are most similar to Bs3, seem to be substrate specific. Interestingly, both enzymes are inhibited by the same competitive inhibitor Yucasin and one can speculate if the putative structure of a Bs3 substrate should be similar to the 1,2,4-triazole-3(4 *H*)-thione moiety present in Yucasin and essential for the inhibitory function (Tsugafune et al., 2017). The future challenge will be to find the Bs3 substrate and to analyse if the increase in oxidation state is an unavoidable side reaction or if it fulfils a necessary additive function during induction of cell death.

Methods

Plants and growth conditions

N. benthamiana and *Capsicum annuum* (cultivar ECW 1-2-3) plants were grown at 20-24°C at 35-60% humidity with a light intensity of 12,3 klx and 16 hours light/ 8 hours dark cycle. Four to six weeks old plants were used for experiments.

DAB staining

Leaves were vacuum infiltrated with DAB staining solution (10 mM Sodium phosphate, 1 mg/ml Diaminobenzidine Tetrahydrochlorid, 0.1% Tween-20, pH 7.2), incubated at room temperature with gentle shaking for at least 5 hours and subsequently de-stained with 80% ethanol at 60°C.

Plasmid construction

For *in planta* expression, the *Bs3* CDS was assembled with a *35S* promoter and *eGFP* into the *LIIa* expression vector via Golden Gate cloning (Binder et al., 2013). The serine to alanine mutation was introduced by PCR (PrimerFW: P-GCCGGGATCGA-TATCTCACTTG PrimerREV: ATTGCCACAGCCAA-CCGC). For bacterial expression, the Bs3 coding sequence was cloned into the pET-53-DEST (Novagen) expression vector via Gateway cloning. Protein solubility could be dramatically improved by deletion of the nucleotides encoding for the recombination site and the codons accounting for the two N-terminal methionines of Bs3. Deletion of these nucleotides was done by PCR mutagenesis (PrimerFW: P-GTGATGGTGGTGGTGATGTG and PrimerREV: AATCAGAATTGCTTTAATTCTTGTTCAC). For expression, in yeast the Bs3 CDS was cloned into the pYES-DEST-52 vector via Gateway cloning without further modification.

Xanthomonas and *Agrobacterium* infiltration

Xanthomonas (82-8 uns*) carrying the pDSK602 vector with either *AvrBs3* or *AvrBs2* were grown at 28°C in NYG medium (5 g/l peptone, 3 g/l yeast exract, 20 g/l glycerol) containing Rifampicin and Spectinomycin at a final concentration of 100 µg/ml. Cultures were pelleted and resuspended in water to OD_{600} = 0.4. Leaves of *C. annuum* were infiltrated with a blunt end syringe from the downside.

Agrobacterium tumefaciens (GV3101) carrying the respective binary plasmids were grown over night at 28°C in YEB medium (5 g/l beef extract, 1 g/l yeast extract, 5 g/l peptone, 5 g/l sucrose, and 0.5 g/l mM MgSO4, pH 7.2) containing Rifampicin and Spectinomycin at a final concentration of 100 µg/ml. Cultures were pelleted and resuspended in water to OD_{600} = 0.4. Leaves of *N. benthamiana* were infiltrated with a blunt end syringe from the downside.

Protein expression

E. coli Rosetta (Novagen) was transformed freshly with *pET-53-DEST_Bs3* or derivatives, plated on LB Agar containing Ampicillin (100 µg/ml) and Chloramphenicol (15 µg/ml) and incubated at 37°C over night. Several colonies were pooled to inoculate LB medium (10g/l NaCl, 5 g/l yeast extract, 10 g/l tryptone) supplemented with Ampicillin (100 µg/ml) and Chloramphenicol (15 µg/ml) and incubated over night at 37°C/180 rpm. This starter culture was used to inoculate 2 l TB Medium (24 g/l yeast extract, 20 g/l tryptone, 4 ml/l glycerol, 0.072 M K_2HPO_4, 0.017 M KH_2PO_4) supplemented with Ampicillin (100 µg/ml) at a starting OD_{600} = 0.05. The culture was grown at 37°C with shaking at 120 rpm until it reached an OD_{600} = 1. Cultures were cooled down in ice water for 15 min and Protein expression was induced with a final

concentration of 1 mM Isopropyl 1-thio-β-D-galactopyranoside (IPTG). The cells were incubated for another 2,5 h at 18°C with shaking and harvested by centrifugation (4500 x g, 30 min, 4°C). Pellets were stored at -20°C until further use.

Protein purification

The pellet was re-suspended in lysis buffer (50 mM potassium phosphate, 10% glycerol, 30 mM Imidazole, 1% Tween, protease inhibitor, 1 µM FAD, 1 mM DTT, pH 8) using 5 ml of buffer per gram of pellet. 30 ml cell suspension were sonicated for 5 min (5s on/10s off, 60% amplitude) with the ¼" microtip probe in the EpiShear Sonicator (Active Motif). The lysate was centrifuged (16000xg, 4°C) for 30 min to pellet cell debris. An ÄKTA Pure 25 FPLC system, equipped with a 5 ml HisTrapFF Crude Column (GE Healthcare), was used for affinity purification. After column equilibration (10 CV of wash buffer 50 mM potassium phosphate, 10% Glycerol, 30 mM Imidazole, pH 8), the supernatant was loaded onto the column and washed with 20 CV wash buffer. The protein was eluted with 2 CV elution buffer (50 mM potassium phosphate, 10% glycerol, 500 mM Imidazole, pH 8). The protein was frozen in liquid nitrogen and stored at -80°C.

Enzyme assays to measure NADPH oxidation

Spectroscopic assays were carried out in buffer (50 mM potassium phosphate, pH 8) containing NADPH in quartz cuvettes with a UV-900 UV-vis spectrometer (Shimadzu) equipped with a temperature-controlled cell holder (TCC-100). Exact NADPH concentrations were calculated from its absorption and the extinction coefficient at 340 nm (ε_{340} = 6220 M^{-1} cm^{-1}).

Detection of H_2O_2 with HyPerBlu

Protein concentration was calculated from the absorption at 280 nm, the predicted extinction coefficent of 53860 l/mol*cm and the Molecular weight (Mw_{Bs3} = 38369 mol/l, Mw_{S211A} = 38353 mol/l). Protein was mixed with NADPH solution (100 µM) and incubated at room temperature for 15 min. Per replicate, 5 µl of the solution were transferred to a white 385 well plate. 5 µl of HyPerBlu solution (Lumigen, Beckman Coulter) were added and the plate was incubated in darkness for 15 min at RT. Subsequently, luminescence was measured using a Berthold Tristar LB 941 plate reader. H_2O_2 concentration was calculated using a standard curve prepared with known concentrations of H_2O_2.

Redox Reporter Microscopy

RoGFP2 (Hanson et al., 2004) fused to *Bs3* and its derivatives were transiently expressed in four to six week old *N. benthamiana* plants via *Agrobacterium* mediated transient transformation. 30 hpi, images were acquired using a Leica TCS SP8 confocal microscope by successive excitation at 405 nm and 488 nm and emission at 498 to 548nm. Images of nuclei were collected using the 63x water immersed objective and 10x digital magnification. Argon laser intensity was adjusted so that pixels were close to saturation for samples with high roGFP2 expression. UV laser intensity was adjusted so that pixels were still visible for samples with low roGFP2 expression. Fiji (Schindelin et al., 2012) was used to crop the surrounding of the nuclei and to calculate mean pixel intensity of the fluorescent area.

Ion leakage measurements

Ion leakage measurements were conducted using the CM100-2 conductivity meter (Reid & Associates). Each well was filled with 1 ml ultrapure water. Leaf discs (Ø 4 mm) were harvested three days post infiltration. One disc was added per well and incubated at RT. Ion leakage was measured after 20 hours of incubation.

References

Alfieri A, Malito E, Orru R, Fraaije MW, Mattevi A (2008) Revealing the moonlighting role of NADP in the structure of a flavin-containing monooxygenase. Proc Natl Acad Sci U S A 105: 6572-6577

Binder A, Lambert J, Morbitzer R, Popp C, Ott T, Lahaye T, Parniske M (2014) A modular plasmid assembly kit for multigene expression, gene silencing and silencing rescue in plants. PLoS One 9: e88218

Dai X, Mashiguchi K, Chen Q, Kasahara H, Kamiya Y, Ojha S, DuBois J, Ballou D, Zhao Y (2013) The biochemical mechanism of auxin biosynthesis by an *Arabidopsis* YUCCA flavin-containing monooxygenase. J Biol Chem 288: 1448-1457

Fiorentini F, Geier M, Binda C, Winkler M, Faber K, Hall M, Mattevi A (2016) Biocatalytic Characterization of Human FMO5: Unearthing Baeyer-Villiger Reactions in Humans. ACS Chem Biol 11: 1039-1048

Forman HJ, Maiorino M, Ursini F (2010) Signaling functions of reactive oxygen species. Biochemistry 49: 835-842

Goncalves LCP, Kracher D, Milker S, Fink MJ, Rudroff F, Ludwig R, Bommarius AS, Mihovilovic MD (2017) Mutagenesis-Independent Stabilization of Class B Flavin Monooxygenases in Operation. Advanced Synthesis & Catalysis 359: 2121-2131

Hanson GT, Aggeler R, Oglesbee D, Cannon M, Capaldi RA, Tsien RY, Remington SJ (2004) Investigating mitochondrial redox potential with redox-sensitive green fluorescent protein indicators. J Biol Chem 279: 13044-13053

Hou X, Liu S, Pierri F, Dai X, Qu LJ, Zhao Y (2011) Allelic analyses of the *Arabidopsis YUC1* locus reveal residues and domains essential for the functions of YUC family of flavin monooxygenases. J Integr Plant Biol 53: 54-62

Krönauer C, Kilian J, Strauß T, Stahl M, Lahaye T (2019) Cell Death Triggered by the YUCCA-like Bs3 Protein Coincides with Accumulation of Salicylic Acid and Pipecolic Acid But Not of Indole-3-Acetic Acid. Plant Physiol 180: 1647-1659

Krueger SK, Williams DE (2005) Mammalian flavin-containing monooxygenases: structure/function, genetic polymorphisms and role in drug metabolism. Pharmacol Ther 106: 357-387

Marinho HS, Real C, Cyrne L, Soares H, Antunes F (2014) Hydrogen peroxide sensing, signaling and regulation of transcription factors. Redox Biol 2: 535-562

Mashiguchi K, Tanaka K, Sakai T, Sugawara S, Kawaide H, Natsume M, Hanada A, Yaeno T, Shirasu K, Yao H, McSteen P, Zhao Y, Hayashi K, Kamiya Y, Kasahara H (2011) The main auxin biosynthesis pathway in *Arabidopsis*. Proc Natl Acad Sci U S A 108: 18512-18517

Meyer AJ, Brach T, Marty L, Kreye S, Rouhier N, Jacquot JP, Hell R (2007) Redox-sensitive GFP in *Arabidopsis thaliana* is a quantitative biosensor for the redox potential of the cellular glutathione redox buffer. Plant J 52: 973-986

Montillet JL, Chamnongpol S, Rusterucci C, Dat J, van de Cotte B, Agnel JP, Battesti C, Inze D, Van Breusegem F, Triantaphylides C (2005) Fatty acid hydroperoxides and H2O2 in the execution of hypersensitive cell death in tobacco leaves. Plant Physiol 138: 1516-1526

Nishimura T, Hayashi K, Suzuki H, Gyohda A, Takaoka C, Sakaguchi Y, Matsumoto S, Kasahara H, Sakai T, Kato J, Kamiya Y, Koshiba T (2014) Yucasin is a potent inhibitor of YUCCA, a key enzyme in auxin biosynthesis. Plant J 77: 352-366

Petrov VD, Van Breusegem F (2012) Hydrogen peroxide-a central hub for information flow in plant cells. AoB Plants 2012: pls014

Potnis N, Timilsina S, Strayer A, Shantharaj D, Barak JD, Paret ML, Vallad GE, Jones JB (2015) Bacterial spot of tomato and pepper: diverse *Xanthomonas* species with a wide variety of virulence factors posing a worldwide challenge. Mol Plant Pathol 16: 907-920

Ritz C, Baty F, Streibig JC, Gerhard D (2015) Dose-Response Analysis Using R. Plos One 10

Schindelin J, Arganda-Carreras I, Frise E, Kaynig V, Longair M, Pietzsch T, Preibisch S, Rueden C, Saalfeld S, Schmid B, Tinevez JY, White DJ, Hartenstein V, Eliceiri K, Tomancak P, Cardona A (2012) Fiji: an open-source platform for biological-image analysis. Nat Methods 9: 676-682

Schwarzländer M, Fricker MD, Muller C, Marty L, Brach T, Novak J, Sweetlove LJ, Hell R, Meyer AJ (2008) Confocal imaging of glutathione redox potential in living plant cells. J Microsc 231: 299-316

Shibata M, Oikawa K, Yoshimoto K, Kondo M, Mano S, Yamada K, Hayashi M, Sakamoto W, Ohsumi Y, Nishimura M (2013) Highly oxidized peroxisomes are selectively degraded via autophagy in *Arabidopsis*. Plant Cell 25: 4967-4983

Shirey C, Badieyan S, Sobrado P (2013) Role of Ser-257 in the sliding mechanism of NADP(H) in the reaction catalyzed by the *Aspergillus fumigatus* flavin-dependent ornithine N5-monooxygenase SidA. J Biol Chem 288: 32440-32448

Siddens LK, Krueger SK, Henderson MC, Williams DE (2014) Mammalian flavin-containing monooxygenase (FMO) as a source of hydrogen peroxide. Biochem Pharmacol 89: 141-147

Tai TH, Dahlbeck D, Clark ET, Gajiwala P, Pasion R, Whalen MC, Stall RE, Staskawicz BJ (1999) Expression of the *Bs2* pepper gene confers resistance to bacterial spot disease in tomato. Proc Natl Acad Sci U S A 96: 14153-14158

Thotsaporn K, Chenprakhon P, Sucharitakul J, Mattevi A, Chaiyen P (2011) Stabilization of C4a-Hydroperoxyflavin in a Two-component Flavin-dependent Monooxygenase Is Achieved through Interactions at Flavin N5 and C4a Atoms. Journal of Biological Chemistry 286: 28170-28180

Tian D, Wang J, Zeng X, Gu K, Qiu C, Yang X, Zhou Z, Goh M, Luo Y, Murata-Hori M, White FF, Yin Z (2014) The Rice TAL Effector-Dependent Resistance Protein XA10 Triggers Cell Death and Calcium Depletion in the Endoplasmic Reticulum. Plant Cell 26: 497-515

Tsugafune S, Mashiguchi K, Fukui K, Takebayashi Y, Nishimura T, Sakai T, Shimada Y, Kasahara H, Koshiba T, Hayashi KI (2017) Yucasin DF, a potent and persistent inhibitor of auxin biosynthesis in plants. Sci Rep 7: 13992

Waszczak C, Akter S, Eeckhout D, Persiau G, Wahni K, Bodra N, Van Molle I, De Smet B, Vertommen D, Gevaert K, De Jaeger G, Van Montagu M, Messens J, Van Breusegem F (2014) Sulfenome mining in *Arabidopsis thaliana*. Proc Natl Acad Sci U S A 111: 11545-11550

Winterbourn CC, Hampton MB (2008) Thiol chemistry and specificity in redox signaling. Free Radic Biol Med 45: 549-561

Zhang J, Yin Z, White F (2015) TAL effectors and the executor *R* genes. Front Plant Sci 6: 641

Zurbriggen MD, Carrillo N, Hajirezaei MR (2010) ROS signaling in the hypersensitive response: when, where and what for? Plant Signal Behav 5: 393-396

Table 1: Yucasin and Methimazole (MMI) decrease NADPH oxidase activity of Bs3 and $Bs3_{S211A}$

Sample	Compound	Activity (nmol/mg*min) ± SD
Bs3	DMSO	63.7 ± 2.6
Bs3	MMI	13.3 ± 2.2
Bs3	YUCASIN	3.4 ± 1.2
$Bs3_{S211A}$	DMSO	137.2 ± 3.6
$Bs3_{S211A}$	MMI	115.5 ± 0.9
$Bs3_{S211A}$	YUCASIN	83.3 ± 3.1

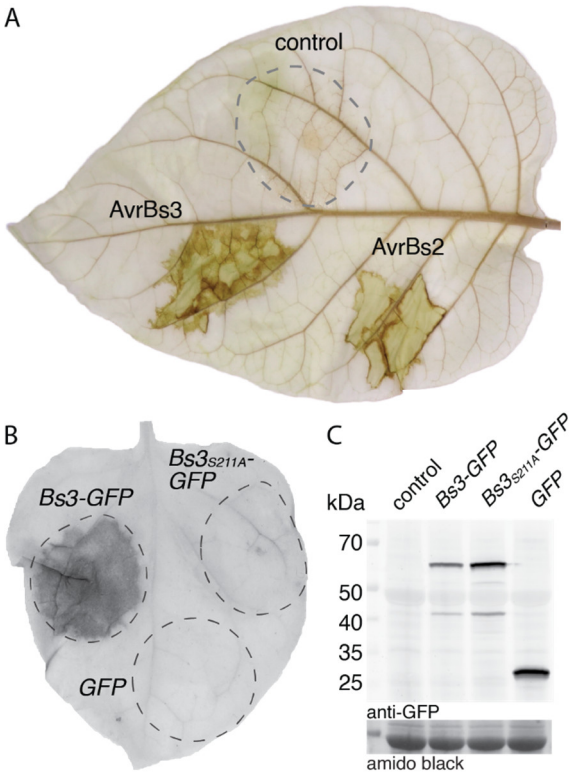

Figure 1: Bs2 and Bs3 trigger HR and ROS accumulation. A) *Capsicum annuum* ECW 1-2-3 leaves were infiltrated with *Xanthomonas* 82-8 uns or 82-8 uns delivering AvrBs2 and AvrBs3, respectively. 30 hpi the leaf was harvested, stained with DAB solution and cleared with ethanol. Dashed lines mark infiltrated areas. B) *35S* driven *Bs3-GFP*, $Bs3_{S211A}$*-GFP* and *GFP* control were expressed in *N. benthamiana* via *Agrobacterium*-mediated transient transformation. At 4 dpi, the leaf was harvested and cleared in ethanol. Dashed lines mark the infiltration site. The HR is visible as dark spot. C) Protein expression was monitored via an immunoblot using an anti-GFP antibody. Amido black staining was used to visualize total protein load.

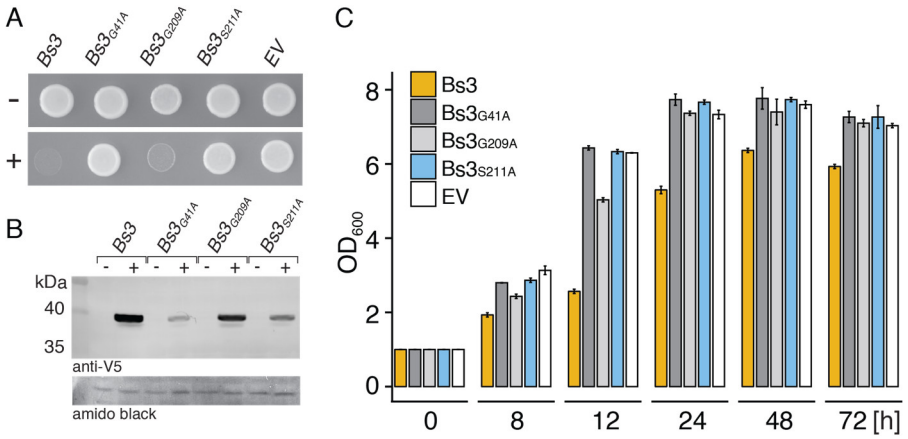

Figure 2: Bs3 but not Bs3$_{S211A}$ impairs growth in yeast A) *Bs3* and *Bs3* mutant derivatives were cloned downstream of a galactose inducible promoter (pGAL1) and transformed into yeast. Cultures were diluted to OD_{600} = 1, dropped onto repressing (-) or inducing (+) medium and incubated at 28°C for one day. B) Yeast cultures carrying the indicated constructs were grown in repressing (-) or inducing (+) liquid medium for 6 hours. Protein expression was monitored via an immunoblot using an anti-V5 antibody. Amido black staining was used to visualize total protein load. C) Yeast strains, carrying the indicated constructs, were grown in repressing medium over night, diluted to OD600 = 1 in inducing medium and incubated at 28°C with shaking. Samples were taken at indicated timepoints and OD600 was measured. Values represent mean +/- SD of three replicates.

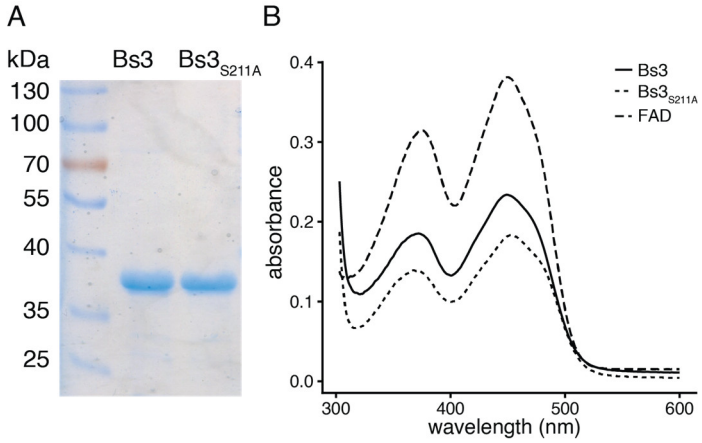

Figure 3: Bs3 and Bs3$_{S211A}$ bind FAD. A) Bs3 and Bs3$_{S211A}$ were loaded onto an SDS gel after affinity purification and dialysis. B) UV/-vis spectrum of FAD (dashed line), Bs3 (solid line) and Bs3$_{S211A}$ (dotted line).

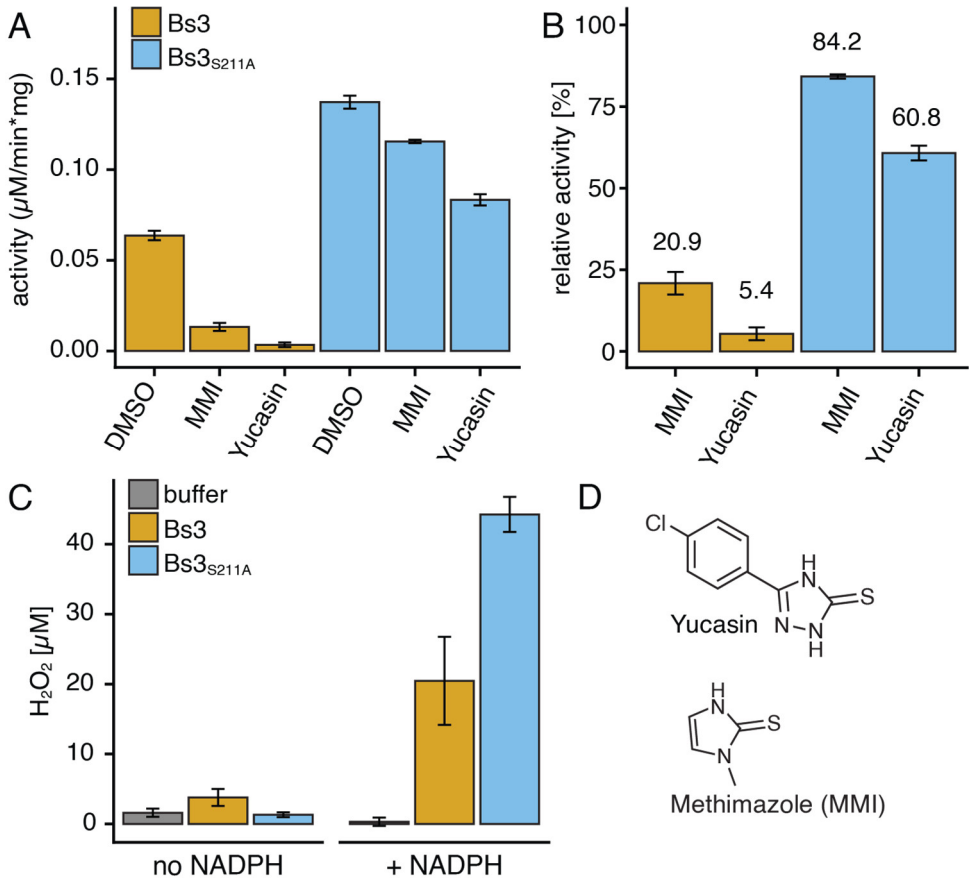

Figure 4: NADPH oxidation and H_2O_2 production by Bs3 and $Bs3_{S211A}$. A) Buffer containing 100 μM NADPH is mixed with 0.2 μM Bs3 or $Bs3_{S211A}$. NADPH oxidation is monitored via absorption at 340 nm at 25°C and activity is calculated. Yucasin and methimazole (MMI) were dissolved in DMSO and added at final concentrations of 50 μM. B) Values of Bs3 and $Bs3_{S211A}$ samples containing MMI and Yucasin (from A) are normalized to DMSO control to show relative activity. C) 0.4 μM of Bs3 and $Bs3_{S211A}$ protein is mixed with buffer containing no or 100 μM NADPH and incubated for five minutes at room temperature. The samples are subsequently mixed with HyPerBlu in a 1:1 ratio. Luminescence is measured after 10 min of incubation. Bars indicated mean +/- SD of three replicates. D) Chemical structures of yucasin and methimazole (MMI).

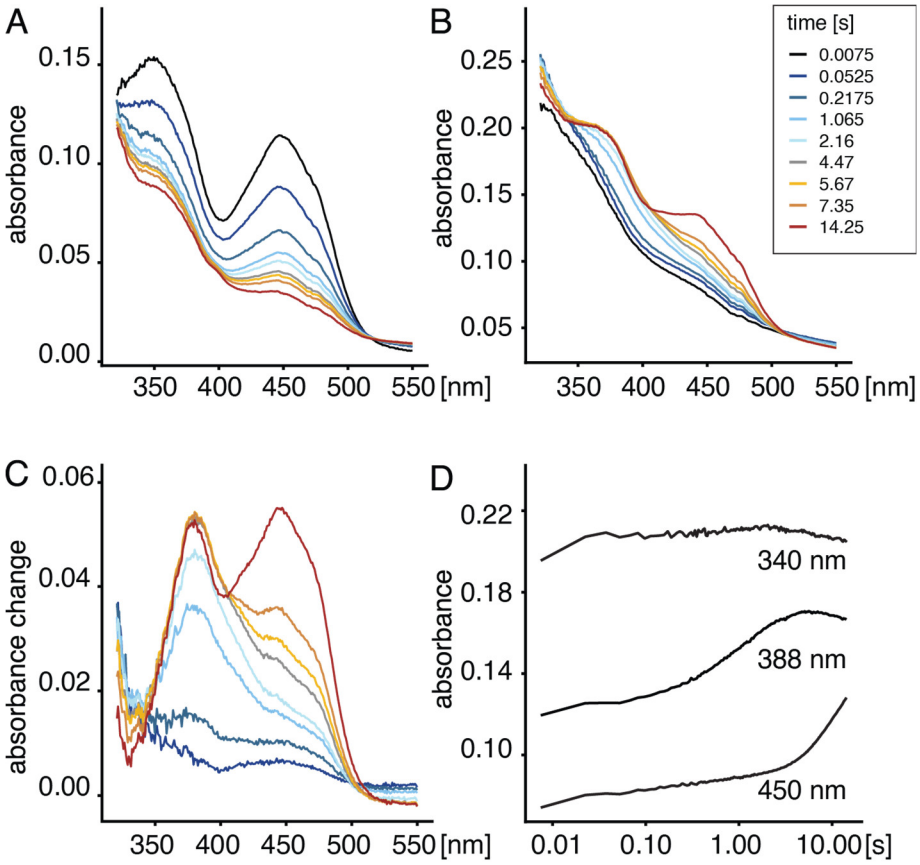

Figure 5. Bs3 forms a C4a-intermediate. A) Bs3 was mixed with 25 μM NADPH under anaerobic conditions. Reduction was followed over time. B) Reduced Bs3 and buffer containing 10% O2 were mixed in the stopped-flow instrument. C) Difference spectra generated by subtracting the first spectrum at 0.0075 s from each successive spectrum. D) In the single wavelength traces formation of the C4a-intermediate, FAD and NADPH consumption are monitored at 340, 388 and 450 nm.

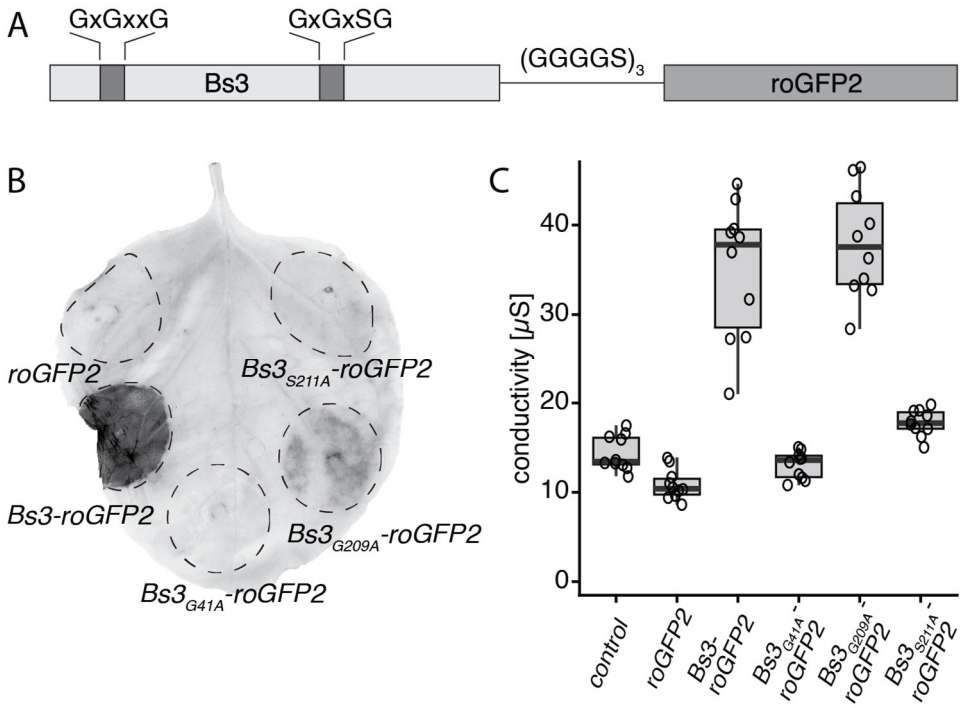

Figure 6: *35S*-driven expression of $Bs3_{G209A}$ triggers HR A) Schematic representation of a Bs3-roGFP2 fusion construct. cofactor binding sites (GxGxx/SG) are depicted as grey bars. Bs3 is fused to roGFP2 via a glycine and serine containing linker $(GGGGS)_3$ B) *Agrobacterium* strains carrying the indicated constructs under control of the 35S promoter were infiltrated into *N. benthamiana* leaves. Four days post infiltration, leaves were harvested and cleared with ethanol. HR is visible as dark spots. Dashed lines mark the infiltrated area. C) Ion leakage measurements of plant tissue expressing *roGFP2* and *Bs3-roGFP2* derivatives. Indicated constructs were expressed under control of the *35S* promoter in *N. benthamiana* via *Agrobacterium*-mediated transient transformation. Three days post infiltration, leaf discs were cut and incubated in ultrapure water. Conductivity was measured after 20 hours of incubation. Boxplots represent values of 10 replicates. Single values are depicted as black circles.

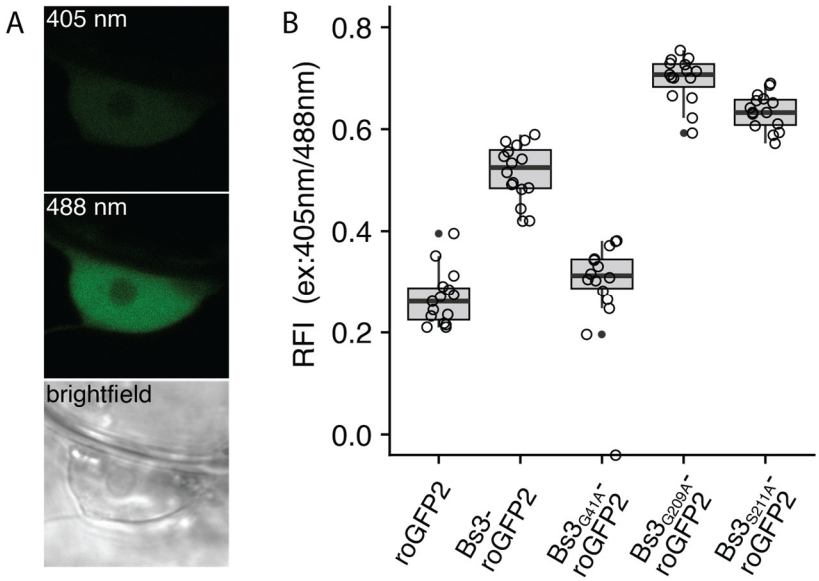

Figure 7. Oxidase function of Bs3 derivatives is independent from HR inducing activity A) Representative pictures of roGFP2 fluorescence in the nucleus with excitation at 405 and 488 nm. Pictures were acquired with a Leica Sp8 confocal laser scanning microscope B) RoGFP2 oxidation is increased in *Bs3*, *Bs3*$_{G209A}$ and *Bs3*$_{S211A}$ expressing leaf tissue. Indicated constructs were expressed under control of the *35S* promoter in *N. benthamiana* via *Agrobacterium*-mediated transient transformation. 30 hpi leaf discs were analysed by ratiometric laser scanning microscopy. Boxplots represent relative fluorescent intensity (RFI) values (emission at ex:405nm/ emission at ex:488nm) of 15 individual nuclei. Single values are depicted as black circles.

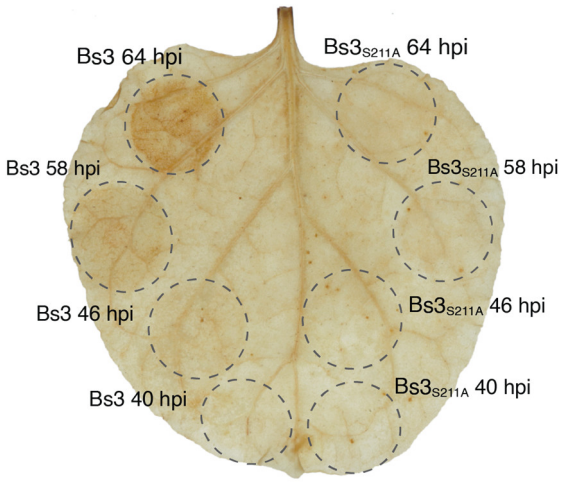

Figure S1: H_2O_2 accumulation during Bs3 HR in *N. benthamiana*. *35S*-driven *Bs3-GFP* and *Bs3*$_{S211A}$*-GFP* were agroinfiltrated into *N. benthamiana* at the depicted timepoints. 64 hours after the first infiltration, the leaf was detached and vacuum infiltrated in DAB solution to visualize ROS accumulation. The leaf was de-stained in hot ethanol. Dashed lines mark infiltrated areas.

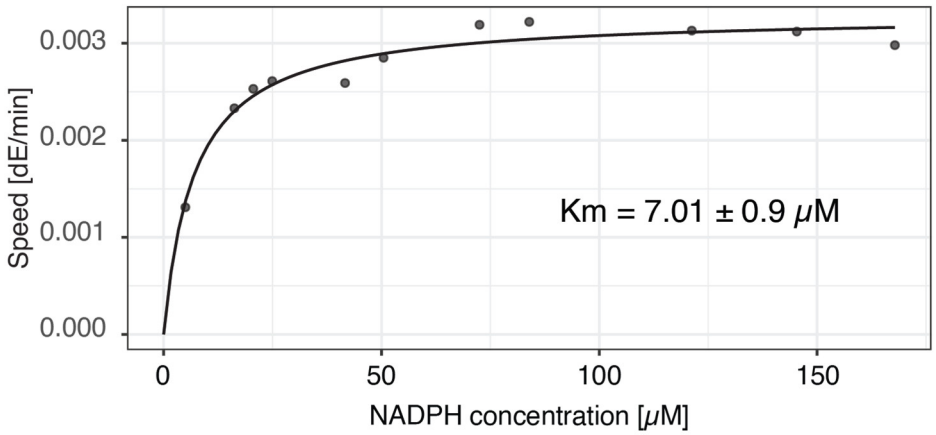

Figure S2: Michaelis Menten Kinetics of Bs3. 0.7 μM Bs3 protein were mixed with 980 μl NADPH of varying concentrations at 25°C. NADPH oxidation was monitored via absorbance change at 340 nm. Km was calculated from slope values using the drm package in R (Ritz et al., 2015)

Statement on author contributions for experiments described in chapter 2.4

Mass spectrometry and data handling of the pull down experiments (section 2.4.1) was conducted by Irina Droste-Borel at the Proteome Center Tübingen. Sulfenome mining (section 2.4.2) was done in collaboration with Frank van Breusegem at Ghent University. Specifically, protein extraction and MS data analysis of the sulfenome mining experiments were carried out by Barbara de Smet.

2.4 Identification of proteins with a putative function in Bs3 HR

No interacting proteins have been identified for any FMO thus far. Nonetheless, it cannot be excluded that interacting proteins exist which are necessary for Bs3 function and it is conceivable, that components acting downstream of Bs3 are involved in a signalling cascade finally leading to HR.

In this work, pull-down and sulfenome mining experiments were carried out to identify putative Bs3 interaction partners. Furthermore, virus induced gene silencing (VIGS) and screening of a yeast knockout library were carried out to find putative pathway components.

2.4.1 Identification of proteins that co-purify with Bs3 via pull down and MS

Assuming that Bs3 forms a stable interaction with another protein, it should be possible to pull down Bs3 from plant extracts and identify the putative interaction partner via mass spectrometry (MS). To follow this approach, *Bs3-GFP*, *Bs3$_{S211A}$-GFP*, *AtYUC8-GFP,* and *GFP* were transiently expressed in *N. benthamiana* and the tagged proteins were purified from leaf extracts with anti-GFP beads. While purification of Bs3, Bs3$_{S211A}$ and GFP worked well, no distinct band indicating the presence of AtYUC8 is visible in either the coomassie stained SDS gel or the anti-GFP western blot (Figure 2.9). Two batches with one replicate for each construct were produced. All immunopurified samples, including AtYUC8-GFP were analysed via tryptic digest and mass spectrometry.

MS spectra derived from Bs3, Bs3$_{S211A}$, YUC8 and GFP containing samples were searched against the Nicotiana_benthamiana_allStrains_19072016.fasta database, including the sequences of Bs3 and GFP. During the evaluation process, candidates with a score <50 and contaminants like keratin were dismissed. Candidates were included into further analysis with a score >50 and a Q value of zero. In general, candidates were regarded as reliable if two or more peptides were identified (Käll et al., 2008). Two independent MS measurements were conducted to identify the proteins in the four samples. A total of 138 and 82 different proteins were identified for measurements of batch one and two, respectively (Table 6.3).

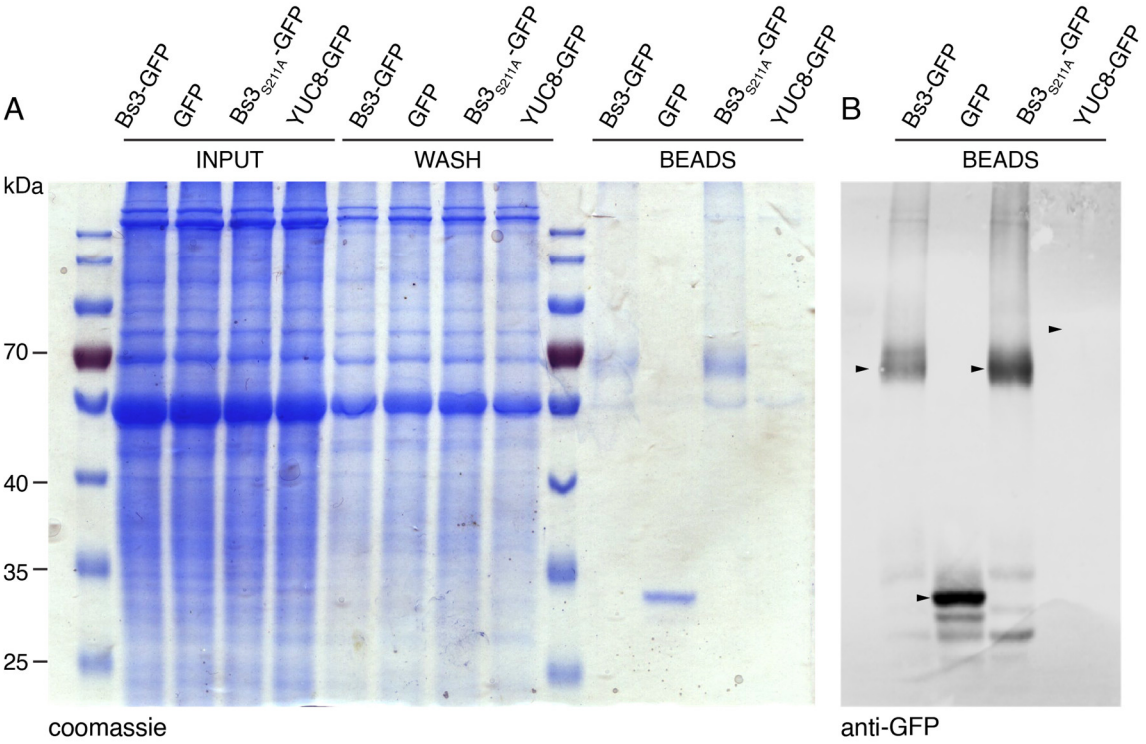

Figure 2.9 Pull down of GFP, Bs3-GFP, Bs3$_{S211A}$-GFP and YUC8-GFP from plant material A) Indicated constructs were expressed in *N. benthamiana* via *Agrobacterium*-mediated transient transformation. 36 hpi, total protein was extracted and incubated with GFP-trap beads for 4 hours. The total protein extract, a wash fraction and the protein bound beads were separated on a denaturing polyacrylamide gel and stained with coomassie. Arrowheads mark the expected size for the indicated fusion proteins. B) Presence of GFP and GFP-tagged proteins was analysed after immunopurification via an anti GFP western blot.

Putative interactors of Bs3 are expected to be present in Bs3 containing samples but absent or very low abundant in GFP containing samples. Since $Bs3_{S211A}$ is non-functional but has a similar sequence, it is not known if putative interaction partners of Bs3 would interact with $Bs3_{S211A}$. Similarly, AtYUC8 and Bs3 contain conserved stretches of amino acids which could serve as interaction sites for the same protein. Therefore, only GFP was considered as negative control.

Table 2.2 Bs3, GFP and candidate proteins that were most abundant in Bs3 samples but not present in GFP or YUC8 samples.

Protein	iBAQ Bs3	iBAQ $Bs3_{S211A}$	iBAQ YUC8	iBAQ GFP	ID
Bs3	1.04E+08	1.61E+08	1.05E+06	3.90E+05	-
GFP	3.35E+08	6.10E+08	4.78E+07	2.20E+08	-
GTP cyclohydrolase (NbRibA)	2.49E+07	0.00E+00	0.00E+00	0.00E+00	D6RUS9
MAP kinase kinase (NbMEK2)	3.89E+06	0.00E+00	0.00E+00	0.00E+00	B2NIC3
Fruktokinase-like protein 1	1.06E+06	0.00E+00	0.00E+00	0.00E+00	D9IWN9
Sucrose phosphate synthase A	9.41E+05	0.00E+00	0.00E+00	0.00E+00	F6L7A2
Lipoxygenase	4.10E+05	0.00E+00	0.00E+00	0.00E+00	R4S2V6
Respiratory burst oxidase homolog (NbRbohB)	1.65E+06	2.83E+04	0.00E+00	0.00E+00	Q84KK7
Ubiquinol oxidase	1.09E+06	1.29E+05	0.00E+00	0.00E+00	U5XH87
5-epi-aristolochene synthase (EAS)	7.76E+05	3.32E+05	0.00E+00	0.00E+00	A0A0H5B1M3
Thioredoxin H-type 1	1.90E+06	5.19E+05	0.00E+00	0.00E+00	C9DFC1
Peroxiredoxin 2B	2.38E+06	1.07E+06	0.00E+00	0.00E+00	R9W2E1
Heat shock protein 70	2.25E+06	1.43E+06	0.00E+00	0.00E+00	Q769C5
NRG1	1.06E+06	2.74E+06	0.00E+00	0.00E+00	Q4TVR0
Heat shock protein 70	3.63E+06	3.11E+06	0.00E+00	0.00E+00	Q6L9F6
DNA gyrase subunit	3.97E+05	8.33E+06	0.00E+00	0.00E+00	Q5YLB4

The presence of peptides of GFP and Bs3 with high intensity values confirm, that the purification of recombinant protein was successful (Table 2.2). Notably, peptides of GFP were found in the AtYUC8 containing sample, indicating that either a small amount of YUC8-GFP fusion protein or free GFP was present in GFP-AtYUC8 samples even though it was not visible in the western blot (Figure 2.9, Table 2.2). Forty-four candidates were identified with higher abundance in Bs3 samples compared to GFP samples according to high intensity based absolute quantification (iBAQ) values (Schwanhausser et al.,

2011, Supplementary Table 6.4). Notably, Bs3 peptides were not only identified in Bs3 and $Bs3_{S211A}$ containing samples but also in YUC8 and GFP samples (Table 2.2). This could either be due to false positive hits or ambiguous peptides. However, intensity values for Bs3 peptides in the sample containing Bs3 are 267-fold higher than values for the presumably false positive identified Bs3 peptides in the sample containing GFP (Supplementary Table 6.4).

The ten candidates with highest iBAQ values in Bs3 containing samples but no peptides in GFP containing samples, are stated in Table 2.2. Many of the identified proteins are associated to defence and immune responses, like MAP kinase kinase (MEK), respiratory burst oxidase homolog B (RbohB) and N requirement gene 1 (NRG1) as well as chaperones like heat shock protein 70 (HSP70).

2.4.2 Identification of proteins sulfenylated during Bs3 HR

H_2O_2 is an important signalling molecule during plant stress and cell death reactions (reviewed in Zurbriggen et al., 2010 and Baxter et al., 2014). The oxidation of cysteine thiols (R-SH) to sulfenic acids (R-SOH) by H_2O_2 is an important posttranslational modification and an example of how a chemical signal can be converted into a biological response. The fact that Bs3, like most FMOs, produces H_2O_2 during the uncoupled reaction (see section 1.4.2) raised the question whether the H_2O_2 generated by Bs3 targets specific proteins to induce a signalling cascade that ultimately causes cell death. Therefore, we were interested in the identification of redox sensitive proteins that are oxidized specifically during Bs3 HR.

Sulfenome mining is based on a linkage of a tandem affinity purification tag to the yeast AP-1 like transcription factor C-terminal domain (YAP1C), that contains a redox sensitive cysteine and is able to form a disulfide bond after reaction with a sulfenic acid (Delaunay et al., 2002). We assume that during Bs3 HR, thiol side chains of target proteins are oxidized to sulfenic acids and subsequently trapped by YAP1C (Figure 2.10).

Creation of a Bs3-YAP1 fusion ensures close proximity of the proteins in the cell

The challenge during these *in vivo* ROS analyses is to distinguish H_2O_2 produced by Bs3 from the indirect production of H_2O_2 originating from other sources after induction of HR. Given that H_2O_2 is scavenged rapidly after its production in the cell (Lim et al., 2015), it is likely that the sulfenylated targets are in the near proximity of Bs3. To improve trapping of Bs3 specific targets, a construct was created that encodes Bs3 with a N-terminal tandem affinity purification tag (TAP) and a C-terminal YAP1C (Figure 2.9). A YAP construct in which the redox sensitive cysteine was mutated to alanine served as a negative control for non-specific protein associations. The $Bs3_{S211A}$ mutant, which does not trigger HR but is able to produce H_2O_2 *in vitro* (Bs3 manuscript, section 2.3.4, Figure 7), was chosen as a control. The four constructs, *TAP-Bs3-YAP1C*, *TAP-*$Bs3_{S211A}$*-YAP1C*, *TAP-Bs3-YAP1A* and *TAP-*$Bs3_{S211A}$*-YAP1A*, were transiently expressed in *N. benthamiana* under the control of the *35S* promoter. Leaf material for Bs3 sulfenome mining was harvested at 30 hpi and sent for tandem affinity purification, mass spectrometry and data analysis. TAP-Bs3-YAP1A/C triggers an HR reaction three days post infiltration (Figure 2.9 B).

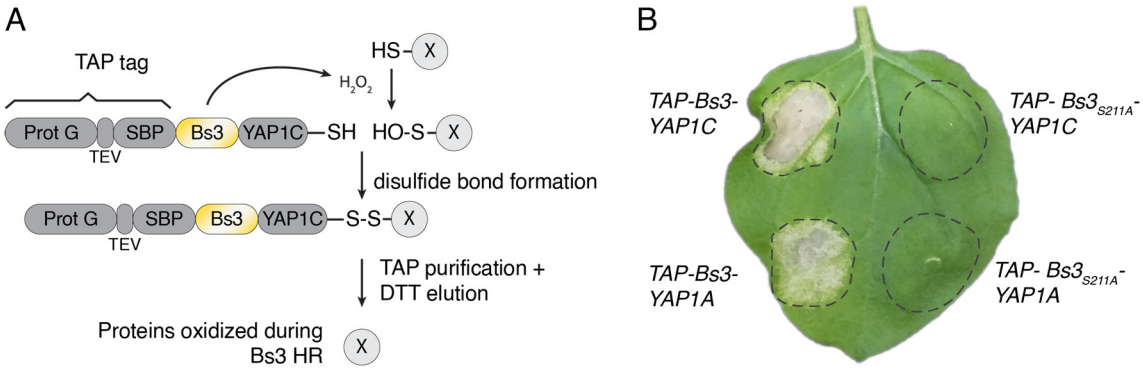

Figure 2.10 Identification of proteins that are sulfenylated during Bs3 HR A) Schematic representation of the sulfenome mining assay with the TAP-Bs3-YAP1C fusion construct. Bs3 derived H_2O_2 reacts with cysteine thiols (-SH) of surrounding proteins and forms a sulfenic acid (-SOH). The sulfenylated protein builds a disulfide bond with the YAP1C domain of the TAP-Bs3-YAP1C construct. Disulfide bridge bound proteins are affinity purified and subsequently identified via mass spectrometry. TAP = tandem affinity purification, TEV = tobacco etch virus protease cleavage site, SBP = streptavidin-binding peptide tag B) Fusion of a N-terminal TAP and a C-terminal YAP does not impair Bs3 function. The four indicated constructs were expressed in *N. benthamiana* via *Agrobacterium* mediated transient transformation. Pictures were taken four days post infiltration. Dashed lines mark the infiltrated area.

Table 2.3 Proteins sulfenylated in *Bs3* expressing *N. benthamiana* leaves. Candidates that were specifically identified in Bs3 but not in $Bs3_{S211A}$ containing samples. Counts display the number of replicates in which the candidate was identified. Candidates that show increased quantitative abundancy in *Bs3* compared to $Bs3_{S211A}$ expressing samples are highlighted in bold. Asteriks indicate candidates that were previously identified in experiments conducted by F. van Breusegem.

DESCRIPTION	Bs3 COUNTS	$Bs3_{S211A}$ COUNTS
V-type proton ATPase subunit C	4	0
Methionine--tRNA ligase	4	0
Pentatricopeptide repeat-containing protein	4	0
Phosphoglucomutase-1	4	0
Peptide methionine sulfoxide reductase MsrB	4	0
Dihydrolipoyllysine-residue acetyltransferase component of pyruvate dehydrogenase complex	4	0
10 kDa chaperonin	4	0
Ferredoxin-dependent glutamate synthase 2	4	0
Thioredoxin family protein	4	0
NAD/NADP-dependent betaine aldehyde dehydrogenase	4	0
Magnesium-protoporphyrin IX monomethyl ester [oxidative] cyclase	4	0
Copper chaperone	4	0
Cystathionine gamma-synthase	4	0
T-complex protein 1 alpha subunit	4	0
Glutamate decarboxylase	4	0
Photosystem I reaction center subunit IV	4	0
Fumarate hydratase class II	4	0
calcium homeostasis regulator CHoR1	4	0
Haloacid dehalogenase-like hydrolase domain-containing protein*	4	0
Beta-ketoacyl synthase*	4	0
NAD-dependent malic enzyme*	4	0
Tripeptidyl-peptidase 2	3	0
Actin-2*	3	0
Cytochrome b6	3	0
Chlorophyll a-b binding protein	3	0
Chlorophyll a-b binding protein	3	0
Chlorophyll a-b binding protein 8	3	0
Phosphoglycerate kinase*	3	0
Acetolactate synthase small subunit*	3	0
NAC domain-containing protein 72	3	0
40S ribosomal protein S10-1	3	0
Methionine--tRNA ligase*	3	0
Cytochrome b559 subunit alpha; PSII reaction center protein L	3	0
SKP1-like protein 1A*	3	0
Glutamate decarboxylase*	3	0
Aquaporin-like superfamily protein	3	0
Glycerol-3-phosphate 2-O-acyltransferase 6	3	0
T-complex protein 1 subunit alpha*	3	0
Photosystem I reaction center subunit IV	3	0
Superoxide dismutase [Mn]*	3	0
Gibberellin receptor GID1*	4	1
Phosphoglucomutase-1	4	1
Chlorophyll a-b binding protein 6A, chloroplastic	3	2

A total of 627 proteins were identified with the YAP1C probe. 88 candidates remained that were not in parallel identified with the YAP1A probe. A full list of candidates with genome identifiers can be found in Supplementary Table 6.4. Notably, one of the four replicates of the $Bs3_{S211A}$-YAP1C did not cluster together with the other replicates in multidimensional scaling (MDS) analysis and was therefore removed from the dataset (B. de Smet, unpublished). 40 of these candidates are not identified in $Bs3_{S211A}$ samples and are therefore proteins that are specifically sulfenylated during Bs3 HR (Table 2.3). In addition to the qualitative comparison, quantitative analysis was carried out and found the three proteins Gibberellin receptor, Phosphoglucomutase-1 and Chlorophyll a-b binding protein 6A to be higher abundant in Bs3-YAP1C than in $Bs3_{S211A}$-YAP1C samples (Table 2.3).

The list of candidates identified with the Bs3 fused YAP1A/C probes was compared to candidates that were previously found in sulfenome mining experiments carried out in the van Breusegem lab. Of the 40 candidates identified in Bs3-YAP1C samples, only eleven were found in other datasets. Out of 48 candidates that were found in Bs3-YAP1C as well as in $Bs3_{S211A}$-YAP1C samples, 28 candidates were found in other datasets. This suggests, that our approach indeed identified proteins that are specifically sulfenylated during Bs3 HR.

2.4.3 Screen of a yeast single gene knockout library

Upon induction, *Bs3* impairs growth in yeast (see section 2.2.2). It is conceivable that the molecular mechanisms leading to the growth defect in yeast may be similar to those being involved in plant HR. Therefore, we decided to conduct a screen for putative pathway components that are indispensable for the Bs3 triggered growth defect in yeast. A yeast single knockout library (Winzeler et al., 1999) was used with the aim to find candidates whose mutation compensates the growth defect caused by Bs3.

Identification of yeast strains that express *Bs3* without being impaired in growth

The yeast library used in this study consists of ~ 4700 pooled homozygous diploid strains with a single gene knocked out. Each target gene is replaced by a cassette conferring resistance to kanamycin/G418 and a unique 20mer barcode.

The library was transformed with either *Bs3* or $Bs3_{S211A}$ under control of a galactose inducible promoter and plated on repressing and inducing solid medium. Figure 2.12 shows a representative picture of one yeast knockout library transformation experiment. The number of clones that grew on repressing medium is similar after transformation of strains with *Bs3* or $Bs3_{S211A}$. Notably, while a lot of $Bs3_{S211A}$ transformed strains grew on inducing medium, only a small number of clones was present on plates with strains transformed with *Bs3* (Figure 2.12). In total 112 clones were picked that were able to grow on inducing solid medium after transformation with *Bs3* (Suppl. Table 6.4).

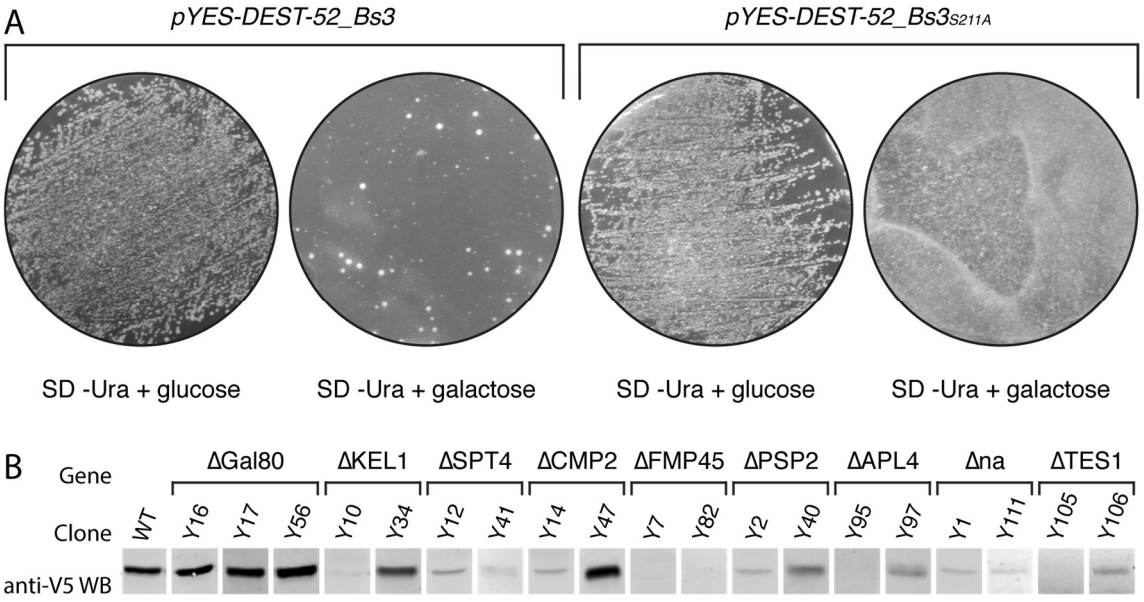

Figure 2.12 Yeast knockout library transformation reveals clones that grow despite expression of *Bs3* A) Representative result of a yeast transformation. The yeast knockout library was transformed with inducible expression vectors containing either *Bs3* or the non-functional $Bs3_{S211A}$ mutant and plated onto solid medium containing either glucose (repressing) or galactose (inducing). Pictures were taken after three days of incubation at 28°C. B) Candidate clones that were found at least twice (see table 2.4) were grown in inducing liquid medium for 6 hours. Western Blot analysis with anti-V5 antibody was carried out to control Bs3 protein abundance.

The barcode sequences of these clones were amplified by PCR and 102 candidates could be identified by sequencing (Supp. Table 6.5). The GAL80 knockout strain (ΔGAL80) was found three times and nine other knockout candidates (ΔKEL1, ΔSPT4, ΔCMP2, ΔFMP45, ΔPSP2 ΔAPL4 and ΔYML051W and ΔTES1) were found twice (Table 2.4). Considering the survival of the ~ 4700 pooled clones to be random, the probability to find some candidates more than once in 112 picked clones, would be very low. Therefore, the finding of

multiple clones in duplication suggests that survival is non-random and probably due to the absence of the respective gene product.

Table 2.4: Candidates that were found at least twice in the yeast knockout library screen

SYSTEMATIC NAME	CLONES	GENE	DESCRIPTION
YML051W	Y16, Y17, Y56	*GAL80*	Transcriptional regulator of galactose genes
YHR158C	Y10, Y34	*KEL1*	Cell morphogenesis
YGR063C	Y12, Y41	*SPT4*	Transcriptional regulation
YML057W	Y14, Y47	*CMP2*	Signaling/ ion homeostasis
YNL194C/ YDL222C	Y7, Y82	*FMP45*	Mitochondrial membrane protein
YML017W	Y2, Y40	*PSP2*	Mitochondrial mRNA splicing
YPR029C	Y95, Y97	*APL4*	Vesicle mediated transport
YGR064W	Y1, Y111	-	Overlaps with SPT4 ORF
YJR019C	Y105, Y106	*TES1*	Fatty acid oxidation

Bs3 expression differs among the identified clones

The aim of this screen was to identify Bs3 pathway components which are required to induce a growth defect in yeast. However, survival can probably also be observed in knockout strains whose mutation causes a reduction of Bs3 protein amounts. Therefore, all identified candidate clones were tested for *Bs3* expression via western blot. In 48 out of 112 strains, the amount of Bs3 was similar compared to expression levels in wild type yeast. In 20 strains, the amount of Bs3 was markedly reduced and in 43 strains, Bs3 could not be detected at all. One out of the 112 colonies did not grow in liquid culture and was therefore not tested for protein abundance. Notably, protein levels in most of the candidates that were identified at least twice were lower compared to wild type and varied among different clones (Figure 2.12). The latter could be a consequence of slight differences in induction time and cell number. Protein levels should be inspected carefully in clones that are chosen for follow up experiments.

String analysis does not reveal significantly enriched interactions

In order to clarify whether the identified yeast knockout candidates are associated, for example by direct interaction, a similar biological function, or involvement in the same process, a pathway analysis was conducted using String (Szklarczyk et al., 2015). 13/92 genes have a connection with at least one other

identified gene (Figure 2.13). No connection was found for 79/92 of the candidate genes (not shown). Notably, the connection of *SPT4* to *YGR064W* is based on their overlapping open reading frames. *YNL194C* is a paralog of *FMP45* that arose via whole genome duplication. The connections of HUB1/ECM2 and CMP2/CPR3 are based on direct interaction found in large scale studies (Decourty et al., 2008) or different species (Huai et al., 2002). Finally, the connection of PXP1, TES1, AGX1, GOR1 and GLC3 is based on their involvement in amino acid biosynthesis.

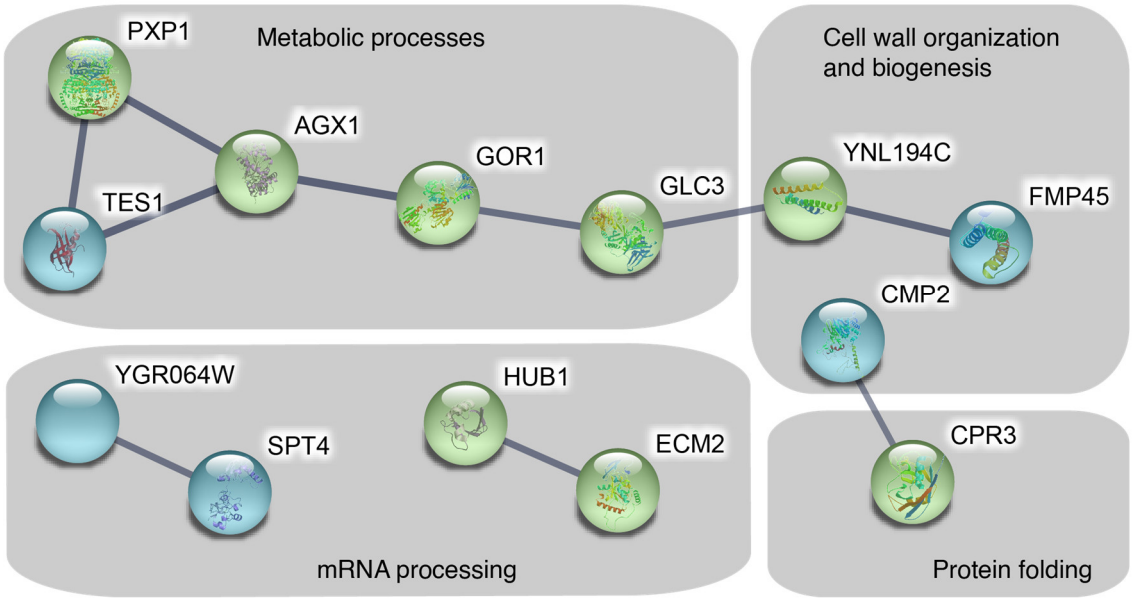

Figure 2.13 String analysis of identified candidate genes. Pathway analysis was performed using String (version 11.0). Only candidates that show association with high confidence (interaction score ≥ 0.7) are shown. Connected nodes are depicted as spheres. Candidates that were found once are coloured in green. Candidates that were found twice are coloured in blue. Disconnected nodes are hidden. Grey boxes highlight shared biological processes.

In general, the amount of identified associations within the 92 candidates is not increased compared to the number of expected associations in the total genome. This indicates, that the identified genes, which are knocked out in the surviving clones, fulfil independent functions within the cell. While we cannot exclude, that these genes are Bs3 associated, it is likely that many of the knockout candidates survive *Bs3* expression because they either suppress protein accumulation or compensate the growth defect via an independent cell developmental mechanism.

2.4.4 Virus induced gene silencing of immune pathway components

To further study the possibility that Bs3 produces a signal that discharges into known signalling pathways, we used Tobacco rattle virus (TRV) based virus induced gene silencing (VIGS) to knock down components involved in immune signalling. *Enhanced disease susceptibility-1* (*EDS1*), *suppressor of G-two allele of skp1* (*SGT1)* and its interactor *req*uired for MLA12 *resistance 1 (RAR1)* are known to be involved in NLR triggered immune pathways (Shirasu, 2009; Bhandari et al., 2019). *Non-race specific disease resistance-1* (*NDR1*) plays a role in ETI as well as SAR establishment and SA signalling (Shapiro and Zhang, 2001). *Isochorismate synthase-1* (*ICS1*) was chosen due to its function in SA biosynthesis. *Arginine decarboxylase 2* (*ADC2*) is described to be essential for HR triggered by the *Xanthomonas* type III effector AvrBsT (Kim et al., 2013). To control the timeframe of efficient silencing, the pepper *phytoene desaturase* (*CaPDS*) and the tomato *heat shock protein 70* (*SlHSP70*) that both cause an obvious leaf bleaching phenotype, were included.

SGT1 and *RAR1* silencing abolish Bs3 HR

Fragments of the respective genes (see supplement section 6.2) were cloned into the TRV2a vector. *Agrobacterium* strains carrying the respective construct and the strain carrying the TRV1 plasmid were co-infiltrated into *N. benthamiana* leaves. After three weeks, *35S* driven *Bs3-GFP* or *GFP* was expressed in silenced plants via agroinfiltration and development of an HR phenotype was monitored (Figure 2.11). None of the three different silencing constructs designed to target *ADC2* had any effect on the Bs3-GFP triggered HR. Similarly, *EDS1*, *NDR1* and *ICS* silencing did not interfere with Bs3-GFP triggered HR (Figure 2.11). By contrast, *RAR1* and *SGT1* silencing strongly reduced the Bs3 triggered HR. As expected, HR was also impaired in *GFP*, *SlHsp70* and *CaPDS* silenced plants (Figure 2.11). These results indicate that HR induction by Bs3 might be dependent on *SGT1* and *RAR1*.

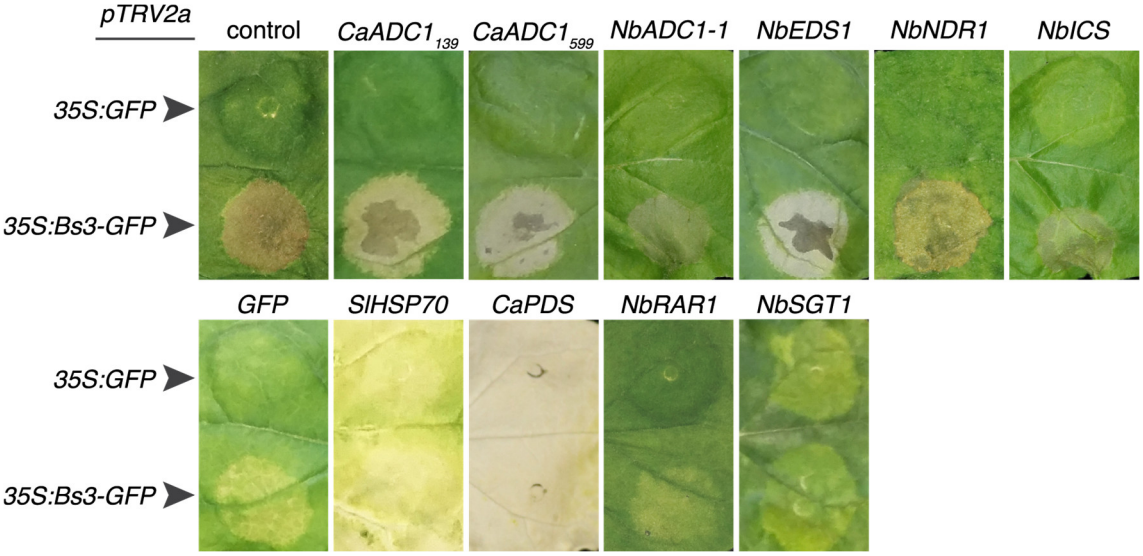

Figure 2.11. *SGT1* and *RAR1* silencing abolishes Bs3 HR pTRV1 and pTRV2a containing fragments of the indicated genes (for sequences see supplement section 6.2) in antisense orientation were delivered via *Agrobacterium* into three-week-old *N. benthamiana* plants. Three weeks later, *35S*-driven *GFP* or *Bs3-GFP* were expressed via *Agrobacterium* mediated transient transformation. Pictures were taken one week later.

2.5 The quest to identify the Bs3 substrate

The findings, that H_2O_2 production of Bs3 is not sufficient to trigger HR and that Bs3 forms a stable C4a-intermediate (see Bs3 manuscript, section 2.3.4) indicate, that Bs3 is converting a substrate to trigger HR. Therefore, we were interested in identifying a putative Bs3 substrate and conducted an untargeted metabolomics experiment. Furthermore, the ability to convert a common FMO substrate was tested with trimethylamine (TMA).

2.5.1 Trimethylamine is not a substrate of Bs3

TMA ($N(CH_3)_3$) is a chemical with a typical fishy odour that is known to be a substrate of hFMO3. As with other human FMOs, hFMO3 possesses a broad substrate specificity and oxygenates a variety of nucleophilic chemicals (Cashman and Zhang, 2006). We were interested if Bs3 would accept TMA as a substrate and oxidize it to Trimethylamine N-oxide (TMAO). Buffer containing 50 µM TMA was mixed with either purified Bs3 or $Bs3_{S211A}$ protein and incubated for 40 minutes at 20°C. TMA (putative substrate) and TMAO (putative product) concentrations were subsequently measured via gas chromatography-mass spectrometry (GC/MS) (Fig. 2.14). TMA concentrations in samples that contained Bs3 were not reduced compared to samples that contained $Bs3_{S211A}$ or buffer control. Furthermore, there was no decrease in TMA concentration

compared to samples without NADPH. Similarly, TMAO concentrations were not increased in samples containing Bs3, compared to samples containing $Bs3_{S211A}$, buffer or without NADPH. Since Bs3 is active and oxidizes NADPH in the presence of TMA (data not shown), these results suggest that TMA is not a Bs3 substrate

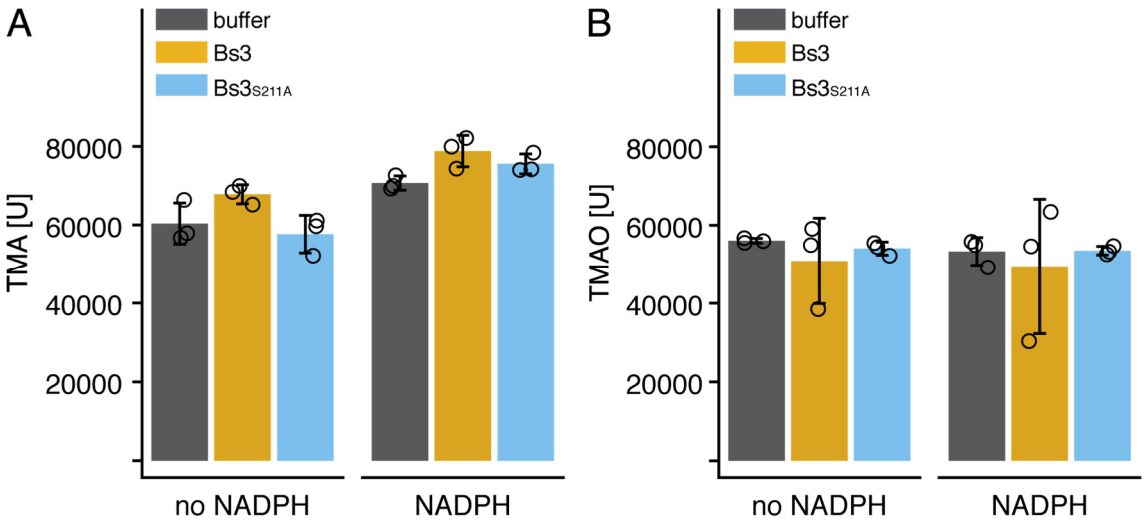

Figure 2.14. Trimethylamine (TMA) is not a Bs3 substrate. Potassium phosphate buffer containing 50 μM TMA was mixed 100 μM of NADPH. Bs3, $Bs3_{S211A}$ or buffer were added, and samples were incubated for 40 min. A) TMA concentrations were quantified by mass spectrometry. B) Trimethylamine-N-oxide (TMAO) was reduced to TMA and concentrations were quantified by mass spectrometry. Bars with error bars indicate mean of three replicates +/- standard deviation. Circles indicate individual measurements. U = units

2.5.2 Purified AtYUC6 converts IPA to IAA *in vitro*

YUCs are known to carry out a defined enzymatic function, the conversion of IPA to IAA (Dai et al., 2013). AtYUC6 was purified with the aim to use it as a control for Bs3 in enzymatic assays. To prove functionality, purified AtYUC6 was tested with its substrate IPA. Buffer containing IPA and NADPH was mixed with AtYUC6 to start the enzymatic reaction. Samples without NADPH or without AtYUC6 serve as negative control. After 40 min of incubation at room temperature, IPA and IAA contents were measured via GC/MS. IPA was almost completely absent in samples containing AtYUC6 and NADPH while higher levels of IPA were still present in samples that only contain buffer or lack NADPH (Figure 2.15). In samples containing AtYUC6 and NADPH, IAA levels are clearly higher when compared to samples without enzyme or NADPH. Notably, two

trimethylsilyl derivatives of IAA (IAA1TMS and IAA2TMS) were existent after derivatization and are shown individually (Figure 2.15). Consistently, IPA was slightly decreased, and IAA was increased in samples containing buffer and NADPH, stating that IPA, to an extent, showed spontaneous conversion without AtYUC6. Overall, the results confirm functionality of AtYUC6 and that it catalyses the enzymatic conversion of IPA to IAA in an NADPH dependant manner.

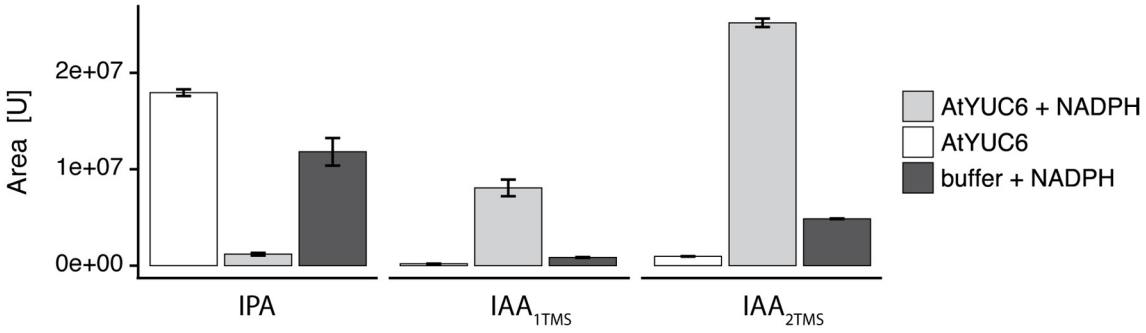

Figure 2.15 AtYUC6 converts IPA to IAA in vitro. Purified AtYUC6 protein was mixed with buffer containing no or 200 μM NADPH and 50 μM indole pyruvic acid (IPA). After 40 min of incubation, IPA and indole-3-acetic acid (IAA) contents were measured via GC/MS. 1TMS and 2TMS are two different Trimethylsilyl derivatives. U = Units.

2.5.3 Glucosinolates accumulate in Bs3 treated *Arabidopsis* extracts

Since there is a nearly indefinite number of chemical substances that could serve as a Bs3 substrate, we decided to conduct non-targeted metabolomic analyses *in planta.* In a first attempt, *35S*-driven *Bs3* and $Bs3_{S211A}$, *GFP* and *CaYUC3* were transiently expressed in *N. benthamiana*. Leaf material was harvested, and metabolites were extracted and analysed via LC/MS. A putative substrate is expected to be downregulated in *Bs3* expressing leaves compared to controls. Vice versa, a putative product is expected to be increased in *Bs3* expressing leaves. Unfortunately, no candidate metabolite with matching characteristics could be identified with this method (data not shown). However, neither increased SA or Pip contents were accounted in leaf material expressing *Bs3*, nor increased IAA values in leaf material expressing *CaYUC3.* Since none of the compounds that are known to be increased upon Bs3 induction (Krönauer et al., 2019) could be confirmed, this may indicate insufficient sensitivity of the employed assay.

The substrate to product conversion during transient expression of *Bs3* might be gradual and probably starts at various time points in different cells, thus limiting the readout of the assay. To overcome this difficulty of the *in vivo* situation, we decided to conduct another metabolite analysis in a cell free context with plant extracts and purified protein. Leaves of three weeks old *Arabidopsis thaliana* plants were harvested, and metabolites were either extracted in 80% methanol or aqueous buffer. Subsequently the extract was mixed with NADPH and either Bs3 or Bs3$_{S211A}$. The test samples were incubated for 20 minutes at room temperature. In control samples, the reaction was immediately stopped after protein addition. LC/MS of the samples was conducted in positive or negative ionisation mode.

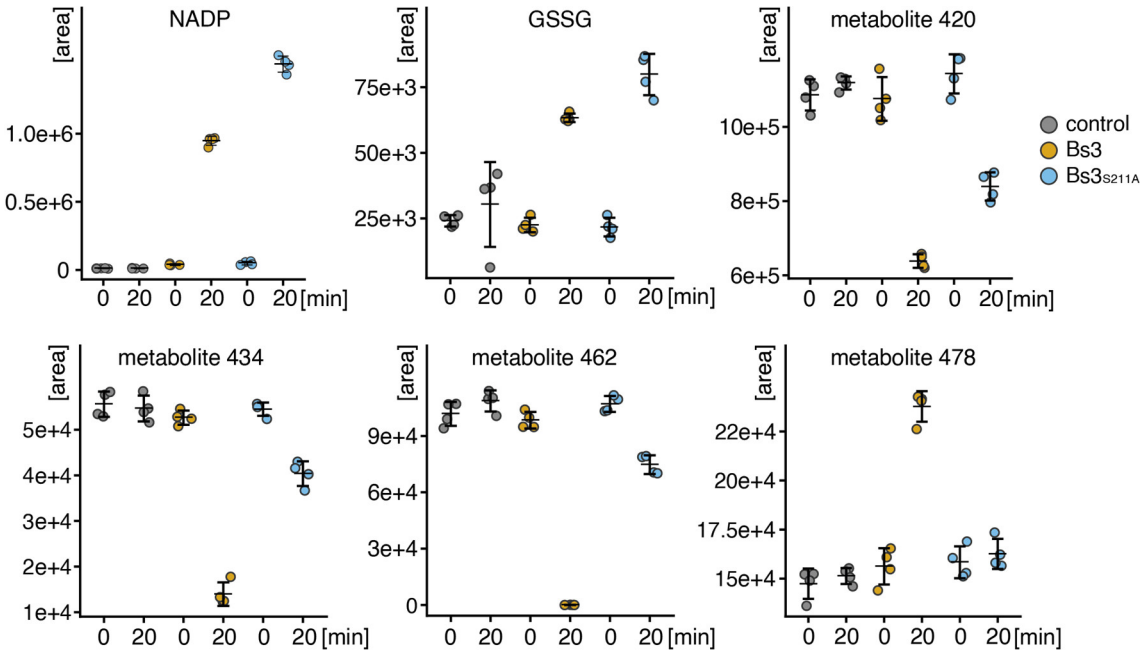

Figure 2.16 Metabolites that were increased or decreased in plant extracts after Bs3 treatment. *A. thaliana* leave extracts were mixed with 100 μM NADPH and either Bs3, Bs3$_{S211A}$ or buffer control. After 0 and 20 min of incubation at RT, the enzymatic reactions were stopped and metabolites were measured via LC-MS. Graphs represent normalized abundance of four replicates (filled circles) with mean and standard deviation. U = units. Metabolites which without reliable identity are numberd according to their mass to charge ratio (m/z).

Six metabolites were identified that were differentially abundant in the plant extract after 20 min of incubation with Bs3 compared to control (Table 2.5, Figure 2.16). Two of the metabolites were identified as $NADP^+$ and glutathione disulfide (GSSG). The oxidation of NADPH to $NADP^+$ confirms, that the purified Bs3 and $Bs3_{S211A}$ proteins are active in the plant extract. The increased values of GSSG match with our previous finding that Bs3 and $Bs3_{S211A}$ produce H_2O_2 and increases the oxidation state of their environment (see Bs3 manuscript, section 2.3.4). Notably, $NADP^+$ and GSSG values are highest in samples treated with $Bs3_{S211A}$ (Figure 2.16). These results confirmed a higher H_2O_2 production of $Bs3_{S211A}$ compared to Bs3.

Table 2.5 Metabolites with differential abundance in Bs3 samples compared to controls. IDs of ambiguous metabolites are based on their mass to charge ration (m/z). Identified metabolites were measured in positive and negative electrospray ionization mode (ESI+ and ESI-, respectively)

ID	MS MODE	M/Z	RETENTION TIME	SUGGESTED FORMULA	SUGGESTED METABOLITE
NADP+	ESI -	742.070	4.579	$C_{21}H_{28}N_7O_{17}P_3$	Nicotinamide adenine dinucleotide phosphate
GSSG	ESI +	307.083	4.774	$C_{20}H_{32}N_6O_{12}S_2$	Glutathione, oxidized
Metabolite 420	ESI -	420.044	6.620	$C_{12}H_{23}NO_9S_3$	Glucoerucin (4-methylthiobutyl glucosinolate)
Metabolite 434	ESI -	434.060	7.599	$C_{20}H_{19}O_{11}$ $C_{13}H_{25}NO_9S_3$	Glucoberteroin (5-Methylthiopentyl glucosinolate)
Metabolite 462	ESI -	462.092	9.554	$C_{15}H_{29}NOS_3$ $C_{25}H_{19}O_9$ $C_{14}H_{18}N_5O_{11}P$	7-Methylthioheptyl glucosinolate
Metabolite 478	ESI -	478.086	6.429	$C_{15}H_{29}NO_2S_3$ $C_{15}H_{22}N_5O_9PS$ $C_{22}H_{23}O_{12}$ $C_{16}H_{25}N_5O_{10}S$	7-Methylthioheptyl glucosinolate + O

Three metabolites (designated according to their mass to charge ratio as 420, 434 and 462) were downregulated in plants extracts that were incubated with Bs3 for 20 minutes, while one metabolite (m/z 478) was increased (Figure 2.16). The amount of metabolite 420 was strongly decreased and metabolites 434 and 462 were slightly decreased in samples that were treated with $Bs3_{S211A}$, indicating that the decrease could be due to oxidation by H_2O_2. However, since $Bs3_{S211A}$ is a stronger oxidase, we would have expected to see a stronger effect in $Bs3_{S211A}$ containing samples compared to Bs3 containing samples, as it is the case for $NADP^+$ and GSSG. All four metabolites were identified as putative glucosinolates

(Table 2.5). Interestingly, metabolite 462, which decreased after Bs3 treatment and 478, which increased after Bs3 treatment showed matching characteristics with 7-Methylthio-heptyl glucosinolate and its oxide, displaying the conversion that would be expected from the Bs3 enzymatic turnover.

2.5.4 Bs3 does not induce N-OH-Pip accumulation *in vitro*

FMO1 from *A. thaliana* (AtFMO1), which is required for the establishment of SAR (Mishina and Zeier, 2006), was recently described to catalyse the oxidation of pipecolic acid (Pip) to N-hydroxypipecolic acid (N-OH-Pip, Figure 2.17 A) (Hartmann et al., 2018). Since Pip levels increase after Bs3 expression in *N. benthamiana* (Krönauer et al., 2019, Figure 9), the question arose whether Bs3 converts Pip to N-OH-Pip in a similar manner like AtFMO1. Therefore, we analysed the presence of Pip and N-OH-Pip in the MS data of our non-targeted metabolomics experiment (section 2.5.3). Pip as well as N-OH-Pip were identified in buffer extracted samples. Since there is no difference in abundance of the two metabolites after 20 min of treatment with Bs3, $Bs3_{S211A}$ or control (Figure 2.17 B), we assume that Pip is not a substrate of Bs3.

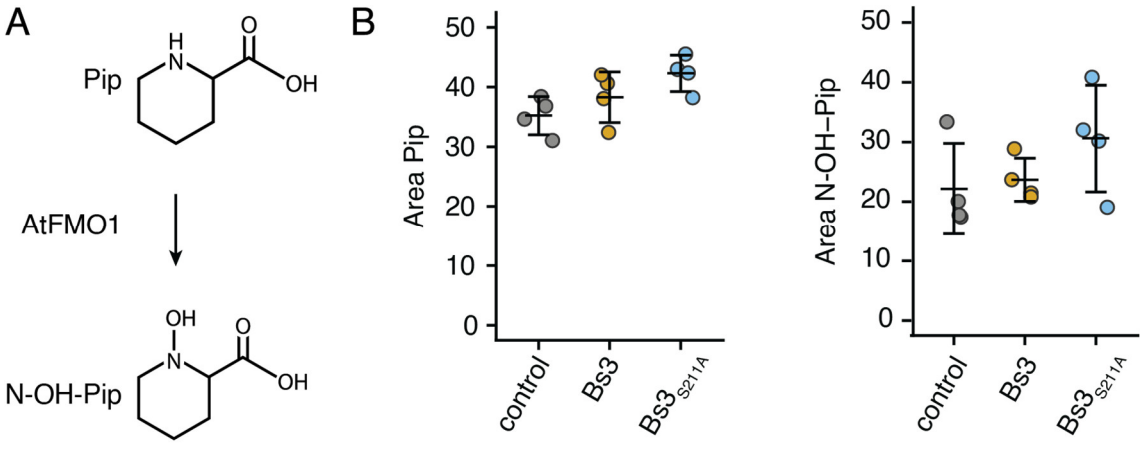

Figure 2.17 Bs3 treatment does not increase N-OH-Pip concentrations in plant extracts. A) Scheme of the conversion of pipecolic acid (Pip) to N-hydroxy-pipecolic acid (N-OH-Pip) by AtFMO1. B) *A. thaliana* leaves were extracted in buffer and mixed with 100 μM NADPH and either Bs3, $Bs3_{S211A}$ or buffer control. After 20 min of incubation at RT, the enzymatic reactions were stopped and metabolites were measured via liquid chromatography mass spectrometry (LC-MS). Graphs represent normalized abundance of four replicates (filled circles) with mean and standard deviation. U = units.

3 Discussion

Numerous resistance genes have been identified and cloned, and many of these genes trigger HR upon activation. However, in most cases, the molecular mechanisms and the signalling pathways leading to HR remain elusive.

Several molecular mechanisms are possible for the Bs3 triggered HR: (1) Bs3 predominantly performs an uncoupling reaction and produces H_2O_2. In case the amount of produced H_2O_2 is high, this could directly lead to cell death via its oxidizing properties. Lower amounts of H_2O_2 could act as signalling compound and trigger a signalling cascade, leading to cell death. (2) Bs3 enzymatically converts a metabolite into a toxic substance which causes cell death. (3) A combination of both. HR is induced by the interplay of a toxic Bs3 product within an increased intracellular oxidation state (Figure 3.1).

In this work, we conducted various *in vivo* and *in vitro* experiments as well as targeted and non-targeted metabolomics with the aim to test our different hypotheses on a possible molecular mechanisms of Bs3 induced HR.

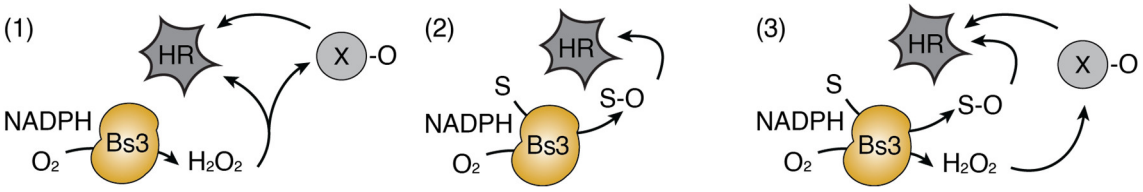

Figure 3.1 Potential mechanisms of HR induction by Bs3. 1) Bs3 triggers HR via production of H_2O_2. This might either directly induce cell death or trigger a signalling cascade via oxidation of specific target proteins. 2) Bs3 converts a substrate into a toxic product 3) Substrate conversion and a H_2O_2 induced change of the intracellular oxidation state in parallel trigger HR. S = Substrate, S-O = oxygenated substrate, X-O = oxygenated protein

3.1 H_2O_2 accumulation is not sufficient to cause HR

Our enzyme assays confirmed that Bs3 not only shows homology to FMOs on the sequence level but also that Bs3 indeed has FMO enzymatic function, like tight binding of an FAD cofactor and oxidation of NADPH with production of H_2O_2 (Section 2.3). Since H_2O_2 is known for its role in plant cell death, we investigated if Bs3 functions exclusively as an NADPH oxidase which triggers cell death by the production of excessive amounts of H_2O_2.

3.1.1 The Bs3$_{S211A}$ mutant does not induce HR but oxidizes NADPH

In order to analyse the function of Bs3 as an NADPH oxidase, a non-functional Bs3 derivative was needed as control. The ideal choice of a negative control would be a non-functional Bs3 derivative with an intact and stable three-dimensional structure. Bs3 contains two conserved GxGxxG motifs, also known as Rossmann fold, which function as FAD and NADPH binding sites, respectively. The six Bs3 derivatives with glycine to alanine exchanges within these conserved motifs, Bs3$_{G39A}$, Bs3$_{G41A}$ and Bs3$_{G44A}$, Bs3$_{G207A}$, Bs3$_{G209A}$ and Bs3$_{G212A}$, have previously been cloned and tested for function (J. Piprek, unpublished). Experiments in which these *Bs3* mutant derivatives were transiently expressed in *N. benthamiana* leaves, under control of the constitutive *35S* promoter, showed that no mutant derivative activated HR except *Bs3$_{G209A}$*, which remains partially functional. These findings were confirmed in additional experiments in yeast (Schiel, 2015). Some of the mutant derivatives, especially Bs3$_{G44A}$ and Bs3$_{G212A}$, showed signs of protein instability in western blots (Piprek, unpublished) and were thus not considered as suitable candidates. Furthermore, Bs3$_{G207A}$ was dismissed as control because the mutation of the first glycine within the Rossmann fold is described to destroy its three-dimensional structure (Rescigno and Perham, 1994). Apart from the glycine residues, the serine at position 211 in Bs3 (S$_{211}$) is conserved within the GxGx**S**G motif. In the flavin-dependent N-hydroxylating monooxygenase of *Aspergillus fumigatus* (SidA), the corresponding serine is known to interact with the pyrophosphate group of $NADP^+$, thereby being essential for the stabilization of the C4a-hydroperoxyflavin (C4a, Shirey et al., 2013). Mutations at this residue are known to cause higher rates of uncoupling. Interestingly, Bs3$_{S211A}$ neither triggers an HR in plants, nor a growth defect in yeast. If the S$_{211}$ in Bs3 functions similarly to the respective serine in SidA, loss of function in Bs3$_{S211A}$ could be explained by the absence of hydrogen bonds in between the introduced alanine and $NADP^+$, which impairs the stability of the C4a. Similar to other FMOs, a less stable C4a-intermediate might inhibit enzymatic turnover of the putative substrate, and consequently disable activation of HR (Krueger et al., 2009).

The Bs3$_{S211A}$ mutant derivative shows stable expression *in planta,* can be purified from *E. coli,* and oxidizes NADPH *in vitro* (See Bs3 manuscript, section 2.3.4). Together, these properties make Bs3$_{S211A}$ a good control in experiments that target the oxidizing properties of Bs3 and its effects *in planta*.

3.1.2 Bs3 produces more H_2O_2 compared to AtYUC6 *in vitro*

During Bs3 HR, high amounts of ROS accumulate in the leaf that can be visualized by DAB staining, (Bs3 manuscript section 2.3.4, Figure 1 and S1). However, accumulation of ROS is not specific to Bs3 HR but a generic response to many stress conditions including pathogen attack (Torres et al., 2006). Moreover, it is challenging to distinguish H_2O_2 originating from different sources during cell death reactions *in planta*. Therefore, we studied H_2O_2 production of Bs3 compared to AtYUC6 *in vitro.*

We found that Bs3 as well as AtYUC6 oxidize NADH and NADPH and thereby produce H_2O_2 (Figure 2.7). Notably, Bs3 produces considerably more H_2O_2 than AtYUC6 (Figure 2.7). In order to exclude the possibility that low NADPH oxidase activity of AtYUC6 is due to a loss of the protein´s native state during purification, functionality of purified AtYUC6 was confirmed by enzyme assays in which the known YUC substrate IPA was converted to IAA *in vitro* (section 2.5.2).

Surprisingly, H_2O_2 contents in samples containing AtYUC6 were sometimes lower than those in buffer control samples (Figure 2.7). Given that AtYUC6 is described to show some uncoupling *in vitro* which is approximately 4 % in presence of the substrate PPA (Dai et al., 2013), we expect the production of small but measurable amounts of H_2O_2 in the enzyme assays. The observation of decreased H_2O_2 levels is remarkable but would be in line with the recently proposed oxidoreductase activity of AtYUC6 which is described to cause decreased accumulation of ROS *in planta* along with increased drought resistance and delayed leaf senescence in *Arabidopsis* (Cheol Park et al., 2013; Kim et al., 2013; Cha et al., 2015). However, the evidence for an actual oxidoreductase activity of AtYUCs is not conclusive so far and it is more likely that the increase of lifespan and the decrease of ROS production in YUC overexpression plants are due to the high levels of auxin and the auxin based morphological differences. Consequently, it can be considered to be more likely that the lower levels of H_2O_2 compared to buffer control in our *in vitro* assays might be due to a stabilizing effect of AtYUC6 on NADPH or on some component of the Amplex Red assay that was used to measure H_2O_2 contents. Additional controls with BSA could be used to test the latter.

While the oxidoreductase function of AtYUC6 proposed by Cha et al. (2015) needs to be confirmed, it is possible that Bs3 and AtYUC6 have some redox active function based on their cysteines. Bs3 contains eleven and AtYUC6 contains 13 cysteines (3.2% and 3.1%, respectively). The cysteine content of the two proteins is double as high as the average cysteine content in plants like tomato and rice (Miseta and Csutora, 2000). Cysteine contains a sulfhydryl group and is therefore able to form inter- and intramolecular disulfide bonds. To test a putative function of cysteines in Bs3, we previously mutated all 11 cysteines individually to serine (C>S), and tested them via transient expression in *N. benthamiana* (Müller, 2017). All of the $Bs3_{C>S}$ mutant derivatives triggered HR. Either the cysteines in Bs3 function redundantly or they do not fulfil a specific function that has an impact on HR induction.

In summary, the levels of H_2O_2 produced by Bs3 are clearly different from those produced by YUCs and it appears rational that during evolution of Bs3, the enzyme properties diversified from YUCs and changed in favour of an increased NADPH oxidase activity. The results of our *in vitro* H_2O_2 measurements are consistent with a model where Bs3 produces high amounts of H_2O_2 that might be the initial trigger of an HR (see Figure 3.1).

3.1.3 Bs3 increases the intracellular oxidation state *in vivo*

The redox sensitive fluorophore roGFP2 allows the *in vivo* detection of H_2O_2 induced redox changes (Meyer et al., 2007). In order to analyse the redox changes in direct proximity of Bs3, we created translational fusions of Bs3 and its mutant derivatives to the fluorescent sensor roGFP2.

Our ratiometric measurements showed, that roGFP2 is in a higher oxidation state when fused to Bs3 or $Bs3_{S211A}$, compared to control samples (Section 2.3.4, Figure 6). This indicates H_2O_2 production by Bs3 and $Bs3_{S211A}$ *in vivo* and is in line with our *in vitro* measurements (Section 2.3.4, Figure 4). Remarkably, $Bs3_{S211A}$ induces a similar increase of the roGFP2 oxidation state as Bs3, even though it does not trigger HR. This demonstrates that NADPH oxidase activity is not sufficient to trigger cell death.

Initially, we also considered to test Bs3 with HyPer and the two other roGFP2 fusion proteins that are available: The fusion of roGFP2 and glutaredoxin (GRX1-roGFP2) and the fusion of roGFP2 and yeast oxidant receptor peroxidase-

1 (roGFP2-Orp1). Bs3 is functional as fusion protein with all three roGFP2 sensor derivatives and with HyPer (Figure 2.8). Due to its sensitivity to changes in pH, HyPer was not included in further experiments (Belousov et al., 2006). Compared to roGFP2, GRX1-roGFP2 is described to respond faster to changes in redox potential in cell culture systems and *in vitro* situations (Gutscher et al., 2008; Meyer and Dick, 2010). It is possible that the 1:1 ratio of GRX1 and roGFP2 and their spatial proximity exhibit an advantage of the fusion protein compared to unlinked roGFP2 but in case of sufficient GRX availability in leaves, the GRX1-roGFP2 fusion might be unnecessary. RoGFP2-Orp1 has been described to be more specific for H_2O_2 (Gutscher et al., 2009). However, similar to roGFP2, roGFP2-Orp1 can be efficiently reduced by the glutathione redox system, which is present in the cytoplasm (Nietzel et al., 2019). Due to the expected redundancy of the three sensor variants *in vivo* and successful reports of measurements with roGFP2 in leaves (Schwarzländer et al., 2008), the experiments were primarily conducted with roGFP2.

Bs3 is localized to the nucleus and the cytoplasm. The midpoint potential of roGFP2 is -280 mV, and therefore, the protein adapts a reduced state within the cytosol (Aller et al., 2013). Since the fluorescence signal to background ratio is favourable in pictures of nuclei, I decided to focus on nuclei in the redox reporter CLSM studies. In general, glutathione oxidation in the nucleus is considered to be similar compared to the cytoplasm. This assumption was supported by yeast immunolocalization studies in which equal GSH concentrations were measured in the nucleus and the cytosol (Zechmann et al., 2011). Similarly, studies in *Arabidopsis* in which the GSH-synthesis inhibitor buthionine sulfoximine was used to decrease GSH values, found an equal redox potential in the nucleus and the cytoplasm (Schnaubelt et al., 2015).

H_2O_2 originating from membrane bound NADPH oxidases can reach the cytoplasm (Nietzel et al., 2019). Hence, the ROS burst observed during later stages of Bs3 HR could cause roGFP2 oxidation in our assay. To avoid roGFP2 oxidation which is not caused by Bs3, the measurements were done 30 hours after agroinfiltration, which is few hours after detectable Bs3 protein accumulation (Krönauer et al., 2019) and no DAB staining or signs of cell death could be observed at that timepoint. Therefore, we are confident, that the increased oxidation state is caused solely by Bs3 activity and not the subsequent activation

of membrane bound NADPH oxidases or peroxidases. The fact that $Bs3_{S211A}$, despite not triggering cell death, is an active oxidase, supports our assumption.

Taken together these results indicate that Bs3 as well as $Bs3_{S211A}$ produce H_2O_2 *in vivo*. Since roGFP2 is not oxidized directly by H_2O_2 but equilibrates with the glutathione redox potential and is highly sensitive towards oxidized glutathione (GSSG, Meyer et al., 2007), it can be assumed that the H_2O_2 which is produced by Bs3 or $Bs3_{S211A}$ induces the oxidation of GSH to GSSG.

The finding that $Bs3_{S211A}$ does not cause cell death despite its similar effect on the cellular redox state compared to Bs3 implies that H_2O_2 production is not sufficient to trigger HR. However, Bs3 produces H_2O_2 even though the potential substrate would be present. This supports a model where substrate conversion and H_2O_2 production are necessary to trigger HR.

3.1.4 Many FMOs produce H_2O_2 with no physiological function

Our experiments confirmed that Bs3 produces H_2O_2 *in vitro* and *in vivo*. The major question, arising from these results is whether the production of H_2O_2 by Bs3 is an unavoidable but meaningless side reaction or if the changed redox state is instigating a response.

Interestingly, there are many examples of FMOs that show a different rate of uncoupling depending on the available substrate or cofactor. For example, *Aspergillus fumigatus* SidA performs N-hydroxylation of its primary substrate, N-ornithine. The hydroxylation of ornithine is highly coupled and 90 % of the NADPH is used for the hydroxylation reaction. By contrast, SidA also hydroxylyzes lysin, but this reaction is only 15 % coupled, due to a slightly different positioning of lysine compared to ornithine within the active site (Franceschini et al., 2012). Similarly, the *Nocardia farcinica* Lys monooxygenase shows 50-70 % uncoupling, dependent on if the cofactor is NADPH or NADH (Binda et al., 2015). Another study of human FMO1-3 found 30-50 % of consumed O_2 is released as H_2O_2 in the presence of the substrate ethylene thiourea (Siddens et al., 2014).

These reports clearly show that uncoupling is not only common in the absence of substrates, but also possible to a high degree in the presence of substrate. Despite some speculations on a possible function of the NADPH oxidase activity, there are no reports so far, that uncovered a purpose of the high degree of uncoupling observed in these N-hydroxylating FMOs. In human FMOs, allelic

variants that lead to a higher degree of uncoupling may potentially lead to a higher toxicity during enzymatic turnover of xenobiotics (Siddens et al., 2014). However, there are no indications of a physiological function of H_2O_2 production in human FMOs so far.

Still it cannot be excluded that the production of H_2O_2 by Bs3 might be meaningful with regard to its function in defence and cell death.

3.1.5 Sulfenome mining reveals redox sensitive proteins present during HR

The finding that Bs3 increases the intracellular oxidation state (see 2.3.4) indicates that Bs3 does produce H_2O_2 *in vivo*. We hypothesized that Bs3 therefore can cause sulfenylation of redox sensitive proteins in the cell. Since protein sulfenylation is known to be decisive for changing protein functionality and inducing or repressing signalling (Waszczak et al., 2015), it is conceivable that H_2O_2 produced by Bs3 can trigger a downstream signalling cascade. Since our results from the analysis of $Bs3_{S211A}$ showed, that H_2O_2 production alone is not sufficient to trigger HR, we expect the presence of additional components which are available after expression of Bs3 but not of $Bs3_{S211A}$ and are crucial for induction of HR. Therefore, we were interested in the identification of target proteins that are sulfenylated after Bs3 expression. Interestingly, 40 candidates were identified which are only present in Bs3-YAP1C samples, but only one candidate (ABC transporter G family member 7, Supp. Table 6.4) was identified which was only present in $Bs3_{S211A}$-YAP1C samples. This supports our assumption that there are proteins present or sulfenylated in the Bs3 environment, which are necessary to trigger HR and are therefore absent in $Bs3_{S211A}$ containing samples. However, it cannot be excluded that the higher number of sulfenylated proteins found specifically in Bs3-YAP1C samples is caused by other sources of ROS that are induced by Bs3 during plant HR.

Interestingly, 29 of these candidates have not been identified in previous studies that aimed to find sulfenylated proteins after treatment with H_2O_2 (B. de Smet, personal communication). This is especially interesting since the amounts of H_2O_2 that were used to induce sulfenylation in these other experiments were in between 0.5 and 20 mM, a concentration that is much higher than what is produced by Bs3 (Akter et al., 2015). The fact that most of the identified

candidates seem to be specific for Bs3 HR highlights the changed intracellular environment caused by Bs3 expression.

In general, the sulfenome mining method can generate some false negative results as non-disulfide based binding to the YAP1A does not exclude the possibility that the protein is also specifically binding to the YAP1C with a disulphide bond. Furthermore, there are two critical points within the assay. One is the less abundant expression of $Bs3_{S211A}$ compared to Bs3 (De Smet, 2019). Uneven protein amounts complicate quantitative analysis and could lead to false positive candidates found in the Bs3-YAP1C samples, that are not detectable in the $Bs3_{S211A}$-YAP1C samples. Another possible difficulty is the *N. benthamiana* peptide databases that was available when these experiments were performed. Despite its importance as a model organism and transient expression system the *N. benthamiana* databases still remain to be completed and fully annotated. It is therefore likely, that possible candidates have been excluded from the analysis because they failed to match with the database.

In summary, some interesting Bs3 specific candidates were identified in the sulfenome mining experiments but it remains unclear, if these candidates are sulfenylated by Bs3 derived H_2O_2 or by other sources of ROS in the cell. Nevertheless, these candidates are redox sensitive proteins that are present during Bs3 mediated induction of HR and might play an important role in signalling. It will be the goal of future experiments to clarify the function of these 40 sulfenylated candidates. Comparative experiments in *Arabidopsis* or re-analysis of the *N. benthamiana* data at a later timepoint might improve the outcome of this approach.

3.2 The Bs3 substrate remains to be determined

3.2.1 YUCs and Bs3 have different substrates but the same inhibitors

The Bs3 protein sequence has high similarity to YUCs (Krönauer et al., 2019, Figures S1 and S2) and it is conceivable that Bs3 and YUCs share an evolutionary origin. However, the cell death phenotype caused by Bs3 is clearly different from the leaf curling caused by YUCs, indicating a different enzymatic function. Our experiments *in planta* and *Agrobacterium* show, that no IAA accumulates after *Bs3* expression (Krönauer et al., 2019, Figure 9 and Figure

S12), suggesting, that Bs3 does not convert IPA to IAA. Presumably, this is due to differences in the amino acid composition of Bs3 compared to YUCs, that cause a conformational change of the active site in Bs3 and prevents binding of IPA or its conversion to IAA *in vivo*.

Bs3 does not convert the tertiary amine TMA into TMAO (Figure 2.14). This indicates, that Bs3 has a different substrate specificity compared to human FMOs. Bs3 might have a narrow substrate range, similar to YUCs, for which only enzymatic conversion of IPA to IAA, and the analogous phenyl pyruvic acid (PPA) to phenyl acetic acid (PAA) is known (Dai et al., 2013). Experiments that previously identified tryptamine as a substrate of YUCs turned out to be erroneous (Zhao et al., 2001; Kim et al., 2007; Tivendale et al., 2010).

Interestingly, Bs3 is inhibited by the two metabolites Yucasin and methimazole (Bs3 manuscript, section 2.3.4, Figure 4). Methimazole serves as substrate and inhibitor of FMOs (Dixit and Roche, 1984; Nace et al., 1997; Eswaramoorthy et al., 2006). Yucasin is described to be a competitive inhibitor of YUCs, indicating that its properties allow it to enter the same active site as the substrate (Nishimura et al., 2014). Since both, Bs3 and AtYUC6 are inhibited by these compounds, we can assume that the active site conformation of Bs3 and YUC is partially conserved. However, as known from pharmacogenetic screens and human drug metabolizing liver FMOs, even minor polymorphisms like single amino acid exchanges can have decisive effects on substrate specificity (Gao et al., 2018). An example is hFMO3 in which more than 30 mutations have been identified thus far, that impaired enzyme activity (Phillips and Shephard, 2008). The N61S mutation in hFMO3 leads to loss of TMA N-oxidation activity but the mutant protein seems to retain its function to S-oxidize methimazole (Dolphin et al., 2000). Detailed studies on this $hFMO3_{N61S}$ revealed that the mutation causes a destabilization of the $NADP^+$ and a much faster decay of the C4a-intermediate (Gao et al., 2017).

Our experiments on IAA as a possible Bs3 substrate only targeted the *in vivo* situation (Krönauer et al., 2019). It could be possible that Bs3, due to specific differences compared to YUCs, has a reduced affinity for IPA and therefore does not produce IAA *in vivo*. In that regard, it would be interesting to test, if Bs3 is able to convert IPA in conditions when IPA is available in excess.

Based on the high similarity of Bs3 to YUCs and the equal response to Yucasin and methimazole, a putative Bs3 substrate might be similar to IPA. However, since already small conformational changes can have an effect on substrate specificity, the prediction of a Bs3 substrate remains speculative.

3.2.2 Does Bs3 oxidize glucosinolates?

Our metabolite experiments with *Arabidopsis* plant extracts and purified Bs3 protein identified several substances which are more abundant in Bs3 compared to control samples (Figure 2.16, Table 2.5). Accumulation of $NADP^+$ and GSSG confirms that the purified proteins are active in the plant extract and that H_2O_2 is produced. Candidate metabolites with higher abundance in Bs3 compared to control, but similar abundance in $Bs3_{S211A}$ treated samples are probably a side product of H_2O_2 production and not responsible for HR. Surprisingly, all metabolites that were found to be more abundant in Bs3 treated samples compared to $Bs3_{S211A}$ and control samples, seem to be glucosinolates. Glucosinolates are amino acid derived, sulfur rich metabolites that are almost exclusively found in the order Brassicales. Upon tissue damage by physical impacts or biotrophic pathogens, glucosinolates get into contact with myrosinases and are hydrolysed. The hydrolysis products are an active compound in plant defence and responsible for the characteristic pungent taste of Brassicaceae (Halkier and Gershenzon, 2006).

Leaf material of *Arabidopsis,* which belongs to the family of Brassicaceae, was chosen for non-targeted metabolite analysis because it contains less substances that interfere with MS analysis compared to *Capsicum* and *Nicotiana* (M. Stahl, personal communication). It is known from transgenic *A. thaliana* lines, that express Bs3 under control of an inducible promoter (Morbitzer, unpublished), that Bs3 expression causes cell death in *Arabidopsis*. Assuming, that HR is triggered by the same compound in *Capsicum* and *Arabidopsis*, all metabolites that are necessary for Bs3 HR should be present in *Arabidopsis*.

Glucosinolates and their breakdown products are associated with stress and defence reactions targeting herbivores and microbes (Tierens et al., 2001; Bruce, 2014). In *Arabidopsis*, glucosinolates are required for callose deposition during innate immune response (Clay et al., 2009). Thus, the metabolic events triggered by these compounds hypothetically could be integrated into the HR.

However, glucosinolates are only present in Brassicaceae and not in Solanaceae like *Capsicum* or *Nicotiana,* which indicates that the identified compound is probably not the primary substrate of Bs3.

Bs3 has 64% identity to YUC FMOs but less than 23% to the seven FMOs of the GS-OX type in *Arabidopsis* ($FMO_{GS\text{-}OX1\text{-}7}$) which catalyse the *S*-oxygenation of glucosinolates (Li et al., 2008; Kong et al., 2016; Krönauer et al., 2019). Glucosinolates are structurally different from IPA, MMI and Yucasin which are substrates or inhibitors of YUCs and Bs3 (Figure 1.3 and 1.5). However, it cannot be excluded, that Bs3 oxygenates glucosinolates.

In summary, the identity of metabolites that were increased after Bs3 treatment need to be confirmed and subsequently analysed further. Leaf material of different plant families should be used to conduct metabolite analyses and pure chemical compounds could be used to test a putative glucosinolate oxygenation of Bs3 *in vitro*.

3.3 Components of the Bs3 environment

Besides the immediate events like substrate conversion and increase in oxidation state, we were interested in the upstream and downstream processes of Bs3 HR. In this work, several experiments were conducted in order to get insights into generated metabolites, possible pathway components of Bs3 triggered HR and putative interacting proteins of Bs3.

3.3.1 Bs3 expression induces SA and Pip but not N-OH-Pip

Expression of *Bs3* in *N. benthamiana* causes strong accumulation of SA and a slight but significant increase of Pip (Krönauer et al., 2019). Based on the time interval between Bs3 expression and SA accumulation, it can be assumed that Bs3 causes an induction of the SA biosynthesis pathway and does not directly produce SA via the conversion of isochorismate. Interestingly, activation of *Bs3* by AvrBs3 carrying *X. euvesicatoria* strains in pepper coincides with increased transcript levels of BAHD Acyltransferase (BAHD) and indole-3-acetic acid-amido synthetase GH3.6-like (GH3.6), which are homologous to EPS1 and PBS3, two proteins that were recently discovered to drive SA biosynthesis from

chorismate in *Arabidopsis* (Rekhter et al., 2019; Torrens-Spence et al., 2019). If SA production is a side effect of Bs3 expression or required for Bs3 induced HR remains to be determined.

The interplay of Pip and SA is known to be required for the induction of SAR. It is known from *Arabidopsis* plants with mutations in *ICS1 or AGD2-LIKE DEFENSE RESPONSE PROTEIN 1* (*ALD1*), that lead to a defective production of SA and Pip, respectively, that a decrease of these metabolites impairs SAR and induction of pathogenesis related genes (Bernsdorff et al., 2016). Another protein required for SAR establishment is *Arabidopsis* FMO1, which converts Pip into N-OH-Pip (Hartmann et al., 2018). Despite the common role in immunity, Bs3 has considerably less similarity to AtFMO1 than to AtYUCs and causes a different phenotype *in planta*. While *Arabidopsis* fmo1 plants are SAR deficient, there is no obvious phenotype in the absence of *Bs3*. Overexpression of AtFMO1 increases resistance to pathogens, while Bs3 expression causes HR. Together with the finding that Bs3 does not change N-OH-Pip levels in *Arabidopsis* extracts (Figure 2.17) this implies that Bs3 fulfils a different enzymatic function than AtFMO1.

3.3.2 VIGS of SGT1 and RAR1 abolishes Bs3 HR in *N. benthamiana*

In recent years, virus induced gene silencing (VIGS) was used as a tool to study essential components of immune signalling pathways, especially in NLR mediated immune reactions. In this work, we used VIGS to silence known elements of immune pathways in order to find candidates that could be required for the Bs3 immune response and to analyse if Bs3 and NLR immune reactions employ common components.

Silencing of *SGT1* and *RAR1* abolished Bs3 triggered HR in *N. benthamiana* (Figure 2.11). This is only partially consistent with results from previous studies which show that *SGT1* but not *RAR1* is required for Bs3 HR (Römer, 2010). However, since RAR1 and SGT1 directly interact with each other and build a ternary complex with the heat shock protein Hsp90 (Zhang et al., 2010; Siligardi et al., 2017), it is possible, that both, RAR1 and SGT1 are required during induction of Bs3 HR. Notably, *SGT1* as well as *RAR1* silencing were found to have a negative effect on protein accumulation (Anand and Mysore, 2013; Yu et al., 2019). Therefore, it is possible that impairment of Bs3 HR in *SGT1* and

RAR1-silenced plants is due to decreased protein accumulation or protein misfolding. In this context it would be interesting to analyse the amounts of Bs3 protein in *RAR1*- and *SGT1*-silenced plants and to test if the present protein is still functional. Interestingly, however, *SGT1* silencing is known to impair accumulation of active mitogen-activated protein kinase kinase in *N. benthamiana* (MEK), that was co-purified with Bs3 in the pull down experiments (section 2.4.1, Table 6.4) and that is known to be required for HR induction of a variety of different R proteins, for example Pto and RPS2 (Oh and Martin, 2011; Ichimura et al., 2016)

The lipase like protein EDS1 builds complexes with PHYTOALEXIN DEFICIENT 4 (PAD4) or SENESCENCE ASSOCIATED GENE 101 (SAG101) and is required for the function of many TIR-NLRs. Similarly, the integrin like protein NDR1 is required for the activation of many CC-NLRs (Qi et al., 2018; Bhandari et al., 2019), (Knepper et al., 2011). The finding that Bs3 HR is neither affected by *EDS1* nor by *NDR1* silencing indicates that Bs3 uses different pathways than NLRs.

In general, the assumption that silencing was effective is based on the phenotypic changes in leaf morphology or impaired Bs3 HR that can be observed in plants in which *SGT1*, *PDS*, *HSP70, GFP and RAR1* are silenced. The silencing of *ADC2*, *ICS*, *NDR1* and *EDS1* did not cause any obvious phenotype in *N. benthamiana* and transcript levels of the target genes remain to be analysed.

In summary, Bs3 HR requires SGT1 and RAR1. However, it remains to be determined if the two proteins fulfil a role in signalling or if they are necessary for proper protein folding and accumulation of Bs3.

3.3.3 Functions of candidates that were co-purified with Bs3

The aim of the pull-down experiments was to identify putative proteins that directly interact with Bs3 and can therefore be extracted from plant leaves alongside with Bs3-GFP via immuno-purification. More than 100 proteins were identified by MS analysis of which approximately 50 are more abundant in samples containing Bs3 compared to controls (Table 2.2 and Supp. Table 6.3).

There have been some indications that Bs3 might indeed interact with other proteins. A previously conducted yeast two hybrid screen (Pascal Braun, unpublished) identified four putative interaction partners of Bs3: AT4G34710/

Arginine decarboxylase (ADC2), AT5G54930/ Metabolic network modulator 1 (MNM1), AT2G45680/ TCP domain protein 9 (TCP9) and AT2G02540/ homeobox protein 21 (ATHB21). Especially TCP9 appeared to be a promising candidate, since the protein belongs to a family of transcription factors that regulate the expression of *ICS1* and induce accumulation of SA. A model where the interaction of Bs3 with TCP9 leads to activation of *ICS1* would therefore be in agreement with the accumulation of SA triggered by Bs3 in *N. benthamiana* (Krönauer et al., 2019). However, none of the candidates that were identified in the co-immunopurification experiments matched with one of the four proteins found previously in the yeast two hybrid screen.

Nevertheless, the majority of identified proteins are known for their role in regulation of SA biosynthesis, cell death and immunity. Two other abundant groups are chaperones and proteins involved in terpenoid biosynthesis.

Identified proteins that are involved in regulation of SA synthesis

Bs3 expression increases SA levels *in planta* (Krönauer et al., 2019, Figure 9). Two interesting candidates that were identified via co-immunopurification with Bs3 that are known to play a role in regulation of SA synthesis were H-type thioredoxin and prohibitin. H-type thioredoxins catalyse disulfide reduction and thereby regulate many cellular processes, especially during stress responses (Arner and Holmgren, 2000). A prominent target of H-type thioredoxins in *Arabidopsis* is NON-EXPRESSOR OF PATHOGENESIS RELATED 1 (NPR1), the master regulator of SA perception (Tada et al., 2008). Thioredoxins catalyse NPR1 oligomer reduction which is the prerequisite for translocation of NPR1 to the nucleus and required for its function.

The *Arabidopsis* homologue of the prohibitin subunit (AtPHB3), was found to associate with the *ICS1* promoter and to induce SA production (Seguel et al., 2018). Silencing of the prohibitin gene decreases the number of mitochondria and increases ROS levels in plants (Ahn et al., 2006). Furthermore, the replicative lifespan in yeast lacking the respective homolog is reduced (Coates et al., 1997). Thus, a putative inhibiting effect of Bs3 on the yeast prohibitin homolog would be consistent with the observed Bs3 induced phenotype in yeast (Figure 2.3 and Bs3 manuscript section 2.3.4, Figure 2).

Identified proteins that are involved in plant immunity and HR

The GTP cyclohydrolase II (D6RUS9), an enzyme encoded by the *RibA* gene, is involved in the biosynthesis of FAD, the cofactor employed by Bs3. Silencing of *RibA* in *N. benthamiana* not only causes a decrease of flavin levels, but also compromises HR triggered by mitogen-activated protein kinase kinase (MEK, Asai et al., 2010). Interestingly, the respective MEK, NbMEK2, which triggers HR in a *RibA* dependent manner was also found to be higher abundant in Bs3 pull down samples compared to controls. The presence of the respiratory burst oxidase homolog B (RbohB) was expected, since Bs3 induction causes ROS accumulation in *N. benthamiana* (section 2.3.4). However, RbohB is induced by MEK2 (Yoshioka et al., 2003), and therefore complements the group of proteins belonging to the same signalling cascade. Together, this group of candidates suggests an overlap of Bs3 triggered HR and the MAP kinase cascade.

The identified Lipoxygenase (R4S2V6) is known to be induced by pathogens and elicitors and to drive peroxidation of lipids during plant immune and abiotic stress responses (Montillet et al., 2005). The transient expression of *35S*-driven lipoxygenase homolog in pepper (*CaLOX1*) triggers cell death (Montillet et al., 2005; Hwang and Hwang, 2010). Reciprocally, silencing of *CaLOX1* delays HR and increases susceptibility to *X. euvesicatoria* (Hwang and Hwang, 2010).

Surprisingly, the CC-NLR protein NRG1 (Q4TVR0) which is encoded by the *N. benthamiana requirement gene 1* (*NRG1*) was one of the identified candidates in the pull down experiment. NRG1 is required for HR mediated by the TIR-NLR N. Together NRG1 and N mediate resistance to tobacco mosaic virus (Peart et al., 2005). A study by Qi et al. (2018) epistatically places NRG1 downstream of EDS1, whose silencing does not affect the Bs3 HR in our VIGS screen. Notably, only one peptide was identified for NRG1 in Bs3 and $Bs3_{S211A}$ samples and the finding needs to be verified.

5-epi-aristolochene synthase (EAS) is an enzyme that catalyses the conversion of 5-epi-aristolochene, a precursor of the terpenoid capsidiol (Figure 3.2). Interestingly, EAS was not only identified after co-immunopurification with Bs3, but also in the sulfenome mining experiments (section 2.4.2). Furthermore, EAS is transcriptionally upregulated in pepper plants after treatment with AvrBs3 carrying *Xanthomonas* strains (Lahaye et al., unpublished). *EAS* is

known to be induced after PAMP treatment (Lee et al., 2017) and capsidiol is known to have antimicrobial effects and to increase the resistance of plants to fungal pathogens like *Phytophtora infestans.*

A promising way to analyse if these immunity-associated candidates are required for Bs3 HR would be to knock down the respective genes via VIGS in *N. benthamiana* and to analyse the possible effect on HR induction after Bs3 expression.

3.3.4 Candidates found in yeast screen are distinct from plant components

Bs3 expression impairs growth in yeast. Phenotypically, yeast cells expressing Bs3 can be distinguished from control cells due to an enlarged vacuole present in many cells (Figure 2.3). In general, yeast vacuole morphology is dependent on growth phase and environmental stimuli. While yeast cells have several medium sized vacuoles during normal growth, fusion to one vacuole which builds a large compartment can be observed during the stationary phase, glucose deprivation and hypotonic conditions (Li and Kane, 2009).

Though it is unknown, if the growth defect in yeast is induced by similar or different processes compared to HR in plants, the activity of Bs3 in yeast provided the possibility to screen a yeast knockout library for strains that are not affected by Bs3 expression. The yeast screen conducted in this work identified a total of 102 candidates whose mutations could rescue the Bs3 induced growth defect (Table 6.4). Only nine of these candidates were found twice or three times and pathway analysis neither revealed any striking links in between the candidates nor any indication of a common function (Figure 2.13).

Little is known about the identified strains from literature. Two candidates, *kel1Δ* and *fmp45Δ* were previously found in a screen on temperature sensitivity caused by *cdc13* mutation. The two knockout strains rescue temperature sensitivity in yeast that contain a mutated version of the telomerase recruiting protein CDC13p (Addinall et al., 2008). However, the result that *kel1Δ* mutation rescues *cdc13Δ* temperature sensitive phenotype while *fmp45Δ* has the opposite effect, makes it difficult to fit the two candidates into a model that explains resistance towards Bs3 induced growth defects.

It is most likely that the major function of the candidates that were found to survive *Bs3* expression is the decrease of Bs3 protein accumulation. This would be in line with our expression analysis (Fig. 2.12) which shows a reduced amount of Bs3 protein in most of the candidates that were identified twice. For *spt4Δ*, globally reduced protein biosynthesis was already reported previously (Cheng et al., 2015).

Surprisingly, the gal80Δ strain rescues the Bs3 induced growth defect without impairing Bs3 protein accumulation (Figure 2.12). Gal80p is known to bind to the activation domain of the Gal4 transcription factor, therefore repressing transcription of genes downstream of the *GAL1* promoter (*pGAL1*) in the absence of galactose (Sil et al., 1999). In the pYES-DEST-52 vector used in our experiments, *Bs3* lies downstream of *pGAL1*. Overexpression of *GAL80* would probably repress Bs3 expression and improve cell survival. Hence, the finding that the *gal80Δ* mutation rescues the *Bs3* induced phenotype is unexpected. A possible explanation is, that gene expression of one of the Gal4p induced genes compensates for the *Bs3* phenotype. Given, that Gal4p activates a variety of genes besides those playing a primary role in galactose metabolism (Traven et al., 2006), it could be possible that one of these genes increases stress resistance and therefore prevents *Bs3* induced cell death. However, there is no further evidence so far that one the Gal4p activated genes is involved in regulation of survival during stress responses.

Like in plants, the main source of ROS in yeast comes from side reactions of aerobic metabolism (Murphy, 2009). In case the *Bs3* triggered growth arrest in yeast is due to production of H_2O_2, we would expect to find knockout strains that are known to have increased resistance towards oxidative stress. Interestingly, depending on the nature of ROS, yeast has a variety of different set of genes that are induced upon treatment and are involved in stress responses (Shapira et al., 2004; Thorpe et al., 2004). None of the key candidates that are known to increase stress survival in yeast, like *yca1Δ* (YOR197W) which is known to abolish H_2O_2 induced apoptosis (Khan et al., 2005) were identified in surviving yeast strains after transformation with *Bs3*. It would be interesting to specifically test consequences of *Bs3* induction in these candidates in future experiments.

In summary, the yeast knockout library screen yielded a number of interesting candidates that could serve as a basis for follow up experiments. Expression levels should be checked thoroughly to exclude that sole reduction of

Bs3 protein amount leads to survival. Also, complementation experiments are needed to confirm the barcode-based identity of the knockout candidates as well as to exclude the occurrence of second site mutations or other rare but possible adverse events that could account for the survival phenotype (Giaever and Nislow, 2014).

3.3.5 Synopsis

Figure 3.2 shows the interplay of selected compounds and components that were identified within the different experiments that were conducted with the objective to find pathway components of Bs3 HR. For the sake of completeness, the identified candidates were compared to a previously conducted RNAseq experiment (Lahaye et al., unpublished) in which differentially upregulated genes of *C. annuum* were identified after inoculation with AvrBs3 carrying *Xanthomonas* strains.

The metabolite analyses as well as pull down- and sulfenome mining-experiments each identified a number of candidates that are highly abundant after expression of *Bs3,* and play a putative role in Bs3 triggered HR. Methods involving MS yielded a higher number of candidates that need to be evaluated thoroughly. The presence of these candidate proteins, especially of those whose discovery is based on a low number of identified peptides, needs to be confirmed. For many candidates that were identified in the different assays, a defence related function has already been described. However, it remains unclear if any of the candidates specifically interacts with Bs3 or if their presence is required for Bs3 HR. Proteins that co-immunopurified with or were sulfenylated by Bs3 may display a snapshot of the compounds that constitute the intracellular environment after *Bs3* expression. Even though the molecular mechanism of Bs3 remains to be determined, these experiments give a first insight into the complex intracellular processes during Bs3 HR.

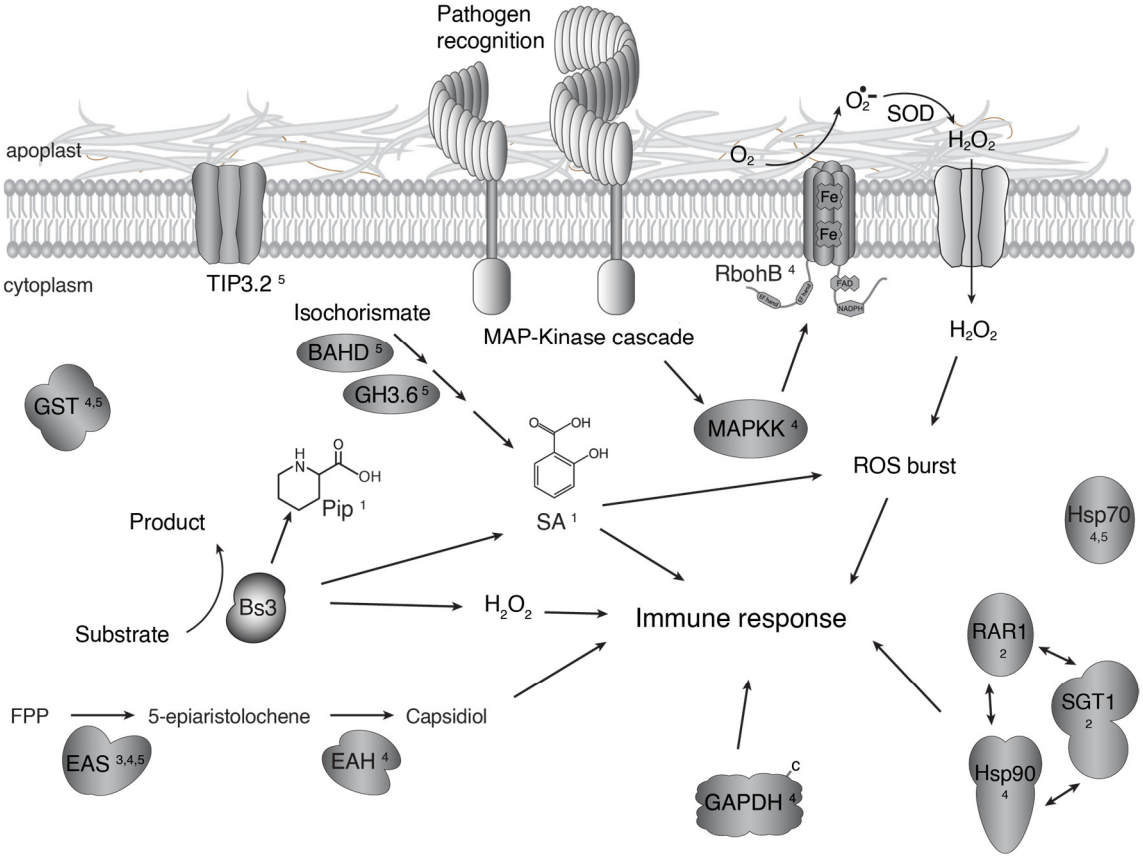

[1] Increased in *N. benthamiana* after expression of *Bs3*
[2] Found by VIGS to be indispensable for Bs3 HR in *N. benthamiana*
[3] Sulfenylatd during Bs3 HR in *N. benthamiana*
[4] Co-purified with Bs3 in *N. benthamiana*
[5] Transcriptionally upregulated in *C. annuum* after infection with *Xanthomonas* carrying AvrBs3

Figure 3.2 Synopsis of selected components identified in screens for Bs3 substrates and interaction partners. Bs3 expression causes accumulation of Pip, SA and H_2O_2. RAR1 and SGT1 are required for HR. Furthermore, the results indicate the involvement of the MAP kinase pathway, chaperones, GAPDH and terpenoid biosynthesis. Bs3 presumably converts a so far unknown substrate. BAHD = BAHD Acyltransferase (XM_0167190254); EAH = 5-epi-aristolochene-1,3-dihydroxylase; EAS = 5-epiaristolochene synthase; FPP = farnesyl diphosphate; GAPDH = glyceraldehyde 3-phosphate dehydrogenase; GH3.6 = indole-3-acetic acid-amido synthetase GH3.6-like (XM_016725827); GST = glutathione-S-transferase; Hsp = heat shock protein; Pip = pipecolic acid; Rboh = respiratory burst oxidase homolog; SA = salicylic acid

4 Material and Methods

4.1 Material

Bacterial strains, tools, antibiotics and media used in this study are listed in Table 4.1 to 4.4. Buffers used for Bs3 purification are listed in Table 4.5 All other solutions are mentioned within the method in which they were utilized. A list with expression vectors and oligonucleotides used in this study can be found in the supplement (Table 6.1 and 6.2).

Table 4.1: Bacteria and yeast strains

STRAIN	RELEVANT CHARACTERISTICS
A. tumefaciens GV3101	C58 (RIF R) Ti pMP90 (pTiC58DT-DNA) (gentR/strepR) Nopaline
X. euvesicatoria 82-8 uns*	RifR ΔAvrBs1 ΔAvrBs2 ΔAvrBs3 AvrBs4Δrep 5-11
E. coli Top 10	F- *mcr*A (*mrr-hsd*RMS-*mcr*Bc) 80d *lacZ*M15 *lac*X74 *deo*R *rec*A1 *ara*D139 (*ara, leu*)7697 *gal*U *gal*K *rps*L (StrR) *end*A1 *nup*G
E. coli Rosetta 2 (DE3)	*F- ompT hsdSB(rB- mB-) gal dcm (DE3) pRARE2 (CamR)*
E. coli ccdB survival	F^- *mcr*A (*mrr-hsd*RMS-*mcr*Bc) 80d *lacZ*M15 *lac*X74 *deo*R *rec*A1 *ara*D139 (*ara, leu*)7697 *gal*U *K rps*L (StrR) *end*A1 *nup*G *ton*A::P*trc-ccd*A
S. cerevisiae BY4742	MATα his3Δ1 leu2Δ0 lys2Δ0 ura3Δ0
S. cerevisiae BY4741	MATα his3Δ1 leu2Δ0 met15Δ0 ura3Δ0
P. pastoris GS115	his4 , Mut+

Table 4.2: Antibiotics

ANTIBIOTIC	STOCK SOLUTION	DILUTION
Ampicillin	100 mg/ml in water	1:1000
Chloramphenicol	15 mg/ml in EtOH	1:1000
Gentamycin	15 mg/ml in water	1:1000 (*E. coli*) 1:300 (*A. tumefaciens*)
Kanamycin	25 mg/ml in water	1:1000 (*E. coli*) 1:250 (*A. tumefaciens*)
Rifampicin	100 mg/ml in DMF	1:1000
Spectinomycin	100 mg/ml in water	1:1000
Zeocin	100 mg/ml in water	1:4000

Table 4.3: Tools used in this study

TOOL	TYPE	COMPANY
Ball mill	TissueLyser II	Qiagen
Laser Scanner	Typhoon FLA 9500	GE
Epifluorescent Microscope	Leica DMI 3000	Leica
CLSM	Leica TCS Sp8	Leica
FPLC	Äkta pure 25	GE
Epifluorescent Microscope	Zeiss Imager M.2	Zeiss
Micro titer plate reader	TriStar LB 941	Berthold
Sonicator	EpiShear probe sonicator	Active Motif
Spectrophotometer (small volumes)	NanoDrop ND-1000	PeqLab
Spectrophotometer (cuvettes)	UV-1900	Shimadzu
Fluorescent plate reader	Safire	Tecan

Table 4.4: Media

MEDIUM	INGREDIENTS
Lysogeny Broth (LB)	5 g/l yeast extract, 10 g/l tryptone, 10g/l NaCl
Yeast Extract Broth (YEB)	5 g/l beef extract, 1 g/l yeast extract, 5 g/l peptone, 5 g/l sucrose, 0.5 g/l $MgSO_4$, pH 7.2
Nutrient Yeast Glycerol (NYG)	5 g/l peptone, 3 g/l yeast extract, 20 g/l glycerol
Terrific Broth (TB)	24 g/l yeast extract, 20 g/l tryptone, 4 ml/L glycerol, 0.017 M KH_2PO_4, 0.072 M KH_2PO_4
Synthetic Defined (SD)	0.77 g/l drop out mix -Ura (Clontech), 6.7 g yeast nitrogen base with ammonium sulfate (w/o AA), pH 6
Yeast Peptone Dextrose (YPD)	10 g/l yeast extract, 20 g/l peptone, 20 g/l dextrose
Buffered Complex Glycerol (BMGY)	10 g/l yeast extract, 20 g/l peptone, 100 mM potassium phosphate pH 6, 13.4 g yeast nitrogen base (w/o AA), 0.4 mg biotin, 10 ml glycerol
Buffered Complex Methanol (BMMY)	10 g/l yeast extract, 20 g/l peptone, 100 mM potassium phosphate pH 6, 13.4 g yeast nitrogen base (w/o AA), 0.4 mg biotin, 5 ml methanol
Agar	15 g/l were added to prepare solid media

Table 4.5: buffers that were used for Bs3 purification

BUFFER	INGREDIENTS
Bs3 resuspension buffer	50 mM potassium phosphate, 10 % glycerol, 30 mM Imidazole, 1 mM DTT, 1 tablet protease inhibitor (Roche, EDTA free) per 40 ml, 10 μM FAD, pH 8 at 4°C
Bs3 wash buffer	50 mM potassium phosphate, 10 % glycerol, 30 mM Imidazole, pH 8
Bs3 elution buffer	50 mM potassium phosphate, 10 % glycerol, 500 mM Imidazole, pH 8
Dialysis buffer	50 mM potassium phosphate, 10 % glycerol, pH 8

4.2 Plant methods

4.2.1 Infiltration of *Capsicum* with *Xanthomonas*

Xanthomonas strain 82-8 uns* which lacks *AvrBs1*, *AvrBs2* and *AvrBs3* and contains a truncated version of *AvrBs4* was transformed with a pDSK602 vector containing either *AvrBs3* or *AvrBs2* via triparental mating *(Daniels et al., 1984)*. Cultures were grown at 28°C in NYG medium containing Rifampicin and Spectinomycin at a final concentration of 100 µg/ml. Cultures were pelleted and resuspended in water to OD_{600} = 0.4. Leaves of *C. annuum* were infiltrated with a blunt end syringe.

4.2.2 Transient transformation of *N. benthamiana*

Preparation of electrocompetent *Agrobacterium* cells and transformation was done according to standard protocols (McCormac et al., 1998). *A. tumefaciens* (GV3101) carrying the respective binary plasmids were grown over night at 28°C in YEB medium containing Rifampicin and Spectinomycin at a final concentration of 100 µg/ml. Cultures were pelleted and resuspended in water to OD_{600} = 0.4. Leaves of *N. benthamiana* were infiltrated with a blunt end syringe.

4.2.3 DAB staining

50 mg of diaminobenzidine tetrahydrochlorid (DAB, Roth CN75.1) were mixed with 50 ml water. 1 ml of a 500 mM Na_2HPO4 solution was added and the pH was adjusted to 7.2 with NaOH. 50 µl of a 50% Tween-20 solution were added to facilitate vacuum infiltration. Leaves were detached and covered with staining solution in a glass petri dish. Then, the leaves were vacuum infiltrated in a desiccator (usually 2x for ~3 min at 150 mbar). Successful infiltration was monitored by darkening of the leaf tissue. Subsequently, leaves were incubated in the solution with gentle shaking for at least 5h or overnight. Leaves were de-stained in hot ethanol to visualize brown staining.

4.2.4 Ratiometric CLSM measurements of roGFP2

Genes fused to *roGFP2* (Hanson et al., 2004), *GRX1-roGFP2* (Gutscher et al., 2008) and *roGFP2-Orp1* (Gutscher et al., 2009) were transiently expressed in four to six week old *N. benthamiana* plants via *Agrobacterium* mediated transient transformation. 24-36 hpi, images were acquired using a Leica TCS SP8 confocal laser scanning microscope by successive excitation at 405 nm and 488 nm and emission at 498 to 548 nm. Images of nuclei were collected using the 63x water immersed objective and 10x digital magnification. Argon laser intensity was adjusted in a way that pixels were close to saturation in samples with high roGFP2 fluorescence. UV laser intensity was adjusted

so that pixels were still visible for samples with low roGFP2 fluorescence. Background fluorescence was recorded for both excitation wavelengths at emission from 600 to 720 nm. A macro (Listing 4.6) was generated in Fiji (Schindelin et al., 2012) and used for fluorescence intensity measurements. For each picture, the surrounding of the nuclei was cropped, and the mean pixel intensity of the fluorescent area recorded in all four channels. Ratios were calculated and plots were generated with R (Wickham, 2009; R Core Team, 2017).

Listing 4.6. Fiji Macro that was used to measure pixel intensities of nuclei from microscopy pictures of Bs3 derivatives fused to roGFP2.

```
macro "Measure roGFP2 [0]" {
Stack.setChannel(4);
setAutoThreshold("Default dark");
//run("Threshold...");
run("Create Selection");
run("Measure");
//run("Channels Tool...");
Stack.setChannel(1);
run("Measure");
//run("Channels Tool...");
Stack.setChannel(2);
run("Measure");
//run("Channels Tool...");
Stack.setChannel(5);
run("Measure");
close();
run("Put Behind [tab]");
}
```

4.2.5 Sulfenome mining

The four binary plasmids *pLIIα_ TAP-Bs3-Yap1A*, *pLIIα_ TAP-Bs3-Yap1C, pLIIα_ TAP-Bs3$_{S211A}$-Yap1A* and *pLIIα_ TAP-Bs3$_{S211A}$-Yap1C* were cloned for sulfenome mining experiments via a Golden Gate cloning strategy. The TAP and YAP1A/C segments were amplified from a plasmid template (pB7WG2_TAP-YAP1A/C; provided by B. de Smet/ F. van Breusegem) with primers attaching BsaI recognition sites and either "BC" (TCTG and CACC) or "DE" (AAGG and AATC) overhangs after restriction digest. The TAP and YAP1A/C fragments were subsequently assembled with the *Bs3* coding sequence (CDS) and the pLIIa (pICH) backbone in a cut ligation reaction. The *Bs3* CDS was separated from the N- and C- terminal tags via a short linker sequence (encoding GGGGS). Four-week-old *N. benthamiana* plants were infiltrated with

A. tumefaciens GV3101 (OD600 = 0.4 in water) carrying the respective plasmids. Two leaves of 24 plants were infiltrated per construct. 5 x 4 g of leaf material were harvested at 30 hpi and immediately frozen in liquid nitrogen and stored at -80°C until shipping. Four replicates were shipped to Barbara De Smet (Research group: Frank Van Breusegem, Center for Plant Systems Biology, University of Gent, Belgium) for affinity purification, mass spectrometry and data analysis. The development of HR was controlled three days post infiltration in residual plants.

4.2.6 Bs3-GFP pull down and LC/MS measurements

Bs3, AtYUC6, Bs3S211A and GFP were expressed in five-week old N. benthamiana plants via Agrobacterium (GV3101) mediated transient transformation. GFP expression was checked by fluorescence microscopy at 24-48 hpi and 7 g of leaf material were harvested per sample, immediately frozen in liquid nitrogen and stored at -80°C until further use. Leaf material was ground using mortar and pestle with liquid nitrogen. 12 ml of Extraction buffer (50 mM Tris-Cl, 100 mM NaCl, 10% Glycerol, 1% Triton X-100, 1 tablet protease inhibitor Roche, EDTA free, per 40 ml, 1 mM EDTA, pH 7.5) were added and the samples were further pestled until the solution was homogenous. Samples were centrifuged at 20.000 x g for 15 min at 4°C. Supernatant was incubated with 80 µl of GFP-Trap®_A bead slurry (Chromotek, 50% slurry equilibrated in wash buffer; 10mM Tris, 100mM NaCl, 0.5mM EDTA, pH 7,5) for 4h at 4°C and constant rocking. Subsequently, beads were pelleted by centrifugation at 1000 x g at 4°C and washed 5 times in wash buffer. Washes were done by repeated short spin down in a mini centrifuge, removal of supernatant and subsequent re-suspension in fresh wash buffer. Finally, beads were pelleted and volume was adjusted to 80 µl with residual supernatant or wash buffer. 20 µl were used for SDS PAGE and 60 µl were used for MS analysis. For SDS PAGE, the 20 µl beads in wash buffer were mixed with 7 µl 4x SDS buffer and incubated at 98°C for 10 min. 10 µl were loaded onto an SDS gel.

Short protocol of analysis done by the proteome center

The samples were purified by SDS PAGE, followed by in-gel digestion with trypsin. LC/MS-MS analysis was done on a Proxeon Easy-nLC coupled to OrbitrapXL (130min, Top10 CID). Data processing was done using MaxQuant software (Version 1.5.2.8. with integrated Andromeda Peptid search engine). The spectra were searched against a *N. bentamiana* database (Nicotiana_benthamiana _allStrains_19072016.fasta) together with sequences for Bs3 and GFP.

4.3 Yeast methods

4.3.1 Yeast transformation

YPD medium containing glucose was inoculated with the respective yeast strain and grown at 28°C with shaking over night. The next day, the culture was used to inoculate 50 ml of YPD medium containing glucose to an OD_{600} of 0.4. Cells were grown for 2-4 hours to reach exponential growth. Cells were subsequently pelleted and resuspended in 40 ml 1x TE buffer (100 mM Tris, 10 mM EDTA, pH 7.5). Cells were again pelleted, resuspended in 1x LiAc/0.5x TE buffer (100 mM LiAc, 5 mM Tris-HCl, 0.5 mM EDTA, pH 7.5) and incubated for 10 min at RT with shaking. For each transformation reaction, 100 µl of the suspension were mixed with 1 µg plasmid DNA and 100 µl salmon sperm (2mg/ ml). 700 µl of PEG solution (100 mM LiAc, 40 % PEG-3350, 10 mM Tris-HCl, 1 mM EDTA, pH 0 7.5) were added an the mix was incubated at 30 °C with shaking for 30 min. 88 µl of DMSO were added, the suspension was thoroughly mixed and incubated for 7 min at 42 °C. Finally, the cells were pelleted, resuspended in 1x TE buffer and plated on selective plates.

4.3.2 Yeast growth curves

S. cerevisiae (BY4742) was transformed with pYES-DEST-52 vectors containing the respective genes. SD-Ura medium (Table 4.3) containing glucose was inoculated with the respective strains and incubated at 30°C with shaking over night. The next day, yeast was pelleted, washed in water once and resuspended in 15 ml SD-Ura medium containing galactose (inducing medium) at a starting $OD_{600} = 1$. The cultures were incubated at 30°C with shaking. To observe yeast growth, OD_{600} was measured every four hours. Three replicates were done per strain.

P. pastoris (GS115) was transformed with pPICZ vectors according to manufacturer's instructions (Thermo Fisher Scientific) and plated on low salt medium containing Zeocin. *P.pastoris* strains were grown in Buffered Complex Glycerol medium (BMGY) over night. The next day the cells were pelleted, washed in water once and resuspended in Buffered Complex Methanol medium (BMMY, inducing) at a starting $OD_{600} = 1$. The cultures were incubated at 30°C with shaking. To observe yeast growth, OD_{600} was measured.

4.3.3 Yeast library screen

The homozygous diploid yeast deletion pool used in this study was purchased from Thermo Fisher Scientific (95401.H1Pool). One tube was thawed and mixed with 200 ml YPD medium containing glucose and incubated at 30°C with shaking at 180 rpm.

Several transformations were done with 20 – 50 ml of culture at different time points (see section 4.3.1 for yeast transformation protocol). 90% of the transformation suspension was plated onto inducing SD-Ura plates containing galactose. 10% of the transformation suspension was plated onto SD-Ura plates containing glucose to control successful transformation. Colonies were visible on glucose plates after 2-3 days and on galactose plates after 4-5 days. Colonies of yeast transformed with Bs3 that appeared on inducing medium ("survivors") were collected and further analysed. The gene knockout of these candidates was identified via PCR amplification and sequencing of the inherent barcode. Bs3 expression was verified via Western Blot (see section 4.3.4).

4.3.4 Yeast sample preparation for PAGE

Six OD units (1 OD unit represents the number of cells in 1 ml of culture at OD600 = 1) were pelleted in a 2 ml tube, resuspended in 200 µl of 0.1 M NaOH and incubated at RT for 15 min. Subsequently, the lysate was centrifuged for one minute at maximum speed. The supernatant was removed and the pellet was resuspended in 50 µl 1x SDS buffer. After incubation at 95°C for 10 min, 10 µl were loaded onto a 10% polyacrylamide SDS gel and run for 80 min at 120 V.

4.4 Human cell methods

4.4.1 Expression vector cloning

The *pVAX_EF-1_3x-HA-Bs3-eGFP* vector was assembled via Golden Gate cloning and ICON toolkit compatible overhangs. The vector backbone module is based on pVAX_Sp6 (C. Wolf). For tag insertion the modules pICH_3x-HA and pICH_eGFP (Weber et al., 2011) were used. The Bs3 coding sequence with silent mutations that modify restriction enzyme recognition sites (designated as Bs3fs) was amplified using Primers CKP133/134 and MP181 as template (Table 6.2). Amplification of eGFP as control was done with Primers CKP193/194. The *EF-1* promoter was amplified from with EMM71T (C. Wolf) with CKP213/214. *Xa10* was amplified from pENTR_Xa10 (R. Morbitzer) with CKP151/152.

4.4.2 Cell growth and FuGENE transfection

HEK-293T cells were grown in Dulbecco's Modified Eagle Medium (DMEM, Sigma) containing 10% FBS (Sigma, F6178) and 1% PenStrep solution (Sigma P0781). Cells were kept in a 250 ml cell culture flask containing 12 ml of medium at 37°C with 10% CO_2. Every second to third day, cells were split 1:20. 1 day before transfection 2.5 x 10^5 cells were seeded in 3 ml medium a 6 well plate. Cells reached a confluency of

60% at the time of transfection. The next day, 6 µl of FuGENE® HD transfection reagent (Promega) were mixed with 2 µg of plasmid DNA and 100 µl of sterile water, vortexed and incubated for 5 min at RT. Subsequently, the FuGENE/DNA mix was added to the medium and the plate was rocked shortly to ensure even dispersion.

4.4.3 Trypan blue staining

In order to distinguish dead and alive cells, HEK293T cells expressing *Bs3-GFP*, *Xa10-GFP* or *GFP* were stained with trypan blue. Two days post transfection, cells were detached from the well by pipetting. Cells were pelleted (5000 g 1min) and resuspended in 500 µl PBS. The cell suspension was mixed 1:1 with 0.4% Trypan blue staining solution (Sigma T8154). Dead cells appear blue after 5 min of incubation. 10 µl of the suspension were transferred to a disposable hemocytometer (C-Chip, NanoEnTek) and dead and alive cell were counted according to manufacturer instructions.

4.5 Protein methods

4.5.1 Bs3 and $Bs3_{S211A}$ expression vector cloning

A total of seven expression vectors (pGS21_6xHis-GST-Bs3-6xHis, pDEST17_6xHis-Bs3, pQE30_6xHis-Bs3, pDEST_6xHis-MBP-Bs3, pET-53-DEST_6xHis-TEV-Bs3, pET-53-DEST_6xHis-Bs3 and pET-53-DEST_6xHis-NQN-Bs3) and four *E. coli* strains (Arctic Express, Rosetta 2, Rosettagami and BL21AI) were used for recombinant expression of soluble and active Bs3 protein. The best results were achieved with pET-53-DEST_6xHis-NQN-Bs3 and *E. coli* Rosetta.

4.5.2 Bs3 and $Bs3_{S211A}$ protein expression

E. coli Rosetta 2 (DE3) (Novagen) were transformed with pET-53-DEST_Bs3 or derivatives, plated on LB Agar containing Ampicillin (100 µg/ml) and Chloramphenicol (15 µg/ml) and incubated at 37°C over night. Incubation at lower temperatures strongly reduced transformation efficiency for vectors carrying functional Bs3 but not non-functional Bs3 mutant derivatives. Several colonies were pooled to inoculate LB medium supplemented with Ampicillin (100 µg/ml) and Chloramphenicol (15 µg/ml). This starter culture was incubated over night at 37°C with shaking. Starter cultures were used to inoculate 2 l TB Medium supplemented with Ampicillin (100 µg/ml) at a starting $OD_{600} = 0.05$. Cultures were grown at 37°C with shaking at 120 rpm until they reached $OD_{600} = 1$. Cultures were cooled down in ice water for 15 min and Protein expression was induced with a final concentration of 1 mM Isopropyl 1-thio-β-D-galactopyranoside

(IPTG). The cells were incubated for another 2,5 h at 18°C with shaking and harvested by centrifugation (4500 x g, 30 min, 4°C). Pellets were stored at -20°C until further use.

4.5.3 Bs3 and $Bs3_{S211A}$ Protein purification

The pellet was re-suspended in lysis buffer (50 mM Potassium phosphate, 10% glycerol, 30 mM Imidazole, 1% Tween, 1 mM DTT, 1 protease inhibitor tablet (Roche, EDTA free), 1 µM FAD, pH 8) using 5 ml of buffer per gram of pellet. 30 ml cell suspension were sonicated for 5 min (5s on/10s off, 60% Amplitude) with the ¼" microtip probe of the EpiShear Sonicator (Active Motif). The lysate was centrifuged (16000 x g, 4°C) for 30 min to pellet cell debris. An ÄKTA Pure 25 FPLC system, equipped with a 5 ml HisTrapFF Crude Column (GE Healthcare), was used for affinity purification. After column equilibration with ten column volumes (CV) of wash buffer (50 mM Potassium phosphate, 10% Glycerol, 30 mM Imidazole, pH 8), the supernatant was loaded onto the column and washed with 20 CV wash buffer. The protein was eluted with 2 CV elution buffer (50 mM Potassium phosphate, 10% Glycerol, 500 mM Imidazole, pH 8). The protein was frozen in liquid nitrogen and stored at -80°C.

4.5.4 Polyacrylamide gel cast

Twelve gels were prepared in parallel in a multicast chamber (BioRad) or a custom-made plastic box (Krönauer, 2018). The standard concentration for separating gels was 10 %. 100 ml of separating gel (40 ml ddH_2O, 25 ml 1.5 M Tris pH 8.8, 1 ml 10% SDS, 1 ml 10% APS, 33 ml 30 % Acrylamide and 100 µl TEMED) and 30 ml 4 % stacking gel (18 ml ddH_2O, 7.5 ml 0.5 M Tris pH 6.8, 300 µl 10% SDS, 300 µl 10% APS, 4 ml 30 % Acrylamide and 30 µl TEMED) were prepared. Short plates and 1 mm spacer plates were assembled, and gels were poured according to manufacturer's instructions.

4.5.5 Polyacrylamide gel electrophoresis

An appropriate amount of 4 x SDS buffer (200 mM Tris-Cl (pH 6.8), 400 mM DTT, 8 % SDS, 0.4 % bromophenol blue, 40 % glycerol) is mixed with protein/plant/yeast samples. Samples are incubated at 95°C for 10 min. 5 – 20 µl of sample were subsequently loaded onto a 10 % SDS polyacrylamide gel. The gel run was carried out in a Mini-Protean Tetra Cell (Bio-Rad) at 120 V with constant voltage and variable amperage for 80 min. The running buffer was diluted from a 10x stock solution (30 g/l Tris base, 144 g/l Glycine, 10 g/l SDS, pH 8.3).

4.5.6 Western Blot

Protein transfer from gels to PVDF membranes (Immobilon-P with 0.45 µm pore size) via a semi dry transfer system (neolab). Assembly of the blotting sandwich was

done as follows: Two layers Whatman filter paper were soaked in anode buffer (25 mM Tris, 40 mM caproic acid, 20 % EtOH, pH 9.4) and placed on the anode plate. The prepared membrane (soaked into methanol for 20 s and incubated in water with rocking for 10 min) is placed on top. The gel was placed on the membrane. Finally, two sheets of Whatman filter paper were soaked in cathode buffer (300 mM Tris, 20 % EtOH, pH 10.4). The transfer is carried out at constant amperage 0.8 mA/cm^2 (approx. 50 mA per gel) and variable voltage for 1 h. After transfer, the membrane is incubated for at least 30 min in blocking solution (5% milk powder in TBST). The membrane was washed twice in TBST (150 mM NaCl, 0.05 % Tween-20, pH 7.6) and incubated for at least 1 h to over night in primary antibody. After two more washes in TBST, the membrane was incubated with an appropriate secondary antibody conjugated to a near infrared fluorescent dye (IRdye 680) for at least 1 hour. Finally, the membrane was washed in TBST and dried. Visualization was done with a Typhoon scanner equipped with a BPFR 700 filter at 680 nm. To control protein transfer, the membrane was stained with amido black solution (0.1% amido black, 25% isopropanol, 10% acetic acid) and rinsed in water or 10% acetic acid until bands were visible.

4.5.7 NADPH oxidation assay

Stocks of 10 mM NADPH dissolved in 50 mM potassium phosphate buffer (pH 8) were stored at -80°C. NADPH was dissolved in buffer to create a solution with a final concentration of approximately 100 µM. The exact concentration is calculated from the absorption values at 340 nm and the extinction coefficient of 6220 M^{-1} cm^{-1}. Quartz cuvettes (Hellma, QS) were used for measurements. Buffer without NADPH served as blank. The reaction was started by adding a defined concentration of purified protein (Usually 0.2 – 1 µM) to the NADPH containing buffer. The absorption at 340 nm was measured every 30 s at constant temperature until the curve progression was non linear (usually 5 – 15 min).

For steady state experiments 0.2 µM of protein were added to buffer containing various concentrations of NADPH. The reaction was run for 5 min at 25°C. The decrease of absorption at 340 nm was followed with a Shimadzu UV1900 photometer equipped with a TCC-100 thermoelectrically temperature controlled cell holder. Slope values and exact NADPH concentrations were calculated for each sample. To fit the Michaelis Menten Model, the drm function of the drc package was used (Ritz et al., 2015). The code was used according to Ritz and Streibig, 2008.

4.5.8 H_2O_2 measurements with HyPerBlu and Amplex Red

HyPerBlu (Lumigen, Beckman Coulter) was used to measure H_2O_2 in enzyme assays. 190 µl of NADPH or buffer were mixed with 10 µl of protein to get a final protein

concentration of 0.2 – 1 µM. The reaction mix were pipetted into a white square 384-well plate and incubated for 15 min at RT. Then 5 µl of HyPerBlu were added to each well. All samples were pipetted in columns and 1 column is left free in between different samples. The wells were covered from light with aluminium foil immediately. After 10 min of incubation in darkness, the luminescent signal was measured with a plate reader (Berthold TriStar LB 941, mode: 1s, 10 repeats). To calculate the absolute amounts of H_2O_2 from HyPerBlu derived luminescence, a H_2O_2 standard ranging from 0 to 50 µM in potassium phosphate buffer pH 8 was prepared from 10 M (~30%) stock solution. The standard concentrations were pipetted in triplicates in the wells of a white square 384-well plate and HyPerBlu was added.

The Amplex™ Red Hydrogen Peroxide/Peroxidase Assay Kit (Invitrogen) was used to measure H_2O_2 production in enzyme assays. The reactions were set up according to manufacturer´s instructions. The fluorescent signal was measured after 30 min of incubation at room temperature with a plate reader (Tecan Safire).

4.5.9 Enzyme assay with AtYUC6 and IPA

AtYUC6 protein was purified from *E. coli* according to Dai et al., 2013. Buffer exchange was done with the ÄKTA FPLC system equipped with a 5 ml HiTrap desalting column. 100 µl of protein were mixed with 400 µl buffer (50 mM sodium phosphate buffer, 0.5 M NaCl, 30% glycerol, pH 8) containing 200 µM of NADPH and 50 µM of IPA. The enzyme-substrate solution was incubated at RT for 40 min. 200 µl of each sample were used for extraction.

Sample preparation for GC/MS analysis

200 µL sample were mixed with 1000 µL ethyl acetate containing 333.33 ng per sample 3HOBA and 0.1% (v/v) formic acid. Subsequently, this solution was incubated for 10 min at 4°C and 1600 rpm followed by centrifugation for 10 min at 4°C and 13000 rpm in a Hettich Micro 220 R SwingOut rotor. 900 µL of supernatant were transferred to a fresh 1.5 ml tube. The samples were dried for 1h in a Speedvac (mode V-HV and 30 mbar). The dried samples were derivatised with 60 µL MSTFA (Sigma) in an Eppendorf Mixer at 40°C for 90 minutes at 1200 rpm. After a short spin down the samples were transferred to 2 mL GC Vials with 100 µL inserts and sealed with PTFE/rubber septa lids. 1 µL was subjected to GCMS analyses.

GC/MS Analysis of IPA and IAA

GC/MS analysis was performed on a Shimadzu TQ-8040 GC/MS system. The injector fitted with a custom glass liner (Restek #550733) was set to Splittless mode at 280°C. The sampling time was 0.5 minutes. Before and after injection the 10 µL syringe was rinsed three times with 8 µL dichlormethane. Separation of the compounds was

achieved by a glass capillary column from Restek (SH-Rxi-17SIL-MS) with a diameter of 0.25 mm, film thickness of 0.25 µm and a length of 30m. The carrier gas was Helium at 1 ml/min column flow at a controlled linear velocity of 36.7 cm/s. Septum purge was set to 3 ml/min. The oven program started at 70°C and was hold for 5 min. Then the oven was heated with a rate of 15 K/min to a final temperature of 280°C which was held for 10 additional minutes. This results in a runtime per sample of approximately 30 minutes. The interface to the mass spectrometer and the ion source were set to 250°C and 200°C, respectively. Single Ion Monitoring (SIM) was used as acquisition mode.

4.5.10 Enzyme assay with Bs3 and TMA

For measurement of trimethylamine (TMA), 1 ml octanol solution (2µg/ml Octanol in 10mM NaOH), 1.5 ml NaOH (1M) and 400 µl H_2O_2 were filled into 10 ml headspace vials equipped with septum lids (screw caps). 100 µl of sample or TMA standard were added. The sample vials were transferred to the Headspace Sampler HS 20 coupled to a GCMS System TQ8040 from Shimadzu

For measurement of trimethylamine oxide (TMAO), 1 ml octanol solution (2µg/mL Octanol in 10mM NaOH), 1.5 ml NaOH (1M), 200 µl H_2O_2 and 200 µL TiCl3 (titanium(III) chloride solution about 15% in about 10% HCl from Merck) were filled into 10 ml headspace vials equipped with septum lids (screw caps). 100 µl of sample or TMAO standard were added. The sample vials were transferred to the Headspace Sampler HS 20 coupled to a GCMS System TQ8040 from Shimadzu

Measurement of TMA

Separation of the compounds was achieved by a glass capillary column from Restek (Stabilwax®) with a diameter of 0.32 mm, film thickness of 1 µm and a length of 30m. The carrier gas was helium at 1.59 ml/min column flow at a controlled linear velocity of 45.5 cm/s. The oven program starts at 40°C and was held for 4 min. Then the oven was heated with a rate of 35 K/min to a temperature of 150°C which was held for 4.5 minutes followed by another ramp of 10 K/min to a final temperature of 190°C which was held for another 10 minutes. This results in a runtime of approximately 30 minutes per sample. The interface to the MS (mass spectrometer) and the ion source were set to 200°C and 200°C, respectively. SIM (Single Ion Monitoring) was used as acquisition mode. Respective peak areas were determined. Results were adjusted to the area of octanol peak. Relative peak area values were compared.

4.5.11 Measurement of IAA and SA from leaf tissue

200 mg (freshweight) of *N. benthamiana* leaf tissue was ground in liquid nitrogen and mixed thoroughly with 1.5 ml extraction solution (ethyl-acetate, 0.1% (v/v) Formic acid containing 16.7 ng/ml 3-hydroxybenzoic acid (3HOBA), and 23.34 ng/ml indole-5-

carboxylic acid (5IFA) as internal standards). Samples were treated for 10 minutes in an ultra sonic water bath and incubated at 28°C with shaking (1600 rpm). After centrifugation at 18500 x *g* at 4°C, 1.2 ml of the supernatant were transferred to a fresh 1.5 ml tube, and the solvent was evaporated in a vacuum concentrator. The dried samples were derivatized in 60 µL N-methyl-N-(trimethylsilyl)trifluoroacetamide (MSTFA, Sigma) for 30 minutes at 40°C and 1200 rpm. Samples were transferred to 2 ml GC Vials with 100 µl inserts and sealed with polytetrafluoroethylene (PTFE) septa lids. 1 µl was subjected to GC/MS analysis.

GC/MS analysis was performed on a Shimadzu TQ-8040 GC/MS system. The injector, fitted with a custom glass liner (Restek #550733), was set to Splitless mode at 280°C. Compounds were separated on a glass capillary column (Restek, SH-Rxi-17SIL-MS, 30 m x 0.25mm x 0.25µm). Helium at 1 ml/min column flow and a controlled linear velocity of 36.7 cm/s was used as carrier gas. Septum purge was set to 3 ml/min. The oven program was set to an: initial temperature of 70°C for 5 min, followed by a gradient of 15 °C/min to a final temperature of 280°C which was held for 10 minutes (Total run time: approximately 30 minutes).

The interface of the mass spectrometer and the ion source were set to 250°C and 200°C, respectively. Multiple Reaction Monitoring (MRM) was used as acquisition mode.

4.6 Metabolomics Methods

4.6.1 *In vitro* Metabolomics assay

Plant growth and tissue harvest

Arabidopsis thaliana (Col-0) plants were grown for 21 days at 18 - 20°C and 30 - 40% humidity under long day conditions (16 hours light/ 8 hours dark). Rosette leaves were harvested and frozen in liquid nitrogen.

Plant extract preparation with methanol/water

Two grams of leaf material were ground to fine powder and transferred to a 50 ml conical tube. 10 ml of 80% methanol were added and the suspension was vortexed for 20s. Suspension was sonicated for 1 min (5s on 10s off at 60% amplitude in the EpiShear™ probe sonicator equipped with ¼ probe). 1.5 ml of extract were transferred to a 1.5 ml tube and centrifuged at 4°C at 20.000xg for 5 min. 1 ml of the supernatant was transferred to a new tube and incubated in a SpeedVac concentrator until the methanol was fully evaporated. 200 µl of potassium phosphate buffer (50 mM, pH 8) were added and mixed with the residual extract by pipetting. Subsequently, 200 µl were transferred to a new tube to start the enzyme reaction.

Plant extract preparation with buffer

Two grams of leaf material were ground to fine powder and transferred to a 50 ml conical tube. 20 ml buffer (50 mM potassium phosphate, pH 8) were added and the suspension was vortexed for 20s. The suspension was sonicated for 1 min (5s on 10s off at 60% amplitude in the EpiShear^{TM} probe sonicator equipped with ¼ probe). 1.2 ml of extract were transferred to a 1.5 ml tube and centrifuged at 4°C at 20.000xg for 2 min. Subsequently, 200 µl were transferred to a new tube to start the enzyme reaction.

Enzymatic reaction

200 µl of plant extract were mixed with 100 µM NADPH and either Bs3, Bs3$_{S211A}$ or dialysis buffer (50 mM KP, 10% glycerol, pH 8) and incubated at room temperature for 20 min. Equal amounts (final concentration 1.8 µM) of Bs3 and Bs3$_{S211A}$ protein, calculated from A280, were used. The reaction was carried out in in 8 replicates. 4 Tubes were subsequently frozen in liquid N2 and 4 were mixed with 5 µl concentrated formic acid to stop the reaction. Samples containing formic acid were directly injected for analysis (see section 4.5.3). Frozen samples were lyophilized and treated similar to samples prepared for in vivo metabolomics (see section 4.6.2).

4.6.2 *In vivo* Metabolomics assay

Bs3, *Bs3$_{S211A}$*, *GFP* and *CaYUC3* coding sequences were expressed in *N. benthamiana* under control of the *35S* Promoter via *Agrobacterium* (GV3101) mediated transient transformation. 30 and 36 hours after infiltration, 100 - 110 mg of leaf tissue were harvested in triplicates and immediately frozen in liquid Nitrogen.

After lyophilization samples were homogenized with a ball mill (twice for 30 s.) and extracted with 80 % methanol containing 0.1 % formic acid followed by a second extraction step with 20 % methanol also containing 0.1 % formic acid. Both supernatants were combined and brought to dryness. Samples were dissolved in 120 µl 20 % methanol containing 0.1 % formic acid out of which 5 µl were injected for analysis. 10 µl of each sample were used to create a pool sample.

4.6.3 LC/MS measurement

Analysis was done with a Waters UPLC-SynaptG2 LC/MS system operated in ESI positive and negative mode. The mass spectrum was scanned in MS and MS^{E} mode from 50 to 2000 mass to charge (m/z) at a scan rate of 0.2 s. For separation a flow rate of 200 µl/min and a 10 min gradient from 99% water to 99 % methanol (both with 0.1 % formic acid) on a Waters Acquity C18 HSST3 100 mm x 2.1 mm, 1.8 µm column was used. Data evaluation was done with ProgenesisQI software from Nonlinear Dynamics.

5 References

Addinall SG, Downey M, Yu M, Zubko MK, Dewar J, Leake A, Hallinan J, Shaw O, James K, Wilkinson DJ, Wipat A, Durocher D, Lydall D (2008) A genomewide suppressor and enhancer analysis of cdc13-1 reveals varied cellular processes influencing telomere capping in *Saccharomyces cerevisiae*. Genetics 180: 2251-2266

Ahn CS, Lee JH, Hwang AR, Kim WT, Pai HS (2006) Prohibitin is involved in mitochondrial biogenesis in plants. Plant Journal 46: 658-667

Akter S, Huang J, Bodra N, De Smet B, Wahni K, Rombaut D, Pauwels J, Gevaert K, Carroll K, Van Breusegem F, Messens J (2015) DYn-2 Based Identification of *Arabidopsis* Sulfenomes. Mol Cell Proteomics 14: 1183-1200

Alfieri A, Malito E, Orru R, Fraaije MW, Mattevi A (2008) Revealing the moonlighting role of NADP in the structure of a flavin-containing monooxygenase. Proc Natl Acad Sci U S A 105: 6572-6577

Aller I, Rouhier N, Meyer AJ (2013) Development of roGFP2-derived redox probes for measurement of the glutathione redox potential in the cytosol of severely glutathione-deficient rml1 seedlings. Front Plant Sci 4: 506

Anand A, Mysore KS (2013) The role of RAR1 in *Agrobacterium*-mediated plant transformation. Plant Signal Behav 8: doi: 10 4161/psb 26784

Arner ES, Holmgren A (2000) Physiological functions of thioredoxin and thioredoxin reductase. Eur J Biochem 267: 6102-6109

Asai S, Mase K, Yoshioka H (2010) A key enzyme for flavin synthesis is required for nitric oxide and reactive oxygen species production in disease resistance. Plant Journal 62: 911-924

Baxter A, Mittler R, Suzuki N (2014) ROS as key players in plant stress signalling. J Exp Bot 65: 1229-1240

Beaty NB, Ballou DP (1980) Transient kinetic study of liver microsomal FAD-containing monooxygenase. J Biol Chem 255: 3817-3819

Belousov VV, Fradkov AF, Lukyanov KA, Staroverov DB, Shakhbazov KS, Terskikh AV, Lukyanov S (2006) Genetically encoded fluorescent indicator for intracellular hydrogen peroxide. Nat Methods 3: 281-286

Bernsdorff F, Doring AC, Gruner K, Schuck S, Brautigam A, Zeier J (2016) Pipecolic Acid Orchestrates Plant Systemic Acquired Resistance and Defense Priming via Salicylic Acid-Dependent and -Independent Pathways. Plant Cell 28: 102-129

Bhandari DD, Lapin D, Kracher B, von Born P, Bautor J, Niefind K, Parker JE (2019) An EDS1 heterodimer signalling surface enforces timely reprogramming of immunity genes in *Arabidopsis*. Nat Commun 10: 772

Binda C, Robinson RM, Martin Del Campo JS, Keul ND, Rodriguez PJ, Robinson HH, Mattevi A, Sobrado P (2015) An Unprecedented NADPH Domain Conformation in Lysine Monooxygenase NbtG Provides Insights Into

Uncoupling of Oxygen Consumption From Substrate Hydroxylation. J Biol Chem

Boch J, Bonas U (2010) *Xanthomonas* AvrBs3 family-type III effectors: discovery and function. Annu Rev Phytopathol 48: 419-436

Boch J, Scholze H, Schornack S, Landgraf A, Hahn S, Kay S, Lahaye T, Nickstadt A, Bonas U (2009) Breaking the code of DNA binding specificity of TAL-type III effectors. Science 326: 1509-1512

Bonas U, Stall RE, Staskawicz B (1989) Genetic and structural characterization of the avirulence gene *avrBs3* from *Xanthomonas campestris* pv. *vesicatoria*. Mol Gen Genet 218: 127-136

Bosland PW, Votava EJ (2012) Peppers: Vegetable and Spice Capsicums, 2nd Edition. Peppers: Vegetable and Spice Capsicums, 2nd Edition 22: 1-230

Bruce TJA (2014) Glucosinolates in oilseed rape: secondary metabolites that influence interactions with herbivores and their natural enemies. Annals of Applied Biology 164: 348-353

Cashman JR, Motika MS (2010) Monoamine Oxidases and Flavin-Containing Monooxygenases,

Cashman JR, Zhang J (2006) Human flavin-containing monooxygenases. Annu Rev Pharmacol Toxicol 46: 65-100

Cha JY, Kim WY, Kang SB, Kim JI, Baek D, Jung IJ, Kim MR, Li N, Kim HJ, Nakajima M, Asami T, Sabir JS, Park HC, Lee SY, Bohnert HJ, Bressan RA, Pardo JM, Yun DJ (2015) A novel thiol-reductase activity of *Arabidopsis* YUC6 confers drought tolerance independently of auxin biosynthesis. Nat Commun 6: 8041

Chen Z, Zheng Z, Huang J, Lai Z, Fan B (2009) Biosynthesis of salicylic acid in plants. Plant Signal Behav 4: 493-496

Cheng HM, Chern Y, Chen IH, Liu CR, Li SH, Chun SJ, Rigo F, Bennett CF, Deng N, Feng Y, Lin CS, Yan YT, Cohen SN, Cheng TH (2015) Effects on murine behavior and lifespan of selectively decreasing expression of mutant huntingtin allele by supt4h knockdown. PLoS Genet 11: e1005043

Cheng Y, Dai X, Zhao Y (2006) Auxin biosynthesis by the YUCCA flavin monooxygenases controls the formation of floral organs and vascular tissues in *Arabidopsis*. Genes Dev 20: 1790-1799

Cheng Y, Dai X, Zhao Y (2007) Auxin synthesized by the YUCCA flavin monooxygenases is essential for embryogenesis and leaf formation in *Arabidopsis*. Plant Cell 19: 2430-2439

Cheol Park H, Cha JY, Yun DJ (2013) Roles of YUCCAs in auxin biosynthesis and drought stress responses in plants. Plant Signal Behav 8: e24495

Clay NK, Adio AM, Denoux C, Jander G, Ausubel FM (2009) Glucosinolate metabolites required for an *Arabidopsis* innate immune response. Science 323: 95-101

Coates PJ, Jamieson DJ, Smart K, Prescott AR, Hall PA (1997) The prohibitin family of mitochondrial proteins regulate replicative lifespan. Curr Biol 7: 607-610

Corpas FJ, Gupta DK, Palma JM (2015) Production Sites of Reactive Oxygen Species (ROS) in Organelles from Plant Cells. *In* DK Gupta, JM Palma, FJ Corpas, eds, Reactive Oxygen Species and Oxidative Damage in Plants Under Stress. Springer International Publishing, Cham, pp 1-22

Dai X, Mashiguchi K, Chen Q, Kasahara H, Kamiya Y, Ojha S, DuBois J, Ballou D, Zhao Y (2013) The biochemical mechanism of auxin biosynthesis by an *Arabidopsis* YUCCA flavin-containing monooxygenase. J Biol Chem 288: 1448-1457

Daniels MJ, Barber CE, Turner PC, Sawczyc MK, Byrde RJ, Fielding AH (1984) Cloning of genes involved in pathogenicity of *Xanthomonas campestris* pv. *campestris* using the broad host range cosmid pLAFR1. EMBO J 3: 3323-3328

De Smet B (2019) Protein cysteine sulfenylation in plant stress responses: a journey through the organelles. Ghent University and Vrije Universiteit Brussel, Ghent

Decourty L, Saveanu C, Zemam K, Hantraye F, Frachon E, Rousselle JC, Fromont-Racine M, Jacquier A (2008) Linking functionally related genes by sensitive and quantitative characterization of genetic interaction profiles. Proc Natl Acad Sci U S A 105: 5821-5826

Delaunay A, Pflieger D, Barrault MB, Vinh J, Toledano MB (2002) A thiol peroxidase is an H_2O_2 receptor and redox-transducer in gene activation. Cell 111: 471-481

Dempsey DA, Klessig DF (1994) Salicylic acid, active oxygen species and systemic acquired resistance in plants. Trends Cell Biol 4: 334-338

Deng D, Yan C, Pan X, Mahfouz M, Wang J, Zhu JK, Shi Y, Yan N (2012) Structural basis for sequence-specific recognition of DNA by TAL effectors. Science 335: 720-723

Dixit A, Roche TE (1984) Spectrophotometric assay of the flavin-containing monooxygenase and changes in its activity in female mouse liver with nutritional and diurnal conditions. Arch Biochem Biophys 233: 50-63

Doidge EM (1920) A tomato canker. J. Dep. Agric. Union S. Afr. 1: 718-721

Dolphin CT, Cullingford TE, Shephard EA, Smith RL, Phillips IR (1996) Differential developmental and tissue-specific regulation of expression of the genes encoding three members of the flavin-containing monooxygenase family of man, FMO1, FMO3 and FMO4. European Journal of Biochemistry 235: 683-689

Dolphin CT, Janmohamed A, Smith RL, Shephard EA, Phillips IR (2000) Compound heterozygosity for missense mutations in the flavin-containing monooxygenase 3 (FMO3) gene in patients with fish-odour syndrome. Pharmacogenetics 10: 799-807

Eswaramoorthy S, Bonanno JB, Burley SK, Swaminathan S (2006) Mechanism of action of a flavin-containing monooxygenase. Proc Natl Acad Sci U S A 103: 9832-9837

Exposito-Rodriguez M, Borges AA, Borges-Perez A, Hernandez M, Perez JA (2007) Cloning and biochemical characterization of *ToFZY*, a tomato gene encoding a flavin monooxygenase involved in a tryptophan-dependent auxin biosynthesis pathway. Journal of Plant Growth Regulation 26: 329-340

FAO (2017) FAOSTAT - Production quantities of Chillies and peppers. URL: http://www.fao.org/faostat/en/#data/QC/visualize accessed at January 21, 2019. 2018

Fiorentini F, Geier M, Binda C, Winkler M, Faber K, Hall M, Mattevi A (2016) Biocatalytic Characterization of Human FMO5: Unearthing Baeyer-Villiger Reactions in Humans. ACS Chem Biol 11: 1039-1048

Fraaije MW, Kamerbeek NM, van Berkel WJ, Janssen DB (2002) Identification of a Baeyer-Villiger monooxygenase sequence motif. FEBS Lett 518: 43-47

Franceschini S, Fedkenheuer M, Vogelaar NJ, Robinson HH, Sobrado P, Mattevi A (2012) Structural insight into the mechanism of oxygen activation and substrate selectivity of flavin-dependent N-hydroxylating monooxygenases. Biochemistry 51: 7043-7045

Fu ZQ, Yan S, Saleh A, Wang W, Ruble J, Oka N, Mohan R, Spoel SH, Tada Y, Zheng N, Dong X (2012) NPR3 and NPR4 are receptors for the immune signal salicylic acid in plants. Nature 486: 228-232

Fürst M, Romero E, Gomez Castellanos JR, Fraaije MW, Mattevi A (2018) Side-Chain Pruning Has Limited Impact on Substrate Preference in a Promiscuous Enzyme. ACS Catal 8: 11648-11656

Gaffney T, Friedrich L, Vernooij B, Negrotto D, Nye G, Uknes S, Ward E, Kessmann H, Ryals J (1993) Requirement of salicylic Acid for the induction of systemic acquired resistance. Science 261: 754-756

Gao C, Catucci G, Castrignano S, Gilardi G, Sadeghi SJ (2017) Inactivation mechanism of N61S mutant of human FMO3 towards trimethylamine. Sci Rep 7: 14668

Gao C, Catucci G, Gilardi G, Sadeghi SJ (2018) Binding of methimazole and NADP(H) to human FMO3: In vitro and in silico studies. Int J Biol Macromol 118: 460-468

Gardner MW, Kendrick JB (1923) Bacterial spot of tomato and pepper. Phytopathology 13: 307-315

Gassmann W, Dahlbeck D, Chesnokova O, Minsavage GV, Jones JB, Staskawicz BJ (2000) Molecular evolution of virulence in natural field strains of *Xanthomonas campestris* pv. *vesicatoria.* J Bacteriol 182: 7053-7059

Giaever G, Nislow C (2014) The yeast deletion collection: a decade of functional genomics. Genetics 197: 451-465

Gitaitis R, Walcott R (2007) The epidemiology and management of seedborne bacterial diseases. Annu Rev Phytopathol 45: 371-397

Greenberg JT, Yao N (2004) The role and regulation of programmed cell death in plant-pathogen interactions. Cell Microbiol 6: 201-211

Gutscher M, Pauleau AL, Marty L, Brach T, Wabnitz GH, Samstag Y, Meyer AJ, Dick TP (2008) Real-time imaging of the intracellular glutathione redox potential. Nat Methods 5: 553-559

Gutscher M, Sobotta MC, Wabnitz GH, Ballikaya S, Meyer AJ, Samstag Y, Dick TP (2009) Proximity-based protein thiol oxidation by H_2O_2-scavenging peroxidases. J Biol Chem 284: 31532-31540

Gygli G, Lucas MF, Guallar V, van Berkel WJH (2017) The ins and outs of vanillyl alcohol oxidase: Identification of ligand migration paths. PLoS Comput Biol 13: e1005787

Halkier BA, Gershenzon J (2006) Biology and biochemistry of glucosinolates. Annu Rev Plant Biol 57: 303-333

Hanson GT, Aggeler R, Oglesbee D, Cannon M, Capaldi RA, Tsien RY, Remington SJ (2004) Investigating mitochondrial redox potential with redox-sensitive green fluorescent protein indicators. J Biol Chem 279: 13044-13053

Hardin C (2014) Scot Nelson: Bacterial leaf spot of pepper; Photograph by Chelsea Hardin. https://www.flickr.com/photos/scotnelson/14954498489 (accessed on 23 January 2019)

Hartmann M, Zeier T, Bernsdorff F, Reichel-Deland V, Kim D, Hohmann M, Scholten N, Schuck S, Brautigam A, Holzel T, Ganter C, Zeier J (2018) Flavin Monooxygenase-Generated N-Hydroxypipecolic Acid Is a Critical Element of Plant Systemic Immunity. Cell

He SY, Bauer DW, Collmer A, Beer SV (1994) Hypersensitive Response Elicited by Erwinia-Amylovora Harpin Requires Active-Plant Metabolism. Molecular Plant-Microbe Interactions 7: 289-292

Heath MC (2000) Hypersensitive response-related death. Plant Molecular Biology 44: 321-334

Higgins BB (1922) The bacterial spot of pepper. Phytopathology 12: 501-517

Hines RN, Cashman JR, Philpot RM, Williams DE, Ziegler DM (1994) The mammalian flavin-containing monooxygenases: molecular characterization and regulation of expression. Toxicol Appl Pharmacol 125: 1-6

Hofius D, Schultz-Larsen T, Joensen J, Tsitsigiannis DI, Petersen NH, Mattsson O, Jorgensen LB, Jones JD, Mundy J, Petersen M (2009) Autophagic components contribute to hypersensitive cell death in Arabidopsis. Cell 137: 773-783

Horsfall JG, McDonnell AD (1940) Varietal susceptibility of peppers to bacterial spot. Plant Dis. Rep. 24: 34 - 36

Huai Q, Kim HY, Liu YD, Zhao YD, Mondragon A, Liu JO, Ke HM (2002) Crystal structure of calcineurin-cyclophilin-cyclosporin shows common but

distinct recognition of immunophilin-drug complexes. Proceedings of the National Academy of Sciences of the United States of America 99: 12037-12042

Hwang IS, Hwang BK (2010) The pepper 9-lipoxygenase gene CaLOX1 functions in defense and cell death responses to microbial pathogens. Plant Physiol 152: 948-967

Ichimura K, Shinzato T, Edaki M, Yoshioka H, Shirasu K (2016) SGT1 contributes to maintaining protein levels of MEK2(DD) to facilitate hypersensitive response-like cell death in *Nicotiana benthamiana.* Physiological and Molecular Plant Pathology 94: 47-52

Ishida JK, Wakatake T, Yoshida S, Takebayashi Y, Kasahara H, Wafula E, dePamphilis CW, Namba S, Shirasu K (2016) Local Auxin Biosynthesis Mediated by a YUCCA Flavin Monooxygenase Regulates Haustorium Development in the Parasitic Plant *Phtheirospermum japonicum.* Plant Cell 28: 1795-1814

Jaenecke C (2011) Etablierung und Durchführung verschiedener Sichtungen zur Identifizierung von Signalwegkomponenten der Paprika Bs3 vermittelten Resistenzreaktion, Martin-Luther-Universität Halle-Wittenberg

Jones JB, Jones JP (1985) The effect of bactericides, tank mixing time and spray schedule on bacterial leaf spot of tomato. Proc. Fla. State Hort. Soc. 98: 244-247

Jones JB, Lacy GH, Bouzar H, Stall RE, Schaad NW (2004) Reclassification of the xanthomonads associated with bacterial spot disease of tomato and pepper. Syst Appl Microbiol 27: 755-762

Jones JD, Dangl JL (2006) The plant immune system. Nature 444: 323-329

Jordan T (2005) Genetische und physikalische Limitierung des Bs3 Resistenzgen-Locus in *Capsicum annuum*, Dissertation, Martin-Luther-Universität Halle-Wittenberg

Jordan T, Romer P, Meyer A, Szczesny R, Pierre M, Piffanelli P, Bendahmane A, Bonas U, Lahaye T (2006) Physical delimitation of the pepper *Bs3* resistance gene specifying recognition of the AvrBs3 protein from *Xanthomonas campestris* pv. *vesicatoria*. Theor Appl Genet 113: 895-905

Käll L, Storey JD, MacCoss MJ, Noble WS (2008) Posterior error probabilities and false discovery rates: two sides of the same coin. J Proteome Res 7: 40-44

Khan MA, Chock PB, Stadtman ER (2005) Knockout of caspase-like gene, *YCA1*, abrogates apoptosis and elevates oxidized proteins in *Saccharomyces cerevisiae*. Proc Natl Acad Sci U S A 102: 17326-17331

Kim B-S, Hartmann RW (1985) Inheritance of a Gene (*Bs3*) Conferring Hypersensitive Resistance to *Xanthomonas campestris* pv. *vesicatoria* in Pepper (*Capsicum annuum*). Plant Disease 3: 233-235

Kim JI, Baek D, Park HC, Chun HJ, Oh DH, Lee MK, Cha JY, Kim WY, Kim MC, Chung WS, Bohnert HJ, Lee SY, Bressan RA, Lee SW, Yun DJ (2013) Overexpression of *Arabidopsis* YUCCA6 in potato results in high-

auxin developmental phenotypes and enhanced resistance to water deficit. Mol Plant 6: 337-349

Kim JI, Sharkhuu A, Jin JB, Li P, Jeong JC, Baek D, Lee SY, Blakeslee JJ, Murphy AS, Bohnert HJ, Hasegawa PM, Yun DJ, Bressan RA (2007) *yucca6*, a dominant mutation in *Arabidopsis*, affects auxin accumulation and auxin-related phenotypes. Plant Physiol 145: 722-735

Kim NH, Kim BS, Hwang BK (2013) Pepper arginine decarboxylase is required for polyamine and gamma-aminobutyric acid signaling in cell death and defense response. Plant Physiol 162: 2067-2083

Kiraly Z, Barna B, Ersek T (1972) Hypersensitivity as a Consequence, Not Cause, of Plant Resistance to Infection. Nature 239: 456-&

Knepper C, Savory EA, Day B (2011) The role of NDR1 in pathogen perception and plant defense signaling. Plant Signal Behav 6: 1114-1116

Kong W, Li J, Yu Q, Cang W, Xu R, Wang Y, Ji W (2016) Two Novel Flavin-Containing Monooxygenases Involved in Biosynthesis of Aliphatic Glucosinolates. Front Plant Sci 7: 1292

Kourelis J, van der Hoorn RAL (2018) Defended to the Nines: 25 Years of Resistance Gene Cloning Identifies Nine Mechanisms for R Protein Function. Plant Cell 30: 285-299

Kraft KH, Brown CH, Nabhan GP, Luedeling E, Luna Ruiz Jde J, Coppens d'Eeckenbrugge G, Hijmans RJ, Gepts P (2014) Multiple lines of evidence for the origin of domesticated chili pepper, *Capsicum annuum*, in Mexico. Proc Natl Acad Sci U S A 111: 6165-6170

Krönauer C (2018) Gel-Gießstand aus Plastikbox. Laborjournal 12: 50

Krönauer C, Kilian J, Strauß T, Stahl M, Lahaye T (2019) Cell Death Triggered by the YUCCA-like Bs3 Protein Coincides with Accumulation of Salicylic Acid and Pipecolic Acid But Not of Indole-3-Acetic Acid. Plant Physiol 180: 1647-1659

Krueger SK, Henderson MC, Siddens LK, VanDyke JE, Benninghoff AD, Karplus PA, Furnes B, Schlenk D, Williams DE (2009) Characterization of sulfoxygenation and structural implications of human flavin-containing monooxygenase isoform 2 (FMO2.1) variants S195L and N413K. Drug Metab Dispos 37: 1785-1791

Krueger SK, Williams DE (2005) Mammalian flavin-containing monooxygenases: structure/function, genetic polymorphisms and role in drug metabolism. Pharmacol Ther 106: 357-387

Lam E (2004) Controlled cell death, plant survival and development. Nat Rev Mol Cell Biol 5: 305-315

Lang DH, Yeung CK, Peter RM, Ibarra C, Gasser R, Itagaki K, Philpot RM, Rettie AE (1998) Isoform specificity of trimethylamine N-oxygenation by human flavin-containing monooxygenase (FMO) and P450 enzymes: selective catalysis by FMO3. Biochem Pharmacol 56: 1005-1012

Lee HA, Kim S, Kim S, Choi D (2017) Expansion of sesquiterpene biosynthetic gene clusters in pepper confers nonhost resistance to the Irish potato famine pathogen. New Phytol 215: 1132-1143

Lee M, Jung JH, Han DY, Seo PJ, Park WJ, Park CM (2012) Activation of a flavin monooxygenase gene *YUCCA7* enhances drought resistance in *Arabidopsis*. Planta 235: 923-938

Li CY, Chen XL, Zhang D, Wang P, Sheng Q, Peng M, Xie BB, Qin QL, Li PY, Zhang XY, Su HN, Song XY, Shi M, Zhou BC, Xun LY, Chen Y, Zhang YZ (2017) Structural mechanism for bacterial oxidation of oceanic trimethylamine into trimethylamine N-oxide. Mol Microbiol 103: 992-1003

Li J, Hansen BG, Ober JA, Kliebenstein DJ, Halkier BA (2008) Subclade of flavin-monooxygenases involved in aliphatic glucosinolate biosynthesis. Plant Physiol 148: 1721-1733

Li SC, Kane PM (2009) The yeast lysosome-like vacuole: endpoint and crossroads. Biochim Biophys Acta 1793: 650-663

Lim JB, Huang BK, Deen WM, Sikes HD (2015) Analysis of the lifetime and spatial localization of hydrogen peroxide generated in the cytosol using a reduced kinetic model. Free Radic Biol Med 89: 47-53

Mak ANS, Bradley P, Cernadas RA, Bogdanove AJ, Stoddard BL (2012) The Crystal Structure of TAL Effector PthXo1 Bound to Its DNA Target. Science 335: 716-719

Marco GM, Stall RE (1983) Control of Bacterial Spot of Pepper Initiated by Strains of *Xanthomonas-Campestris* Pv-*Vesicatoria* That Differ in Sensitivity to Copper. Plant Disease 67: 779-781

McCormac AC, Elliott MC, Chen DF (1998) A simple method for the production of highly competent cells of *Agrobacterium* for transformation via electroporation. Mol Biotechnol 9: 155-159

Meyer AJ, Brach T, Marty L, Kreye S, Rouhier N, Jacquot JP, Hell R (2007) Redox-sensitive GFP in *Arabidopsis* thaliana is a quantitative biosensor for the redox potential of the cellular glutathione redox buffer. Plant Journal 52: 973-986

Meyer AJ, Dick TP (2010) Fluorescent protein-based redox probes. Antioxid Redox Signal 13: 621-650

Miseta A, Csutora P (2000) Relationship between the occurrence of cysteine in proteins and the complexity of organisms. Mol Biol Evol 17: 1232-1239

Mishina TE, Zeier J (2006) The *Arabidopsis* flavin-dependent monooxygenase FMO1 is an essential component of biologically induced systemic acquired resistance. Plant Physiology 141: 1666-1675

Montillet JL, Chamnongpol S, Rusterucci C, Dat J, van de Cotte B, Agnel JP, Battesti C, Inze D, Van Breusegem F, Triantaphylides C (2005) Fatty acid hydroperoxides and H_2O_2 in the execution of hypersensitive cell death in tobacco leaves. Plant Physiology 138: 1516-1526

Morel JB, Dangl JL (1997) The hypersensitive response and the induction of cell death in plants. Cell Death Differ 4: 671-683

Muller-Moule P, Nozue K, Pytlak ML, Palmer CM, Covington MF, Wallace AD, Harmer SL, Maloof JN (2016) *YUCCA* auxin biosynthetic genes are required for *Arabidopsis* shade avoidance. PeerJ 4: e2574

Müller J (2017) Funktionelle Analyse konservierter Cysteine in Bs3 und YUCCA Bachelorarbeit, Eberhard Karls Universität Tübingen

Murphy MP (2009) How mitochondria produce reactive oxygen species. Biochemical Journal 417: 1-13

Nace CG, Genter MB, Sayre LM, Crofton KM (1997) Effect of methimazole, an FMO substrate and competitive inhibitor, on the neurotoxicity of 3,3'-iminodipropionitrile in male rats. Fundam Appl Toxicol 37: 131-140

Nawrath C, Metraux JP (1999) Salicylic acid induction-deficient mutants of *Arabidopsis* express *PR-2* and *PR-5* and accumulate high levels of camalexin after pathogen inoculation. Plant Cell 11: 1393-1404

Nietzel T, Elsasser M, Ruberti C, Steinbeck J, Ugalde JM, Fuchs P, Wagner S, Ostermann L, Moseler A, Lemke P, Fricker MD, Muller-Schussele SJ, Moerschbacher BM, Costa A, Meyer AJ, Schwarzländer M (2019) The fluorescent protein sensor roGFP2-Orp1 monitors in vivo H_2O_2 and thiol redox integration and elucidates intracellular H_2O_2 dynamics during elicitor-induced oxidative burst in *Arabidopsis*. New Phytol 221: 1649-1664

Nishimura T, Hayashi K, Suzuki H, Gyohda A, Takaoka C, Sakaguchi Y, Matsumoto S, Kasahara H, Sakai T, Kato J, Kamiya Y, Koshiba T (2014) Yucasin is a potent inhibitor of YUCCA, a key enzyme in auxin biosynthesis. Plant J 77: 352-366

Normanly J, Slovin JP, Cohen JD (2004) The Plant Hormones. Biosynthesis, Signal Transduction, Action!, 3rd edition. Kluwer Academic Publishers

Oh CS, Martin GB (2011) Tomato 14-3-3 protein TFT7 interacts with a MAP kinase kinase to regulate immunity-associated programmed cell death mediated by diverse disease resistance proteins. J Biol Chem 286: 14129-14136

Orru R, Pazmino DE, Fraaije MW, Mattevi A (2010) Joint functions of protein residues and NADP(H) in oxygen activation by flavin-containing monooxygenase. J Biol Chem 285: 35021-35028

Peart JR, Mestre P, Lu R, Malcuit I, Baulcombe DC (2005) NRG1, a CC-NB-LRR protein, together with N, a TIR-NB-LRR protein, mediates resistance against tobacco mosaic virus. Curr Biol 15: 968-973

Phillips IR, Shephard EA (2008) Flavin-containing monooxygenases: mutations, disease and drug response. Trends Pharmacol Sci 29: 294-301

Pickersgill B (1997) Genetic resources and breeding of *Capsicum* spp. *Euphytica* 96: 129-133

Pierre M, Noël L, Lahaye T, Ballvora A, Veuskens J, Ganal M, U B (2000) High-resolution genetic mapping of the pepper resistance locus Bs3 governing

recognition of the *Xanthomonas campestris* pv. *vesicatoria* AvrBs3 protein. Theor Appl Genet 101: 255-263

Poulsen LL, Ziegler DM (1995) Multisubstrate Flavin-Containing Monooxygenases - Applications of Mechanism to Specificity. Chemico-Biological Interactions 96: 57-73

Qi T, Seong K, Thomazella DPT, Kim JR, Pham J, Seo E, Cho MJ, Schultink A, Staskawicz BJ (2018) NRG1 functions downstream of EDS1 to regulate TIR-NLR-mediated plant immunity in *Nicotiana benthamiana*. Proc Natl Acad Sci U S A 115: E10979-E10987

R Core Team (2017) R: A language and environment for statistical computing. *In*. R Foundation for Statistical Computing, Vienna, Austria

Rao ST, Rossmann MG (1973) Comparison of Super-Secondary Structures in Proteins. Journal of Molecular Biology 76: 241-&

Rekhter D, Ludke D, Ding Y, Feussner K, Zienkiewicz K, Lipka V, Wiermer M, Zhang Y, Feussner I (2019) Isochorismate-derived biosynthesis of the plant stress hormone salicylic acid. Science 365: 498-502

Rescigno M, Perham RN (1994) Structure of the NADPH-binding motif of glutathione reductase: efficiency determined by evolution. Biochemistry 33: 5721-5727

Ritchie DF (2000) Bacterial spot of pepper and tomato. The Plant Health Instructor

Ritz C, Baty F, Streibig JC, Gerhard D (2015) Dose-Response Analysis Using R. Plos One 10

Ritz C, Streibig JC (2008) Nonlinear Regression with R. 10 - 11

Römer P (2010) Isolierung des Paprika *Bs3*-Resistenzgens und Interaktionsanalyse zwischen TAL-Effektoren und pflanzlichen Promotoren. Martin-Luther-Universität Halle-Wittenberg, Halle (Saale)

Römer P, Hahn S, Jordan T, Strauss T, Bonas U, Lahaye T (2007) Plant pathogen recognition mediated by promoter activation of the pepper *Bs3* resistance gene. Science 318: 645-648

Romero E, Gomez Castellanos JR, Gadda G, Fraaije MW, Mattevi A (2018) Same Substrate, Many Reactions: Oxygen Activation in Flavoenzymes. Chem Rev 118: 1742-1769

Schiel D (2015) Characterization of *Bs3/YUC* homologs from *Capsicum annuum* and analysis of *Bs3* expression in *Saccharomyces cerevisiae*. Masterthesis. University of Tübingen, Tübingen

Schindelin J, Arganda-Carreras I, Frise E, Kaynig V, Longair M, Pietzsch T, Preibisch S, Rueden C, Saalfeld S, Schmid B, Tinevez JY, White DJ, Hartenstein V, Eliceiri K, Tomancak P, Cardona A (2012) Fiji: an open-source platform for biological-image analysis. Nat Methods 9: 676-682

Schlaich NL (2007) Flavin-containing monooxygenases in plants: looking beyond detox. Trends Plant Sci 12: 412-418

Schnaubelt D, Queval G, Dong Y, Diaz-Vivancos P, Makgopa ME, Howell G, De Simone A, Bai J, Hannah MA, Foyer CH (2015) Low glutathione regulates gene expression and the redox potentials of the nucleus and cytosol in *Arabidopsis thaliana*. Plant Cell Environ 38: 266-279

Schornack S, Minsavage GV, Stall RE, Jones JB, Lahaye T (2008) Characterization of AvrHah1, a novel AvrBs3-like effector from *Xanthomonas gardneri* with virulence and avirulence activity. New Phytol 179: 546-556

Schwanhausser B, Busse D, Li N, Dittmar G, Schuchhardt J, Wolf J, Chen W, Selbach M (2011) Global quantification of mammalian gene expression control. Nature 473: 337-342

Schwarzländer M, Fricker MD, Muller C, Marty L, Brach T, Novak J, Sweetlove LJ, Hell R, Meyer AJ (2008) Confocal imaging of glutathione redox potential in living plant cells. J Microsc 231: 299-316

Seguel A, Jelenska J, Herrera-Vasquez A, Marr SK, Joyce MB, Gagesch KR, Shakoor N, Jiang SC, Fonseca A, Wildermuth MC, Greenberg JT, Holuigue L (2018) Prohibitin 3 Forms Complexes with Isochorismate Synthase 1 to Regulate Stress-Induced Salicylic Acid Biosynthesis in *Arabidopsis*. Plant Physiol 176: 2515-2531

Shapira M, Segal E, Botstein D (2004) Disruption of yeast forkhead-associated cell cycle transcription by oxidative stress. Mol Biol Cell 15: 5659-5669

Shapiro AD, Zhang C (2001) The role of *NDR1* in avirulence gene-directed signaling and control of programmed cell death in *Arabidopsis*. Plant Physiol 127: 1089-1101

Shirasu K (2009) The HSP90-SGT1 chaperone complex for NLR immune sensors. Annu Rev Plant Biol 60: 139-164

Shirey C, Badieyan S, Sobrado P (2013) Role of Ser-257 in the sliding mechanism of NADP(H) in the reaction catalyzed by the *Aspergillus fumigatus* flavin-dependent ornithine N5-monooxygenase SidA. J Biol Chem 288: 32440-32448

Siddens LK, Krueger SK, Henderson MC, Williams DE (2014) Mammalian flavin-containing monooxygenase (FMO) as a source of hydrogen peroxide. Biochem Pharmacol 89: 141-147

Sil AK, Alam S, Xin P, Ma L, Morgan M, Lebo CM, Woods MP, Hopper JE (1999) The Gal3p-Gal80p-Gal4p transcription switch of yeast: Gal3p destabilizes the Gal80p-Gal4p complex in response to galactose and ATP. Mol Cell Biol 19: 7828-7840

Siligardi G, Zhang M, Prodromou C (2017) The Stoichiometric Interaction of the Hsp90-Sgt1-Rar1 Complex by CD and SRCD Spectroscopy. Front Mol Biosci 4: 95

Stall RE, Jones JB, Minsavage GV (2009) Durability of resistance in tomato and pepper to xanthomonads causing bacterial spot. Annu Rev Phytopathol 47: 265-284

Stehr M, Diekmann H, Smau L, Seth O, Ghisla S, Singh M, Macheroux P (1998) A hydrophobic sequence motif common to N-hydroxylating enzymes. Trends in Biochemical Sciences 23: 56-57

Stoyanova M, Vancheva T, Moncheva P, Bogatzevska N (2014) Differentiation of *Xanthomonas* spp. Causing Bacterial Spot in Bulgaria Based on Biolog System. Int J Microbiol 2014: 495476

Strauß T (2008) Mutationsanalyse des Resistenzgens *Bs3* aus Paprika, Diplomarbeit, Martin-Luther-Universität Halle-Wittenberg

Suh JK, Poulsen LL, Ziegler DM, Robertus JD (1996) Molecular cloning and kinetic characterization of a flavin-containing monooxygenase from *Saccharomyces cerevisiae*. Arch Biochem Biophys 336: 268-274

Suh JK, Poulsen LL, Ziegler DM, Robertus JD (1999) Yeast flavin-containing monooxygenase generates oxidizing equivalents that control protein folding in the endoplasmic reticulum. Proceedings of the National Academy of Sciences of the United States of America 96: 2687-2691

Szklarczyk D, Franceschini A, Wyder S, Forslund K, Heller D, Huerta-Cepas J, Simonovic M, Roth A, Santos A, Tsafou KP, Kuhn M, Bork P, Jensen LJ, von Mering C (2015) STRING v10: protein-protein interaction networks, integrated over the tree of life. Nucleic Acids Res 43: D447-452

Tada Y, Spoel SH, Pajerowska-Mukhtar K, Mou Z, Song J, Wang C, Zuo J, Dong X (2008) Plant immunity requires conformational changes [corrected] of NPR1 via S-nitrosylation and thioredoxins. Science 321: 952-956

Thorpe GW, Fong CS, Alic N, Higgins VJ, Dawes IW (2004) Cells have distinct mechanisms to maintain protection against different reactive oxygen species: Oxidative-stress-response genes. Proceedings of the National Academy of Sciences of the United States of America 101: 6564-6569

Tian D, Wang J, Zeng X, Gu K, Qiu C, Yang X, Zhou Z, Goh M, Luo Y, Murata-Hori M, White FF, Yin Z (2014) The Rice TAL Effector-Dependent Resistance Protein XA10 Triggers Cell Death and Calcium Depletion in the Endoplasmic Reticulum. Plant Cell 26: 497-515

Tierens KF, Thomma BP, Brouwer M, Schmidt J, Kistner K, Porzel A, Mauch-Mani B, Cammue BP, Broekaert WF (2001) Study of the role of antimicrobial glucosinolate-derived isothiocyanates in resistance of Arabidopsis to microbial pathogens. Plant Physiol 125: 1688-1699

Tivendale ND, Davies NW, Molesworth PP, Davidson SE, Smith JA, Lowe EK, Reid JB, Ross JJ (2010) Reassessing the role of N-hydroxytryptamine in auxin biosynthesis. Plant Physiol 154: 1957-1965

Torrens-Spence MP, Bobokalonova A, Carballo V, Glinkerman CM, Pluskal T, Shen A, Weng JK (2019) PBS3 and EPS1 Complete Salicylic Acid Biosynthesis from Isochorismate in *Arabidopsis*. Mol Plant 12: 1577-1586

Torres MA, Jones JD, Dangl JL (2005) Pathogen-induced, NADPH oxidase-derived reactive oxygen intermediates suppress spread of cell death in *Arabidopsis thaliana*. Nat Genet 37: 1130-1134

Torres MA, Jones JDG, Dangl JL (2006) Reactive oxygen species signaling in response to pathogens. Plant Physiology 141: 373-378

Traven A, Jelicic B, Sopta M (2006) Yeast Gal4: a transcriptional paradigm revisited. EMBO Rep 7: 496-499

Tsuda K, Katagiri F (2010) Comparing signaling mechanisms engaged in pattern-triggered and effector-triggered immunity. Curr Opin Plant Biol 13: 459-465

USDA (2019) USDA, Agricultural Research Service, National Plant Germplasm System. 2019. Germplasm Resources Information Network (GRIN-Taxonomy). National Germplasm Resources Laboratory, Beltsville, Maryland.URL:https://npgsweb.arsgrin.gov/gringlobal/taxon/taxonomy simple.aspx. Accessed 20 January 2019.

van Doorn WG, Beers EP, Dangl JL, Franklin-Tong VE, Gallois P, Hara-Nishimura I, Jones AM, Kawai-Yamada M, Lam E, Mundy J, Mur LA, Petersen M, Smertenko A, Taliansky M, Van Breusegem F, Wolpert T, Woltering E, Zhivotovsky B, Bozhkov PV (2011) Morphological classification of plant cell deaths. Cell Death Differ 18: 1241-1246

van Wees SC, Glazebrook J (2003) Loss of non-host resistance of *Arabidopsis* NahG to *Pseudomonas syringae* pv. *phaseolicola* is due to degradation products of salicylic acid. Plant J 33: 733-742

Waszczak C, Akter S, Jacques S, Huang J, Messens J, Van Breusegem F (2015) Oxidative post-translational modifications of cysteine residues in plant signal transduction. J Exp Bot 66: 2923-2934

Waterhouse A, Bertoni M, Bienert S, Studer G, Tauriello G, Gumienny R, Heer FT, de Beer TAP, Rempfer C, Bordoli L, Lepore R, Schwede T (2018) SWISS-MODEL: homology modelling of protein structures and complexes. Nucleic Acids Res 46: W296-W303

Weber E, Engler C, Gruetzner R, Werner S, Marillonnet S (2011) A modular cloning system for standardized assembly of multigene constructs. PLoS One 6: e16765

Weigel D, Ahn JH, Blazquez MA, Borevitz JO, Christensen SK, Fankhauser C, Ferrandiz C, Kardailsky I, Malancharuvil EJ, Neff MM, Nguyen JT, Sato S, Wang ZY, Xia Y, Dixon RA, Harrison MJ, Lamb CJ, Yanofsky MF, Chory J (2000) Activation tagging in *Arabidopsis*. Plant Physiol 122: 1003-1013

Wickham H (2009) ggplot2: Elegant Graphics for Data Analysis. Ggplot2: Elegant Graphics for Data Analysis: 1-212

Wildermuth MC, Dewdney J, Wu G, Ausubel FM (2001) Isochorismate synthase is required to synthesize salicylic acid for plant defence. Nature 414: 562-565

Winzeler EA, Shoemaker DD, Astromoff A, Liang H, Anderson K, Andre B, Bangham R, Benito R, Boeke JD, Bussey H, Chu AM, Connelly C, Davis K, Dietrich F, Dow SW, El Bakkoury M, Foury F, Friend SH, Gentalen E, Giaever G, Hegemann JH, Jones T, Laub M, Liao H, Liebundguth N,

Lockhart DJ, Lucau-Danila A, Lussier M, M'Rabet N, Menard P, Mittmann M, Pai C, Rebischung C, Revuelta JL, Riles L, Roberts CJ, Ross-MacDonald P, Scherens B, Snyder M, Sookhai-Mahadeo S, Storms RK, Veronneau S, Voet M, Volckaert G, Ward TR, Wysocki R, Yen GS, Yu K, Zimmermann K, Philippsen P, Johnston M, Davis RW (1999) Functional characterization of the *S. cerevisiae* genome by gene deletion and parallel analysis. Science 285: 901-906

Wojtaszek P (1997) Oxidative burst: an early plant response to pathogen infection. Biochem J 322 (Pt 3): 681-692

Yamamoto Y, Kamiya N, Morinaka Y, Matsuoka M, Sazuka T (2007) Auxin biosynthesis by the *YUCCA* genes in rice. Plant Physiol 143: 1362-1371

Yoshioka H, Numata N, Nakajima K, Katou S, Kawakita K, Rowland O, Jones JD, Doke N (2003) *Nicotiana benthamiana* gp91phox homologs NbrbohA and NbrbohB participate in H_2O_2 accumulation and resistance to *Phytophthora infestans*. Plant Cell 15: 706-718

Yu G, Xian L, Sang Y, Macho AP (2019) Cautionary notes on the use of *Agrobacterium*-mediated transient gene expression upon *SGT1* silencing in *Nicotiana benthamiana*. New Phytol 222: 14-17

Zechmann B, Liou LC, Koffler BE, Horvat L, Tomasic A, Fulgosi H, Zhang Z (2011) Subcellular distribution of glutathione and its dynamic changes under oxidative stress in the yeast *Saccharomyces cerevisiae*. FEMS Yeast Res 11: 631-642

Zhang J, Yin Z, White F (2015) TAL effectors and the executor *R* genes. Front Plant Sci 6: 641

Zhang M, Kadota Y, Prodromou C, Shirasu K, Pearl LH (2010) Structural basis for assembly of Hsp90-Sgt1-CHORD protein complexes: implications for chaperoning of NLR innate immunity receptors. Mol Cell 39: 269-281

Zhang Y, Li X (2019) Salicylic acid: biosynthesis, perception, and contributions to plant immunity. Curr Opin Plant Biol 50: 29-36

Zhao Y (2010) Auxin biosynthesis and its role in plant development. Annu Rev Plant Biol 61: 49-64

Zhao Y, Christensen SK, Fankhauser C, Cashman JR, Cohen JD, Weigel D, Chory J (2001) A role for flavin monooxygenase-like enzymes in auxin biosynthesis. Science 291: 306-309

Zurbriggen MD, Carrillo N, Hajirezaei MR (2010) ROS signaling in the hypersensitive response: when, where and what for? Plant Signal Behav 5: 393-396

6 Supplementary Information

6.1 Expression vectors and Oligonucleotides

Table 6.1: Expression vectors used in this study

PLASMID	PROJECT	NUMBER
pLIIα_35S_Bs3G209A_GFP_dy	Bs3 mutant analysis	CK-MP303
pLIIα_35S_Bs3G41A_GFP_dy	Bs3 mutant analysis	CK-MP302
pLIIα_35S_Bs3S211A_GFP_dy (DS)	Bs3 mutant analysis	CK-MP304
pLIIα_Bs3-C6S-GFP	Bs3 mutant analysis	CK-MP676
pLIIα_Bs3-C10S-GFP	Bs3 mutant analysis	CK-MP677
pLIIα_Bs3-C25S-GFP	Bs3 mutant analysis	CK-MP678
pLIIα_Bs3-C29S-GFP	Bs3 mutant analysis	CK-MP679
pLIIα_Bs3-C66S-GFP (JM)	Bs3 mutant analysis	CK-MP567
pLIIα_Bs3-C88S-GFP (JM)	Bs3 mutant analysis	CK-MP521
pLIIα_Bs3-C138S-GFP (JM)	Bs3 mutant analysis	CK-MP568
pLIIα_Bs3-C158S-GFP (JM)	Bs3 mutant analysis	CK-MP569
pLIIα_Bs3-C190S-GFP (JM)	Bs3 mutant analysis	CK-MP570
pLIIα_Bs3-C208S-GFP (JM)	Bs3 mutant analysis	CK-MP571
pLIIα_Bs3-C295S-GFP (JM)	Bs3 mutant analysis	CK-MP572
pLIIα_35S_CaYUC3-GFP_noster (DS)	*Capsicum* YUCs	CK-MP817
pLIIα_35S_CaYUC4-GFP_noster (DS)	*Capsicum* YUCs	CK-MP818
pLIIα_35S_CaYUC5-GFP_noster (DS)	*Capsicum* YUCs	CK-MP819
pLIIα_35S_CaYUC6-GFP_noster (DS)	*Capsicum* YUCs	CK-MP820
pLIIα_35S_Bs3_GFP	Divers	CK-MP338
pLIIα_35S_GFP_noster_dy	Divers	CK-MP92
pLIIα_35S_YUC8_GFP	Divers	CK-MP339
pLIIα_Bs3S211A-GFP	Divers	CK-MP556
pYES-DEST-52_PGal1_Bs3G209A-V5-6xhis (DS)	Expression in yeast	CK-MP805
pYES-DEST-52_PGal1_Bs3G41A-V5-6xhis (DS)	Expression in yeast	CK-MP804
pYES-DEST-52_PGal1_Bs3S211A-V5-6xhis (DS)	Expression in yeast	CK-MP806
pYES-DEST-52_PGal1_Bs3-V5-6xhis (DS)	Expression in yeast	CK-MP802
pYES-DEST-52_PGal1_GFP-V5-6xhis (DS)	Expression in yeast	CK-MP807
pYES-DEST-52_PGal1_YUC8-V5-6xhis (DS)	Expression in yeast	CK-MP808
pLIIα_35S_AB1b2CDE_GFP_noster_dy	Gene shuffling	CK-MP82
pLIIα_35S_Ab1B2CDE_GFP_noster_dy	Gene shuffling	CK-MP83
pLIIα_35S_AB1b2cdE_GFP_noster_dy	Gene shuffling	CK-MP84
pLIIα_35S_Ab1B2cdE_GFP_noster_dy	Gene shuffling	CK-MP85
pLIIα_35S_aBCDe_GFP_NosTer_dy #10	Gene shuffling	CK-MP28
pLIIα_35S_AbcDE_GFP_NosTer_dy #11	Gene shuffling	CK-MP29
pLIIα_35S_AbCdE_GFP_NosTer_dy #12	Gene shuffling	CK-MP30
pLIIα_35S_AbCDe_GFP_NosTer_dy #13	Gene shuffling	CK-MP31
pLIIα_35S_ABcdE_GFP_NosTer_dy #14	Gene shuffling	CK-MP32
pLIIα_35S_ABCde_GFP_NosTer_dy #15	Gene shuffling	CK-MP33
pLIIα_35S_AbcDe_GFP_NosTer_dy #16	Gene shuffling	CK-MP34
pLIIα_35S_Abcde_GFP_NosTer_dy #17	Gene shuffling	CK-MP35
pLIIα_35S_AbCde_GFP_NosTer_dy #18	Gene shuffling	CK-MP36
pLIIα_35S_AbcDe_GFP_NosTer_dy #19	Gene shuffling	CK-MP37
pLIIα_35S_aBCDE_GFP_NosTer_dy #2	Gene shuffling	CK-MP20

Table 6.1 (continued)

pLIIα_35S_AbcdE_GFP_NosTer_dy #20	Gene shuffling	CK-MP38
pLIIα_35S_aBCde_GFP_NosTer_dy #21	Gene shuffling	CK-MP39
pLIIα_35S_aBcDe_GFP_NosTer_dy #22	Gene shuffling	CK-MP40
pLIIα_35S_aBcdE_GFP_NosTer_dy #23	Gene shuffling	CK-MP41
pLIIα_35S_abCDe_GFP_NosTer_dy #24	Gene shuffling	CK-MP42
pLIIα_35S_abCdE_GFP_NosTer_dy #25	Gene shuffling	CK-MP43
pLIIα_35S_abcDE_GFP_NosTer_dy #26	Gene shuffling	CK-MP44
pLIIα_35S_abcdE_GFP_NosTer_dy #27	Gene shuffling	CK-MP45
pLIIα_35S_Abcde_GFP_NosTer_dy #28	Gene shuffling	CK-MP46
pLIIα_35S_aBcde_GFP_NosTer_dy #29	Gene shuffling	CK-MP47
pLIIα_35S_AbCDE_GFP_NosTer_dy #3	Gene shuffling	CK-MP21
pLIIα_35S_abCde_GFP_NosTer_dy #30	Gene shuffling	CK-MP48
pLIIα_35S_abcDe_GFP_NosTer_dy #31	Gene shuffling	CK-MP49
pLIIα_35S_AbcDE_GFP_NosTer_dy #4	Gene shuffling	CK-MP22
pLIIα_35S_ABCdE_GFP_NosTer_dy #5	Gene shuffling	CK-MP23
pLIIα_35S_ABCDe_GFP_NosTer_dy #6	Gene shuffling	CK-MP24
pLIIα_35S_abCDE_GFP_NosTer_dy #7	Gene shuffling	CK-MP25
pLIIα_35S_aBcDE_GFP_NosTer_dy #8	Gene shuffling	CK-MP26
pLIIα_35S_aBCdE_GFP_NosTer_dy #9	Gene shuffling	CK-MP27
pLIIα_35S_Bs3+AA-GFP_noster_dy #1	Gene shuffling	CK-MP400
pLIIα_35S_YUC8-AA-GFP_noster_dy #1	Gene shuffling	CK-MP401
pLIIα_NLS_Bs3+AA_GFP_noster_dy	Gene shuffling	CK-MP86
pLIIα_NLS_YUC8-AA_GFP_noster_dy	Gene shuffling	CK-MP87
pLIIα_35S_Bs4C-GFP_noster	HR induction	CK-MP823
pLIIα_35S_Xa10-GFP_noster	HR induction	CK-MP821
pLIIα_35S_Xa23-GFP_noster	HR induction	CK-MP822
pLIIα_35S_NES-Bs3-GFP_noster_dy	Localisation studies	CK-MP94
pLIIα_35S_NES-YUC8-GFP	Localisation studies	CK-MP341
pLIIα_35S_NLS-Bs3-GFP_noster_dy	Localisation studies	CK-MP95
pLIIα_35S_NLS-Bs3-GFP_noster_dy	Localisation studies	CK-MP126
pLIIα_35S_NLS-YUC8-GFP_noster_dy	Localisation studies	CK-MP125
pLIIα_35S_YUC8PartIV-GFP_noster_dy	Localisation studies	CK-MP774
pLIIα__GAG-Bs3	N-terminal deletions	CK-MP761
pLIIα__GPL-Bs3	N-terminal deletions	CK-MP756
pLIIα__IQV-Bs3	N-terminal deletions	CK-MP752
pLIIα__IVG-Bs3	N-terminal deletions	CK-MP759
pLIIα__LIV-Bs3	N-terminal deletions	CK-MP758
pLIIα__NGP-Bs3	N-terminal deletions	CK-MP755
pLIIα__PLI-Bs3	N-terminal deletions	CK-MP757
pLIIα__QVN-Bs3	N-terminal deletions	CK-MP753
pLIIα__VGA-Bs3	N-terminal deletions	CK-MP760
pLIIα__VNG-Bs3	N-terminal deletions	CK-MP754
pPICZ_GST_sBs3 #C	Pichia survival analysis	CK-MP350
pPICZ_sBs3	Pichia survival analysis	CK-MP357
pET-53-DEST_6xhis-NQN-Bs3	Protein purification	CK-MP660
pET-53-DEST_6xhis-NQN-Bs3S211A	Protein purification	CK-MP665
pET-53-DEST_YUC6	Protein purification	CK-MP374

Table 6.1 (continued)

pLIIα_35S_roGFP2	Redox reporter	CK-MP848
pLIIα_35S_Bs3-roGFP2	Redox reporter	CK-MP490
pLIIα_35S_Bs3G41A-roGFP2	Redox reporter	CK-MP869
pLIIα_35S_Bs3G209A-roGFP2	Redox reporter	CK-MP873
pLIIα_35S_Bs3S211A-roGFP2	Redox reporter	CK-MP542
pLIIα_35S_GRX1-roGFP2	Redox reporter	CK-MP850
pLIIα_35S_Bs3-GRX1-roGFP2	Redox reporter	CK-MP489
pLIIα_35S_Bs3G41A-GRX1-roGFP2	Redox reporter	CK-MP870
pLIIα_35S_Bs3G209A-GRX1-roGFP2	Redox reporter	CK-MP875
pLIIα_35S_Bs3S211A-GRX1-roGFP2	Redox reporter	CK-MP540
pLIIα_35S_roGFP2-Orp1	Redox reporter	CK-MP868
pLIIα_35S_Bs3-roGFP2-Orp1	Redox reporter	CK-MP547
pLIIα_35S_Bs3G41A-roGFP2-Orp1	Redox reporter	CK-MP871
pLIIα_35S_Bs3G209A-roGFP2-Orp1	Redox reporter	CK-MP876
pLIIα_35S_Bs3S211A-roGFP2-Orp1	Redox reporter	CK-MP554
pLIIα_TAP-Bs3-Yap1A	Sulfenome mining	CK-MP652
pLIIα_TAP-Bs3-Yap1C	Sulfenome mining	CK-MP654
pLIIα_TAP-Bs3S211A-Yap1A	Sulfenome mining	CK-MP656
pLIIα_TAP-Bs3S211A-Yap1C	Sulfenome mining	CK-MP657
pTRV1	VIGS	CK-MP727
pTRV2a_CaADC1_135bp	VIGS	CK-MP161
pTRV2a_CaADC1_500bp #1	VIGS	CK-MP159
pTRV2a_CaPDS	VIGS	CK-MP731
pTRV2a_NbEDS1	VIGS	CK-MP728
pTRV2a_NbNDR1	VIGS	CK-MP738
pTRV2a_NbRAR1	VIGS	CK-MP739
pTRV2a_NbSGT1	VIGS	CK-MP732
pTRV2a_SlHsp70	VIGS	CK-MP730
pTRV2a_smGFP	VIGS	CK-MP729
TRV2a_NbADC1-1 250	VIGS	CK-MP830
TRV2a_NbICS	VIGS	CK-MP831

Table 6.2: Oligonucleotides

DESIGNATION	SEQUENCE	PROJECT
343Bs3C6Sfw	GAATCAGAATaGCTTTAATTCTtGTTCACCTCTAAC	Bs3 C>S mutagenesis
344Bs3C6Srev	GAATTAAAGCtATTCTGATTCATCATGGTGAGAG	Bs3 C>S mutagenesis
345Bs3C10Sfw	GCTTTAATTCTaGTTCACCTCTAACTGTTGATGC	Bs3 C>S mutagenesis
346Bs3C10Srev	GAGGTGAACtAGAATTAAAGCAATTCTGATTC	Bs3 C>S mutagenesis
347Bs3C25Sfw	CCTCTaGTGCTGCTAAATGCATACAAGTAAATGG	Bs3 C>S mutagenesis
348Bs3C25Srev	GCATTTAGCAGCACtAGAGGATTTTTTTGG	Bs3 C>S mutagenesis
349Bs3C29Sfw	GTGCTGCTAAAaGCATACAAGTAAATGGTCC	Bs3 C>S mutagenesis
350Bs3C29Srev	CCATTTACTTGTATGCtTTTAGCAGCACAAGAGG	Bs3 C>S mutagenesis
288Bs3C88Sfw	CAATACaGCGAATTGCCTGGCTTGCC	Bs3 C>S mutagenesis (JM)
289Bs3C88Srev	GGCAATTCGCtGTATTGTCGTGGCAC	Bs3 C>S mutagenesis (JM)
301Bs3C66Sfw	CGCGGACaGCATTGCTTCTCTGTGGCAAC	Bs3 C>S mutagenesis (JM)
302Bs3C66Srev	GAAGCAATGCtGTCCGCGCGTTCAATGATTAC	Bs3 C>S mutagenesis (JM)
303Bs3C88Sfw	CAATACaGCGAATTGCCTGGCTTGCCA	Bs3 C>S mutagenesis (JM)
304Bs3C88Srev	GGCAATTCGCtGTATTGTCGTGGCACG	Bs3 C>S mutagenesis (JM)
305Bs3C138Sfw	GAGACAaGTGGTTTATGGAAGGTGAAAAC	Bs3 C>S mutagenesis (JM)
306Bs3C138Srev	CATAAACCACtTGTCTCATCATATCCAGCC	Bs3 C>S mutagenesis (JM)
307Bs3C158Sfw	GAATACATGaGTAAGTGGCTTATTGTGGCC	Bs3 C>S mutagenesis (JM)
308Bs3C158Srev	CCACTTACtCATGTATTCAGAGGTTGAACC	Bs3 C>S mutagenesis (JM)
309Bs3C190Sfw	CATGCTaGTGAGTACAAGACTGGGG	Bs3 C>S mutagenesis (JM)
310Bs3C190Srev	GTACTCACtAGCATGAATAACCTGGCC	Bs3 C>S mutagenesis (JM)
311Bs3C208Sfw	GGTTGGCaGTGGGAATTCAGGGATAGATATCTCACTTG	Bs3 C>S mutagenesis (JM)
312Bs3C208Srev	GAATTCCCACtGCCAACCGCCAGCACATTTTC	Bs3 C>S mutagenesis (JM)
313Bs3C295Sfw	GGGAaGTCCAAAAAGCCCATTCCCAAATGG	Bs3 C>S mutagenesis (JM)
314Bs3C295Srev	GGCTTTTTGGACtTCCCTCCCTTGAAAACAATTC	Bs3 C>S mutagenesis (JM)
200Bs3G209Afw	GGCTGTGcCAATTCCGGGATCGATATCTC	Bs3 mutagenesis G209A
201Bs3G209Arev	GGAATTGgCACAGCCAACCGCCAGCAC	Bs3 mutagenesis G209A
163-Bs3S211Afw	P- GCC GGG ATC GAT ATC TCA CTT G	Bs3 mutagenesis S211A (DS)
164-Bs3S211Arev	ATT GCC ACA GCC AAC CGC	Bs3 mutagenesis S211A (DS)
360-IQV-Bs3fw	aaacgtctctCACCATGATACAAGTAAATGGTCCTCTTAT	Bs3 N-terminal deletions
361-QVN-Bs3fw	aaacgtctctCACCATGCAAGTAAATGGTCCTCTTATTG	Bs3 N-terminal deletions
362-VNG-Bs3fw	aaacgtctctCACCATGGTAAATGGTCCTCTTATTGTT	Bs3 N-terminal deletions
363-NGP-Bs3fw	aaacgtctctCACCATGAATGGTCCTCTTATTGTTG	Bs3 N-terminal deletions
364-GPL-Bs3fw	aaacgtctctCACCATGGGTCCTCTTATTGTTGGA	Bs3 N-terminal deletions
365-PLI-Bs3fw	aaacgtctctCACCATGCCTCTTATTGTTGGAGCTG	Bs3 N-terminal deletions
366-LIV-Bs3fw	aaacgtctctCACCATGCTTATTGTTGGAGCTGGC	Bs3 N-terminal deletions
367-IVG-Bs3fw	aaacgtctctCACCATGATTGTTGGAGCTGGCC	Bs3 N-terminal deletions
368-VGA-Bs3fw	aaacgtctctCACCATGGTTGGAGCTGGCCCTTC	Bs3 N-terminal deletions
369-GAG-Bs3fw	aaacgtctctCACCATGGGAGCTGGCCCTTCAG	Bs3 N-terminal deletions
Yuc8partIfw	tttcgtctctCACCATGGAGAATATGTTTCG	Bs3/YUC8 chimeras
Yuc8partIrev	aaacgtctctAGCAGTCGCTAAGCCCG	Bs3/YUC8 chimeras
Yuc8partIIfw	aaacgtctctTGC TGC TTG TCT CCA TG	Bs3/YUC8 chimeras
Yuc8partIIrev	aaacgtctctTGA ACT GAC GCT TCG TC	Bs3/YUC8 chimeras
Yuc8partIIIfw	aaacgtctctTTCATCGACTACCTCGAGTC	Bs3/YUC8 chimeras

Table 6.2 (continued)

Yuc8partIIIrev	aaacgtctctGAGCTTCTCACGACCATC	Bs3/YUC8 chimeras
Yuc8partIVfw	tttcgtctctGCTCTCTTCACGTGATGC	Bs3/YUC8 chimeras
Yuc8partIVrev	tttcgtctctCCAATATGGGACGTTGC	Bs3/YUC8 chimeras
Yuc8partVfw	aaacgtctctTTGGCTACAAGAGAATGAG	Bs3/YUC8 chimeras
Yuc8partVrev	aaacgtctctCCTTGAACTGTTGAGAGATAC	Bs3/YUC8 chimeras
Bs3partIfw	aaacgtctctCACCATGATGAATCAGAATTG	Bs3/YUC8 chimeras
Bs3partIrev	aaacgtctctAGCAGTAGCCAGCCCTG	Bs3/YUC8 chimeras
Bs3partIIfw	aaacgtctctTGCTGCCGTCCTTAAGC	Bs3/YUC8 chimeras
Bs3partIIrev	tttcgtctctTGAATTGGTTTTTGGTTGG	Bs3/YUC8 chimeras
Bs3partIIIfw	aaacgtctctTTCATCAGCTACCTGGTATC	Bs3/YUC8 chimeras
Bs3partIIIrev	aaacgtctctGAGCTTCGTACTACCATGAATG	Bs3/YUC8 chimeras
Bs3partIVfw	aaacgtctctGCTCGGTACAGGGTCGTA	Bs3/YUC8 chimeras
Bs3partIVrev	aaacgtctctCCAAGAAGTTACATTGCTGG	Bs3/YUC8 chimeras
Bs3partVfw	aaacgtctctTTGGTTAATGGAGAGTG	Bs3/YUC8 chimeras
Bs3partVrev	aaacgtctctCCTTCATTTGTTCTTTCC	Bs3/YUC8 chimeras
CKP52partIVaBs3rev	aaacgtctctGAACCACGTTTATTTCCTCGG	Bs3/YUC8 chimeras
CKP53partIVaYuc8rev	aaacgtctctGAACTATGTTGATCTTTCCTAAG	Bs3/YUC8 chimeras
CKP54partIVbBs3fw	aaacgtctctGTTCCAGCAATCAAGAAATTTAC	Bs3/YUC8 chimeras
CKP55partIVbYuc8fw	aaacgtctctGTTCCCGGGATCAAAAG	Bs3/YUC8 chimeras
CKP70Bs3pIIarev	aaacgtctctCGTAGGTCTTGTGTTGCCAC	Bs3/YUC8 chimeras
CKP71Bs3pIIbfw	aaacgtctctTACGATCGGTTAAGGCTTAAC	Bs3/YUC8 chimeras
CKP72YUCpIIarev	aaacgtctctCGTAAGTACGTTTTTGCCATAG	Bs3/YUC8 chimeras
CKP73YUCpIIbfw	aaacgtctctTACGATCGACTAAAGCTTCACC	Bs3/YUC8 chimeras
CKP66ADC1vigsBsaIfw	aaaggtctctcaccATGCCGGCCTTAGGTTGTTG	Clonig of CaADC1
CKP85CaADC1rev	aaaggtctctccttAGCAGTGCAATAGGACCAAATCTC	Clonig of CaADC1
175cat2FWcacc	tttcgtctcTCACCATGGATCCTTACAAG	Cloning of AtCat2
176cat2REVaagg	tttcgtctctccttCTGAGACCAGTAAGAGATCCAG	Cloning of AtCat2
229TCP15fw	ATGGATCCGGATCCGGATC	Cloning of AtTCP15
230TCP15rev	CTAGGAATGATGACTGGTGCTTCC	Cloning of AtTCP15
255TCP15#2fw	tttGGTCTCACACCATGGATCCGGATCCGGATCATAACC	Cloning of AtTCP15
256TCP15#2rev	tttGGTCTCACCTTGGAATGATGACTGGTGCTTCCATC	Cloning of AtTCP15
259TCP15nostoprev	tttGGTCTCACCTTGGAATGATGACTGGTGCTTCC	Cloning of AtTCP15
225TCP8fw	ATGGATCTCTCCGACATC	Cloning of AtTCP8
226TCP8rev	TCACTCAGAGCTATTTGAGTTC	Cloning of AtTCP8
243TCP8CACC	tttGGTCTCACACCATGGATCTCTCCGACATC	Cloning of AtTCP8
244TCP8AAGG	tttGGTCTCACCTTTCACTCAGAGCTATTTGAGTTC	Cloning of AtTCP8
257TCP8nostoprev	tttGGTCTCACCTTCTCAGAGCTATTTGAGTTCTCC	Cloning of AtTCP8
227TCP9fw	ATGGCGACAATTCAGAAGC	Cloning of AtTCP9
228TCP9rev	TCAGTGGTTCGATGACCG	Cloning of AtTCP9
245TCP9CACC	tttGGTCTCACACCATGGCGACAATTCAGAAGC	Cloning of AtTCP9
246TCP9AAGG	tttGGTCTCACCTTTCAGTGGTTCGATGACCG	Cloning of AtTCP9
258TCP9nostoprev	tttGGTCTCACCTTGTGGTTCGATGACCGTG	Cloning of AtTCP9
CKP58AvrBsTfw	ATGAAGAATTTTATGCGTTCACTTG	Cloning of AvrBsT (Kim et al. 2010)
CKP59AvrBsTrev	TTATGATTCAATAGTTTTCCTAATTTT	Cloning of AvrBsT (Kim et al. 2010)

Table 6.2 (continued)

CKP90AvrBsTFLAGcaccF	aaaggtctctcaccATGAAGAATTTTATGCGTTCAC	Cloning of AvrBsT-FLAG
CKP91AvrBsTFLAGaaggR	aaaggtctctccttTTACTTGTCATCGTCGTCC	Cloning of AvrBsT-FLAG
CKP60CaADC1fw	ATGCCGGCCTTAGGTTG	Cloning of CaADC1
CKP61CaADC1rev	TCAAGCAGTGCAATAGGACC	Cloning of CaADC1
CKP125Bs3H1cacc	tttggtctctcaccATGAATCAATATTGTAATAGTCCTTGTTC	Cloning of CaYUC3 (DS)
CKP126Bs3H1aagg	aaaggtctcaccttGAAATGTGACTTGCTTCTTCTATG	Cloning of CaYUC3 (DS)
CKP127Bs3H2cacc	tttcgtctctcaccATGTTTAGTTTCTCAGAAAACGATTTC	Cloning of CaYUC4 (DS)
CKP128Bs3H2aagg	aaacgtctcaccttGAAGGTTGAGATGCAACGTC	Cloning of CaYUC4 (DS)
CKP131Bs3H4cacc	tttcgtctctcaccATGGTTAACTTCAATGATCAAG	Cloning of CaYUC5 (DS)
CKP132Bs3H4aagg	aaacgtctcaccttATTTACACATAAGGTTGACATG	Cloning of CaYUC5 (DS)
CKP129Bs3H3cacc	tttggtctctcaccATGTTTACCTTTTCGTCAGAAC	Cloning of CaYUC6 (DS)
CKP130Bs3H3aagg	aaaggtctcaccttAAAAGTTGAGATGCATCTTCTATG	Cloning of CaYUC6 (DS)
391NahGII	tttcgtctctCACCATGAAAAACAATAAACTTGGCTTGC	Cloning of NahG
392NahGII	aaacgtctctCCTTCCCTTGACGTAGCGCACC	Cloning of NahG
318xa27cacc	tttGGTCTCACACCATGCAACTGATGCTGACG	Cloning of Xa27
319xa27AAGG	tttGGTCTCACCTTCACCGGGCTGATTTCTTC	Cloning of Xa27
260-15aaGrx1roGFP2fw	tttGGTCTCAAAGGGAggtggaggaggttctggaggcggtggaagt ggtggcggaggTAGCatggctcaagagtttgtgaac	Redox reporter
261-15aaroGFP2fw	tttGGTCTCAAAGGGAggtggaggaggttctggaggcggtggaagt ggtggcggaggTAGCgtgagcaagggcgaggag	Redox reporter
450roGFP2CDfw	tttGGTCTCACACCATGGTGAGCAAGGGCG	Redox reporter
451roGFP2CDrev	aaaGGTCTCACCTTaCTTGTACAGCTCGTCCATGC	Redox reporter
452GRX1roGFP2CDfw	tttGGTCTCACACCatggctcaagagtttgtgaac	Redox reporter
453roGFP2orpCDrev	aaaGGTCTCACCTTaCTATTCCACCTCTTTCAAAAGTTC	Redox reporter
CKP44 LIIa fw	GAGTGGTGATTTTGTGCC	Sequencing
CKP45 LIIa rev	GATAAACCTTTTCACGCC	Sequencing
CKP46 35S fw	CATCGTGGAAAAAGAACAC	Sequencing
CKP47 gfp rev	GTCAGCTTGCCGTAGGT	Sequencing
CKP48 pGS21a seq fw	TAATACGACTCACTATAGGG	Sequencing
CKP49 pGS21a seq rev	GCTAGTTATTGCTCAGCGG	Sequencing
266Yap1-fw	tttGGTCTCACACCATGAGTGTGTCTACCGCC	Sulfenome mining
267Yap1-rev-stop	tttGGTCTCACCTTTTAGTTCATATGCTTATTCAAAGC	Sulfenome mining
268Yap1-rev-nostop	tttGGTCTCACCTTGTTCATATGCTTATTCAAAGC	Sulfenome mining
336NmTAPfwBC	tttGGTCTCAtctgATGGAATTCATGGGCACCcc	Sulfenome mining
337NmTAPrevBC	tttGGTCTCAggtgGAACCGCCTCCACCCGG	Sulfenome mining
338YAPfwDE	tttGGTCTCAaaggGTGGAGGCGGTTCAAAC	Sulfenome mining
339YAPrevDE	tttGGTCTCAgattTTAATTCATATGTTTATTAAGTGCAAG	Sulfenome mining
316orp1rev	tttggtctcagattCTATTCCACCTCTTTCAAAAGTTC	use with CKP261
CKP64ADC1vigsfw	ATGCCGGCCTTAGGTTGTTG	VIGS CaADC1 (Kim et al. 2013)
CKP65ADC1vigsrev	AGAAGAGCATCAGCGCTGCCC	VIGS CaADC1 (Kim et al. 2013)
CKP81ADC1vigs139fw	aaaggtctctcaccGCCTTACCTTGTGGCACCTTC	VIGS CaADC1 construct 139bp (Kim et al. 2013)
CKP82ADC1vigs139re	aaaggtctctccttTCAAGCAGTGCAATAGGACCAAA	VIGS CaADC1 construct 139bp (Kim et al. 2013)
357TRV2	TGAGCTCGGTACCGGATC	VIGS fragment sequencing
372TRV2aSEQrev	GATTCTGTGAGTAAGGTTACCG	VIGS fragment sequencing
381NbADCvigs250fw	aaaggtctctcaccTGTTCGAGACTCTCAAGCAC	VIGS NbADC construct 250

Table 6.2 (continued)

382NbADCvigs250rev	aaaggtctctccttCAAGCAGTGCAATAGGACC	VIGS NbADC construct 250
387NbICSvigs126fw	aaaggtctctcaccAGGTTCCTCTCCAAGAAATG	VIGS NbICS fragment
388NbICSvigs126rev	aaaggtctctccttATTTACCTGAGGGACCATG	VIGS NbICS fragment
358NbICSvigsFW	GCATGGGATAATGCTGTCTCTTG	VIGS NbICS fragment (Catinot et al. 2008)
359NbICSvigsREV	CCCACAAACTGCTGGAGTAGG	VIGS NbICS fragment (Catinot et al. 2008)
443yeastU1	GATGTCCACGAGGTCTCT	Yeast library screen
444yeastU2	CGTACGCTGCAGGTCGAC	Yeast library screen
445yeastD1	CGGTGTCGGTCTCGTAG	Yeast library screen
446yeastD2	ATCGATGAATTCGAGCTCG	Yeast library screen
447yeastKanB	CTGCAGCGAGGAGCCGTAAT	Yeast library screen
448yeastKanC	TGATTTTGATGACGAGCGTAAT	Yeast library screen
449KanMXrev	GTCGGAAGAGGCATAAATT	Yeast library screen

6.2 Coding sequences used for VIGS

The CDS sequences of genes that were used for Virus induced gene silencing (VIGS) were downloaded from NCBI. Shaded sequences mark the segments that were cloned into pTRV2a in antisense direction. Underlined sequences are 3`UTR sequences.

>*NbSGT1* (accession LC314285)

ATGGCGTCCGATCTGGAGATTAGGGCTAAAGAAGCTTTCATCGACGACCACTTTGAGCTCGCCGTTGACCTTTACACGCAAGCAATCG
CCATGACTCCTAAGAACGCTGAGCTTTTCGCCGACCGTGCTCAGGCCAACATCAAACTCAACTACTTCACTGAAGCTGTTGTTGATGC
GAACAAGGCCATTGAGTTAGATCCTTCAATGTCAAAAGCATATTTGCGTAAGGGGTTGGCCTGTATGAAGCTTGAAGAGTACCAAACT
GCAAAAGCAGCTTTGGAAACTGGTGCTAGTTTAGCACCGGCAGAGTCAAGGTTCACAAAGTTAATCAAAGAATGTGATGAACGCATTG
CAGAGGAAGCTGGAGAACTACCTAATCAGTCGGTGGATAAAACCTCGGGAAATGTCGTAGCTCCCCCTGCATCTGAGTCTTTGGGCAA
TGTTGCTGTTGCGCCTAAAGATGCTCAACCAACTGTCAACCTGTCCTATCAAGGATCTGCTGCCAGACCAAAATACAGGCATGAATTT
TACCAGAAGCCAGAGGAGGTGGTGGTGACTATATTTGCCAAGGGAATACCAGCCAAGAATGTTATTGTTGACTTTGGTGAACAAATAC
TTAGTGTTAGCATTGATGTGCCGGGTGACGAAACTTATTCTTTCCAGCCTAGGTTGTTTGGGAAGATAACACCTGCAAAATGCAGATA
TGAAGTGATGTCCACCAAAATTGAGATCCGCCTTGCAAAAGCTGAACCCTTACACTGGACATCTCTCGAATATACGAGAGAGTCTGCT
GTAGTGCAGAGGCCTAATGTGTCATCAGATGCCCCCCGGCCCAGTTATCCTTCCTCGAAATTGAGACATACGGATTGGGATAAATTAG
AGGCTGAAGTGAAAAAGGAGGAAAAAGACGAAAAATTGGATGGAGATGCAGCATTGAACAAATTTTTCCGAGACATTTACAAAGATGC
CGATGAGGACACCAGAAGAGCCATGATGAAATCCTTTGTGGAATCTAATGGGACTGTTCTGTCTACAAACTGGAAAGAAGTCGGTGCA
AAGAAGGTAGAAGGAAGCCCTCCAGATGGCATGGAGCTGAAGAAATGGGAAATCTAG

>*NbEDS1* (accession AF479625)

ATGGTGAGAATTGAAGAGGGGAGAGAAGTGAAAGATGAGCTGATCAAGAAAGCTTGTAACTTAGCAATGGAAGCTCACAGTTTGTCTT
CTGGGAAGCCTTATATTTTCAAGAAAAAAAGTGGATCGATGGATGTTTTTTTGGCTTTTGCTGGAAATTGGTCTGTTGATGGTTGGTA
CAGTTGTAGCACTTCTTTTGGAGAGAAAAAATCTTCGTTTCCATCATTGAAAAGTGTTGGCACAGATGAGGTAGCCATGGTTAATGAA
GCATTTGCTAGCAGATTTGAACACATATTGAACAACTCTTCTCTTAAAAATGAGGTGGAGAAGGCGATGTCAGAAGGAAAACAGATAG
TGTTTGCAGGGCACTCGTCGGGTGGCCCTATTGCGATTTTGGCAGCCCTATGGTGTCTAGAACATTGTTGCACAAGACCAAATGACAA
CCTGGTTTGTCCATACTGTATAACTTTTGGATGCCCTCTTGTTGGTGACAGAATATGGTCTCATGCCCTCATGCGCGAAAACTGGGCT
CGTTACTTCATACATTTTGTCACGAAATATGATATCGTTCCTCGGATGATGCTTGCTCCCCTTTCATCGATTCAAGAATGGCTTCAAG
CAATCTTTGACTTCATCAATCCAAAATCCCGGAATTATCAGCACGAGGTAGTTGTAAGATCATATGATGCATCGAAGAATTTCTTTAT
GACTGTAATGAGGAGTGCATCCTCTGTTGCAAGTTATGCTGCATGTAATCTGAAAGGATGCACAAACTTGTTGTTAGAAACAGTTTCT
AACATTGTTCAACTCAGCCCTTATAGACCTTTTGGAACTTACATCTTCTGCACTGGAAATGGGAAACTGGTGGTCGTTGAGAATCCAG
ATGCTGTTCTGCAGTTACTGTTCTATTGTGCTCAAATGAGTTCCGAAACAGAAGTTGAAGAAGTTGTTACCAGAAGCTTAAACGAACA
TTTGTTATATAGAAAAGAAATGCAGGAAAGCTTAGAGATGCAGGATGTGGTTCATCTCAATAATCTTACCGATATTCCCTTGTCTTCA
AATGCCATTGCATTAGCTAGTGATGAAGTGGTAACGATGAATTTAGCCCTGAATGACTTAGGCCTGAGTACAAGAGCACGGTTGTGTC
TTCGTGCAGCAGGACAATGGGAGAAGCAGAAAAGGAAGAACGAGGAAAAGATTGATGGTAATAAGAACAGCATCATGGAAGGATTAAG
CAAGATACAGGAGTACCAGACCAAGTGTGATATTCAGAAAGTCGGGTATTATGATGCGTTCAAGCTTCAAGAGACCATCGATGACTTC
AATGCTAATGTGAAAAGGCTGGAGCTAGCAGGAATATGGGACGAAATCATTGAAATGTTGAAAAGGTATGAGCTCCCAGATAGTTTTG
AGGGAAGAAAGGAATGGATAAAACTAGGGACGCAGTTCCGCAGGCAAGTTGAGCCCTTGGATATTGCAAACTATTACAGGCATTTGAA
GAATGAAGATACAGGACCTTACATGATCAGGGCTAGGCCGAAGCGTTATAGGTTCACACAACGATGGTTAGAGCATGAAGAGAGGGTG
CAAACAGGTGAACGCTCTGAGTCTTGTTTTTGGGCAGAAGTGGAGGAACTAAGAAACAAGCCAATTATGGAAGTGCAAAACAGGATTT
TGAGTTTAGAAACAAAGGCATGGGATTGGTCCCAGAGTGGCCTTCTGGGCGATGATGTTTTCTTCCCTGAGTCTACCTTTACCAAATG
GTGGAAACAACTCCCTACTCAGCACAGAATGACATCTTGGATATCAGGGAAAGTAAATTCTTAG

>NbNdr1 (accession AY438029)

ATGTCAGACTATGGATCCAATAATACATGCTGCTTTAAGTGCATCCAATTCATATTAACAGCAGGCTTAACAGCTCTTTTCATTTGGC
TAAGTCTAAGAACCACAAAACCATCTTGCTCTTTAGATAATTTTTACTTACCTGCCCTTAACAACTCTGATAACTCCAACTCCACAAG
ATCCAATCATACACTTTCCTTTCAGCTCAATTTGAACAACAAGATGAAGGACAAAGGTGTTCGTTACGATGACATTAAACTTAGTTTT
TATTATGGTACAAATACAAGTTTTCCTATAGGTAATTATACAGTACCTGGCTTTTACCAAGGTCATGACAAGAAAGCACATAAAAAAG
GTATACTGGAAACTCAGAAAATGCCTTGGAATGATGCTTTAAAGATGGTTTCAAATGGGTCTAAAGTGGTTTTCAGGGTGGATGTAGC
TACTAGAGTCAGGTACAAGGTCATTCTTTGGTATACTAAGAGGCATAATTTTACTGTGGAAAATAGTAAAGTGAAAGTGGATGGTTCA
GGTAAATCAAGCGCACAGAAGCTTCATTGCTGTTTTATGACTTTTGGACTTCCCCGAATTGTTTTATTCACCTTGCTTCTTTTGTTGT
AAAAGATTCCTCGGGTATTCAAGATTTAAGCTTGATTAGTTCAGTTTTACAATTGCAGGTTCAGGTTTTAGTATTTGGTAACATTCTA
GTAATTCTTTTAATTATGTATCATTTAAAAAATGTTGGACTCAGTTGATTGCATGCTGTCGGTGCAAACTGACTGTAGTTGG

>NbRar1 (accession LC314307)

ATGGAGAGACTTCGTTGCCAGAGGATCGGTTGCAACGCCACCTTCACAGAGGATGATAACCCTGAAAATTCCTGCACTTATCACGAAT
CCGGTCCTCTATTTCATGATGGAATGAAGAAGTGGAGTTGTTGCAAGAAAAGCAGTCATGATTTCAGCTTATTTCTCGAAATTCCTGG
TTGTAAGACAGGAAAACACACAGCAGAAAAACCAGTGATAGCAAAGCCAGCTGCTAACCAGAATAGAGCAATTCCCGCACCGACTTCT
ATGGCCAATGTATCACCGAAGGATGCTTGTCCTAGATGCTGCCAGGGATTCTTTTGTTCTGATCATGGTTCACAACCTAGAGAAGCAA
TTCGAAAAGCATCAAAGAGTAATACAGTAACATCTGTACCTTCTGAGAGCAATACAGATGTACAGCAATGCGATCCTGCTCCGGTGAA
GAAGAAAGTTGATATAAACGAGCCCCAAATTTGTAAAAACAAGGGCTGTGGTAAGACCTTTACAGAAAAGGAAAATCATGACACTGCT
TGCAGTTACCATCCTGGCCCCGCTATCTTCCATGACCGGATGAGAGGATGGAAATGCTGTGATATTCATGTCAAAGAATTTGATGAGT
TCATGAGCATATCGCCATGCACCACAGGATGGCACAACGCCAGCCCAGCGTCCTAA

>smGFP (accession XXU70495)

ATGAGTAAAGGAGAAGAACTTTTCACTGGAGTTGTCCCAATTCTTGTTGAATTAGATGGTGATGTTAATGGGCACAAATTTTCTGTCA
GTGGAGAGGGTGAAGGTGATGCAACATACGGAAAACTTACCCTTAAATTTATTTGCACTACTGGAAAACTACCTGTTCCATGGCCAAC
ACTTGTCACTACTTTCTCTTATGGTGTTCAATGCTTTTCAAGATACCCAGATCATATGAAGCGGCACGACTTCTTCAAGAGCGCCATG
CCTGAGGGATACGTGCAGGAGAGGACCATCTCTTTCAAGGACGACGGGAACTACAAGACACGTGCTGAAGTCAAGTTTGAGGGAGACA
CCCTCGTCAACAGGATCGAGCTTAAGGGAATCGATTTCAAGGAGGACGGAAACATCCTCGGCCACAAGTTGGAATACAACTACAACTC
CCACAACGTATACATCACGGCAGACAAACAAAAGAATGGAATCAAAGCTAACTTCAAAATTAGACACAACATTGAAGATGGAAGCGTT
CAACTAGCAGACCATTATCAACAAAATACTCCAATTGGCGATGGCCCTGTCCTTTTACCAGACAACCATTACCTGTCCACACAATCTG
CCCTTTCGAAAGATCCCAACGAAAAGAGAGACCACATGGTCCTTCTTGAGTTTGTAACAGCTGCTGGGATTACACATGGCATGGATGA
ACTATACAAATAA

>CaPDS (accession NM_001324813)

ATGCCCCAAATTGGACTTGTTTCTGCTGTCAACTTGAGAGTCCAAGGTAATTCAGCTTATCTTTGGAGCTCGAGGTCTTCTTTGGGAA
CTGATAGTCAAGATGGTTGCTCGCAAAGGAATTCGTTATGTTTTGGTGGTAGTGACTCAATGAGTCATAGGTTAAAGATTCGTAATCC
CCATTCCATAACGAGAAGATTGGCTAAGGATTTCCGGCCTTTAAAGGTTGTTTGCATTGATTATCCAAGGCCAGAGCTAGACAATACA
GTTAACTATTTGGAGGCTGCATTCTTATCATCATCATTCCGATCTTCTCCGCGCCCAACCAAACCACTGGAGATTGTTATTGCTGGTG
CAGGTTTGGGTGGTTTGTCTACAGCAAAATATTTGGCAGATGCTGGTCACAAACCAATACTGCTGGAGGCAAGGGATGTTCTAGGTGG
AAAGGTAGCTGCATGGAAAGATGATGATGGAGATTGGTATGAGACTGGTTTGCACATATTCTTTGGGGCTTACCCAAATATGCAGAAC
CTATTTGGAGAATTAGGGATAAATGATCGATTGCAATGGAAGGAACATTCGATGATATTTGCAATGCCAAACAAGCCAGGAGAATTCA
GCCGCTTTGATTTCCCCGAAGCTTTACCTGCTCCTTTAAATGGAATTTTGGCAATCCTAAAGAACAATGAAATGCTTACATGGCCAGA
AAAAGTCAAATTTGCAATTGGACTCTTGCCAGCAATGCTTGGTGGGCAATCTTATGTTGAAGCTCAAGACGGGATAAGTGTTAAGGAC
TGGATGAGAAAACAAGGTGTGCCGGATAGGGTGACGGATGAGGTGTTCATCGCCATGTCAAAGGCACTTAACTTCATAAATCCTGATG
AGCTTTCGATGCAGTGCATCTTGATCGCGTTGAACAGATTTCTTCAGGAGAAACATGGTTCAAAAATGGCCTTTTTAGATGGTAATCC
TCCTGAGAGACTTTGCATGCCGATTGTTGAACATATCGAGTCAAAAGGTGGACAAGTCAGACTGAACTCACGAATAAAAAAGATTGAG
CTGAATGAGGATGGAAGTGTCAAGTGTTTTATACTGAACGATGGTAGTACAATTGAGGGAGATGCTTTTGTGTTTGCGACTCCAGTGG
ATATTTTCAAGCTTCTTTTGCCTGAAGACTGGAAAGAGATTCCATATTTCCAAAAGTTGGAGAAGTTAGTTGGAGTACCTGTGATAAA
TGTCCATATATGGTTTGACAGAAAACTGAAGAACACATCTGATAATTTGCTCTTCAGCAGAAGCCCACTGCTCAGTGTGTATGCTGAC
ATGTCCGTCACATGTAAGGAATATTACGACCCCAACAAGTCCATGTTGGAATTGGTCTTTGCGCCTGCAGAAGAGTGGGTATCTCGCA
GTGACTCTGAAATTATTGATGCTACAATGAAGGAACTAGCAAAGCTATTTCCTGATGAAATTTCGGCGGATCAGAGCAAAGCAAAAAT
ATTGAAGTATCATGTTGTCAAAACTCCAAGGTCTGTATATAAAACTGTGCCAGGTTGTGAACCCTGTCGGCTCTTGCAAAGATCCCCT
GTAGAGGGGTTTTATTTAGCTGGTGACTACACGAAACAGAAATACTTGGCTTCAATGGAAGGTGCTGTCTTATCAGGAAAGCTTTGTG
CACAAGCTATTGTACAGGATTACGAGTTACTTGTTGGCCGGAGCCAGAGGAAGTTGGCAGAAACAAGTGTAGTTTAG

> NbADC1-1 (Niben101Scf00466g03022.1 *N. benthamiana* Genome v1.0.1)

ATGCCGGCCCTAGGTTGTTGTGTGGACGCGGCTGTTGTTTCCCCTCCTCTCGGCTATGCCTTCTCTCGGGATAGCTCTCTTCCCGTGC
CGGAGTTCTTCACCTCCGGCGTACCTCCGACAAATTCCGCCGCCTCTTCCCATTGGTCTCCGGATTTATCATCTGCTTTGTACGGGGT
CGATGGGTGGGGAGCTCCTTATTTCTCTGTTAACTCTAATGGAGATATCTCCGTCCGACCACATGGTACGGGCACTCTCCCTCACCAG
GAAATTGACCTTCTCAAGGTCGTGAAAAAAGCCTCCGATCCGAAACATTCAGGTGGTCTTGGTCTTCAGCTGCCTCTTGTTGTTCGCT
TCCCTGATGTGCTGAAAAACCGGTTGGAATCTCTGCAATCGGCTTTTGATCTCGCGGTTCATTCCCAGGGCTATGGGGCCCACTACCA
AGGTGTTTATCCCGTGAAATGCAATCAGGACAGGTTCGTGGTGGAAGATATTGTCAAATTCGGGTCGTCATTCCGGTTCGGGTTGGAA
GCGGGGTCTAAACCTGAGCTCCTGTTAGCCATGAGCTGTCTCTGCAAGGGAAGTGCTGAGGGCCTTCTCGTTTGCAATGGTTTCAAGG
ACGCTGAGTACATTTCGCTTGCTTTGGTTGGAAGAAAGCTCATGTTAAACACTGTAATTGTGCTTGAACAAGAGGAGGAGCTTGACCT
TGTGATTGATATAAGCCGTAAGATGGCTGTTCGGCCTGTAATTGGACTTCGGGCTAAGCTCAGGACCAAGCATTCAGGCCATTTTGGA
TCCACTTCTGGAGAAAAAGGTAAGTTTGGGCTTACAACTACCCAAATTGTTCGTGTAGTGAAGAAGCTGGAAGAATCCGGAATGCTGG
ATTGCCTTCAGTTGCTGCATTTTCACATTGGATCTCAGATCCCTTCAACGGCGTTGCTTGCTGACGGTGTTGGTGAGGCTGCTCAGAT
TTATTGTGAATTAGTTCGTCTTGGTGCGGGTATGAAGTTCATTGATACTGGAGGTGGGCTCGGAATCGACTATGATGGTACTAAATCA
TGTGATTCTGATGTCTCTGTTGGCTATGGCATTCAAGAATATGCCTCCACAGTTGTCCAGGCTGTTCAATATGTATGCGATCGTAAGG
GCGTGAAGCACCCAGTGATTTGCAGCGAAAGTGGCAGAGCAATTGTTTCTCATCACTCAATTCTGATTTTCGAAGCGGTGTCTGCTTC
TAGTACTCATCTTTCTTCTTCACACCTGTCTTCTGGTGTCCTCCAATCCATGGCGGAGACGCTCAATGAAGATGCCCTTGCTGATTAC
CGCAATTTATCTGCTGCTGCAGTTCGTGGAGAGTACGAGACATGTGTACTTTACTCCGATCAGCTGAAACAGAGATGTGTGGATCAGT
TTAAAGAAGGGTCCTTGGGTATTGAACATCTTGCTGCTGTTGATAGCATCTGTGACTTTGTATCAAAGGCTATGGGGGCTGCTGATCC
TGTCCGCACTTACCATGTGAATCTGTCAATTTTCACTTCAATTCCTGATTTTTGGGCCTTTGGTCAATTGTTTCCAATTGTTCCAATA
CACCGTTTAGATGAAAAACCTGCAGTAAGGGGAATATTATCGGACTTGACTTGTGACAGTGATGGGAAGGTTGATAAGTTCATTGGTG
GCGAATCAAGCTTGCCGCTGCATGAATTGGGAAGTAATGGCGATGGTGGTGGTTATTATCTGGGGATGTTTTTGGGTGGGGCTTATGA
GGAGGCGCTCGGAGGACTCCACAACTTGTTTGGTGGACCAAGCGCTGTGCGCGTGGTGCAGAGCGATAGCGCTCACAGCTTCGCCACG
ACATGCTCTGTCCCTGGCCCGTCCTGTGCGGACGTGCTCCGAGCAATGCAGCACGAGCCCGAGCTCATGTTCGAGACTCTCAAGCACC
GTGCAGAGGAATTCTTGGAACAAGAAGATGACAAAGGGCTGGCTGTTGAATCTTTGGCCAGCAGCTTAGCTCAGTCCTTCCATAACAT
GCCTTACCTTGTGGCGCCTTCATCTTGCTGCTTCACTGCAGCTACTGATAACAATGGTGGCTATAATTACTATTATAGTGATGAGAAT
GCAGCAGATTCTGCTACAGGGGAGAATGAGATTTGGTCCTATTGCACTGCTTGA

> SlHsp70 (accession XM_004230397.4)

ATGGCGTCTTCAACTGCTCAAATTCATGCTCTTGGAGCTACATATTTCGCTAATTCATCTTCTTCCACTAGAAAACCTTTAAAGTCTG
TGTTTTTGGGCCAGAAACTGAACAATAGAACCCTAGCTTTTGGATTGAAGCAGAAGAAGAGCCGGGGGAATAACGGTGGTTATGCACC
GATGCGTGTGGTGGCGGAGAAGGTGGTGGGAATTGACTTGGGGACTACTAATTCTGCTGTGGCTGCTATGGAAGGAGGGAAGCCTACC
ATAGTGACGAATGCTGAAGGACAGAGGACAACTCCTTCAGTGGTCGCTTATACTAAGAGTGGGGATAGGCTTGTTGGTCAAATTGCTA
AGCGTCAGGCTGTGGTGAACCCGGAGAATACCTTCTTTTCAGTGAAGAGATTCATTGGAAGGAAGATGAATGAGGTGGATGAGGAGTC
GAAGCAGGTGTCCTACAATGTCATCAGAGATGAGAATGGAAATGTCAAGCTTGATTGCCCTGCCATTGGCAAATCATTCGCTGCTGAA
GAAATTTCAGCTCAGGTCCTGAGGAAGTTGGTGGATGATGCATCCAAATTTTTGAATGACAAGGTTTCCAAGGCTGTTGTCACGGTTC
CTGCATACTTCAATGATTCTCAGAGGACAGCAACTAAGGATGCAGGTCGCATTGCTGGATTAGAAGTTCTTCGGATAATTAATGAACC
CACTGCTGCCTCCTTGGCTTATGGTTTTGAAAAGAAAAGTAACGAAACAATTTTGGTTTTTGATCTTGGAGGTGGTACTTTTGATGTA
TCAGTTCTTGAGGTTGGTGACGGTGTCTTTGAGGTGTTGTCAACTTCTGGTGACACCCATCTTGGTGGTGATGATTTTGACAAGAGGA
TTGTTGATTGGCTTGCTGCAAGTTTCAAAAGAGATGAAGGTATTGATCTTCTAAAGGACAAACAAGCTCTTCAACGTCTGACTGAGAC
TGCTGAGAAAGCTAAGATGGAACTGTCATCGCTGACCCAGACTAACATCAGTTTACCATTCATTACGGCTACTGCTGATGGTCCTAAA
CACATTGAGACCACTATCACACGTGGGAAATTTGAAGAACTATGCTCAGATCTGCTTGACAGGCTTAAAACTCCTGTTCAGAATTCCT
TGAGAGATGCCAAGCTCTCCTTCAGCGATATTGATGAGGTCATCCTTGTTGGTGGTTCTACACGTATCCCAGCTGTTCAGGAACTTGT
TAAGAAATTGACTGGAAAGGACCCCAATGTTACAGTTAATCCCGATGAAGTCGTTGCTCTTGGTGCTGCAGTGCAGGCTGGAGTTTTG
GCCGGAGATGTCAGCGATATTGTCCTTTTAGATGTCACACCATTGTCCATTGGTTTGGAAACACTTGGTGGTGTGATGACAAAGATCA
TTCCAAGAAATACAACATTGCCTACCTCCAAATCAGAAGTGTTCTCTACCGCTGCTGATGGTCAGACAAGTGTAGAAATTAATGTCCT
CCAAGGAGAGCGAGAATTTGTTAGGGACAACAAATCTTTAGGTAGCTTCCGGCTTGATGGAATTCCTCCTGCCCCAAGAGGGGTTCCA
CAAATTGAAGTGAAATTTGACATTGATGCCAATGGTATTCTTTCCGTGACTGCTATTGACAAGGGTACTGGGAAGAAGCAAGACATCA
CCATTACAGGTGCCAGCACATTGCCTGGTGATGAGGTCGAGAGAATGGTTAAAGAAGCTGAAAGATTTGCCCAGGAAGACAAAGAGAA
GAGAGACGCCATAGACACAAAGAACCAGGCCGATTCTGTTGTCTACCAGACAGAGAAGCAGTTGAAGGAACTTGGAGACAAAGTACCA
GGGCCAGTGAAAGAAAAGGTTGAGGCTAAACTTGGAGAGCTTAAAGAAGCAATCTCAGGAGGGTCAACTCAGACCATGAAGGATGCTA
TGGCTGCCCTTAACCAAGAAGTAATGCAGCTTGGTCAGTCACTCTACAACCAGCCTGGTGCTGCACCAGGTGCTGGTCCAGCACCTGG
CGGTGCTGATGGACCTTCAGAATCATCATCTGGGAAGGGACCTGATGGAAATGACGTAATTGATGCTGATTTCACCGACAGCAAGTGA

>NbICS (accession EU257505, partial CDS)

CTTCATGCTCAGAACCATGTCCTCCTCCCGCGCTGTTTCTTCTCCGGTCGAAGGGCAGCTGCTGATTCTGAAATGTGCTTCAACGGAA
CTTCTCACCCCTCTTCTAAAGTGGTCAGTGTAGCTGGTGTCGGCTCTGCTGTCTTCTTTACTCATTTACGCCCTTTTTCCTTTGACGA
TTGGCGTGCTATACGCAGGTTCCTCTCCAAGAAATGTCCTCTAATTCGTGCTTATGGGGCAATTCGATTTGATGCAACAGCCAACATA
GGTCCTGAATGGAATGCTTTTGGTTCATTTTATTTCATGGTCCCTCAGGTTGAGTTCGATGAGCTTGAAGGAAGTTCAGTTATTGCTG
CAACTATTGCATGGGATAATGCTGTCTCTTGCACGTACCAGATGGCAATAGAAGCACTTCAGGCCACAATATGGCAGGTTTCCTCCGT
TCTTATGAGGGTGCAGAAAAAAATATCTCGTTCACATCTACTCGCAAGTACTCATGTCCCTGGTAAAGCATCTTGGGACCAAGCTGTT
AAGCGTGCTTTGCAAAAAATAAGAAGAAATAACCCGATGCTTATCAAGGTGGTACTTGCTCGTAGCTCCAGAGTTGTGACAGCTGCCG
ACATTGATCCTTTAACATGGTTATCTTGCTTAAAGGTTGAAGGAGAAAATGCATATCAGTTCTGTTTGCAACCTCCCCAGTCAGCGGC
ATTCATTGGGAACACTCCAGAGCAGCTATTTCATCGGGACTGCCTCAGCATTTGTAGCGAGGCTTTAGCTGGAACACGGGCTAGGGGT
GGATCAGAGCTTCTGGATCTTAGGATAGGACAGGATTTACTATCCAGTGGTAAGGACCATAATGAGTTTGCTATAGTACGGGAGTGCA
TAAGAAGAAAATTGGAGGCTGTGTGTTCCAGCGTTTTAATTGAACCAAAGAAAGCAATAAGAAAATTTCCAAGAGTTCAACATCTCTA
TGCTCGATTGAGGGGGAGACTCCAGACTGAAGATGATGAGTTTAAGATCTTGTCGTCCATTCACCCTACTCCAGCAGTTTGTGGGTAT
CCTACAGAAGATGCACGGGCTTTTATTTCAGAAACCGAAATGTTTGACCGAGGAATGTATGCTGGTCCTGTTGGTTGGTTTGGAGGGG
AAGAGAGTGAGTTTGCTGTTGGAATAAGGTCAGCTTTGGTTGAAAAGGGTCTTGGTGCTTTAATTTATGCGGGAACTGGGATAGTGGA
AGGAAGTGATTCATCTCTAGAATGGGAAGAGCTCGAGCTGAAGACTTCACAGTTCACCAAATTGATGAAACTTGAGGCTCCTCTTTTG
ACAAGAGGAGAAATTAGGACTATCAATCAGAATCAGAAAGCGAGATGA

>CaADC1 (accession KC160547)

ATGCCGGCCTTAGGTTGTTGTGTAGACGCTACTGTTTCACCTCCTCTCGGCTATGCCTTCTCTTCGGATAGCTCTCTTCCCACGCCGG
AATTCTTTTCCTCCGGCGTACCTCCGATGACAAACGCCGCCGCCGGTCATTCCCATTGGTCACCGGATCTGTCCTCTGCTCTTTACCG
GGTTGATGGGTGGGGTGCTCCTTATTTCTCTGTTAACTCCTCCGGTGATATCTCCGTCCGGCCACATGGTACGGATACTCTTCCTCAC
CAGGAGATTGACCTTCTTAAGGTTGCGAAGAAGGCGGCTGACCCGAAACATTTGGGTGGGCTTGGACTTCAGATGCCTCTTGTTGTTC
GTTTCCCTGATATTCTGAAGAACCGTTTGGAGACTTTGCAATCGGCTTTTGATATGGCGGTTCGTTCCAGGGGATATGAGGCTCATTA
CCAAGGTGTTTATCCTGTGAAATGTAATCAAGACAGGTTCGTGGTGGAAGATATCGTGAAATTCGGATCGCCATATCGATTCGGGTTG
GAAGCCGGGTCGAAACCGGAGCTCCTTTTGGCCATGAACTGTCTGTCCAAGGGCAGCGCTGATGCTCTTCTTGTTTGCAATGGTTTCA
AGGATACTGAGTATATTTCGCTTGCTTTGATCGCAAGAAAGCTCCTTTTGAACACTGTAATTGTGCTTGAACAAGAGGAGGAGCTTGA
CCTGGTGATTGATATCAGCCGTAAGATGGCTGTCCGGCCCGTAATTGGACTTCGTGCTAAGCTGAGGACCAAGCATTCGGGCCATTTT
GGATCCACTTCTGGAGAAAAGGGCAAATTTGGGTTGACAACAACTCAGATTCTTCGTGTAGTGAAGAAGTTGGAGGGGTCTGGGATGC
TTGATTGTCTTCAGTTATTGCATTTTCACATTGGATCTCAGATCCCAACAACGGAGTTGCTTGCTGATGGTGTTGGTGAGGCCACTCA
GATTTACTCTGAGTTAGTCCGTCTTGGAGCTGGTATGAAATTCATTGATATTGGAGGTGGCCTTGGAATTGACTATGACGGTTCGAAA
TCATCCGATTCGGATGTCTCTGTTGCCCATGGCATTGAGGAATATGCCTCTGCTGTTGTCCAGGCTGTCCAATTTGTCTGTGACCGTA
AGGGCGTTAAGCATCCAGTGATTTGCAGCGAAAGTGGCAGGGCAATTGTTTCTCACCATTCAATTATGATTTTTGAAGCTGTGTCTGC
TTCTACTACTAATGTTTCTCCACAGCTGTCTTCCGGTGGTCTTCAATCACTGGCGGAAACTCTCAATGAAGATGCCCGTGCTGATTAC
CGAAACCTATCTGCTGCTGCTGTCCGTGGCGAATATGATACATGTCTCCTTTACTCTGATCAGTTGAAACAGAGATGTGTGGAACAGT
TCAATGATGGTTCCTTGGATATTGAGCAGCTTGCTGCAGTGGATAGCATCTGTGACTTGGTGTCGAAAGCTATCGGGGTTTCTGATCC
TGTTCGCGCTTACCATGTGAATCTGTCAGTTTTCACCTCAATTCCTGATTTTTGGGCATTTGGCCAATTGTTTCCGATCGTTCCAATT
CATCGTTTGGATGAAAAGCCTACAATGAGAGGAATACTGTCGGACCTGACCTGTGACAGTGATGGGAAGGTAGACAAGTTCATTGGGG
GCGAATCAAGCTTGCCACTCCATGATTTGGGAAGCAATGGTGGTGATGGTGGGCGGTATTATCTGGGGATGTTTTTGGGTGGGGCTTA
TGAGGAGGCGCTCGGAGGGCTCCACAACCTGTTTGGTGGACCAAGCGTCGTGCGTGTGTTGCAGAGCGATAGCCCTCACAGCTTCGCT
GTGACTCGCTCTGTCCCTGGCCCGTCCTGTGCTGACGTGCTCCGGGCGATGCAGTTCGAGCCTGAACTCATGTTCGAGACTCTCAAGC
ACCGTGCAGAGGAATCCTTTGATCAAGAAGAAGAAATAGAAGATAAAGGCCTGGCCTTTGAATCTTTAATCAGCGGCTTAGCTCAGTC
CTTCCACAACATGCCTTACCTTGTGGCACCTTCGTCTTGCTGCTTCACCGCAGCAACCGCGAAAGGTGGGGGCTATTACTACTACAAT
GAAGACAATGCTGCTGATTGTGCAACAGCGGAGGATGAGATTTGGTCCTATTGCACTGCTTGA

6.3 CLSM pictures of Bs3-AtYUC8 chimeras

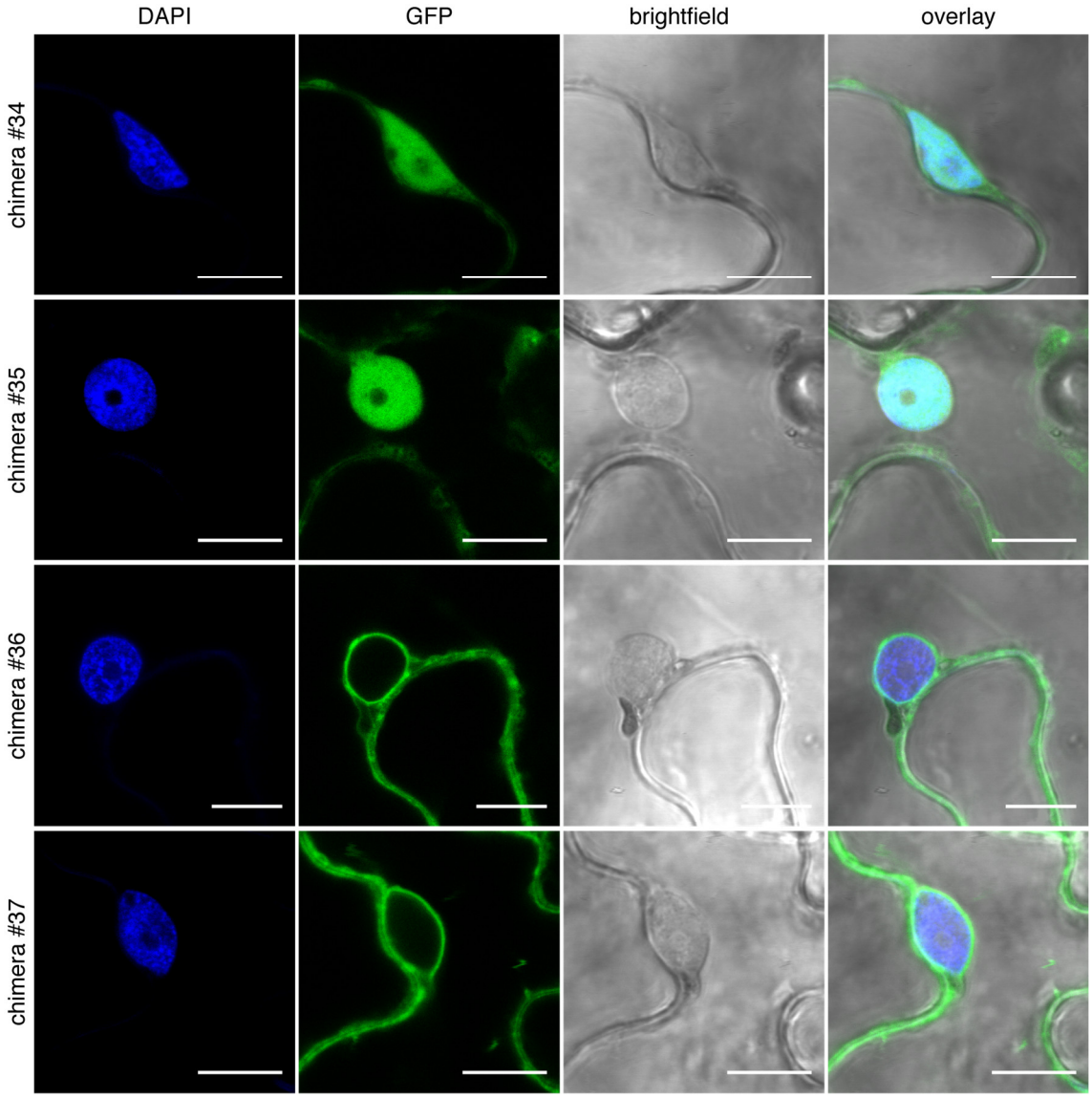

Figure 6.1 Chimeras #34 and #35 are located to the nucleus while chimeras #36 and #37 are excluded from the nucleus. *Bs3-AtYUC8* chimera (see Figure 2.1 and 6.3) were expressed in *N. benthamiana* leaves under control of the *35S* promoter via *Agrobacterium*-mediated transient transformation. 30 hpi, 0.1% DAPI solution was infiltrated into leaves to stain nuclei. After 30 min of incubation pictures were taken with a Leica CLSM. Pictures show DAPI and GFP fluorescence, brightfield and overlay. Scale bar = 10 μM.

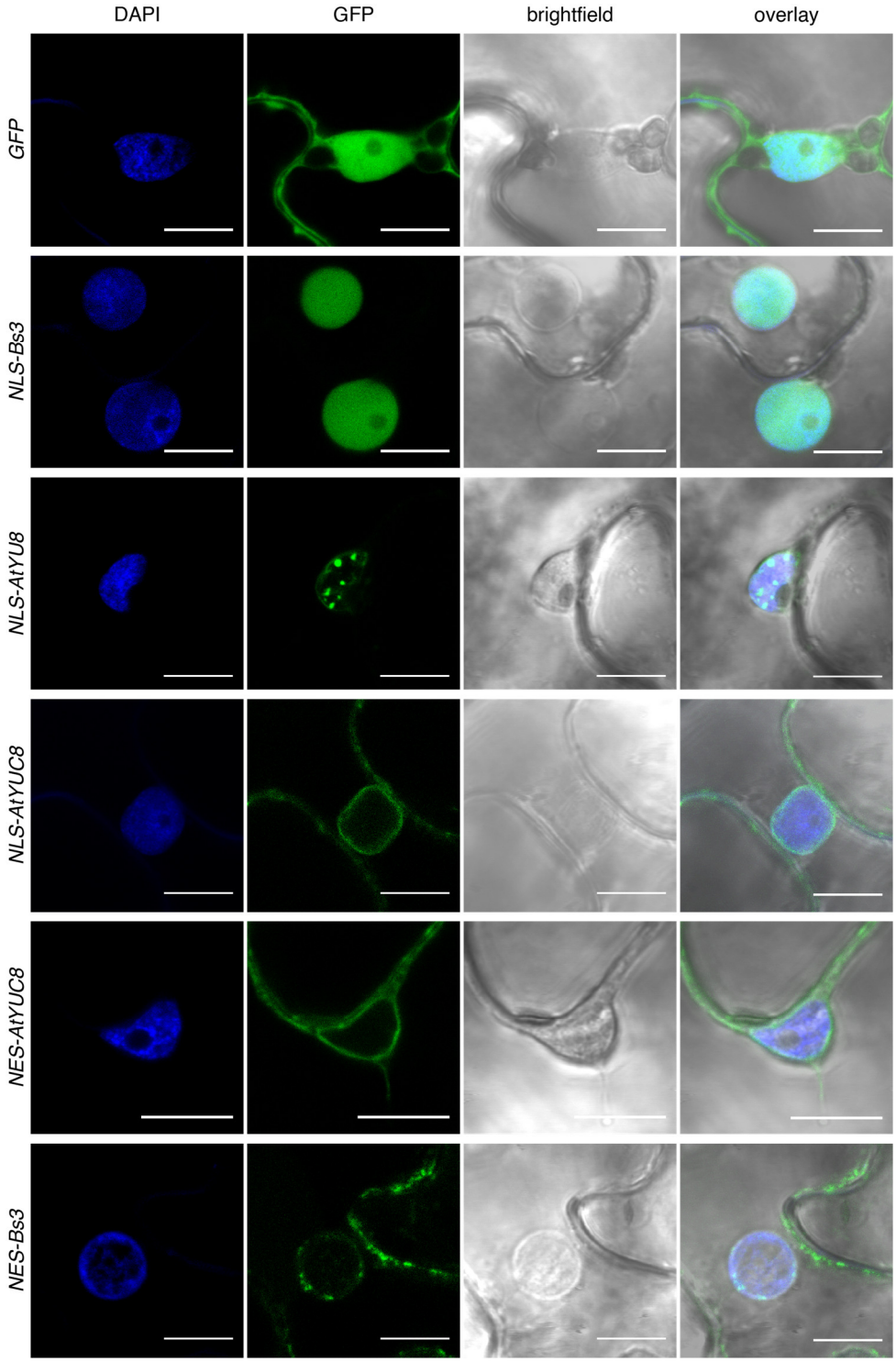

Figure 6.2 Subcellular localization of NES- and NLS-tagged Bs3 and AtYUC8 in *N. benthamiana*. Indicated constructs were expressed in *N. benthamiana* leaves under control of the *35S* promoter via *Agrobacterium*-mediated transient transformation. 30 hpi, 0.1% DAPI solution was infiltrated into leaves to stain nuclei. Pictures were taken after 30 min of incubation with a Leica Sp8 CLSM. Pictures show DAPI and GFP fluorescence, brightfield and overlay. NLS = nuclear localisation signal, NES = nuclear export signal. Scale bar = 10 μM.

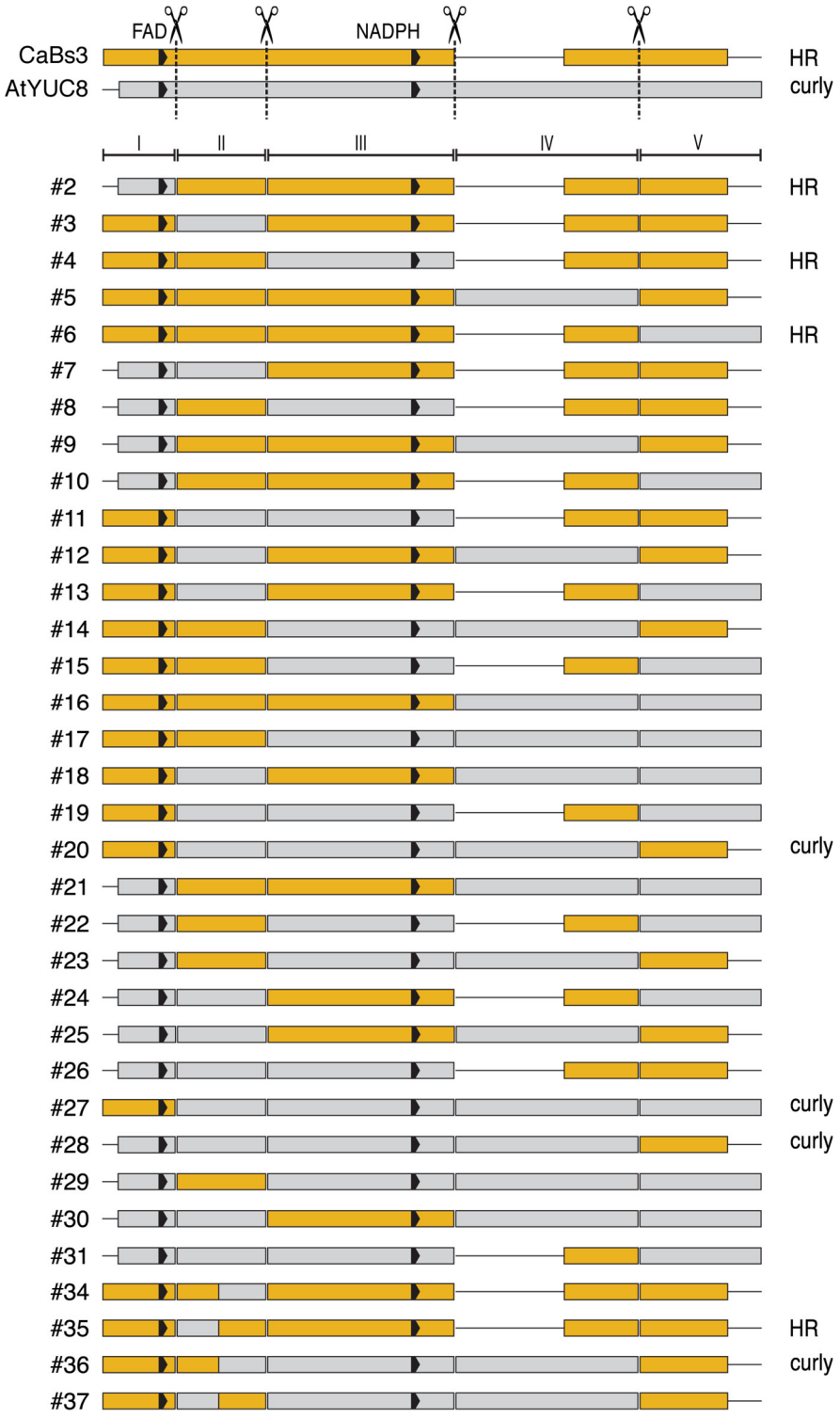

Figure 6.3: Complete overview of Bs3-AtYUC8 chimeras. Schematic alignment of Bs3, AtYUC8 and all Bs3-AtYUC8 chimeras. Bs3 derived parts are depicted in yellow, AtYUC8 derived parts are depicted in grey. FAD and NADPH binding site are depicted as black arrows. Gaps are indicated by black lines. Scissor symbols indicate cutting points.

6.4 Result tables of pull down experiments

Table 6.3 Pull down and MS. Candidate proteins that were higher abundant in Bs3 containing samples than in GFP and YUC8 containing samples.

Protein	PEP Bs3	PEP $Bs3_{S211A}$	PEP YUC8	PEP GFP	iBAQ Bs3	iBAQ $Bs3_{S211A}$	iBAQ YUC8	iBAQ GFP	Batch	ID
GFP	21	22	8	22	3.35E+08	6.10E+08	4.78E+07	2.20E+08	2	-
Bs3	12	14	2	1	1.04E+08	1.61E+08	1.05E+06	3.90E+05	2	-
GTP cyclohydrolase II	1	0	0	0	2.49E+07	0.00E+00	0.00E+00	0.00E+00	1	D6RUS9
Ubiquitin/s27a 40S ribosomal protein	6	3	3	3	1.83E+07	8.54E+06	1.59E+06	8.22E+06	2	Q5EC25
Sesquiterpene synthase	13	5	7	2	1.83E+07	1.86E+06	6.09E+06	1.10E+05	1	W8SIT3
Glyceraldehyde-3-phosphate dehydrogenase	13	13	5	3	1.46E+07	3.25E+07	3.21E+06	4.88E+05	2	A0A0F7JJ49
Translation elongation factor 1 alpha	8	10	3	2	1.31E+07	4.55E+07	2.26E+06	1.34E+06	2	Q6XX19
Prohibitin subunit PHB1	6	8	4	6	1.24E+07	6.87E+06	2.81E+06	1.65E+06	1	Q45Q24
Endopeptidase inhibitor	1	0	0	1	1.01E+07	0.00E+00	0.00E+00	6.11E+05	1	C9DFA9
Heat shock protein 70-like	8	7	1	0	8.98E+06	4.61E+06	7.23E+05	0.00E+00	2	C9DFB9
ADP-ribosylation factor 1	6	6	3	2	7.77E+06	8.26E+06	1.95E+06	6.16E+05	2	A7IYM9
Glukose-6-phosphate 1-dehydrogenase	7	2	1	6	5.94E+06	1.20E+06	0.00E+00	7.16E+05	1	F2Z9R2
Fibrillarin	3	0	0	1	4.41E+06	0.00E+00	0.00E+00	1.04E+05	1	Q1EI36
Epi-aristolochene dihydroxylase	5	3	3	1	4.07E+06	4.82E+05	1.40E+06	6.41E+04	1	A0A0A7HDA5
TSC13 protein	2	1	0	1	4.06E+06	5.09E+05	0.00E+00	1.23E+05	1	Q3IAA0
MAP kinase kinase (NbMEK2)	2	0	0	1	3.89E+06	0.00E+00	0.00E+00	0.00E+00	1	B2NIC3
Heat shock protein 70	5	4	0	0	3.63E+06	3.11E+06	0.00E+00	0.00E+00	2	Q6L9F6
ELI3	1	0	1	1	3.47E+06	0.00E+00	2.38E+05	2.37E+05	1	B8R6B6
Eukarytic translation initiation factor	1	1	0	1	3.46E+06	1.13E+06	0.00E+00	2.18E+05	1	U6BM52
Actin depolymerizing factor	1	1	1	1	2.54E+06	9.22E+05	4.28E+05	6.72E+04	1	A5H0M2
Peroxiredoxin 2B	2	2	0	0	2.38E+06	1.07E+06	0.00E+00	0.00E+00	2	R9W2E1
Chaperone like	1	0	0	1	2.30E+06	0.00E+00	0.00E+00	9.61E+04	1	G5DBJ0
Heat shock protein 70	1	1	0	0	2.25E+06	1.43E+06	0.00E+00	0.00E+00	1	Q769C5
Glyceraldehyde-3-phosphate dehydrogenase	12	12	4	2	2.06E+06	4.34E+06	4.87E+05	0.00E+00	2	A0A0F7JLU6
Thioredoxin H-type 1	2	1	0	0	1.90E+06	5.19E+05	0.00E+00	0.00E+00	1	C9DFC1
ER luminal-binding protein	9	3	1	0	1.70E+06	6.58E+05	2.38E+04	0.00E+00	2	B7U9Z3
Geranylgeranyl reductase	7	6	4	1	1.67E+06	2.43E+06	3.75E+05	4.52E+04	2	A0A0A8K9V3
Respiratory burst oxidase homolog	5	1	0	0	1.65E+06	2.83E+04	0.00E+00	0.00E+00	1	Q84KK7
Alpha-tubulin	5	8	2	0	1.65E+06	6.45E+06	4.64E+05	0.00E+00	2	A0A0S0N5Y9
MIP1.1	5	2	2	2	1.14E+06	0.00E+00	0.00E+00	2.31E+04	1	U5Q1Q7
Heat shock protein 90-1	9	10	2	0	1.14E+06	2.46E+06	1.57E+05	0.00E+00	2	A0A0M4J3A8
Glycine decarboxylase	3	5	1	1	1.14E+06	3.43E+06	1.60E+05	4.69E+05	2	E0X585
Ubiquinol oxidase	1	1	0	0	1.09E+06	1.29E+05	0.00E+00	0.00E+00	1	U5XH87
Fruktokinase-like	1	0	0	0	1.06E+06	0.00E+00	0.00E+00	0.00E+00	1	D9IWN9
NRG1	1	1	0	0	1.06E+06	2.74E+06	0.00E+00	0.00E+00	1	Q4TVR0
Glucose-6-phosphate 1-dehydrogenase	6	2	1	6	9.52E+05	0.00E+00	0.00E+00	1.72E+05	1	F2Z9R3
Sucrose phosphate synthase A	1	0	0	0	9.41E+05	0.00E+00	0.00E+00	0.00E+00	1	F6L7A2

Table 6.3 (continued)

Molecular chaperone	30	23	30	20	8.36E+05	0.00E+00	1.49E+05	5.40E+04	1	Q6UJX5
Eukaryotic translation initiation factor 4A	7	13	1	0	8.28E+05	6.78E+06	3.71E+04	0.00E+00	2	A0A0P0INT0
5-epi-aristolochene synthase	5	2	0	0	7.76E+05	3.32E+05	0.00E+00	0.00E+00	2	A0A0H5B1M3
Phospholipase D	3	2	1	0	7.48E+05	2.28E+05	2.49E+04	0.00E+00	1	A0A0M4UPT2
Acetylglutamate kinase	1	0	0	1	6.37E+05	0.00E+00	0.00E+00	3.47E+05	1	F8WQS2
Chloroplast PsbP2	2	0	1	0	4.63E+05	0.00E+00	1.75E+05	0.00E+00	2	I0B7J6
Lipoxygenase	4	0	0	0	4.10E+05	0.00E+00	0.00E+00	0.00E+00	2	R4S2V6
DNA gyrase subunit	1	1	0	0	3.97E+05	8.33E+06	0.00E+00	0.00E+00	1	Q5YLB4
NUb93b	2	0	0	1	1.75E+05	0.00E+00	0.00E+00	2.52E+04	1	W6JLE2

6.5 Result tables of Sulfenome mining experiments

Table 6.4: Sulfenome mining. Candidates that were identified with the YAP1C probe for Bs3 (from 4 replicates) and $Bs3_{S211A}$ (from 3 replicates). Candidates with significantly increased peptide abundance are marked in bold. Asterisks mark candidates that were previously found with sulfenome mining techniques in F. van Breusegem´s lab in different experiments.

#	DESCRIPTION	Bs3 COUNTS	$Bs3_{S211A}$ COUNTS	ID
1	V-type proton ATPase subunit C	4	0	Niben101Scf01182g03013.1
2	Methionine--tRNA ligase	4	0	Niben101Scf01146g09022.1
3	Pentatricopeptide repeat-containing protein	4	0	Niben101Scf01697g19001.1
4	Phosphoglucomutase-1	4	0	Niben101Scf01697g23018.1
5	Peptide methionine sulfoxide reductase MsrB	4	0	Niben101Scf01999g06013.1
6	Dihydrolipoyllysine-residue acetyltransferase component of pyruvate dehydrogenase complex	4	0	Niben101Scf02517g18011.1
7	10 kDa chaperonin	4	0	Niben101Scf08651g04006.1
8	Ferredoxin-dependent glutamate synthase 2	4	0	Niben101Scf04198g01002.1
9	Thioredoxin family protein LENGTH = 488	4	0	Niben101Scf04765g00002.1
10	NAD/NADP-dependent betaine aldehyde dehydrogenase	4	0	Niben101Scf05250g02011.1
11	Magnesium-protoporphyrin IX monomethyl ester [oxidative] cyclase	4	0	Niben101Scf10305g01003.1
12	Copper chaperone	4	0	Niben101Scf13029g03026.1
13	Cystathionine gamma-synthase	4	0	Niben101Scf04133g01027.1
14	T-complex protein 1 alpha subunit	4	0	Niben101Scf08606g00014.1
15	Glutamate decarboxylase	4	0	Niben101Scf00440g01018.1
16	Photosystem I reaction center subunit IV	4	0	Niben101Scf01220g04007.1
17	Fumarate hydratase class II	4	0	Niben101Scf01112g02010.1
18	Calcium homeostasis regulator CHoR1 [Zea mays]	4	0	Niben101Scf02730g00005.1
19	Haloacid dehalogenase-like hydrolase domain-containing protein*	4	0	Niben101Scf02853g02003.1
20	Beta-ketoacyl synthase*	4	0	Niben101Scf10810g01009.1
21	NAD-dependent malic enzyme*	4	0	Niben101Scf10055g07005.1
22	Tripeptidyl-peptidase 2	3	0	Niben101Scf00595g08041.1
23	Actin-2*	3	0	Niben101Scf00672g00001.1

Table 6.4 (continued)

24	Cytochrome b6	3	0	Niben101Scf01281g01007.1
25	Chlorophyll a-b binding protein, chloroplastic	3	0	Niben101Scf04318g01016.1
26	Chlorophyll a-b binding protein, chloroplastic	3	0	Niben101Scf02128g00025.1
27	Chlorophyll a-b binding protein 8, chloroplastic	3	0	Niben101Scf11767g01011.1
28	Phosphoglycerate kinase*	3	0	Niben101Scf02461g00003.1
29	Acetolactate synthase small subunit*	3	0	Niben101Scf04035g00002.1
30	NAC domain-containing protein 72	3	0	Niben101Scf14516g00019.1
31	40S ribosomal protein S10-1	3	0	Niben101Scf10636g00008.1
32	Methionine--tRNA ligase*	3	0	Niben101Scf09424g06007.1
33	Cytochrome b559 subunit alpha	3	0	Niben101Scf02160g06002.1
34	SKP1-like protein 1A*	3	0	Niben101Scf02658g00008.1
35	Glutamate decarboxylase*	3	0	Niben101Scf01958g05004.1
36	Aquaporin-like superfamily protein	3	0	Niben101Scf02576g00011.1
37	Glycerol-3-phosphate 2-O-acyltransferase 6	3	0	Niben101Scf02806g00013.1
38	T-complex protein 1 subunit alpha*	3	0	Niben101Scf02814g02005.1
39	Photosystem I reaction center subunit IV	3	0	Niben101Scf04172g02006.1
40	Superoxide dismutase [Mn]*	3	0	Niben101Scf04451g00026.1
41	60S ribosomal protein L7	4	1	Niben101Scf10798g00006.1
42	5-methyltetrahydropteroyltriglutamate-homocysteine methyltransferase*	4	1	Niben101Scf01812g02025.1
43	**Gibberellin receptor GID1***	**4**	**1**	**Niben101Scf02420g08013.1**
44	**Phosphoglucomutase-1**	**4**	**1**	**Niben101Scf02665g09004.1**
45	Aspartate aminotransferase 5 LENGTH=462*	4	1	Niben101Scf04437g00011.1
46	Xyloglucan endotransglucosylase/hydrolase	4	1	Niben101Scf09075g03002.1
47	1-aminocyclopropane-1-carboxylate oxidase*	4	1	Niben101Scf09217g00024.1
48	Glycogen synthase*	4	1	Niben101Scf14955g00012.1
49	Non-specific lipid-transfer protein 1	4	1	Niben101Scf29144g00011.1
50	Histone H2A	4	3	Niben101Scf08328g00009.1
51	30S ribosomal protein S6	4	2	Niben101Scf31903g00003.1
52	Nucleoside diphosphate kinase family protein*	2	2	Niben101Scf00324g02022.1
53	Nucleoside diphosphate kinase*	3	3	Niben101Scf02471g01008.1
54	**Chlorophyll a-b binding protein 6A, chloroplastic**	**3**	**2**	**Niben101Scf01105g00001.1**
55	Nucleotide/sugar transporter family protein	4	3	Niben101Scf00414g08001.1
56	Ras-related protein Rab*	3	2	Niben101Scf09317g00006.1
57	NAD(P)H-quinone oxidoreductase subunit 2 B	1	2	Niben101Scf00509g00005.1
58	Photosystem I P700 chlorophyll a apoprotein A2	3	1	Niben101Scf00568g04071.1
59	50S ribosomal protein L3*	4	3	Niben101Scf14636g02013.1
60	60S ribosomal protein L23a*	3	3	Niben101Scf01025g04007.1
61	ADP/ATP carrier 2*	3	2	Niben101Scf03587g00002.1
62	40S ribosomal protein S17*	3	2	Niben101Scf03138g01017.1
63	Glutamine synthetase PR-1*	3	3	Niben101Scf00952g03003.1
64	26S proteasome non-ATPase regulatory subunit 6*	2	2	Niben101Scf03038g06010.1
65	Aspartate aminotransferase, mitochondrial*	3	1	Niben101Scf09082g00016.1
66	60S ribosomal protein L13*	4	2	Niben101Scf05767g04004.1
67	UTP--glucose-1-phosphate uridylyltransferase*	3	1	Niben101Scf01556g01007.1
68	Heavy metal transport/detoxification superfamily protein	4	3	Niben101Scf01695g01016.1
69	ABC transporter G family member 7	0	2	Niben101Scf01837g02001.1

Table 6.4 (continued)

70	40S ribosomal protein S21	3	1	Niben101Scf02248g00007.1
71	60S ribosomal protein L35a-3	2	2	Niben101Scf07320g00021.1
72	Receptor-like protein kinase*	3	2	Niben101Scf02323g01010.1
73	60S ribosomal protein L18a	3	2	Niben101Scf07826g04012.1
74	Alcohol dehydrogenase*	4	3	Niben101Scf02907g06031.1
75	40S ribosomal protein S8*	4	2	Niben101Scf08447g02008.1
76	Aldehyde dehydrogenase family 1 member A3*	3	1	Niben101Scf02921g00003.1
77	Oxygen-dependent coproporphyrinogen-III oxidase*	3	1	Niben101Scf09708g10001.1
78	50S ribosomal protein L2, chloroplastic; 30S ribosomal protein S19	3	1	Niben101Scf05776g01052.1
79	Phosphoenolpyruvate carboxylase 1*	4	2	Niben101Scf03628g14021.1
80	Terpene synthase (EAS)	3	2	Niben101Scf03993g05005.1
81	Glycine-rich RNA-binding protein 3 (Fragments)*	4	2	Niben101Scf04659g00004.1
82	1,4-alpha-glucan branching enzyme GlgB*	3	1	Niben101Scf05222g04012.1
83	50S ribosomal protein L19	4	2	Niben101Scf06078g00003.1
84	Monodehydroascorbate reductase 1*	3	2	Niben101Scf07005g00008.1
85	Kinesin-related protein 5*	3	1	Niben101Scf09234g01003.1
86	Calcium-binding protein 7	3	3	Niben101Scf10103g03013.1
87	Apocytochrome f	3	1	Niben101Scf11178g01001.1
88	Ferredoxin-dependent glutamate synthase*	3	1	Niben101Scf12966g00016.1

6.6 Result table of Yeast knockout experiments

Table 6.5 Yeast knockout library screen. Yeast clones that formed colonies after transformation with Bs3 on plates containing galactose (induction medium). nd = not determined, na = not available

CLONE	COLONY SIZE	BARCODE	WB	REC NUMBER	ORF	GENE	PUTATIVE FUNCTION
Y1 = Y111	medium	CCTGTACTTTAAGAGTTGGG	no	34694	YGR064W	na	ORF, dubious
Y2 = Y40	medium	ATATGACAGCCAGTGGTACG	weak	30556	YML017W	PSP2	mRNA splicing
Y3	small	CATGCTCGGTCAGAGGATCT	no	31180	YNL264C	PDR17	phospholipid composition
Y4	small	TTGTACCCCCTAGACGTGCG	weak	33612	YDR253C	MET32	Transcription factor
Y5	small	TTATGTCACCTCTGCCAGTG	no	30565	YML010W-A	na	ORF, dubious
Y6	large	TACCTAACGACATTTGTGGC	no	35277	YLR368W	MDM30	Part of E3 ubiquitin ligase complex SCF
Y7 = Y82par.	large	GCGCTGCCATAATCCAAATA	no	32018	YNL194C	na	Sphingolipid content
Y8	large	CCGGACCTGTAACTTATTAG	no	36985	YGR053C	na	unknown function
Y9	large	GCACCTTCATCATGTCAGTG	no	36549	YMR109W	MYO5	Myosin motors
Y10 = Y34	large	TTGAAGAGTCCATTGTACTG	no	32852	YHR158C	KEL1	Cell morphology
Y11	large	GACCCTTAACTCAGATTCAG	yes	35667	YFL046W	FMP32	Cytochrome c oxidase assembly
Y12 = Y41	medium	CTAACGTCTTTGAACTTGGG	no	36986	YGR063C	SPT4	Transcription elongation factor
Y13	medium	mixed sequence	yes	35649	YFL030W	AGX1	Glycine biosynthesis
Y14 = Y47	small	CGGAGCTACTGATGTCTATT	weak	30513	YML057W	CMP2	Calcineurin A
Y15	large	CCTATGCACTGATTCCAGAT	no	30370	YAL036C	RBG1	Translation
Y16 = Y17	large	GGCCACCATAAATGAGTCCA	yes	30520	YML051W	Gal80	Gal80 Transcriptional regulator
Y17 = Y16	large	GGCCACCATAAATGAGTCCA	yes	30520	YML051W	Gal80	Gal80 Transcriptional regulator
Y18	large	ACTATTATGGCAGATGACGG	yes	32102	YPL150W	na	Protein kinase
Y19	large	ATGTACCACTACGCGCTGAG	no	31799	YOR023C	AHC1	Histone acetyltransferase subunit
Y20	medium	GGCCGCACTCAATAATCATA	no	30289	YEL048C	TCA17	Transport
Y21	large	TCAGCTTCGATAGCCGAGGT	no	32930	YNL146W	na	unknown function
Y22	large	ACACGATGGTAAGATTTGCG	no	36076	YNR032C-A	HUB1	mRNA splicing
Y23	medium	TGGGACTCAACCAACATCGA	yes	32723	YLR112W	na	unknown function
Y24	large	GGTTAATCCGAACTACCTAC	no	34727	YGR097W	ASK10	Channel regulator
Y25	large	ACAGTCTTGTAATCTGCTGG	weak	36486	YML074C	FPR3	Transcriptional regulator
Y26	medium	GGAGCGTACATCACTCACAG	weak	30739	YMR157C	AIM36	unknown function
Y27	medium	CCATACACTACAAGTTCGGA	no	33457	YCL050C	APA1	Phosphorylase
Y28	large	ATACATACGTGGAGAAGGCC	yes	35122	YKR051W	na	unknown function
Y29	large	GATCACGTCTTCTAACACTA	yes	36915	YJR107W	LIH1	Lipase
Y30	medium	nd	yes				
Y31	large	ATTGCGATACGAGCGGCCA	yes	32057	YNL155W	CUZ1	Proteasome pathway
Y32	large	CTGATTCCACGAGGTATGTG	no	30844	YMR258C	ROY1	Transport regulator
Y33	medium	CTGTGGTAACAGCACACATA	weak	31528	YLL040C	VPS13	Morphogenesis
Y34 = Y10	small	TAGAGGAGTCCATTGTACTG	yes	32852	YHR158C	KEL1	Cell morphology
Y35	small	TTTAGTCCGCGACGGGATCT	yes	34566	YGL199C	na	ORF, dubious
Y36	small	ATATGATGAGCACCCGCGTC	weak	30348	YAL059W	ECM1	Ribosome associated
Y37	small	ATCCTGATTTAAGGTGAGCG	yes	33164	YBR027C	na	ORF , Uncharacterized
Y38	small	TTTAGCCGCCGAGGTTCGT	no	34580	YGL214W	na	ORF, dubious
Y39	medium	ATGACGAGCCCATGACCTAG	yes	35344	YNL016W	PUB1	RNA-binding protein

Table 6.5 (continued)

Y40	medium	ATATGACAGCCAGTGGTACG	weak	30556	YML017W	PSP2	mRNA splicing
Y41 = Y12	medium	CTAACGTCTTTGAACTTGGG	no	36986	YGR063C	SPT4	Transcription elongation factor
Y42 = Y40	medium	ATATGACAGCCAGTGGTACG	weak	30556	YML017W	PSP2	mRNA splicing
Y43	small	TTACAGGGTCATAAGGTGTC	not grown	32777	YPL051W	ARL3	Membrane traffic
Y44	medium	CTACCACGATACCTAGTTAG	weak	34430	YGL063W	PUS2	Transcription
Y45	medium	CAGTATGCTAGATTCCGGGT	yes	33888	YDL190C	UFD2	Ubiquitin chain assembly factor
Y46	medium	GGAGACGCACACTCTTCTAT	weak	35319	YLR410W	VIP1	Inositol hexakisphosphate
Y47 = Y14	small	CGGAGCTACTGATGTCTATT	yes	30513	YML057W	CMP2	Calcineurin A
Y48	small	CCCTTGTAGTAATGGTTAG	yes	34684	YGR054W	na	Eukaryotic initiation factor eIF2A
Y49	small	nd	yes				
Y50	small	nd	yes				
Y51	medium	TAGTATATCCCATAACCGGC	yes	35237	YLR328W	NMA1	NAD biosynthesis
Y52	large	AAGTCTGTCTAACCTTCGCA	weak	32984	YNL092W	na	Methyltransferase
Y53	large	ACTACTGTGGTCCATGTGGT	yes	33345	YBR205W	KTR3	Protein glycosylation
Y54	large	AGAGCTCGGTAACTCGCACG	yes	32827	YPL001W	HAT1	Histone acetyl-transferase complex
Y55	large	double peaks! best fit	weak	30879	YMR292W	GOT1	Secretory transport
Y56 = Y16+17	large	GGCCACCATAAATGAGTCCA	yes	30520	YML051W	Gal80	Gal80 Transcriptional regulator
Y57	large	nd	no				
Y58	large	TGCATCTGCTGAATCGTATC	yes	30918	YHL045W	na	unknown function
Y59	large	TAAGAGTGGACAACTGCTGA	yes	34817	YGR187C	HGH1	unknown function
Y60	medium	nd	yes				
Y61	small	TAAGTCTTCACAAGCCGTCA	yes	32707	YLR096W	KIN2	Serine/threonine protein kinase
Y62	large	AATCGTCACCAACGTGCATA	yes	36388	YEL011W	GLC3	Glycogen accumulation
Y63	large	CCATCGTTTAGAAGTTTGCC	no	34385	YGL017W	ATE1	Arginyl-tRNA-protein transferase
Y64	large	AACTGAGTCGTACCGAGCTT	no	34320	YDR486C	VSP60	Transport
Y65	large	CCAGGTAGTGAACTGCTATC	yes	30347	YAL060W	BDH1	Metabolism
Y66	large	TGCGCCATGAGCACAAATAC	yes	34983	YKL133C	RCI50	Respiration
Y67	large	TCTTGGACGGGTTACATACG	no	32829	YPR002W	PDH1	Respiration
Y68	large	CCGATATTTCCAAGGCTGTA	no	34864	YKL015W	PUT3	Transcriptional activator
Y69	large	ACCTGAGCAGTATAGACGCG	no	36003	YKR087C	OMA1	Metalloendopeptidase
Y70	large	CAAGGGCCCCCAAGTGTCTA	yes	33499	YCR019W	MAK32	unknown function
Y71	large	CTATACGGCCAGATCCAGG	yes	33202	YBR065C	ECM2	mRNA splicing
Y72	large	CCGATATTTCCAAGGCTGTA	no	34864	YKL016C	ATP7	ATP synthase subunit
Y73	large	CTATCAGCCACGATAGGTAG	no	33127	YBL101C	ECM21	Membrane traffic
Y74	large	CCATCTCAGTGGGTGCAATG	no	30427	YAR040C	na	unknown function
Y75	large	GCCTGACAGACAATCTATCA	no	31625	YOR328W	PDR10	ABC transporter
Y76	large	GCCATCGGTGTCATGTACTT	yes	36432	YLR034C	SMF3	Metal ion transporter
Y77	large	nd	yes				
Y78	large	GCAGTCGATAGACCCGATTC	no	36930	YJR131W	MNS1	ER protein degradation
Y79	large	nd	no				
Y80	large	ACGGCAGATTCATTACATCG	no	36089	YNR062C	na	unknown function
Y81	large	TACGCTCGCGCAGATGTTTG	no	31923	YHR095W	na	ORF, dubious
Y82 = Y7 paralog	medium	GGTCCGCCCCCCAGGTAACA	no	33920	YDL222C	FMP45	Sphingolipid content
Y83	medium	GCAGCAGCATCTAAGGTAAG	yes	30612	YMR036C	MIH1	Cell cycle control
Y84	medium	TCAGGATGAGCCATTATCGG	no	36220	YMR086C-A	na	ORF, dubious

Table 6.5 (continued)

Y85	medium	CCAGGGCTCAAATGGCATAA	no	31449	YIL056W	VHR1	Transcriptional activator
Y86	medium	CCTTTCTTTACATGCGCTGC	weak	31535	YLL047W	na	ORF, dubious
Y87	medium	nd	yes				
Y88	medium	nd	no				
Y89	medium	GTACTCCGGTTCAGCATGT	yes	33572	YDR213W	na	Sterol biosynthesis
Y90	small	CAGTATAGTGAATCAGGTGC	yes	31795	YOR019W	na	unknown function
Y91	large	ATGACGTGAGCACCTATTGG	yes	30360	YAL045C	na	ORF, dubious
Y92	large	CATCACTCATCAGAGATACG	no	30492	YML078W	CPR3	Protein refolding
Y93	large	GTGAGACATATAACCTCCGC	yes	37327	YOR269W	PAC1	Transport
Y94	large	ATACCTGAGCCAGAGTTGCG	yes	36072	YMR174C	PAI3	Catabolism
Y95 = Y97	large	GGACTATCTTAACACCTGTC	no	35448	YPR029C	APL4	Vesicle mediated transport
Y96	large	TTAGTCACGCCACTGGTTCG	yes	33621	YDR262W	na	unknown function
Y97 = Y95	large	GGACTATCTTAACACCTGTC	weak	35448	YPR029C	APL4	Vesicle mediated transport
Y98	large	AGTGCTACTCTGACCTACTT	no	33389	YBR249C	ARO4	Amino acid biosynthesis
Y99	large	TGAGCACCTTTCACGAAGTC	weak	34051	YDR117C	TMA64	unknown function
Y100	large	CTAGAACACGCATGTAGAGC	yes	31416	YIL023C	YKE4	Zinc transporter
Y101	large	ACAGTTTAGGAAGC	yes	33101	YBL075C	SSA3	Hsp70 family
Y102	large	CAGATGACTGAATGGCTCTC	yes	30261	YEL020C	PXP1	unknown function
Y103	large	GTTACAACCAAACTGGCCGA	no	34492	YGL125W	MET13	Methionine biosynthesis
Y104	large	ATAATACGTCTGCAACCGGc	yes	33081	YBL055C	na	Nuclease involved in apoptosis
Y105 = 106	large	GGCAGATATACATACCCATC	no	36817	YJR019C	TES1	Fatty acid oxidation
Y106 = 105	medium	GGCAGATATACATACCCATC	weak	36817	YJR019C	TES1	Fatty acid oxidation
Y107	medium	ATCAGCCTGTCATGGTCCGT	weak	31723	YOL032W	OPI1	Phospholipid biosynthesis
Y108	medium	CCTGAGATTACATGACCTTC	yes	35509	YPR092W	na	ORF, dubious
Y109	medium	ACTGCATAGTCACTGTGGTG	no	36645	YNL274C	GOR1	Glyoxylate reductase
Y110	small	CACGATGGCCGATATTGCGT	yes	31820	YOR044W	IRC23	unknown function
Y111 = Y1	small	CCTGTACTTTAAGAGTTGGG	weak	34694	YGR064W	na	ORF, dubious
Y112	small	GTCGCCTTCATAACAAAGCA	weak	36567	YMR126C	DLT1	unknown function

Acknowledgements

First, I would like to thank Prof. Dr. Thomas Lahaye for his supervision and the opportunity to conduct my thesis in his research group. Thank you for your trust and your multitude of scientific ideas.

I also want to thank Prof. Dr. Ulrike Zentgraf for the useful advice as part of my thesis advisory committee and for the evaluation of my thesis.

Thanks to all current members of this lab: Dr. Annett Strauß, Dr. Robert Morbitzer, Dousheng Wu, Kyrylo Schenstnyi, Trang Phan and Erin Ritchie. It was a pleasure to work with you in this veritably cosmopolitan atmosphere. Special thanks to Danalyn Holmes for continuing the exciting Bs3 research project and for proofreading a lot of pages.

I especially thank Dr. Mark Stahl, Dr. Joachim Kilian and Bettina Stadelhofer for analysis of hundreds of mass spectrometry samples, fruitful collaboration, the transfer of knowledge, outstanding ideas and scientific discussion for many (happy) hours.

Thank you to Sergej, Jan, David, Patrizia and Sascha who supported my work on Bs3 with their Bachelor- Master- and research internship projects.

Thank you to Betty, Anne, Lisi and Kathi for all the good times and memories.

I would like to thank my parents and my brother for encouraging me to pursue my goals, wherever they may take me.

Finally, I want to thank Stefan, with whom I share my love for science - hopefully for the rest of my life. Thank you for your help and support.

Christina Krönauer

Functional and biochemical analysis of the *Capsicum annuum* resistance protein Bs3